ADAPTIVE TRANSLATIONAL MEDICINE

TOWARDS NEW THERAPEUTIC APPROACHES FOR METABOLIC DISEASES

GAUTAM KOK

.

Adaptive Translational Medicine

Towards New Therapeutic Approaches For Metabolic Diseases

Gautam Kok

Adaptive Translational Medicine

Towards New Therapeutic Approaches For Metabolic Diseases

Thesis with a summary in Dutch, Utrecht University

.

Adaptive Translational Medicine
Towards New Therapeutic Approaches
For Metabolic Diseases

Adaptieve Translationele Geneeskunde
Richting Nieuwe Therapeurische Benaderingen Voor Metabole Ziekten

(met een samenvatting in het Nederlands)

Proefschrift

ter verkrijging van de graad van doctor aan de Universiteit Utrecht op gezag van de rector magnificus, prof. dr. H.R.B.M. Kummeling, ingevolge het besluit van het college voor promoties in het openbaar te verdedigen op dinsdag 25 april 2023 des middags te 4.15 uur

door

Gautam Kok

geboren op 4 juni 1992 te Zevenaar

| **Promotor:** | prof. dr. E.E.S. Nieuwenhuis |
| | |

Promotor: prof. dr. E.E.S. Nieuwenhuis

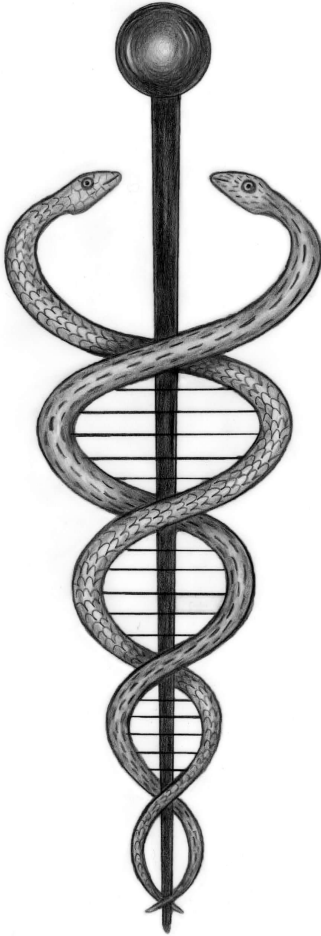**Copromotor:** dr. S.A. Fuchs

Beoordelingscommissie: prof. dr. K.P.J. Braun
prof. dr. J. Frenkel
prof. dr. J.B.F. Hulscher
prof. dr. C.D.M. van Karnebeek
prof. dr. A.B.J. Prakken

Table of contents

THE START

Prologue

YOUNG SCIENTISTS AIM TO PRIORITIZE PATIENTS

Remi Stevelink & Gautam Kok

Translational medicine helps to prevent scientific research from being wasted by focusing on the long-term benefits for patients. As early-career researchers, we want to accelerate that process - rather than waiting for senior researchers to spearhead the necessary changes.

Our international network of aspiring clinician–scientists, called Apollo, collaborates with senior scientists from the EUREKA Institute for Translational Medicine in Syracuse, Italy. We aim to learn about the goals, opportunities and challenges of translational medicine, including finding a more-efficient way to use research funding and balancing the competing interests of the different parties involved in research. We organize meetings, student workshops, mentorship programmes and an annual training programme.

We hope to develop the skills to navigate and improve the drug-discovery pipeline. Speeding up research delivery from bench to bedside will also entail changing how scientists are evaluated, as well as promoting collaboration across disciplines.[1]

References

1. Benedictus R, Miedema F, Ferguson MWJ. Fewer numbers, better science. *Nature* 2016; 538: 453–5.

Chapter 1

GENERAL INTRODUCTION

Translation is derived from translate, defined as "to change words into a different language", and "to change something into a new form, especially to turn a plan into something real".[1] This thesis is about translation: translating the need for new therapies to laboratory based research, then translating the results back from the lab to therapies for these patients.

Translational medicine: from DNA to RNA to proteins

Heritable information is stored in the nucleus of every cell, in two copies of DNA. The DNA contains thousands of genes, specific stretches of DNA that encode protein molecules. Differences in these genes account for people's inherited traits. The fact that there are two full copies of the DNA gives a form of redundancy. With some exceptions, most single gene (monogenetic) traits, and hence also monogenetic diseases, are inherited in an autosomal dominant or autosomal recessive fashion.[2] An autosomal dominant inheritance pattern means that one altered gene copy is sufficient to affect a person, while in autosomal recessive inheritance patterns, both gene copies need to be altered.

Genes give rise to specific traits by being translated into enzymes. Enzymes are special proteins that carry out all necessary cellular functions, including synthesis, degradation, and transport of nutrients and other molecules. Proteins can also be important for cellular structure and stability and function as messengers.[3] When needed, special proteins (DNA polymerases) transcribe the genes to pre-messenger RNA (pre-mRNA). Unneeded regions (introns) are then removed from protein-coding regions (exons) in a process called splicing, resulting in mature messenger RNA (mRNA). DNA and RNA consist of four nucleotides: A, T (DNA) or U (RNA), G, and C. Nucleotides triplets are called codons and encode amino acids. There are 20 different amino acids, hence multiple codons can encode the same amino acid (Table 1). These amino acids are carried to the ribosome by small, highly specific transfer RNA (tRNA) molecules. Aminoacyl-tRNA synthetases (ARS1) are the enzymes responsible for charging these specific tRNAs with the cognate amino acids in the cytosol.[4] Ribosomes then 'read' the mRNA, pair the codons with the specific tRNA, and attach the amino acids to each other. This forms an amino acid chain, called a polypeptide. After translation, polypeptides are modified and folded to become mature proteins, and transported to the correct location to carry out their function.[3]

Table 1. Nucleotide triplets (codons) encoding each amino acid, and the one- and three-letter abbreviations of the amino acids. Three codons specify a translational stop instead of an amino acid (AA). The methionine-codon AUG functions as a start codon.

AA	Ala	Arg	Asp	Asn	Cys	Glu	Gln	Gly	His	Ile	Leu	Lys	Met	Phe	Pro	Ser	Thr	Trp	Tyr	Val	Stop
	A	R	D	N	C	E	Q	G	H	I	L	K	M	F	P	S	T	W	Y	V	*
Co-don	GCA	AGA	GAC	AAC	UGC	GAA	CAA	GGA	CAC	AUA	UUA	AAA	AUG	UUC	CCA	AGC	ACA	UGG	UAC	GUA	UAA
	GCC	AGG	GAU	AAU	UGU	GAG	CAG	GGC	CAU	AUC	UUG	AAG		UUU	CCC	AGU	ACC		UAU	GUC	UAG
	GCG	CGA						GGG		AUU	CUA				CCG	UCA	ACG			GUG	UGA
	GCU	CGC						GGU			CUC				CCU	UCC				GUU	
		CGG									CUG					UCG					
		CGU									CUU					UCU					

Besides the nuclear DNA, each cell contains mitochondrial DNA (mtDNA). Mitochondria are subcellular organelles responsible for producing the energy the cell and all its processes need. One cell contains multiple mitochondria that all contain many copies of mtDNA.[3] As mitochondria have an evolutionary bacterial origin, the processes of DNA replication, transcription and translation differ from the nuclear/cytosolic processes. Many of the mitochondrial functions rely on proteins encoded in the nucleus. For example, the mtDNA replication and maintenance relies on a nucleus encoded protein (POLG).[5] Similarly, there are nucleus encoded mitochondrial ARS enzymes (ARS2) exist to attach the amino acids to mitochondrial tRNAs.[6] Hence, human cells and their mitochondria are heavily dependent on one another.

Inborn errors of metabolism

Inborn errors of metabolism, also known as metabolic diseases, are caused by pathogenic monogenetic variants and often follow autosomal recessive inheritance.[7] These variants cause a change in enzyme function, including a partial or total loss of function or gained abnormal function. As enzymes are responsible for cellular metabolism, e.g., synthesis, breakdown or change of cellular metabolites, these changes disrupt cellular homeostasis. Thousands of enzymes, thus thousands inborn errors of metabolism exist with an enormous variation in presentation and symptomology, severity, and disease-course.[8]

For several of the well-known diseases that are included in newborn screening programs, rapid diagnosis led to vast improvements of patient quality of life and survival.[9] However, if the disorder is not diagnosed at birth, it is often not diagnosed until onset of symptoms. Whole exome sequencing (WES) has significantly increased the number of patients diagnosed with inborn errors of metabolism, and at the same time

massively increased the number of genes associated with disease. The improved re-cognition of inborn errors of metabolism has not always improved care for patients. Most importantly, for many of these (relatively) new disorders, no treatment options are available for the patients.

Developing treatments for inborn errors of metabolism

Treatments of inborn errors of metabolism vary, but are generally based on one of the following principles: dietary changes to reduce or stop intake of food or medicines that cannot be metabolized; replace the dysfunctional or missing enzyme or metaboli-te; or remove accumulating toxic metabolites.[10] These established options offer decent therapeutic possibilities for a subset of the many inborn errors of metabolism. Howe-ver, they are limited to very specific diseases and are not curative. Hence, there is an urgent need for (curative) treatment options that are applicable to multiple diseases or that can be rapidly adapted for use in different diseases.

In this thesis, three levels of possible therapeutic interventions are discussed, all developed for patients from our own hospital (Wilhelmina Children's Hospital in Utrecht, The Netherlands).

The conventional approach

In **part 2**, using the conventional approach on ARS deficiencies, we utilize charac-terization of the disease and evaluation of the molecular mechanism to develop and test a substrate therapy. This approach is specific to this group of inborn errors of meta-bolism.

ARS enzymes, both the cytosolic ARS1, the mitochondrial ARS2, and the combined mitochondrial and cytosolic glycyl- and lysyl-ARS1 (GARS1 and KARS1, respectively) are responsible for the covalent binding of amino acids to their cognate tRNAs for use in protein translation. Pathogenic variants in these genes are increasingly associated with disease. Autosomal dominant variants in the cytosolic ARS1 genes cause Charcot-Marie-Tooth neuropathies, putatively due to a toxic gain-of-function.[19] In **chapter 2**, **chapter 3**, and the **addendum to part 2** we gain insights in the phenotype of autoso-mal recessive variants in these genes, which cause severe multi-organ diseases. Under-standing of the disease mechanism is essential for development of treatment. As our index patient was isoleucyl-ARS1 (IARS1) deficient, our primary interest was IARS1 deficiency. IARS1 is known to be able to misactivate isoleucine-tRNA with structurally

similar amino acid valine (1 valine for 180 isoleucine),[4] but subsequent editing activity ensures extreme specificity (1 valine for 50.000 isoleucine).[20–22] In **chapter 4**, we investigate the mechanism of IARS1 deficiency. Upon deprivation of specific essential amino acids, unicellular organisms may sacrifice translational fidelity to preserve protein synthesis.[23] Recently, a similar mechanism was identified in tryptophanyl-ARS1 (WARS1) which was found to be able to substitute tryptophan (W) by phenylalanine (F) in cancer cells.[24] In **chapter 5**, we re-analyze the publicly available proteomics data to investigate whether the mass spec techniques can be used to find other amino acid substitutions,[25] and to investigate if W>F substitutions are limited to tumor cells or not. With increased understanding of the mechanism, in **chapter 6** and **chapter 7** we develop the first therapeutic strategy for all ARS1 deficiencies. Motivated by the effects, in **chapter 8** we further elucidate the mechanism of and develop a similar strategy various mitochondrial ARS2, the combined cytosolic and mitochondrial KARS1, and the cytosolic glutaminyl-ARS1 (QARS1) deficiencies, all of which cause a distinctive mitochondrial phenotype.

The novel approach

In **part 3**, we target the liver. The liver has a central role in metabolism. Many inborn errors of metabolism can thus be treated or cured by (pediatric) liver transplantation. This includes intra- and extrahepatic conditions with and without liver injury.[26] Unfortunately, long-term survival of liver transplantation recipients has remained suboptimal. Especially the long-term use of immunosuppressants is associated with malignancies, infections and organ dysfunction.[27–29] Strategies that reduce the need for immunosuppressive therapy can potentially improve long-term quality of life and transplantation outcomes. Improved donor-recipient compatibility could help achieve this. A strategy that we have been working on is transplantation of bankable stem cells.[30] Such stem cell transplantations could be either healthy allogeneic cells or autologous cells derived from the patient. Autologous stem cells could be genetically corrected in vitro prior to re-transplantation.[14] Allogeneic stem cells could be derived from healthy donors, which would allow for accurate matching for nearly every parameter.

Most solid organ transplantations are matched for numerous criteria including human leukocyte antigen (HLA), but liver transplants are matched only for ABO blood group, and hepatitis serology.[31] HLA matching has improved outcomes for most solid

organ transplantations,[32–38] but studies on liver transplantations have been inconsistent.[39–44] Most studies have focused on serological HLA typing, which may not detect all clinically relevant mismatches. Therefore, in **chapter 9**, we investigate the effect of genetic HLA locus mismatching on liver transplantation outcomes in a meta-analysis. Not every mismatch has similar consequences. Therefore, more precise methods for HLA matching are being developed.[45] HLAMatchmaker uses B-cell epitopes,[46] and has been shown to corelate with graft outcome in various solid organ transplantations. PIRCHE (Predicted Indirectly Recognizable HLA Epitopes) uses T-cell epitopes,[47] and has been shown to correlate with kidney graft loss.[48] In **chapter 10**, we investigate the correlations between both HLAMatchmaker scores and PIRCHE-II scores on liver transplantation outcomes in a large cohort of patients transplanted in the Erasmus University Medical Center in Rotterdam, The Netherlands. Additionally, in the **addendum to part 3**, we develop a tool for transcriptomic comparison and selection of the best in vitro hepatocyte model systems for experimental use.

The future approach

As all inborn errors of metabolism are caused by genetic defects, targeting the underlying genetic defects hold the potential to cure all inborn errors of metabolism. In **part 4**, we use this approach to develop a treatment for DNA polymerase gamma (POLG)-related disease.

There are two major forms of gene therapy. In gene replacement therapy, as currently in use for spinal muscular atrophy, additional copies of the wildtype gene are inserted permanently or temporarily in patient cells.[11] These genes are then transcribed and translated to functional enzymes. Unfortunately, these genes are not placed under endogenous control, and can therefore not respond to environmental influences like the original gene. Recent advances in gene editing technologies evolved from the Nobel Prize winning CRISPR/Cas9 techniques have enabled us to precisely target the patient-specific genetic defects.[12] The most promising of these advances is prime editing. This versatile search-and-replace technique does not create double-strand breaks, significantly increasing safety.[13] This holds the potential to permanently correct any genetic defect in a multitude of cells in theoretically any target organ. We have previously genetically and functionally corrected primary, patient-derived liver cells, and in the **addendum to part 4** develop a dual-fluorescent reporter to improve *in vitro* editing efficiency.[14,15]

———

We aim to use this technique in vivo to target the most common variant in *POLG* causing Alpers-Huttenlocher syndrome. Combinations of more than 200 known pathogenic autosomal recessive *POLG* variants cause a wide spectrum of disease, ranging from very severe early onset encephalopathy syndromes to adult-onset spinocerebellar ataxia and epilepsy. The Alpers-Huttenlocher syndrome is characterized by a triad of refractory epilepsy, psychomotor regression and muscle weakness, often with acute onset in childhood or adolescence.[16] No curative therapeutic options exist, thus treatment is limited to supportive care. Common anti-epileptic drugs may induce acute liver failure.[17] The most common variant found in patients with Alpers-Huttenlocher syndrome and other *POLG*-related diseases is c.1399G>A p.(A467T), which reduces enzyme activity by 96%.[18] Therefore, in **chapter 11**, we pave the way towards the first curative in vivo prime editing strategy to treat patients with this common variant.

References

1. McIntosh C, ed. Cambridge Advanced Learner's Dictionary. 4th ed. *Klett*; 2013.

2. Mendel G. Versuche über Pflanzen-Hybriden. 1866.

3. Alberts B, ed. Molecular Biology of the Cell. 5. ed. *Garland Science*; 2008.

4. Rubio Gomez MA, Ibba M. Aminoacyl-tRNA synthetases. *RNA*. 2020; 26: 910-936.

5. Naviaux RK, Nguyen KV. POLG mutations associated with Alpers' syndrome and mitochondrial DNA depletion. *Ann Neurol*. 2004; 55: 706-712.

6. Christian BE, Spremulli LL. Mechanism of protein biosynthesis in mammalian mitochondria. *Biochim Biophys Acta Gene Regul Mech*. 2012; 1819: 1035-1054.

7. Raghuveer TS, Garg U, Graf WD. Inborn errors of metabolism in infancy and early childhood: an update. *Am Fam Physician*. 2006; 73: 1981-1990.

8. Ferreira CR, Rahman S, Keller M, et al. An international classification of inherited metabolic disorders (ICIMD). *J Inher Metab Dis*. 2021; 44: 164-177.

9. Champion M. An approach to the diagnosis of inherited metabolic disease. *Archives of Disease in Childhood - Education and Practice*. 2010; 95: 40-46.

10. Cameron P, ed. Textbook of Paediatric Emergency Medicine. 3rd edition. *Elsevier*; 2018.

11. Mendell JR, Al-Zaidy S, Shell R, et al. Single-Dose Gene-Replacement Therapy for Spinal Muscular Atrophy. *N Engl J Med*. 2017; 377: 1713-1722.

12. Jinek M, Chylinski K, Fonfara I, Hauer M, Doudna JA, Charpentier E. A Programmable Dual-RNA–Guided DNA Endonuclease in Adaptive Bacterial Immunity. *Science*. 2012; 337: 816-821.

13. Anzalone AV, Randolph PB, Davis JR, et al. Search-and-replace genome editing without double-strand breaks or donor DNA. *Nature*. 2019; 576: 149-157.

14. Schene IF, Joore IP, Oka R, et al. Prime editing for functional repair in patient-derived disease models. *Nat Commun*. 2020; 11: 5352.

15. Schene IF, Joore IP, Baijens JHL, et al. Mutation-specific reporter for optimization and enrichment of prime editing. *Nat Commun*. 2022; 13: 1028.

16. Saneto RP, Cohen BH, Copeland WC, Naviaux RK. Alpers-Huttenlocher Syndrome. *Pediatr Neurol*. 2013; 48: 167-178.

17. Hikmat O, Eichele T, Tzoulis C, Bindoff L. Understanding the Epilepsy in POLG Related Disease. *Int J Mol Sci*. 2017; 18: 1845.

18. Chan SSL, Longley MJ, Copeland WC. The Common A467T Mutation in the Human Mitochondrial DNA Polymerase (POLG) Compromises Catalytic Efficiency and Interaction with the Accessory Subunit. *J Biol Chem*. 2005; 280: 31341-31346.

19. Meyer-Schuman R, Antonellis A. Emerging mechanisms of aminoacyl-tRNA synthetase mutations in recessive and dominant human disease. *Hum Mol Genet*. 2017; 26: R114-R127.

20. Mohler K, Ibba M. Translational fidelity and mistranslation in the cellular response to stress. *Nat Microbiol*. 2017; 2: 17117.

21. Loftfield RB, Vanderjagt D. The frequency of errors in protein biosynthesis. *Biochem J*. 1972; 128: 1353-1356.

22. Hale SP, Auld DS, Schmidt E, Schimmel P. Discrete Determinants in Transfer RNA for Editing and Aminoacylation. *Science*. 1997; 276: 1250-1252.

23. Mordret E, Dahan O, Asraf O, et al. Systematic Detection of Amino Acid Substitutions in Proteomes Reveals Mechanistic Basis of Ribosome Errors and Selection for Translation Fidelity. *Mol Cell*. 2019; 75: 427-441.e5.

24. Pataskar A, Champagne J, Nagel R, et al. Tryptophan depletion results in tryptophan-to-phenylalanine substitutants. *Nature*. 2022; 603: 721-727.

25. Baranov PV, Atkins JF. Immune cells alter genetic decoding in cancer. *Nature*. 2022; 603: 582-583.

26. Mazariegos G, Shneider B, Burton B, et al. Liver transplantation for pediatric metabolic disease. *Mol Genet Metab*. 2014; 111: 418-427.

27. Ojo AO, Held PJH, Port FK, et al. Chronic Renal Failure after Transplantation of a Nonrenal Organ. *N Engl J Med*. 2003; 349: 931-940.

28. Åberg F, Gissler M, Karlsen TH, et al. Differences in long-term survival among liver transplant recipients and the general population: A population-based nordic study. *Hepatology*. 2015; 61: 668-677.

29. Tasdogan BE, Ma M, Simsek C, Saberi B, Gurakar A. Update on Immunosuppression in Liver Transplantation. *Euroasian J Hepatogastroenterol*. 2019; 9: 98-101.

30. Ardisasmita AI, Schene IF, Joore IP, et al. A comprehensive transcriptomic comparison of hepatocyte model systems improves selection of models for experimental use. *Commun Biol*. 2022; 5: 1094.

31. Eurotransplant. Liver - Eurotransplant. Accessed October 31, 2022. https://www.eurotransplant.org/organs/liver/

32. Opelz G. Effect of HLA matching in 10,000 cyclosporine-treated cadaver kidney transplants. *Transplant Proc*. 1987; 19: 641-646.

33. Opelz G. Importance of Hla Antigen Splits for Kidney Transplant Matching. *The Lancet*. 1988; 332: 61-64.

34. Anasetti C, Amos D, Beatty PG, et al. Effect of HLA Compatibility on Engraftment of Bone Marrow Transplants in Patients with Leukemia or Lymphoma. *N Engl J Med*. 1989; 320: 197-204.

35. Gjertson DW, Terasaki PI, Takemoto S, Mickey MR. National Allocation of Cadaveric Kidneys by HLA Matching. *N Engl J Med*. 1991; 324: 1032-1036.

36. Opelz G. Effect of HLA matching in heart transplantation. *Transplant Proc*. 1989; 21: 794-796.

37. Doxiadis IIN, Smits JMA, Persijn GG, Frei U, Claas FHJ. It takes six to boogie: Allocating cadaver kidneys in Eurotransplant. *Transplantation*. 2004; 77: 615-617.

38. Eurotransplant. Chapter 10 Histocompatibility Testing. *Eurotransplant Manual*. 2018: 1-21.

39. Gubernatis G, Kemnitz J, Tusch G, Pichlmayr R. HLA compatibility and different features of liver allograft rejection. *Transpl Int*. 1988; 1: 155-160.

40. Markus BH, Duquesnoy RJ, Gordon RD, et al. Histocompatibility and liver transplant outcome. Does HLA exert a dualistic effect? *Transplantation*. 1988; 46: 372-377.

41. O'Grady JG, Sutherland S, Harvey F, et al. Cytomegalovirus Infection and Donor/Recipient Hla Antigens: Interdependent Co-Factors in Pathogenesis of Vanishing Bileduct Syndrome After Liver Transplantation. *The Lancet*. 1988; 332: 302-305.

42. Chen M, Wade J, Levy GA, Greig PD. Effect of HLA matching and T- and B-cell crossmatch on acute rejection and graft survival following liver transplantation. *Transplant Proc*. 1994; 26: 2695-2696.

43. Nikaein A, Backman L, Jennings L, et al. HLA compatibility and liver transplant outcome: Improved patient survival by HLA and crossmatching. *Transplantation*. 1994; 58: 786-792.

44. Balan V, Ruppert K, Demetris AJ, et al. Long-term outcome of human leukocyte antigen

mismatching in liver transplantation: Results of the National institute of diabetes and digestive and kidney diseases liver transplantation database. *Hepatology*. 2008; 48: 878-888.

45. Erlich HA, Opelz G, Hansen J. HLA DNA typing and transplantation. *Immunity*. 2001; 14: 347-356.

46. Duquesnoy RJ. HLAMatchmaker: a molecularly based algorithm for histocompatibility deter-

mination. I. Description of the algorithm. *Hum Immunol*. 2002; 63: 339-352.

47. Geneugelijk K, Thus KA, Spierings E. Predicting alloreactivity in transplantation. *J Immunol Res*. 2014; 2014: 159479.

48. Geneugelijk K, Niemann M, Drylewicz J, et al. PIRCHE-II Is Related to Graft Failure after Kidney Transplantation. *Front Immunol*. 2018; 9: 321.

1
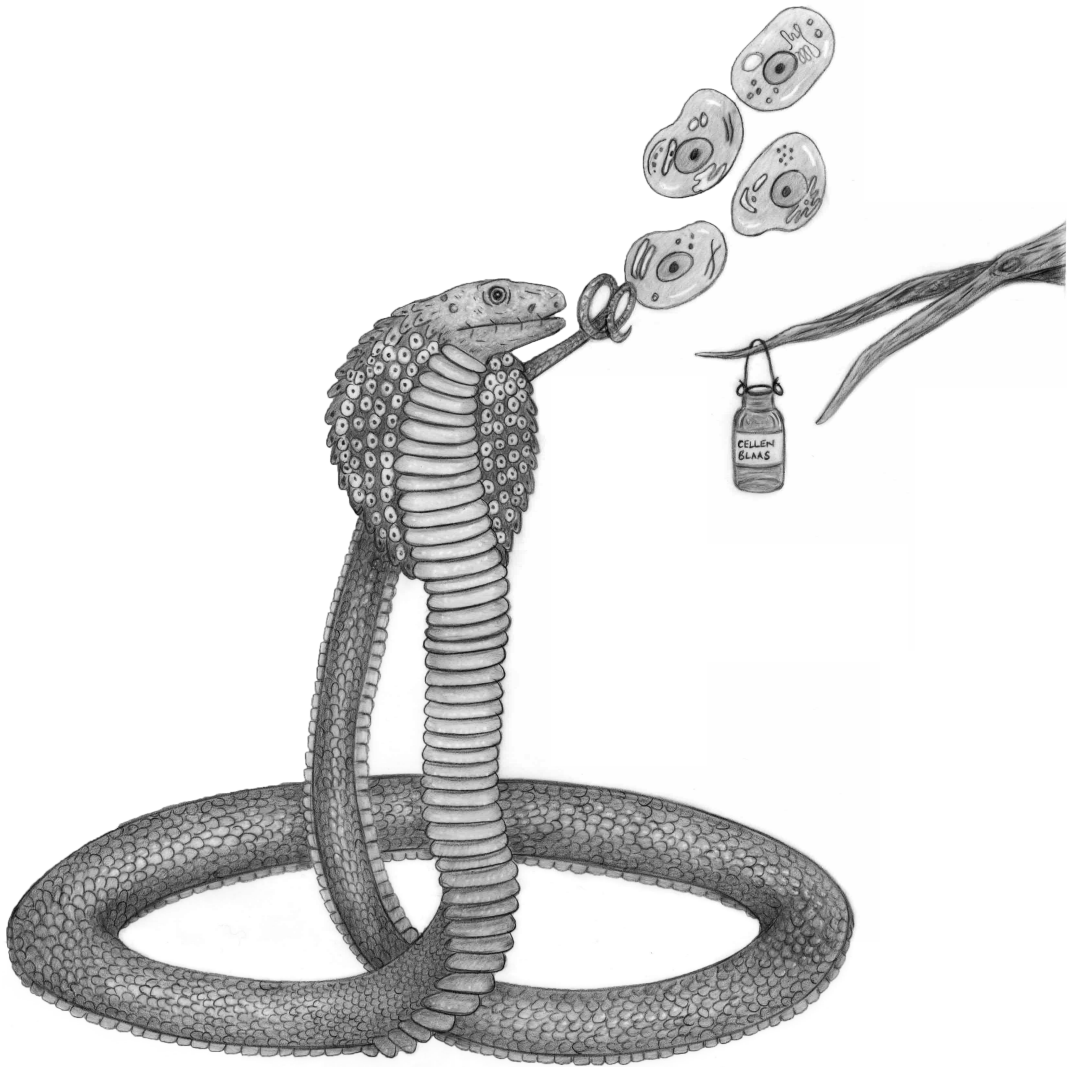
THE CONVENTIONAL APPROACH

DISEASE CHARACTERIZATION, MOLECULAR MECHANISM, AND SUBSTRATE THERAPY

Chapter 2

AMINOACYL-TRNA SYNTHETASE DEFICIENCIES:
IN SEARCH OF COMMON THEMES

Sabine Fuchs, Imre Schene*, Gautam Kok*, Jurriaan Jansen, Peter Nikkels, Koen van Gassen, Suzanne Terheggen-Lagro, Saskia van der Crabben, Sanne Hoeks, Laetitia Niers, Nicole Wolf, Maaike de Vries, David Koolen, Roderick Houwen, Margot Mulder, Peter van Hasselt

Abstract

Purpose

Pathogenic variations in genes encoding aminoacyl-tRNA synthetases (ARSs) are increasingly associated with human disease. Clinical features of autosomal recessive ARS deficiencies appear very diverse and without apparent logic. We searched for common clinical patterns to improve disease recognition, insight into pathophysiology, and clinical care.

Methods

Symptoms were analyzed in all patients with recessive ARS deficiencies reported in literature, supplemented with unreported patients evaluated in our hospital.

Results

In literature, we identified 107 patients with AARS1, DARS1, GARS1, HARS1, IARS1, KARS1, LARS1, MARS1, RARS1, SARS1, VARS1, YARS1, and QARS1 deficiencies. Common symptoms (defined as present in ≥4/13 ARS deficiencies) included abnormalities of the central nervous system and/or senses (13/13), failure to thrive, gastrointestinal symptoms, dysmaturity, liver disease, and facial dysmorphisms. Deep phenotyping of 5 additional patients with unreported compound heterozygous pathogenic variations in IARS1, LARS1, KARS1, and QARS1 extended the common phenotype with lung disease, hypoalbuminemia, anemia, and renal tubulopathy.

Conclusion

We propose a common clinical phenotype for recessive ARS deficiencies, resulting from insufficient aminoacylation activity to meet translational demand in specific organs or periods of life. Assuming residual ARS activity, adequate protein/amino acid supply seems essential instead of the traditional replacement of protein by glucose in patients with metabolic diseases.

Introduction

Protein translation is essential for all forms of life. Within this process, aminoacyl-transfer RNA (tRNA) synthetases (ARSs) play an important role. This highly conserved ubiquitously expressed class of enzymes is responsible for correct coupling of amino acids to their cognate tRNAs,[1-3] which base pair with messenger RNA (mRNA) triplets.[4] This ensures incorporation of correct amino acids in the growing polypeptide chain during protein synthesis. Each proteinogenic amino acid is coupled to its corresponding tRNA by a specific ARS,[1] as reflected in the ARS nomenclature (for example IARS1 for isoleucine-tRNA synthetase; LARS1 for leucine-tRNA synthetase). Because protein translation takes place in both the cytosol and mitochondria, mammalian cells possess cytosolic and mitochondrial ARSs. Mitochondrial ARSs are encoded by separate nuclear genes (nomenclature: ARS2), with the exception of KARS1, GARS1, and QARS1, which encode both the cytosolic and mitochondrial ARSs.[1]

Over the past 15 years, an increasing proportion of ARS genes has been associated with human disease. In the first description, a heterozygous missense pathogenic variation in *GARS1* was found to cause Charcot–Marie–Tooth disease type 2D, a peripheral axonal neuropathy.[5] Subsequently, other dominant pathogenic variations in *GARS1*,[6-16] *YARS1*,[17,18] *AARS1*,[19-24] *HARS1*,[25] *KARS1*,[26] and MARS1[27] have been associated with peripheral axonal neuropathies. In the past 10 years, pathogenic variations in mitochondrial *ARSs* (*DARS2*, *RARS2*, *EARS2*, *MARS2*, *FARS2*, *YARS2*, *SARS2*, *AARS2*, and *HARS2*)[28] have emerged as a cause of human disease. The clinical presentation of these mitochondrial diseases was reported to depend on the affected ARS, with encephalopathy as the most common manifestation. Only in the past 5 years have homozygous and compound heterozygous pathogenic variations been identified in cytosolic *LARS1*,[29,30] *AARS1*,[31-32] MARS1,[33-35] *IARS1*,[36,37] *YARS1*,[38] *VARS1*,[39] *RARS1*,[40] *DARS1*,[41] *HARS1*,[42] *SARS1*,[43] and in the combined cytosolic and mitochondrial *QARS1*,[44-47] *GARS1*,[48-50] and *KARS1*[26,51-54] genes. The resulting autosomal recessive diseases show considerable clinical variability and involve numerous organs without apparent logic.

With the increasing number of diagnosed patients, insight in the pathophysiological mechanism is crucial for optimal clinical care. To this end, we reviewed literature for patients with autosomal recessive ARS deficiencies. We additionally deep phenotyped five patients with novel compound heterozygous pathogenic variations in IARS1, LARS1, KARS1, and QARS1 and illustrate the common themes in disease presentation.

Part 2

		Cytosolic										Cytosolic and mito-chondrial			Including our patients			
Ref		36, 37	29, 30	33-35	38	31, 32	43	39	40	41	42	26, 51-54	48-50	44-47	36, 37, P1, P2	29, 30, P3	51-55, P4	44-47, P5
		IARS	LARS	MARS	YARS	AARS	SARS	VARS	RARS	DARS	HARS	KARS	GARS	QARS	IARS	LARS	KARS	QARS
N		4	10	32	2	5	4	3	4	10	2	18	3	10	6	11	19	11
Central nervous system	MRI abnormalities																	
	Psychomotor retardation																	
	Microcephaly																	
	Hypotonia																	
	Seizures																	
	Encephalopathy																	
	Spasticity																	
	Ataxia																	
	Episodic excited states																	
Senses	Sensorineuronal deafness																	
	Visual loss/retinal abnormalities																	
	Strabismus																	
	Nystagmus																	
Dysmorphisms	Chubby cheeks																	
	Facial dysmorphisms																	
	Abnormalities hands/feet/fingers																	
Growth	Dysmaturity																	
	Failure to thrive																	
Gastrointestinal tract	Poor feeding (tube/parenteral)																	
	Diarrhea/constipation/vomiting																	
Liver	Liver failure/hepatomegaly																	
	↓ albumin/protein																	
Lungs	Interstitial lung disease																	
	Clubbing																	
	Cystic lung disease																	
	Oxygen dependency																	
Bone marrow	Anemia																	
	Leukocytosis																	
	Thrombocytosis/thrombocytopenia																	
Kidneys	Tubulopathy																	
	Acute kidney failure																	
	Anatomical/ultrasound abnormalities																	
Spleen	Splenomegaly																	
	Accessory spleen																	
Heart	Cardiomyopathy/LVH																	
	Anatomical abnormalities																	
Muscles	Exercise intolerance/myalgia/weakness																	
Other symptoms	Skin abnormalities																	
	Hydrocele testis																	
	Hernia inguinalis																	
Laboratory findings	Endocrine abnormalities																	
	Various																	
	Mitochondrial dysfunction																	
	Other metabolic abnormalities																	
Periods of increased symptom severity	First years of life																	
	Infections																	

COLOR LEGEND

■ (grey) Reported for 1 patient

■ (black) Reported for > 1 patient

■ (orange) Threshold > 25% of ARSs with a common symptom within the category, in patients described in literature

■ (red) Threshold > 25% of ARSs with a common symptom within the category, in patients described in literature plus our patients

Fig. 1: clinical symptoms of patients with autosomal recessive ARS deficiencies reported in literature (left part) and supplemented with P1–5 (right part).

Gray squares represent symptoms reported for 1 patient, black squares symptoms reported for >1 patient. Categories of symptoms occurring in > 30% of the individual ARS deficiencies are marked in orange for patients reported in literature and in red after addition of P1–5. MRI magnetic resonance imaging, LVH left ventricular hypertrophy.

Materials and methods

A literature search was performed up to July 2017 in PubMed and Embase (search terms tRNA synthetase deficiency, ARS deficiency, (individual) ARS pathogenic variations) and through references in retrieved publications. Clinical details and laboratory results were retrieved from the manuscripts and supplementary material. The search was supplemented with all patients seen in our hospital with recessive ARS deficiencies diagnosed through exome sequencing. Exomes were enriched using Agilent Sure-Select XT Human All Exon kit V5 and sequenced on a HiSeq sequencing system (Illumina). Reads were aligned to hg19 using Burrows–Wheeler Aligner. Variants were called using Genome Analysis Toolkit variant caller and annotated, filtered, and prioritized using the Bench NGS Lab platform (Agilent-Cartagenia, Leuven, Belgium) and/or an in-house designed "variant interface" and manual curation. Patients were evaluated according to our clinical practice and all laboratory analyses were performed in ISO 9001/ISO15189 accredited diagnostic laboratories. Clinical and laboratory findings were categorized. Findings reported in >30% (≥ 4/13) of individual ARS deficiencies were considered common among ARS deficiencies.

Results

We identified 107 children with homozygous or compound heterozygous pathogenic variations in 10 different cytosolic and 3 combined cytosolic and mitochondrial *ARS* genes (Fig. 1, Table S1). All reported ARS deficiencies were associated with affected central nervous system (CNS) and/or senses (hearing/sight), most with failure to thrive (10/13) and many with feeding problems (6/13), dysmaturity (5/13), and liver symptoms (4/13). Signs of mitochondrial dysfunction and facial dysmorphisms were common (6/13 and 4/13, respectively, including all three combined cytosolic and mitochondrial ARSs) and various endocrine abnormalities (4/13). Symptoms were most

severe in the first year of life (4/13) and during infections and included acute liver failure and status epilepticus and/or encephalopathy (4/13).

We additionally identified five patients with pathogenic variations in *ARS* genes (nomenclature according to Human Genome Variation Society [HGVS] guidelines):

- P1, female, died at age 4 months, compound heterozygous pathogenic variations in *IARS1* (NM_002161.5): c.1305G>C p.(Trp435Cys) and c.3377dup p.(Asn1126fs)

- P2, male, now age 5 years, compound heterozygous pathogenic variations in *IARS1* (NM_002161.5): c.1305G>C p.(Trp435Cys) and c.3377dup p.(Asn1126fs). The parents originate from the same region as P1, which may suggest a founder effect for their common pathogenic variation

- P3, female, now age 5.5 years, compound heterozygous pathogenic variations in *LARS1* (NM_020117.10): c.3420del p.(Ile1141fs) and c.1283C>T p.(Pro428Leu)

- P4, male, died at age 4 years, compound heterozygous pathogenic variations in *KARS1* (NM_001130089.1): c1732_1744delGGCATTGATCGAG, p.(Gly578SerfsX20) and c.683C>T p.(Pro228Leu)

- P5, male, now age 4 years, compound heterozygous pathogenic variations in *QARS1* (NM_005051.2): c.2084+2_2084+3del p.(?) and c.793C>T p.(Arg265Cys)

Similar to the patients reported in literature, we observed CNS symptoms, growth/ feeding problems, and liver disease (Fig. 1, Table S1).

CNS symptoms

P1, P2, and P5 were born and remained microcephalic (< –2 SDS, Fig. 2). Head circumference at birth of P3–4 are unknown, but subsequent measurements were normal. CNS was most seriously affected in P4–5 with combined mitochondrial and cytosolic ARS deficiencies. Both patients had severe global developmental delays. P4 had an estimated developmental age of 4 months at age 4 years, involving eye contact, intentional laugh, recognition of parents, hypotonia, bipyramidal syndrome combined with extrapyramidal movements, but no rolling nor independent sitting. P5 had an estimated developmental age of 9 months at age 3.5 years, involving independent sitting and standing with support, but no crawling, language development, or interest in toys. Both patients had severe epilepsy. P4 had a permanent electroencephalogram
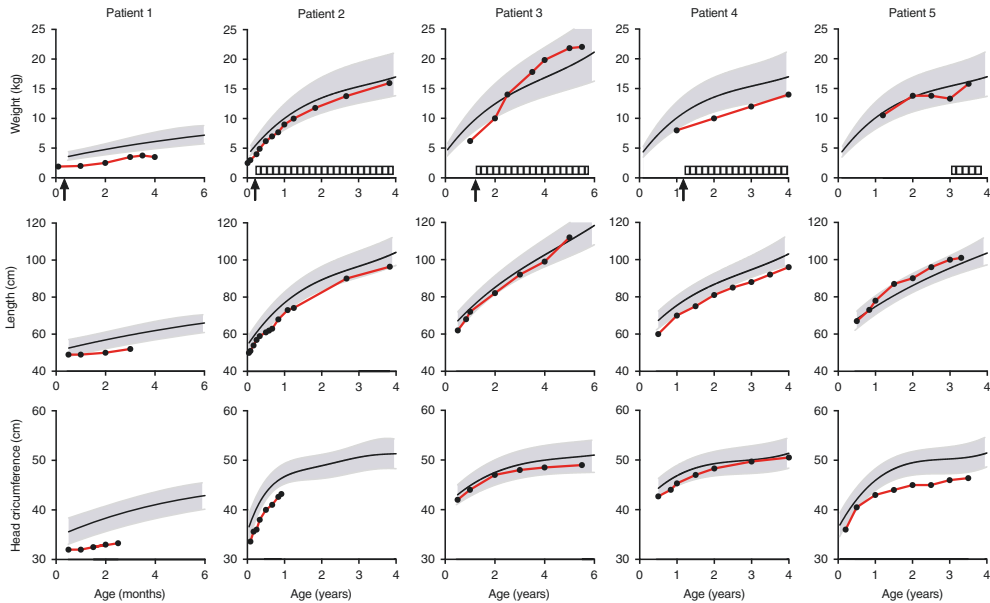
Fig. 2: growth curves of weight, length, and head circumference of P1–5.

Arrows indicate hospitalization due to feeding problems requiring nasogastric tube feeding (P1–4). Striped bars represent periods of feeding by percutaneous endoscopic gastrostomy (P2, P3, P5) or nasogastric tube (P4). Notice that the ranges of the x-axes are not synchronized between patients due to age differences.

(EEG) pattern of a (non)convulsive status epilepticus and from the age of 6 months jerky movements of the extremities, head, and/or eyes, somewhat improving with levetiracetam and clonazepam. P5 had a refractory epileptic encephalopathy despite ketogenic diet, deteriorating with vaccination/infections. In addition, P4 had severe perceptive hearing deficit, treated with cochlear implants and P5 severe occipital visual disturbance, with random eye movements and almost absent eye fixation or following.

Symptoms were milder in P1–3. Due to young age and hospitalization, development in P1 was difficult to judge. She was hypotonic, alert, made good eye contact, and passed her hearing test. P2–3 showed evidence of delayed global development (P2: global hypotonia, developmental quotients for global development, motoric skills, and verbal capacities ranging from 49 to 75 at age 3.5 years; P3: motor functioning p16, verbal IQ 81, performal IQ 70 at 5.5 years). P1–2 showed no evidence of epilepsy. P3 was hospitalized in her second and third year of life for three proven and one

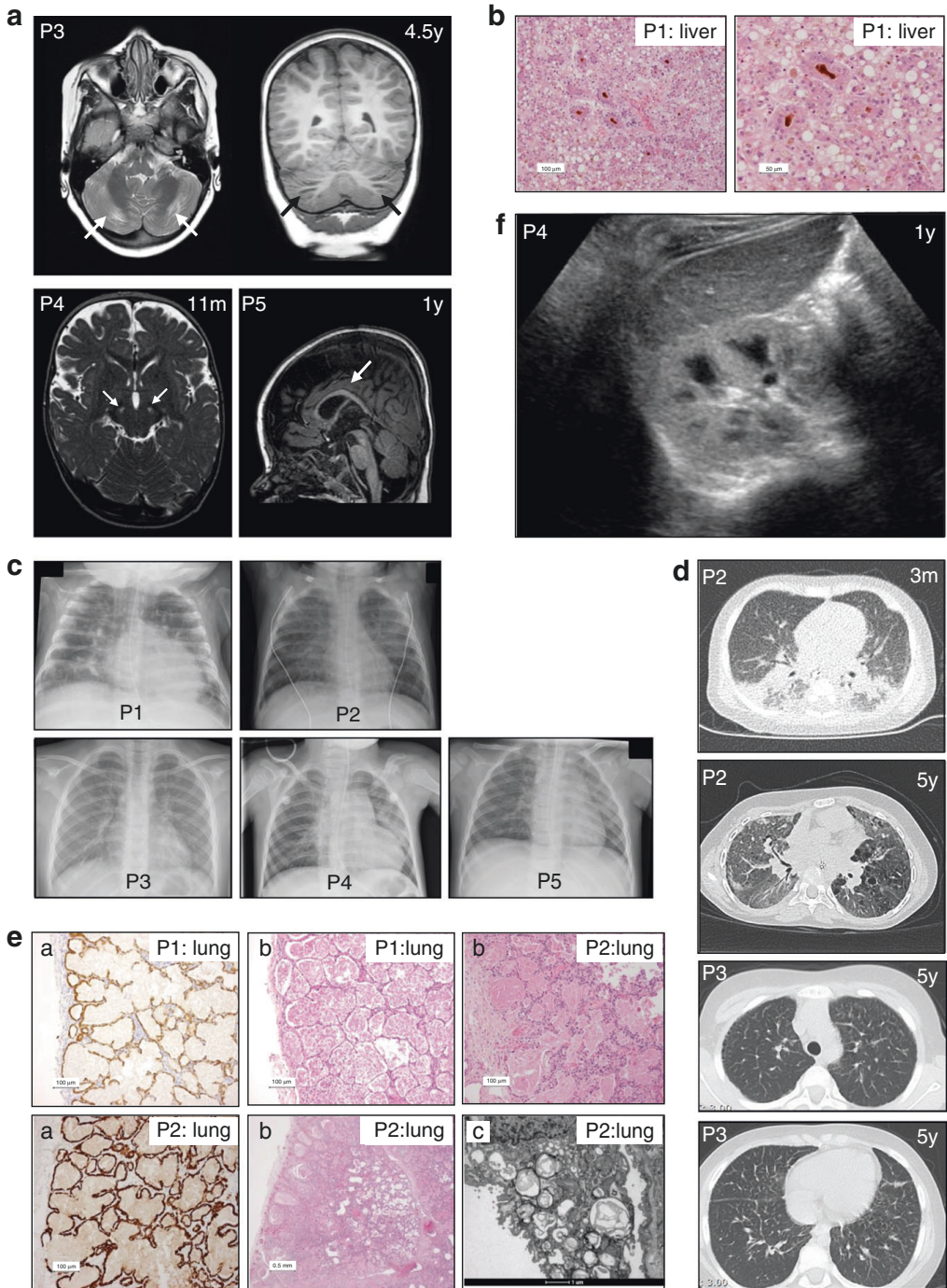**Fig. 3**: radiologic and histologic findings.

a, Brain magnetic resonance image (MRI) scans of P3, P4, and P5. T2-weighted axial and T1-weighted coronal MRI in P3 at age 4.5 years show focal atrophy of the cerebellar cortex. T2-weighted MRI in P4 at age 11 months shows abnormalities in the substantia nigra. T1-weighted MRI in P5 at age 1 year shows delayed myelination with a relatively thin corpus callosum. **b**, Histology shows severe cholestasis and steatosis in liver tissue (P1) in H&E staining (pseudorosette formation around bile plugs (brown). **c**, Chest X-rays of P1–5. Interstitial abnormalities are visible in P1–P4. **d**, Thoracic computed tomography (CT) scan in P2 at age 3 months shows extensive bilateral peribronchial consolidations, bronchus dilation, and subpleural ground glass consolidation with a remarkable dorso-basal distribution; at age 5 years it shows diffuse ground glass abnormalities, cystic lesions in a paraseptal–subpleural–bronchovascular distribution, and some thickening of interlobular septae. Thoracic CT scan in P3 at age 5 years shows thickening of interlobular septae in the upper and lower thorax. **e**, Histology shows severe pulmonary alveolar proteinosis in lung tissue (P1 and P2) by staining for pankeratin marker CKAE1/3: (a: highlights the lining of the alveoli with reactive type 2 pneumocytes, b: H&E staining; b: P1 and P2 alveoli are filled with a dense, eosinophilic, amorphous, protein-lipid precipitate; P2 shows granular material in multivesicular bodies and absent formation of lamellar bodies in type 2 pneumocytes, and c: electron microscopy;c: alveoli contain laminated annular structures [lamellar bodies]). **f**, Ultrasound of the kidneys in P4 shows a hyperechogenic cortex of the kidneys. The global intensity of the kidney cortex versus medulla and liver is too intense.

---

suspected status epilepticus, all triggered by infections. Electroencephalogram showed a focal left temporo-occipital lesion. Lamotrigine was started and no signs of epilepsy were noted after the age of 4 years.

Brain imaging of P3–5 showed distinct abnormalities (Fig. 3a). In P3, brain MRI showed periventricular white matter abnormalities (at age 13 months and 4.5 years), and focal cerebellar atrophy, without other neurodegenerative abnormalities or abnormalities of the thalami and basal ganglia. Magnetic resonance spectroscopy (MRS) showed elevated lactate peaks in white and gray matter. In P4, brain MRI at age 11 months showed hyperintense abnormalities in the substantia nigra. In P5, brain MRI was relatively normal at age 3 months, but displayed delayed white matter myelination, gradual loss of frontal periventricular white matter, and a relatively thin corpus callosum at age 1 year. At autopsy, microscopic evaluation of the brain of P1 (age 4 months) showed sparse white matter with decreased occipital myelination of U fibers.

Neuronal damage, presumably toxic, was seen in the basal ganglia and thalamus and minor recent hypoxic/ischemic damage in cerebellar neurons.

Intrauterine growth restriction, feeding problems, and failure to thrive

Intrauterine growth restriction was noted at 20 weeks of pregnancy in P1 and 3. P1–3 were born severely dysmature (P1: 1770 g; P2: 2250 g; P3: 1495 g, Fig. 2), P4 p2.3–5 (2800 g) and P5 P20–50 (3125 g). There were no signs of placental insufficiency or infections. In P1–4, the neonatal period was characterized by feeding problems and grossly insufficient growth, requiring hospitalization and nasogastric/duodenal tube feeding (P1: age < 1 week, P2: 2 months, P3: 13 months, P4: 13 months), in P3 prompted by fasting intolerance (4.5–10 h). Percutaneous endoscopic gastrostomy was performed in P2, P3, and P5. Extensive analyses including gastrointestinal passage studies and esophagogastroduodenoscopy showed no anatomic, histologic abnormalities, nor malabsorption. With enteral feeding, growth normalized in P2, 3, and 5, but remained deficient in P4.

Liver disease

P1–3 had markedly elevated liver enzymes (Fig. 4) in the first year of life, normalizing with age in P2 and to a lesser extent in P3. There were no signs of known (metabolic) liver diseases. During infections, liver enzymes rose dramatically in these patients, accompanied by transient (P3) and refractory (P1) ascites in the context of progressive liver failure. Liver ultrasound imaging showed normal homogeneous aspect at age 1 month and progressive enlargement from age 2 months onwards in P1; a slightly enlarged, diffusely hyperechogenic liver and left lobe hypertrophy, with normalization of echogenicity from age 2.5 years onwards in P2; and an enlarged liver with multiple hypoechogenic masses at 13 months, confirmed with MRI abdomen and persistent at age 5.5 years, with then also echogenic nodules in the pancreas in P3. Liver biopsy showed micro- and macrovesicular steatosis in P1 and combined steatosis and cirrhosis in P3. Liver steatosis, cholestasis, and extensive fibrosis were present at autopsy in P1 (Fig. 3b). Conversely, P4 only showed elevated liver enzymes in the final stage of his disease and P5 only during two episodes of antiepileptic drug introduction.

Additional common clinical symptoms

Hypoalbuminemia

Blood albumin concentrations were severely decreased P1–4 in their first year of age and increased temporarily upon albumin infusions in P1–2 (Fig. 4). There were no signs of intestinal or renal protein loss. Protein electrophoresis showed proportional protein deficiency, suggestive of a general protein synthesis defect. In P2–4, hypoalbuminemia resolved spontaneously with age (P2: 11 months, P3: 18 months, and P4: 30 months, followed by severe hypoalbuminemia in his last episode of life). Albumin was only determined after age 17 months in P5 and was normal.

Inflammation

In the first 6 months of life, P1 and P2 showed an inflammatory reaction with severe leukocytosis with predominantly neutrophils, varying thrombocytosis (P1: normal to 600×10^9/L; P2: $400–1400 \times 10^9$/L; reference range: $150–450 \times 10^9$/L), elevated C-reactive protein (CRP) and ferritin concentrations (P1: 680–1050 µg/L, reference range: 20–150 µg/L) (Fig. 4). Treatment with corticosteroids temporarily normalized CRP and leukocytes in P1. After age 1 year, leukocytes and thrombocytes gradually normalized in P2. However, CRP remains elevated (>15 mg/L) up to his current age of 4.5 years. Bone marrow aspiration and blood smear showed myeloid and lymphoid dysplasia as seen in aberrant stimulation, without evidence of malignancies. P4 also displayed inflammatory reactions in the first month of life and during infections, with leukocytosis, thrombocytosis ($550–600 \times 10^9$/L), and elevated CRP, and complete normalization thereafter. P3 and P5 had normal CRP and leukocyte concentrations and adequate inflammatory response during infections.

Pulmonary alveolar proteinosis

Respiratory symptoms were most prominent in P2, with respiratory distress at age 2 months requiring high-flow nasal oxygen administration and two days of invasive ventilation. Thoracic chest X-ray and high-resolution CT (HR-CT) scan (Fig. 3c,d) showed extensive bilateral interstitial pulmonary abnormalities. Lung histology revealed pulmonary alveolar proteinosis (PAP) (Fig. 3e). He is still dependent on oxygen administration and recently developed cystic abnormalities (Fig. 3d). P1 required invasive ventilation during respiratory syncytial virus infection and could not be weaned from
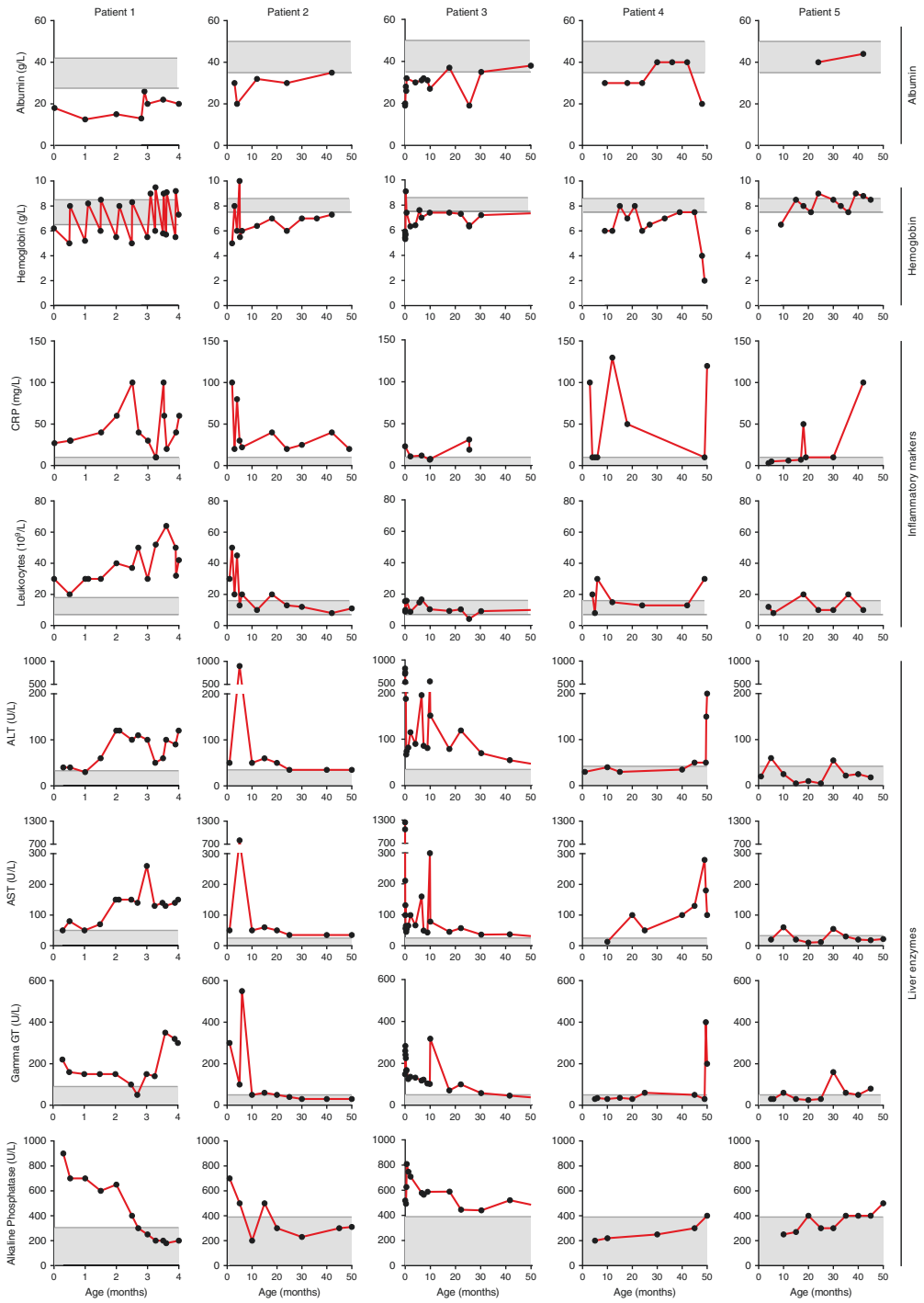
Fig. 4: laboratory findings of P1–5.

Notice that the ranges of the *x*-axes are not synchronized between patients due to age differences. ALT alanine transaminase, AST aspartate transaminase, CRP C-reactive protein, gamma-GT, gamma-glutamyltransferase

the ventilator nor oxygen. At autopsy, severe PAP was evident (Fig. 3e). P3 has been hospitalized once for pneumonia. She is easily fatigued, without overt respiratory symptoms. She has digital clubbing like her father. Aware of PAP in P1–2, chest X-rays were performed (Fig. 3c). Interstitial abnormalities, compatible with PAP, were noted and confirmed by thoracic HR-CT scan at age 5 years (Fig. 3d). P4 presented with fever, dyspnea, and respiratory insufficiency requiring ventilatory support at age 4 years. Chest X-ray showed signs of infection without clear interstitial pulmonary abnormalities (Fig. 3c). Further investigations were not conducted. P5 has no history of respiratory symptoms. Thoracic chest X-ray was performed once (Fig. 3c) upon presentation with fever and tachypnea. Symptoms resolved after antibiotic treatment.

Metabolic abnormalities

Analysis of urine from P1–2 showed increased excretion of galactose (maximal 1219 mmol/mol creatinine and 2534 mmol/mol creatinine, respectively, reference range: < 838 mmol/mol creatinine) and galactitol (maximal 1082 mmol/mol creatinine and 378 mmol/mol creatinine, respectively, reference range: < 107 mmol/mol creatinine), which normalized after lactose free feeding in P1 and spontaneously in P2. Enzyme activities involved in galactose breakdown and neonatal screening results for galactosemia were reviewed and normal in P1.

P1–2 and sporadically P4–5 displayed generalized aminoaciduria, which normalized with age in P2. Renal ultrasound in P4 showed bilateral increased renal cortex echogenicity (Fig. 3f), but no other signs of renal pathology.

Other metabolic abnormalities were only seen in individual patients, including for P1 increased cholesterol intermediates (cholestanol-7 and 8-dehydrocholesterol), putatively resulting from cholestasis or hypoalbuminemia and abnormal isoelectric focusing of serum transferrins, possibly secondary to liver failure or inflammation; for P2 increased urinary excretion of ethylmalonic acid (maximally 55 mmol/mol creatinine at age 5 months, reference range: < 20 mmol/mol creatinine) and bile acids, and elevated chitotriosidase blood concentration (62.5 μmol/hour/L, reference range: < 37.1 μmol/hour/L) at age 3 months, putatively reflecting the inflammatory state; for P5 ele-

vated blood and urine methylmalonic acid concentrations (maximally 3.11 µmol/L; reference range: 0.12–0.25 µmol/L; and 102 mmol/mol creatinine; reference range: 0–20 mmol/mol creatinine, respectively) at age 3 months; there was no evidence of nutritional deficiencies with normal vitamin B12 and homocysteine concentrations. All abnormalities normalized with age.

Metabolic investigations were performed in P3 at age 13 months upon presentation with hypoglycemia, abnormal liver enzymes, and status epilepticus. She displayed elevated cerebrospinal fluid (CSF) lactate concentrations, but normal lactate/pyruvate ratio and alanine concentrations. Urinary lactate and pyruvate excretion were elevated, but organic acid excretion was normal. Oral glucose tolerance test showed a slight rise in lactate and low–normal ketone body production. Muscle biopsy revealed decreased substrate oxidation velocity and ATP + CrP production (10.9 nmol/h.mUCS, reference range: 15.4–30.2 nmol/h.mUCS), but normal enzyme activities of all respiratory chain enzymes, complex V, pyruvate dehydrogenase complex (PDHc) PDHc, and citrate synthetase. There were no signs of mitochondrial depletion syndromes or *POLG*, *DGUOK*, and *MPV17* pathogenic variations. Glycogen storage diseases and lysosomal diseases (Niemann–Pick, lysosomal acid lipase deficiency [LALD]) were ruled out by enzyme assays and tyrosinemia and aberrant sugar or polyol metabolism by urinary analyses.

As might be expected, P4 showed evidence of mitochondrial dysfunction with elevated lactate levels in CSF (5.3 mmol/L, reference range: 1.1–2.1 mmol/L) and plasma (3.5–10 mmol/L, reference range: 0–2.2 mmol/L). Values rose after glucose challenge, with concomitantly increased urinary excretion of citric acid cycle intermediates. Lactate, pyruvate, alanine, and citric acid cycle intermediates dramatically increased in the final stage of disease. Muscle biopsy showed decreased substrate oxidation velocity and ATP + CrP production (7.4 nmol/h.mUCS, reference values 15.4–30.2 nmol/h.-mUCS), but normal enzyme activities of the respiratory chain enzymes, complex V, and citrate synthetase. Pathogenic variation analysis of *POLG* revealed no pathogenic variations. P5 showed normal lactate concentrations in blood and CSF, except during the period of epileptic encephalopathy (blood lactate concentration: 5.2 mmol/L).

Discussion

Autosomal recessive ARS deficiencies represent a rapidly growing group of severe inherited diseases, involving multiple organs, currently without curative options. The rising number of recognized patients allows us to search for a potential common clini-
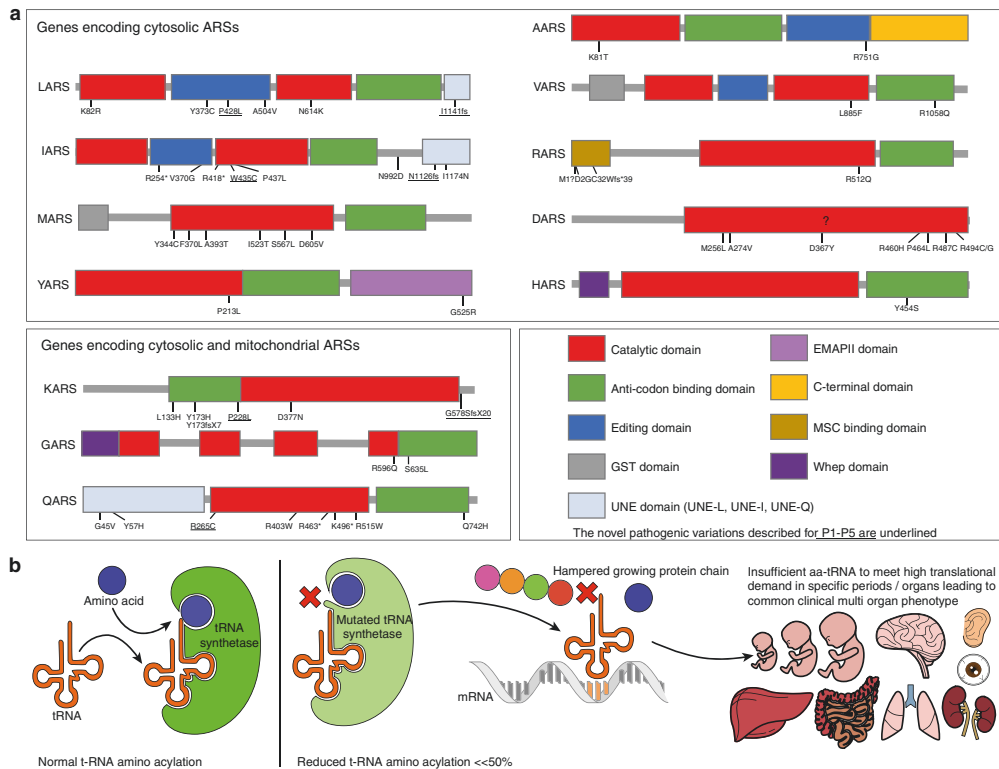
Fig. 5: putative disease mechanism for autosomal recessive ARS deficiencies.

a, Overview of the pathogenic variations found in autosomal recessive ARS deficiencies, concentrated in the domains associated with the canonical function in protein translation. The novel pathogenic variations described for P1–P5 are underlined. **b**, Schematic representation of the putative disease mechanism: insufficient aminoacylation to meet translational demand in specific organs or periods. tRNA transfer RNA

cal phenotype, which might improve clinical recognition, insight into the disease mechanism, and clinical care. To this end, we compared clinical phenotypes of 112 patients with pathogenic variations in 10 cytosolic and 3 combined cytosolic and mitochondrial ARS genes, including all previously described patients with autosomal recessive ARS deficiencies we could identify in literature, supplemented with five new patients.

All ARS deficiencies were associated with CNS symptoms, including deficient hearing and/or sight, and most with failure to thrive, feeding, and gastrointestinal pro-

blems. Liver disease, chubby cheeks/facial dysmorphisms, various endocrine abnorma-
lities, and mitochondrial dysfunction were reported for >30% of the different ARS defi-
ciencies (Fig. 1, orange) as was the pattern of severe symptoms in the first months of
life and during infections. Identification of common clinical features from literature
might underestimate true symptom overlap. Sometimes, not all clinical features were
described, especially when studies were performed in specific cohorts of patients
(HARS1)[42] or for specific clinical features (intellectual disability [SARS1],[43] leukoen-
cephalopathy and leg spasticity [DARS1],[41] hypomyelination [RARS1],[40] neurogenetic
disease [VARS1],[39] nonsyndromic hearing impairment [KARS1]).[51] We emphasize the
importance of deep phenotyping in novel genetic diseases with five supplementary
patients and encourage reporting all symptoms, also when not suspected as a core cli-
nical feature. This allowed us to also classify lung disease, hypoalbuminemia, bone
marrow, and kidney abnormalities as common (Fig. 1, red). Moreover, some symptoms
might only be noted after specific diagnostic evaluation, as illustrated for restrictive
lung disease in our IARS1 (P1) and LARS1 (P3) deficient patients.

Our findings suggest a strikingly common clinical phenotype for LARS1, MARS1,
and IARS1 and to a slighter extent YARS1 and AARS1 deficiencies. Potentially, all
symptoms reported for cytosolic ARS deficiencies represent the spectrum of a common
clinical phenotype. Conversely, some features might be characteristic for specific ARS
deficiencies. Nine cytosolic ARSs (IARS1, LARS1, MARS1, QARS1, KARS1, RARS1,
DARS1, and EPRS1) form a multisynthetase complex (MSC). The major role ascribed to
the MSC is to improve translational efficiency. Putatively, pathogenic variations in this
subset of *ARSs* result in common symptoms based on deficient MSC function. Alterna-
tively, symptoms might relate to specific amino acids (individually or to groups like
branched chain amino acids), based on abundance in specific proteins or to common
(non)canonical amino acid or ARS functions. Combined cytosolic and mitochondrial
ARS deficiencies obviously represent a specific subgroup, with mitochondrial dysfunc-
tion reflected in laboratory findings, muscle biopsy, and affected organs with high oxi-
dative metabolism (brain, heart). Similarly, sensorineural hearing impairment is fre-
quently seen in other mitochondrial ARS deficiencies, including LARS2, HARS2,
RARS2,[55] and IARS2.[54] However, anemia and hypoalbuminemia in our KARS1 defi-
cient patient and hepatosplenomegaly during infancy in QARS1 deficiencies[46] might
imply involvement of the cytosolic ARS deficiency. Conversely, although the multi-or-
gan phenotype might suggest a mitochondriopathy, we did not find evidence for mito-
chondrial dysfunction caused directly by the cytosolic ARS deficiency.

—

The overlap in clinical phenotype between pathogenic variations in different *ARS*s suggests a general disease mechanism. Pathogenic variations causing recessive ARS deficiencies generally reside in catalytic or anticodon binding domains of *ARS* genes (Fig. 5a). The most straightforward hypothesis therefore confers that aminoacylation is insufficient to meet translational demand in specific organs, especially during high demands in the first year of life and infections (Fig. 5b). Concurrently, aminoacylation activity was decreased in mutant alleles from patients with AARS1,[31,32] MARS1,[33,34] IARS1,[36] HARS1,[42] SARS1,[43] QARS1,[44,46] and KARS1[26] deficiencies, but never to an enzyme activity of < 8% from normal (Table S2). The fact that heterozygous parents of patients are unaffected suggests that on the other hand there is some excess capacity in ARS activity.

Intrauterine growth restriction and failure to thrive seem closely related to a disease mechanism involving reduced aminoacylation activity, translational slowdown or inefficiency, and consequential decreased proliferation. Indeed, growth was diminished in complementation assays in yeast with mutant *AARS1*,[31] *IARS1*,[36] *MARS1*,[34] *GARS1*,[50] and *KARS1*[53] alleles. Similarly, hypoalbuminemia would well align with this disease mechanism, because albumin synthesis is very sensitive to amino acid depletion, particularly for leucine, isoleucine, and tryptophan.[56] Moreover, organs most prominently affected in recessive ARS deficiencies are the organs with highest amino acid incorporation rates: liver (2.4 %/hr), lung (1.0 %/hr), brain (0.6 %/hr), and muscle (0.4–0.7 %/hr)[57] or high proliferation rates (intestine). This also concurs with the prominence of symptoms during perinatal growth and infections, periods of high translational demand. It remains unclear why other highly proliferative organs like the skin are not affected, except in one patient with IARS1 deficiency and skin hyperelasticity,[37] and two sibs with QARS1 deficiency with a dry rough skin.[46]

PAP was previously thought to be a specific feature of MARS1 deficiency.[33-35] We show that other recessive ARS deficiencies (IARS1 and LARS1) can also cause PAP. Furthermore, our IARS1 deficient patient developed cystic abnormalities with time, as reported in YARS1 deficient patients.[38] PAP results from the accumulation of lipoproteins in pulmonary alveoli, leading to restrictive lung disease and respiratory failure.[58] Most commonly involved in the pathogenesis is defective granulocyte-macrophage colony-stimulating factor (GM-CSF) receptor activation, either through GM-CSF autoantibodies[59] or rare pathogenic variations in GM-CSF receptor genes.[60] This leads to deficient alveolar macrophage maturation, which is essential for macrophages to clear and recycle surfactant. Interestingly, among patients with autoimmune antisynthetase

syndromes, antibodies against ARSs strongly predict interstitial lung disease.[61] In addition, PAP is also a clinical characteristic of lysinuric protein intolerance (LPI), a rare inherited metabolic disease[62] caused by a defective cationic amino acid transporter in the kidney, small bowel, lung, spleen, monocytes, and macrophages, resulting in leakage of cationic amino acids (arginine, ornithine, and lysine). Thus a shortage of amino acids, antibodies against ARSs, and genetic ARS deficiencies can all result in PAP, putatively through reduced aminoacylation and deficient translation to ensure adequate surfactant composition or homeostasis. Interestingly, LPI patients show considerable overlap in clinical phenotype with recessive ARS deficiencies, involving neurological impairment, failure to thrive, hepatosplenomegaly, PAP, renal tubulopathy, and hemophagocytic lymophohistiocytosis.[62] The fact that both reduced amino acid concentrations and ARS deficiencies can result in common clinical symptoms concurs with insufficient aminoacylation for efficient translation as disease mechanism.

If reduced aminoacylation leads to symptoms in patients with recessive ARS deficiencies and if patients have some residual enzyme activity, then supplementation of the corresponding amino acid or high protein intake might improve symptoms. This is in sharp contrast with the traditional management of replacing protein by glucose in patients with metabolic hepatic disease, but aligns with the previous advice to patients with LARS1 pathogenic variations[29-30] to supply a minimum of 2.5 g/kg of whole protein either enterally or parenterally while unwell. This is supported by the restoration of growth upon increased intake with tube feeding in P1–3 (Fig. 2). Similarly, the clinical phenotype in a patient with MARS1 deficiency improved after starting parenteral nutrition[33] and MARS1 aminoacylation activity and proliferation in yeast with mutant MARS1 alleles improved upon methionine supplementation.[34]

In conclusion, through deep phenotyping of five patients with novel compound heterozygous IARS1, LARS1, KARS1, and QARS1 pathogenic variations, we were able to add lung disease, hypoalbuminemia, anemia, and renal tubulopathy to the common phenotype we derived from literature for cytosolic ARS deficiencies, involving CNS abnormalities, growth restriction, liver symptoms, and facial dysmorphisms. This highlights the importance of deep phenotyping in patients with novel rare genetic diseases. Identification of a common clinical phenotype implies that recessive pathogenic variations in newly identified cytosolic ARSs may result in similar clinical symptoms, which might improve disease recognition and guide diagnostic work-up. Insufficient aminoacylation activity to meet high translational demand as common disease mechanism would also guide therapeutic care. As some residual enzyme activity seems essential

for life, adequate supply of protein/amino acids is crucial, especially during periods of increased translational demand, including the first year of life and infections.

2

References

1. Antonellis A & Green ED. The role of aminoacyl-tRNA synthetases in genetic diseases. *Annu Rev Genom Hum Genet*. 2008; 9: 87–107.

2. Yao P & Fox PL. Aminoacyl-tRNA synthetases in medicine and disease. *EMBO Mol Med*. 2013; 5: 332–43.

3. Storkebaum E. Peripheral neuropathy via mutant tRNA synthetases: Inhibition of protein translation provides a possible explanation. *BioEssays*. 2016; 38: 818–29.

4. Scheper GC, van der Knaap MS & Proud CG. Translation matters: protein synthesis defects in inherited disease. *Nat Rev Genet*. 2007; 8: 711–23.

5. Antonellis A, Ellsworth RE, Sambuughin N, et al. Glycyl tRNA synthetase mutations in Charcot-Marie-Tooth disease type 2D and distal spinal muscular atrophy type V. *Am J Hum Genet*. 2003; 72: 1293–9.

6. Sivakumar K, Kyriakides T, Puls I, et al. Phenotypic spectrum of disorders associated with glycyl-tRNA synthetase mutations. *Brain*. 2005; 128: 2304–14.

7. James PA, Cader MZ, Muntoni F, Childs AM, et al. Severe childhood SMA and axonal CMT due to anticodon binding domain mutations in the GARS gene. *Neurology*. 2006; 67: 1710–2.

8. Del BoR, Locatelli F, Corti S, et al. Coexistence of CMT-2D and distal SMA-V phenotypes in an Italian family with a GARS gene mutation. *Neurology*. 2006; 66: 752–4.

9. Seburn KL, Nangle LA, Cox GA, et al. An active dominant mutation of glycyl-tRNA synthetase causes neuropathy in a Charcot-Marie-Tooth 2D mouse model. *Neuron*. 2006; 51: 715–26.

10. Rohkamm B, Reilly MM, Lochmüller H, et al. Further evidence for genetic heterogeneity of distal HMN type V, CMT2 with predominant hand involvement and Silver syndrome. *J Neurol Sci*. 2007; 263: 100–6.

11. Abe A & Hayasaka K. The GARS gene is rarely mutated in Japanese patients with Charcot-Marie-Tooth neuropathy. *J Hum Genet*. 2009; 54: 310–2.

12. Lee HJ, Park J, Nakhro K, et al. Two novel mutations of GARS in Korean families with distal hereditary motor neuropathy type V. *J Peripher Nerv Syst*. 2012; 17: 418–21.

13. Eskuri JM, Stanley CM, Moore SA, et al. Infantile onset CMT2D/dSMA V in monozygotic twins due to a mutation in the anticodon-binding domain of GARS. *J Peripher Nerv Syst*. 2012; 17: 132–4.

14. Kawakami N, Komatsu K, Yamashita H, et al. A novel mutation in glycyl-tRNA synthetase caused Charcot-Marie-Tooth disease type 2D with facial and respiratory muscle involvement. *Rinsho Shinkeigaku*. 2014; 54: 911–5.

15. Sun A, Liu X, Zheng M, Sun Q, Huang Y, Fan D. A novel mutation of the glycyl-tRNA synthetase (GARS) gene associated with Charcot–Marie–Tooth type 2D in a Chinese family. *Neurol Res*. 2015; 37: 782–7.

16. Liao YC, Liu YT, Tsai PC, et al. Two novel de novo GARS mutations cause early-onset axonal Charcot-Marie-Tooth disease. *PLoS One*. 2015; 10: e0133423.

17. Jordanova A, Irobi J, Thomas FP, et al. Disrupted function and axonal distribution of mutant tyrosyl-tRNA synthetase in dominant intermediate Charcot-Marie-Tooth neuropathy. *Nat Genet*. 2006; 38: 197–202.

18. Hyun YS, Park HJ, Heo SH, et al. Rare variants in methionyl- and tyrosyl-tRNA synthetase genes in late-onset autosomal dominant Charcot-Marie-Tooth neuropathy. *Clin Genet*. 2014; 86: 592–4.

19. Latour P, Thauvin-Robinet C, Baudelet-Méry C, et al. A major determinant for binding and aminoacylation of tRNAAla in cytoplasmic

alanyl-tRNA synthetase is mutated in dominant axonal Charcot-Marie-Tooth disease. *Am J Hum Genet*. 2010; 86: 77–82.

20. Lin K-P, Soong B-W, Yang C-C, et al. The mutational spectrum in a cohort of Charcot-Marie-Tooth disease type 2 among the Han Chinese in Taiwan. *PLoS One*. 2011; 6:e29393.

21. Zhao Z, Hashiguchi A, Hu J, et al. Alanyl-tRNA synthetase mutation in a family with dominant distal hereditary motor neuropathy. *Neurology*. 2012; 78: 1644–9.

22. Bansagi B, Antoniadi T, Burton-Jones S, et al. Genotype/phenotype correlations in AARS-related neuropathy in a cohort of patients from the United Kingdom and Ireland. *J Neurol*. 2015; 262: 1899–908.

23. Motley WW, Griffin LB, Mademan I, et al. A novel AARS mutation in a family with dominant myeloneuropathy. *Neurology*. 2015; 84: 2040–7.

24. McLaughlin HM, Sakaguchi R, Giblin W, et al. A recurrent loss-of-function alanyl-tRNA synthetase (AARS) mutation in patients with charcot-marie-tooth disease type 2N (CMT2N). *Hum Mutat*. 2012; 33: 244–53.

25. Safka Brozkova D, Deconinck T, Beth Griffin L, et al. Loss of function mutations in HARS cause a spectrum of inherited peripheral neuropathies. *Brain*. 2015; 138: 2161–72.

26. McLaughlin HM, Sakaguchi R, Liu C, et al. Compound heterozygosity for loss-of-function lysyl-tRNA synthetase mutations in a patient with peripheral neuropathy. *Am J Hum Genet*. 2010; 87: 560–6.

27. Gonzalez M, McLaughlin H, Houlden H, et al. Exome sequencing identifies a significant variant in methionyl-tRNA synthetase (MARS) in a family with late-onset CMT2. *J Neurol Neurosurg Psychiatry*. 2013; 84: 1247–9.

28. Konovalova S & Tyynismaa H. Mitochondrial aminoacyl-tRNA synthetases in human disease. *Mol Genet Metab*. 2013; 108: 206–11.

29. Casey JP, McGettigan P, Lynam-Lennon N, et al. Identification of a mutation in LARS as a novel cause of infantile hepatopathy. *Mol Genet Metab*. 2012; 106: 351–8.

30. Casey JP, Slattery S, Cotter M, et al. Clinical and genetic characterisation of infantile liver failure syndrome type 1, due to recessive mutations in LARS. *J Inherit Metab Dis*. 2015; 38: 1085–92.

31. Simons C, Griffin LB, Helman G, et al. Loss-of-function alanyl-tRNA synthetase mutations cause an autosomal-recessive early-onset epileptic encephalopathy with persistent myelination defect. *Am J Hum Genet*. 2015; 96: 675–81.

32. Nakayama T, Wu J, Galvin-Parton P, et al. Deficient activity of alanyl-tRNA synthetase underlies an autosomal recessive syndrome of progressive microcephaly, hypomyelination, and epileptic encephalopathy. *Hum Mutat*. 2017; 38: 1348–54.

33. van Meel E, Wegner DJ, Cliften P, et al. Rare recessive loss-of-function methionyl-tRNA synthetase mutations presenting as a multiorgan phenotype. *BMC Med Genet*. 2013; 14: 106.

34. Hadchouel A, Wieland T, Griese M, et al. Biallelic mutations of methionyl-tRNA synthetase cause a specific type of pulmonary alveolar proteinosis prevalent on Réunion Island. *Am J Hum Genet*. 2015; 96: 826–31.

35. Sun Y, Hu G, Luo J, et al. Mutations in methionyl-tRNA synthetase gene in a Chinese family with interstitial lung and liver disease, postnatal growth failure and anemia. *J Hum Genet*. 2017; 62: 647–51.

36. Kopajtich R, Murayama K, Janecke AR, et al. Biallelic IARS mutations cause growth retardation with prenatal onset, intellectual disability, muscular hypotonia, and infantile hepatopathy. *Am J Hum Genet*. 2016; 99: 414–22.

37. Orenstein N, Weiss K, Oprescu SN, et al. Biallelic IARS mutations in a child with intrauterine growth retardation, neonatal cholesta-

sis, and mild developmental delay. *Clin Genet*. 2017; 91: 913–7.

38. Nowaczyk MJM, Huang L, Tarnopolsky M, et al. A novel multisystem disease associated with recessive mutations in the tyrosyl-tRNA synthetase (YARS) gene. *Am J Med Genet Part A*. 2017; 173: 126–34.

39. Karaca E, Harel T, Pehlivan D, et al. Genes that affect brain structure and function identified by rare variant analyses of Mendelian neurologic disease. *Neuron*. 2015; 88: 499–513.

40. Wolf NI, Salomons GS, Rodenburg RJ, et al. Mutations in RARS cause hypomyelination. *Ann Neurol*. 2014; 76: 134–9.

41. Taft RJ, Vanderver A, Leventer RJ, et al. Mutations in DARS cause hypomyelination with brain stem and spinal cord involvement and leg spasticity. *Am J Hum Genet*. 2013; 92: 774–80.

42. Puffenberger EG, Jinks RN, Sougnez C, et al. Genetic mapping and exome sequencing identify variants associated with five novel diseases. *PLoS One*. 2012; 7: e28936.

43. Musante L, Püttmann L, Kahrizi K, et al. Mutations of the aminoacyl-tRNA-synthetases SARS and WARS2 are implicated in the etiology of autosomal recessive intellectual disability. *Hum Mutat*. 2017; 38: 621–36.

44. Zhang X, Ling J, Barcia G, et al. Mutations in QARS, encoding glutaminyl-tRNA synthetase, cause progressive microcephaly, cerebral-cerebellar atrophy, and intractable seizures. *Am J Hum Genet*. 2014; 94: 547–58.

45. Kodera H, Osaka H, Iai M, et al. Mutations in the glutaminyl-tRNA synthetase gene cause early-onset epileptic encephalopathy. *J Hum Genet*. 2015; 60: 97–101.

46. Leshinsky-Silver E, Ling J, Wu J, et al. Severe growth deficiency, microcephaly, intellectual disability, and characteristic facial features are due to a homozygous QARS mutation. *Neurogenetics*. 2017; 18: 141–6.

47. Datta A, Ferguson A, Simonson C, et al. Case report: QARS deficiency and favorable outco-

me following treatment of seizures with ketogenic diet. *J Child Neurol*. 2017; 32: 403–7.

48. McMillan HJ, Schwartzentruber J, Smith A, et al. Compound heterozygous mutations in glycyl-tRNA synthetase are a proposed cause of systemic mitochondrial disease. *BMC Med Genet*. 2014; 15: 36.

49. Nafisinia M, Riley LG, Gold WA, et al. Compound heterozygous mutations in glycyl-tRNA synthetase (GARS) cause mitochondrial respiratory chain dysfunction. *PLoS One*. 2017; 12: e0178125.

50. Oprescu SN, Chepa-Lotrea X, Takase R, et al. Compound heterozygosity for loss-of-function GARS variants results in a multisystem developmental syndrome that includes severe growth retardation. *Hum Mutat*. 2017; 38: 1412–20.

51. Santos-Cortez RLP, Lee K, Azeem Z, et al. Mutations in KARS, encoding lysyl-tRNA synthetase, cause autosomal-recessive nonsyndromic hearing impairment DFNB89. *Am J Hum Genet*. 2013; 93: 132–40.

52. McMillan HJ, Humphreys P, Smith A, et al. Congenital visual impairment and progressive microcephaly due to lysyl–transfer ribonucleic acid (RNA) synthetase (KARS) mutations. *J Child Neurol*. 2015; 30: 1037–43.

53. Verrigni D, Diodato D, Di Nottia M, et al. Novel mutations in KARS cause hypertrophic cardiomyopathy and combined mitochondrial respiratory chain defect. *Clin Genet*. 2017; 91: 918–23.

54. Kohda M, Tokuzawa Y, Kishita Y, et al. A comprehensive genomic analysis reveals the genetic landscape of mitochondrial respiratory chain complex deficiencies. *PLoS Genet*. 2016; 12: e1005679.

55. Glamuzina E, Brown R, Hogarth K, et al. Further delineation of pontocerebellar hypoplasia type 6 due to mutations in the gene encoding mitochondrial arginyl-tRNA synthetase, RARS2. *J Inherit Metab Dis*. 2012; 35: 459–67.

56. Hutson SM, Stinson-Fisher C, Shiman R & Jefferson LS. Regulation of albumin synthesis by hormones and amino acids in primary cultures of rat hepatocytes. *Am J Physiol*. 1987; 252: E291–8.

57. Shahbazian FM, Jacobs M & Lajtha A. Rates of protein synthesis in brain and other organs. *Int J Dev Neurosci*. 1987; 5: 39–42.

58. de Blic J. Pulmonary alveolar proteinosis in children. *Paediatr Respir Rev*. 2004; 5: 316–22.

59. Uchida K, Beck DC, Yamamoto T, et al. GM-CSF autoantibodies and neutrophil dysfunction in pulmonary alveolar proteinosis. *N Engl J Med*. 2007; 356: 567–79.

60. Dirksen U, Nishinakamura R, Groneck P, et al. Human pulmonary alveolar proteinosis associated with a defect in GM-CSF/IL-3/IL-5 receptor common beta chain expression. *J Clin Invest*. 1997; 100: 2211–7.

61. Marie I, Josse S, Decaux O, et al. Comparison of long-term outcome between anti-Jo1- and anti-PL7/PL12 positive patients with antisynthetase syndrome. *Autoimmun Rev*. 2012; 11: 739–45.

62. Mauhin W, Habarou F, Gobin S, et al. Update on lysinuric protein intolerance, a multi-faceted disease retrospective cohort analysis from birth to adulthood. *Orphanet J Rare Dis*. 2017; 12: 3.

Acknowledgments

Supplementary tables

Table S1: common clinical symptoms in patients with autosomal recessive cytosolic/combined cytosolic and mitochondrial ARS deficiencies.

Table S2: aminoacylation activity of mutated ARSs.

May be downloaded from doi.org/10.1038/s41436-018-0048-y.

Chapter 3

PHENOTYPIC FEATURES OF QARS1 DEFICIENCY

3

Gautam Kok, Clara van Karnebeek, Sabine Fuchs

Since publication of our previous paper on aminoacyl-tRNA synthetase (ARS) deficiencies,[1] the number of recognized patients suffering from these diseases has steadily increased, putatively through progressively genetic diagnostic testing, aided by recognition of the clinical phenotype. To further improve disease recognition, counseling, prognostic prediction, and potential treatment development and evaluation, further understanding of the disease mechanism, genotypes, and clinical phenotypes remains crucial.

Shen et al. provide interesting additional clinical information on QARS1 deficiency,[2] one of these ARS deficiencies. They show that serum protein levels were consistently decreased in their three patients with QARS1 deficiency, while albumin was only slightly and inconsistently decreased, which they attribute to the relatively low glutamine content of albumin (3.3%). Hypoalbuminemia is common to multiple ARS deficiencies,[1] including IARS1, LARS1, MARS1, and possibly KARS1. However, the abundance of the corresponding amino acids varies (isoleucine: 1.5%, leucine: 10.5%, methionine: 1.1%, and lysine: 9.9%). Therefore, a more general mechanism seems more plausible.

Of the QARS1 deficient patients we previously described,[1,3] the first[1] displayed normal serum albumin concentrations at ages 1.5 years (40 g/l, normal values: 35–50 g/l), and 3 years (43 g/l), but decreased concentrations at age 5.5 years (28 g/l). The second patient[3] also displayed mostly normal concentrations except at age 12 years (31 g/l, normal values: 34–42 g/l). Total plasma protein concentration was only measured once in both patients and was normal (63 g/l, normal 60–80 g/l) at age 1.5 years in the first patient[1] and decreased (54 g/l, normal 60–80 g/l) at age 13 years in the second.[3] In this second patient, serum prealbumin concentrations were normal, and marginally reduced once (185 g/l, normal 186–335 g/l) at age 9 years. When looking at our other ARS deficient patients,[1] IARS1 deficient patient 1 also had low plasma protein levels (33 and 34 g/l at age 1 month and 2.5 months, respectively), but IARS1 deficient patient 2 had normal levels (80 g/l) at age 4 years and so did KARS1 deficient patient 4 (64 g/l) at age 1 year. Plasma protein concentration was not determined in our LARS1-deficient patients. Collectively, these data suggest that both plasma albumin and protein concentrations may be decreased in ARS deficiencies, putatively through a common mechanism shared among the ARS deficiencies involving either insufficient protein synthesis, mistranslation, and/or increased peptide/protein degradation. Affected proteins may depend on the specific amino acid corresponding to the ARS deficiency.
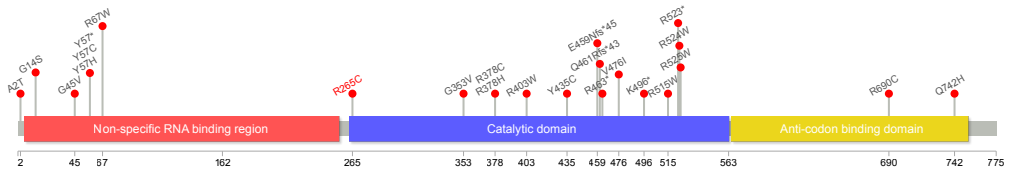
Fig. 1: genetic localization of reported *QARS1* mutations.

Since QARS1 deficiency is a predominantly neurological disease, Shen et al. sought to extend the hypothesis of decreased protein synthesis to the central nervous system.[2] However, they did not find decreased protein levels in cerebrospinal fluid (CSF). Similarly, our QARS1 deficient patients[1,3] did not have decreased CSF protein levels (0.36 g/l, normal range 0–0.40 g/l, and 0.36 g/l, normal values 0.10–0.35 g/l, respectively), nor did our KARS1 deficient patient (0.31 g/l) and our IARS1 deficient patient (0.75 g/l; but this sample was contaminated with >80,000 erythrocytes and >400 leukocytes). Shen et al. then propose an interesting hypothesis of excitotoxicity induced by increased glutamate/glutamine ratios due to QARS1 deficiency.[2] Indeed, severe neurological symptoms have been associated with increased glutamate/glutamine ratios in several inborn errors of metabolism.[4] However, CSF amino acid analysis in our reported QARS1 patients[1,3] revealed normal glutamate (3 µmol/l, normal range 0–7.8 µmol/l and < 8.5 µmol/l, normal range: < 8.5 µmol/l, respectively) and nearly normal glutamine concentrations (488 µmol/l, normal range 363–785 µmol/l and 688 µmol/l, normal range 260–684 µmol/l, respectively). The first patient[1] also had slightly decreased taurine concentrations (2 µmol/l, normal range 4–13 µmol/l) and the second[3] marginally decreased serine concentrations (24.4 µmol/l, normal 25–56 µmol/l). Although the proposed disease mechanism would be QARS1 specific, the underlying mechanistic hypothesis would suggest alterations in the corresponding amino acids in CSF of other ARS deficiencies. However, CSF amino acids were also normal in our KARS1-deficient patient.

As a global central nervous system fluid, CSF may not reflect local concentrations of amino acids in the brain. We performed brain magnetic resonance (MR) spectroscopy in the white matter of our QARS1 patient,[1] which revealed low N-acetyl aspartic acid peaks compatible with white matter disease, and prominent glutamate/glutamine peaks. Unfortunately, these 3-Tesla MRI scans do not allow distinction between glutamate and glutamine. Further studies with more advanced spectroscopy in different brain areas may provide further insight in this hypothesis. Similarly, as also mentioned

by Shen et al.,[2] the response to treatments affecting the glutamate/glutamine balance (like glutamine supplementation) and/or excitotoxicity (like memantine, which antagonizes the interaction between glutamate and the NMDA receptor and pyridoxine, which is required for the conversion of glutamate to GABA) may provide further support for this hypothesis and guide therapeutic strategies. Nevertheless, since neurological symptoms are shared among many cytosolic, combined cytosolic and mitochondrial, and mitochondrial ARS deficiencies, a more common translational deficiency or mitochondrial dysfunction may also contribute to the neurological phenotype.

When interpreting genetic variations, their potential pathogenicity, associated clinical phenotype. and response to specific treatments, their precise genetic location is crucial. This is the reason we dedicated Fig. 5 of our previous article[1] to the genetic locations of all reported *ARS* variants. We have updated this figure (Fig. 1) with novel pathogenic variants,[5-10] and hope this genetic information, the additional clinical features, and deduced mechanistic hypotheses will aid other researchers and clinicians to improve understanding of ARS deficiencies and care for this expanding group of patients.

References

1. Fuchs SA, Schene IF, Kok G, et al. Aminoacyl-tRNA synthetase deficiencies in search of common themes. *Genet Med*. 2019; 21: 319–330.

2. Shen YW, Zou LP. A possible natural model for excitation/inhibition imbalance in epilepsy. *Genet Med*. 2021; 23: 587-588.

3. Salvarinova R, Ye CX, Rossi A, et al. Expansion of the QARS deficiency phenotype with report of a family with isolated supratentorial brain abnormalities. *Neurogenetics*. 2015; 16: 145–149.

4. Rumping L, Vringer E, Houwen RHJ, Hasselt PM, Jans JJM, Verhoeven-Duif NM. Inborn errors of enzymes in glutamate metabolism. *J Inherit Metab Dis*. 2020; 43: 200–215.

5. Datta A, Ferguson A, Simonson C, et al. Case report: QARS deficiency and favorable outcome following treatment of seizures with ketogenic diet. *J Child Neurol*. 2017; 32: 403–407.

6. Kodera H, Osaka H, Iai M, et al. Mutations in the glutaminyl-tRNA synthetase gene cause early-onset epileptic encephalopathy. *J Hum Genet*. 2015; 60: 97–101.

7. Johannesen KM, Mitter D, Janowski R, et al. Defining and expanding the phenotype of QARS -associated developmental epileptic encephalopathy. *Neurol Genet*. 2019; 5: e373.

8. Alabdullatif MA, Al Dhaibani MA, Khassawneh MY, El-Hattab AW. Chromosomal microarray in a highly consanguineous population: diagnostic yield, utility of regions of homozygosity, and novel mutations. *Clin Genet*. 2017; 91: 616–622.

9. Leshinsky-Silver E, Ling J, Wu J, et al. Severe growth deficiency, microcephaly, intellectual disability, and characteristic facial features are due to a homozygous QARS mutation. *Neurogenetics*. 2017; 18: 141–146.

10. Kuperberg M, Lev D, Blumkin L, et al. Utility of whole exome sequencing for fenetic diagnosis of previously undiagnosed pediatric neurology patients. *J Child Neurol*. 2016; 31: 1534–1539.

ISOLEUCINE-TO-VALINE SUBSTITUTIONS SUPPORT CELLULAR PHYSIOLOGY DURING ISOLEUCINE DEPRIVATION

....

Gautam Kok*, Imre Schene*, Eveline Ilcken, Paula Sobrevals, Tim Hoek, Robert van Es, Holger Rehmann, Edward Nieuwenhuis, Harmjan Vos, Sabine Fuchs

Abstract

Aminoacyl-tRNA synthetases (ARSs) couple tRNAs with their corresponding amino acids. While ARSs can bind structurally similar amino acids, extreme specificity is ensured by subsequent editing activity. Yet, we found that upon isoleucine (I) restriction, healthy fibroblasts consistently incorporated valine (V) into proteins at isoleucine codons, resulting from mis-aminoacylation of tRNA$^{\text{Ile}}$ with valine by wildtype IARS1. Using a dual-fluorescent reporter of translation, we found that valine supplementation could fully compensate for isoleucine depletion and restore translation to normal levels in healthy, but not IARS1 deficient cells. Similarly, the antiproliferative effects of isoleucine deprivation could be fully restored by valine supplementation in healthy, but not IARS1 deficient cells. This indicates I>V substitutions help prevent translational termination and maintain cellular function in human primary cells during isoleucine deprivation. We suggest that this is an example of a more general mechanism in mammalian cells to preserve translational speed at the cost of translational fidelity in response to (local) amino acid deficiencies.

Introduction

Correct charging of tRNAs with their corresponding amino acid is crucial for accurate translation of the genetic code into proteins. Central in this process are aminoacyl-tRNA synthetases (ARSs), enzymes that charge tRNAs with their corresponding amino acids. For each amino acid (a), a specific ARS (aARS) performs this role either in the cytosol (aARS1), in the mitochondria (aARS2), or both (KARS1, GARS1). Variants in ARS-genes are increasingly associated with human disease.[1] Autosomal dominant variants in ARS-genes result in Charcot Marie Tooth polyneuropathies.[2] The underlying mechanism was recently described for autosomal dominant GARS1 disease. By abnormal binding dynamics of GARS1 to Gly-tRNA^{Gly}, ribosome stalling occurs specifically in sensory neurons, leading to the GCN2-dependent stress response and peripheral neuropathy.[3,4] Autosomal recessive variants in ARS-genes cause multi organ disease.[1] We previously hypothesized that symptoms arise in different organs due to insufficient canonical aminoacylation of tRNAs to meet translational demands, especially during times of high translation. This formed the basis for amino acid supplementation therapies for patients with aARS1 deficiencies, resulting in strikingly beneficial effects.[5–7]

Nevertheless, the precise mechanism explaining how deficient aminoacylation of tRNAs leads to translational failure and organ-specific effects remains elusive. To address this, we analysed the molecular consequences of IARS1 deficiency in fibroblasts from two unrelated patients with the same compound heterozygous IARS1 variants (NM_002161.5): c.1305G>C p.(Trp435Cys) and c.3377dup p.(Asn1126fs) (OMIM 600709).[1,5] Both variants are expected to affect the canonical aminoacylation function, with the Trp435Cys variant residing in the catalytic domain of IARS1, and the Asn1126fs variant likely leading to unexpressed protein.[1,5] Accordingly, catalytic activity for these donors was severely decreased to 23% and 21%.[5] We hypothesized that decreased catalytic activity would result in insufficient loaded tRNA^{Ile}, which may be compensated by mis-aminoacylation. To our surprise, we consistently found that upon isoleucine restriction, healthy fibroblasts but not IARS1 deficient fibroblasts incorporated valine instead of isoleucine into proteins.

Sacrificing translational fidelity may represent a strategy to preserve protein synthesis during deprivation of specific essential amino acids, as is increasingly reported for unicellular organisms (bacteria and yeast).[8] It is known that aminoacyl-tRNA synth-eta-

ses (ARSs) can mis-activate tRNAs with structurally similar amino acids,[9] but subsequent editing activity ensures extreme specificity under physiological conditions.[10–12] To explore a putative rescue mechanism for unfavourable circumstances like (local) amino acid deficiencies induced by nutrition, physiological stress, or disease states, we investigated the nature and consequences of mis-aminoacylation by IARS1. We uncovered that IARS1 can indeed induce amino acid substitutions in healthy primary human cells. These substitutions were beneficial in preserving translation and promoting cell viability during nutritional stress. Not only does this contribute to further understanding of the consequences of IARS1 deficiency, but this may also represent a more general human strategy of aARSs to cope with unfavourable conditions.

Materials and Methods

Ethical approval

Local medical ethical approval (Institutional Review Board of the University Medical Center Utrecht (STEM: 10-402/K, TC Bio 190489)) was obtained for use of the patient materials in this study. Written informed consent was obtained from all patients' parents.

Cell culture

Fibroblasts were obtained and cultured as described previously.[5] Media with specific amino acid concentrations were based on amino-acid free DMEM/F12 (DF12; US Biological cat. D9811), supplemented with all amino acids (compared to advanced (A)DF12, ThermoFisher cat. 12634028), 1% GlutaMax, 1% penicillin/streptomycin (pen/strep) and 10% dialyzed foetal bovine serum (FBS; ThermoFisher cat. 26400044), or custom-made ADF12 (based on ThermoFisher cat. 12634010) without isoleucine/valine, supplemented with 1% GlutaMax, 1% pen/strep, 1% HEPES and 10% dialyzed FBS. HEK293T were cultured in DMEM (ThermoFisher cat. 10569010), supplemented with 1% pen/strep and 10% FBS. Cultures were tested for mycoplasma every two months. Experimental isoleucine and valine concentrations were calculated as percentage of average plasma concentrations of vegetarians.[13]

Aminoacylation activity

IARS1 activity was measured as described previously, with four technical replicates per condition and donor.[5]

Lentivirus production

Lentiviruses were produced in HEK293T cells (15 cm dish). At 80% confluency, they were transfected with 10 µg GFP-α-catenin lentiviral plasmid DNA, 6.6 µg psPAX2 (Addgene #12260), 3.3 µg pMD2.G (Addgene #12259) and PEI MAX (3:1 PEI:DNA), in 1 mL OptiMEM. Both psPAX2 and PMD2.G were a gift from Trono et al. Media were refreshed after 24 hrs. Then, media containing the virus was collected after 48 and 72 hrs. Virus was concentrated using Lenti-X concentrator (Takara, cat. 631231), resuspended in 2 mL DMEM and stored at 4 °C for short-term use, and at -80 °C for long-term use.

Lentiviral transduction

Fibroblasts were harvested by trypsinization, washed, and resuspended in culture medium with 12 µg/mL polybrene, then mixed 1:1 with concentrated virus, and incubated for 1 hr at 37 °C. Cells were plated on a 6-well plate with 6 µg/mL polybrene and incubated for 24 hrs. Culture media were refreshed and cells were allowed to grow to 70% confluency. Transduced cells were selected by fluorescence-activated cell sorting (FACS).

Amino acid substitution mass-spectrometry

Stable GFP-α-catenin-expressing fibroblasts were created by lentiviral transduction. GFP+ cells were selected by FACS and cultured to 6x15cm dishes per condition. At 70% confluency, cells were washed once with phosphate-buffered saline (PBS), then incubated for 72 hrs. with the desired concentrations of isoleucine and valine. After washing with ice-cold PBS, cells were harvested with a cell scraper and pooled per condition. Pooled samples were washed twice with PBS and immediately lysed in RIPA buffer (ThermoFisher cat. 89900) with 1% Halt (ThermoFisher cat. 87786) for 30 min. Immunoprecipitation using GFP-Trap Agarose (Chromotek cat. GTA-20) was performed according to manufacturer's protocol. Cells were additionally washed three times in ice-cold PBS, and transferred to new Eppendorf tubes before the final wash. Samples were stored at -80 °C before mass spectrometry.

Part 2

Mass spectrometry

After immuno-precipitation of GFP-α-catenin, proteins were denatured in 8 M Urea, 1 M Ammonium BiCarbonate (ABC) containing 10 mM tris (2-carboxyethyl) phosphine hydrochloride to reduce and 40 mM 2-chloro-acetamide to alkylate the cysteines. After 4-fold further dilution with 1 M ABC and digestion with trypsin (250 ng/200 µl), peptides were separated from the beads and desalted with homemade C-18 stage tips (Affinisep). Peptides were separated on-a 25 cm column (75 µm ID fused silica capillary with emitter tip, made in house) packed with 1.9 µm aquapur gold C-18 material (Dr Maisch, Ammerbuch-Entringen, Germany) using a 2-hour gradient (0-80% Acetonitrile), delivered by an easy 1200 nano HPLC (Thermo Scientific). Peptides were electrosprayed directly into a Fusion Tribrid-Orbitrap (Thermo Scientific) and analysed in data-dependent mode with the resolution of the full scan set at 240,000, after which the top N peaks were selected for Higher energy Collision-induced Dissociation (HCD) fragmentation (set at a normalized energy of 30%) and detection in the Iontrap with a target setting of 5000 ions. Raw files were analysed with Proteome Discoverer (PD) software (Thermo, versions 2.4.0.305 & 2.5.0.400). For identification, a fasta file of the Homo sapiens protein Catenin alpha-1 (CTNA1, Uniprot P35221) was used to perform a search with the standard Consensus Workflow for Label free quantification of the precursor peptide and the standard Processing Workflow for Orbitrap, Sequest and Percolator, with carbamido-methylation of cysteine set as fixed modification. The required substitutions from Isoleucine (Ile) to other amino-acids were set as a variable modification in consecutive analysis runs. The mass accuracy of the recalibration (RC) node was set to 20 ppm for the precursor and the fragmentation to 0.5 Da. The Main search settings were 5 ppm for the precursor and 0.5 Da for the fragments. The traces of the peptides chromatograms were extracted from the result files of PD and plotted using R (version 4.0.4) through RStudio (version 1.5.64). The mass spectrometry proteomics data have been deposited to the ProteomeXchange Consortium via the PRIDE partner repository (http://www.ebi.ac.uk/pride with the dataset identifier PXD033426).

Cloning of dual-fluorescent reporter

Three custom dual-fluorescent reporters of translation termination were adapted from pmGFP-P2A-K0-P2A-RFP (Addgene #105686) and pmGFP-P2A-K20(AAA)-P2A-RFP (Addgene #105688), which were gifted by Juszkiewicz et al.[14] The CMV-GFP-P2A-K0/K20(AAA)-P2A-RFP cassettes were amplified by PCR and subcloned into a pJET1.2

—

backbone vector (ThermoFisher cat. K1231). To create the CMV-GFP-P2A-15xIle-P2A-RFP reporter, a geneblock containing 15x isoleucine codons was ordered (Integrated DNA technologies) and cloned in-frame in-between the P2A sites using In-Fusion HD cloning (Takara cat. 639648). The complete sequences of the GFP-P2A-[K0(=empty)/K20(AAA)(=20xLys^{AAA})/15xIle]-P2A-RFP cassettes are provided in the Supplementary Information. These plasmids can be obtained through Addgene (#185618, #185619, #185620).

Dual-fluorescent reporter of translation

A 6-well of fibroblasts per condition was washed with PBS, and media were replaced to culture media with normal concentrations of isoleucine and valine, isoleucine depletion (0%) or isoleucine depletion with valine depletion or supplementation (1% or 1000% of plasma). Cells were immediately transfected with pJET-CMV-GFP-[empty/15xIle/20xLys$_{AAA}$]-mCherry using Lipofectamine 3000 according to manufacturer's protocol, except replacing OptiMEM by isoleucine- and valine-free custom-made AD-F12 without supplements. After 24 hours, cells were washed once with PBS, harvested by trypsinization, and kept on ice onwards. Cells were resuspended in ice-cold fluorescence-activated cell sorting (FACS) buffer (PBS with 2 mM ethylenediaminetetraacetic acid and 0.5% bovine serum albumin) with 1x DAPI and transferred to filter-capped FACS tubes. Fluorescence was measured on a CytoFLEX S (Beckman Coulter) flowcytometer (405→450±45 nm, 488→525±40 nm, 561→610±20 nm). Gating and calculations were performed in FlowJo V10.8 (BD Biosciences). The gating strategy is attached in Supplementary Fig. 4. In summary, from single cells selected by FSC/SSC, live cells (DAPI$^-$) were selected. From the GFP$^+$ cells, the median ratio between the red- and green fluorescence was calculated, and each condition was normalized to the normal isoleucine value. Statistical analyses and data visualization were performed in GraphPad Prism 9.

Proliferation assay

Fibroblasts were seeded in quadruplicate on E-Plate 96 PET (Agilent, cat. 300600910) at 3,500 cells/well in normal culture medium. After 24 hours, wells were washed twice with PBS, and medium with the desired amino acid concentrations was applied. Proliferation of fibroblasts was evaluated by continuous impedance analysis over two or five days using a real-time cell analyser (xCELLigence MP, ACEA Bioscien-

ces). Per donor, impedance was normalized against the 100% amino acid concentration condition.

Prediction of functional effect of amino acid substitutions

Lists of all tryptophan (W) and isoleucine (I) residues in human transcripts were prepared using the 'whole human exome sequence space' (WHESS) database. The effects of W>F and I>V amino acid substitutions on protein structure and function was predicted using Polymorphism Phenotyping v2 (PolyPhen-2) in batch mode and HumVar classifier model.[15]

RNA sequencing and analysis

A 6-well of fibroblasts per condition was washed with PBS, and media were replaced to culture media with normal concentrations of isoleucine or isoleucine depletion (1% of plasma). After 72 hours, before confluency was reached in any condition, total RNA was isolated using Trizol LS reagent (Invitrogen) and stored at –80°C until further processing. mRNA was isolated using Poly(A) Beads (NEXTflex). Sequencing libraries were prepared using the Rapid Directional RNA-Seq Kit (NEXTflex) and sequenced on a NextSeq500 (Illumina) to produce 75 base long reads (Utrecht DNA Sequencing Facility). Sequencing reads were mapped against the reference genome (genome sequence release 33 (GRCh38.p13)) using BWA41 package (mem –t 7 –c 100 –M –R). Normalized counts were obtained by applying the DESeq2 variance-stabilizing transformation (VST) to the read counts using the DESeq2 R package.[16] Principal component analysis was performed with the 5000 most variable genes and plotted using the DESeq2 'plotPCA' function. Differentially expressed genes between normal and 1% isoleucine conditions were calculated using DESeq2, correcting for Control/Patient-batch effects (design = ~type ('control' or 'IARS1') + isoleucine ('1%' or '100%'), using thresholds of 'padj' < 0.05 and 'log2FoldChange' > 1. Finally, genes that were upregulated in IARS1 patient vs. control lines, which were also upregulated upon isoleucine depletion, were extracted using a threshold of 0.5-fold (log2) increase between the average of groups. Similarly, genes that were downregulated in IARS1 patient and downregulated upon isoleucine depletion, were extracted using a threshold of 0.5-fold (log2) decrease between the average of groups. Heatmaps were created using Microsoft Excel. Gene set enrichment analysis of genes that were up/down regulated upon isoleucine depletion, and in IARS1 patient vs. control lines, was performed using Enrichr.[17]

Results

IARS1 generates I>V substitutions in human fibroblasts upon isoleucine deprivation

To investigate if isoleucine deprivation causes amino acid substitutions, we created primary fibroblast lines derived from healthy donors that stably express a fusion protein of green fluorescent protein (GFP) and alpha catenin (CTNA1). We immunoprecipitated the fusion protein from protein lysates and performed mass spectrometry analysis to search for isoleucine substitutions in stable CTNA1 peptides containing a single isoleucine residue (TSVQTEDDQL**I**AGQSAR and NAGNEQDLG**I**QYK) (Fig. 1a). We did not observe any I>V substitutions in fibroblasts cultured under normal conditions. However, upon isoleucine depletion (1% of normal plasma concentrations), we found a strong increase of I>V substitutions in both peptides, which did not further increase upon additional valine supplementation (Fig. 1b, Supplementary Fig 1b). Isoleucine deprivation did not introduce I>V substitutions in fibroblasts from patients with impai-
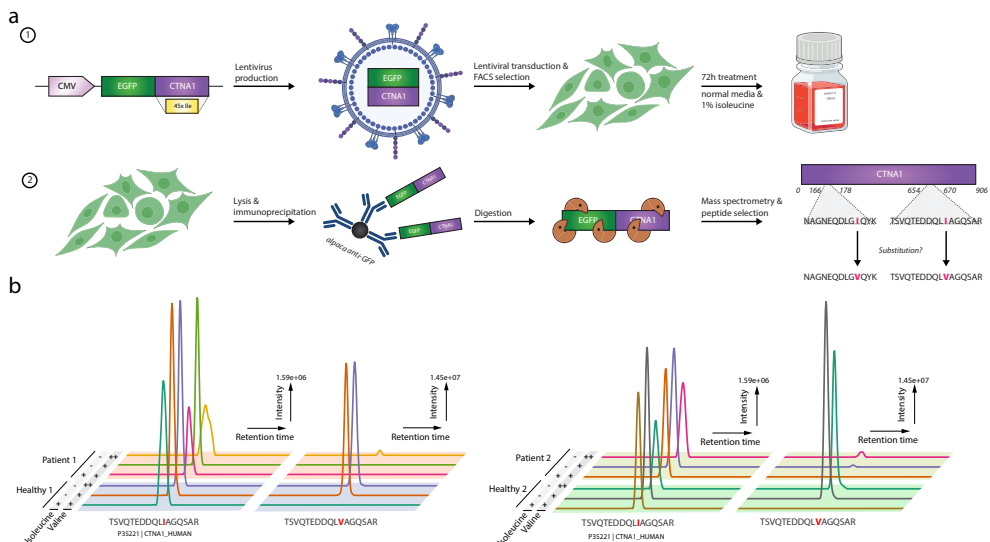
4

Fig. 1: detection of I>V substitutions upon isoleucine restriction.

a, Schematic representation of sample preparation for mass spectrometry to identify amino acid substitutions in peptides of the Catenin Alpha 1 protein (CTNA1). **b**, Identification of peptides containing a single isoleucine or isoleucine > valine substitution in healthy fibroblasts or fibroblasts from patients with IARS1 deficiency.

red catalytic IARS1 activity while supplementation of additional valine led to minimal I>V substitutions (Fig. 1b). This suggests that mis-aminoacylation of tRNA[Ile] by wildtype IARS1 is responsible for the observed I>V substitutions. Additionally, we found I>M substitutions upon isoleucine depletion in both healthy control- and patient-derived cells (Supplementary Fig. 1a,b). These likely result from ribosomal mispairing, since isoleucine (AUU, AUC, AUA) and methionine (AUG) codons only differ at the third codon wobble position.[8] We could not reliably identify any other I>X substitutions upon thorough screening of the mass-spectrometric data.

I>V substitutions support translation and proliferation in human fibroblasts

To test whether isoleucine-deprived cells benefit from a certain rate of I>V substitution to maintain translation of isoleucine-rich regions, we adapted a dual-fluorescent reporter[14] to contain a cassette of eGFP and mCherry, interceded by an isoleucine-rich region (Fig. 2a). Regular translation of this cassette results in equal amounts of GFP and Cherry fluorescence while translational termination in the interceding region decreases Cherry to GFP ratios (Supplementary Fig. 2a,b). We transfected the reporter into four healthy donor fibroblast lines and the two fibroblast lines from patients with IARS1 deficiency, incubated the cells for 24 hours in various medium conditions, and analysed translational function by flow cytometry. As expected, isoleucine deprivation impaired translation of the isoleucine-rich region, and this effect was stronger in IARS1 patient fibroblasts than in healthy fibroblasts (Fig. 2b). Supplementation of additional valine rescued translation to normal levels in healthy cells but not in IARS1 deficient cells (Fig. 2b, Supplementary Fig. 2c). This indicates that I>V substitutions help to prevent translational termination during isoleucine deprivation and that this mechanism depends on IARS1 catalytic activity.

To determine the effect of I>V substitutions on cellular functions, we quantified proliferation of human fibroblasts cultured under various medium conditions. In healthy fibroblasts, proliferation decreased upon isoleucine deprivation (1% of plasma concentrations) and decreased further upon additional valine deprivation (1% isoleucine and 1% valine, p=0.021) (Fig. 2c). In comparison, fibroblasts from patients with IARS1 deficiency were more severely affected by isolated isoleucine deprivation (p=0.039) but not by isolated valine deprivation (p=0.422). Strikingly, additional valine supplementation (1000% of plasma concentration) could rescue the antiproliferative effects of isoleucine deprivation almost completely in healthy cells (p=0.007), while additional leucine, methionine, or serine could not (Fig. 2c, Supplementary Fig. 3). In

—
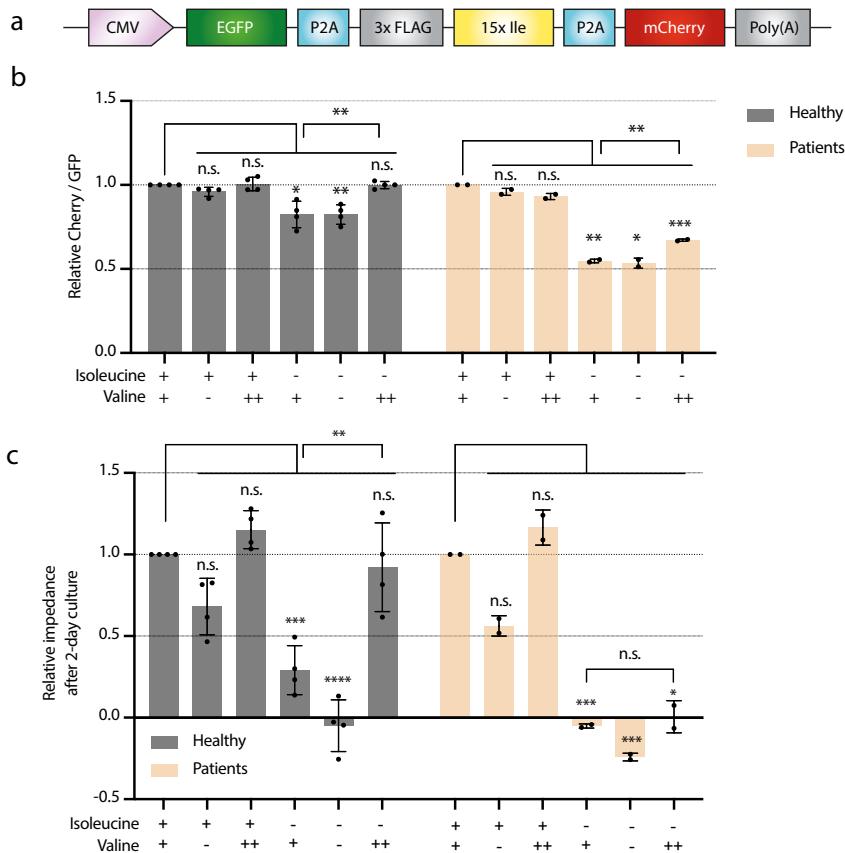
Fig. 2: I>V substitutions prevent translational termination and maintain cellular growth.

a, Design of the ribosomal stalling reporter plasmid. **b**, Relative fluorescence of Cherry / GFP in healthy and IARS1 deficient patient-derived fibroblasts under varying concentrations of isoleucine and valine (isoleucine: + = 100%, - = 0% | valine: + = 100%, - = 1%, ++ = 1000% of plasma); two-sided unpaired Student's t-test with equal variance, with Bonferroni correction for multiple testing: n.s. p ≥ 0.05, * p < 0.05, ** p < 0.01, *** p < 0.001. **c**, Normalized impedance measured with the xCELLigence MP real-time-cell-analyser as read-out for proliferation after 2-day culture in varying concentrations of isoleucine and valine (isoleucine: + = 100%, - = 1% | valine: + = 100%, - = 1%, ++ = 1000% of plasma concentrations); two-sided unpaired Student's t-test with equal variance, with Bonferroni correction for multiple testing: n.s. p ≥ 0.05, * p < 0.05, ** p < 0.01, *** p < 0.001, **** p < 0.0001; each dot represents the average of four technical replicates; bars depict mean ± SD.
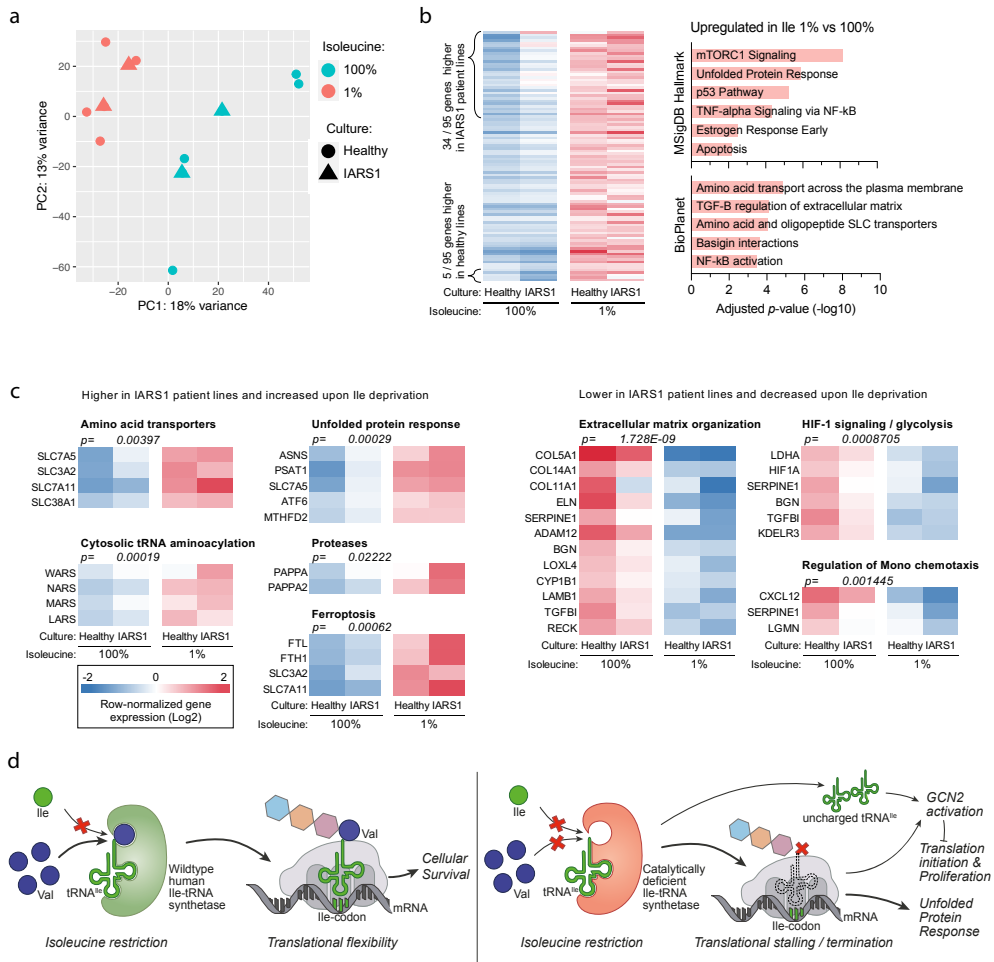
Fig. 3: reaction to isoleucine deprivation is aggravated by IARS1 deficiency.

a, Principal component plot of fibroblasts from healthy persons and patients with IARS1 deficiency cultured in normal (100%) and isoleucine deprived medium (1% of normal plasma concentrations). **b**, Genes with increased expression in fibroblasts cultured in 1% versus 100% isoleucine concentrations and corresponding pathways. **c**, Differentially expressed genes between fibroblasts from healthy controls and patients with IARS1 deficiency, which further deviate with isoleucine deprivation. **d**, Proposed IARS1 function and disease mechanism in IARS1 deficiency in response to isoleucine deprivation. Wildtype (catalytically active) IARS1 attaches the structurally similar valine instead of isoleucine to tRNA^Ile upon (local) isoleucine restriction. I>V substitutions in proteins are generally benign and thus support translation and cellular function. Catalytically deficient IARS1 cannot attach valine instead of

isoleucine, leading to an increase of uncharged tRNA$^{\text{Ile}}$ which activated GCN2, inhibiting translation initiation and proliferation. Termination of translation further activates the unfolded protein response and apoptosis.

IARS1 deficient cells, additional valine supplementation did not rescue the antiproliferative effects of isoleucine deprivation (p=0.511) (Fig. 2c). Together, these findings indicate that I>V substitutions, originating from mis-aminoacylation of tRNA$^{\text{Ile}}$ with valine by catalytically active IARS1 help to preserve cellular functions and viability during isoleucine deprivation.

Translation termination and unfolded protein response aggravated by IARS1 deficiency

As observed with the dual fluorescent reporter, isoleucine deprivation led to translation termination in fibroblasts and this effect was more pronounced and could not be rescued by valine in fibroblasts from patients with IARS1 deficiency. Principal component analysis of RNA sequencing data of these fibroblasts discriminated two clusters based on isoleucine concentrations rather than on healthy versus patient status (Fig. 3a). Genes that were upregulated upon isoleucine deprivation were associated with mTORC1, amino acid transport, the unfolded protein response, NF-κB signaling, and apoptosis and were generally expressed higher in IARS1 deficient than healthy fibroblasts (Fig. 3b). Reasoning that IARS1 deficiency may induce an exaggerated physiological response to isoleucine deprivation, we found IARS1 specific upregulation of amino acid transporters, cytosolic tRNA amino acid synthetases, the unfolded protein response, proteases and ferroptosis, while pathways associated with proliferation (glycolysis, extracellular matrix organization) were downregulated (Fig. 3c). Together, these results support a disease mechanism of insufficient tRNA$^{\text{Ile}}$ aminoacylation to meet translational demands, resulting in translation termination at isoleucine codons, leading to an increase in (poly)peptides terminated prior to isoleucine incorporation and increased unfolded protein response, cellular stress, and apoptosis. In case of isoleucine deprivation, this reaction is more pronounced in IARS1 deficiency because of an additional failure to compensate with mis-aminoacylation of tRNA$^{\text{Ile}}$ with valine (Fig. 3d).

Discussion

In this study, we show that healthy human primary cells deprived of isoleucine substitute isoleucine for valine and thereby maintain translation and proliferation. Using cells derived from patients with catalytically deficient IARS1, we were able to attribute the observed isoleucine-to-valine substitutions to IARS1 mis-aminoacylation of tRNA[Ile] with valine and not to alternative ribosomal decoding.

Accurate protein translation (1:3,300) is believed to be essential to life.[11] Indeed, IleS from Escherichia coli (corresponding to mammalian IARS1) evolved an editing domain to hydrolyse non-cognate amino acids such as valine that are frequently mis-activated by the catalytic domain (1:180).[18] This mechanism ensures low error rates (1:50,000) under normal conditions.[11] Very recently, it was discovered that this IleS editing domain does not display higher hydrolysis rates of amino acids that are often mis-activated compared to amino acids that are rarely mis-activated.[19] This suggests that IARS1 evolved to prevent hydrolysis of correctly activated Ile-tRNA[Ile] and not to minimize mis-aminoacylation of tRNA[Ile], thus supporting translational speed at the expense of translational fidelity. This is in line with our finding that human IARS1 with normal catalytic activity can mis-aminoacylate tRNA[Ile] with valine, especially during isoleucine deprivation, and that mis-aminoacylation is largely prevented by patient mutations that lead to impaired catalytic but conserved editing activity of IARS1.

Recently, a similar mechanism of WARS1-induced W>F substitutions was discovered in both cancer cells[20] and in adjacent normal tissue (Schene et al., Matters Arising to Pataskar et al., manuscript number 2022-08-13333). These W>F substitutions preserved translation but generated dysfunctional proteins that were expected to activate T cell-mediated killing and reduce survival of cells.[20] Besides W>F substitutions, Y>F and F>Y substitutions were also observed during tryptophan depletion.[20] Although many amino acid substitutions may result in dysfunctional proteins (Fig. 4a), we observed beneficial cellular effects from I>V substitutions in healthy primary fibroblasts. PolyPhen-2 HumVar analyses and substitutions in conserved regions support benign effects and tolerance to I>V as opposed to W>F substitutions (Fig. 4a,b).[21] aARS recognize amino acids primarily based on size and physiochemical properties.[22] When predicting the effect of an amino acid substitution on protein function as benign based on > 50% substitutions with a low probability of damage score according to Poly-Phen2 HumVar analyses (Fig. 4a), specific substitutions of the essential amino acids
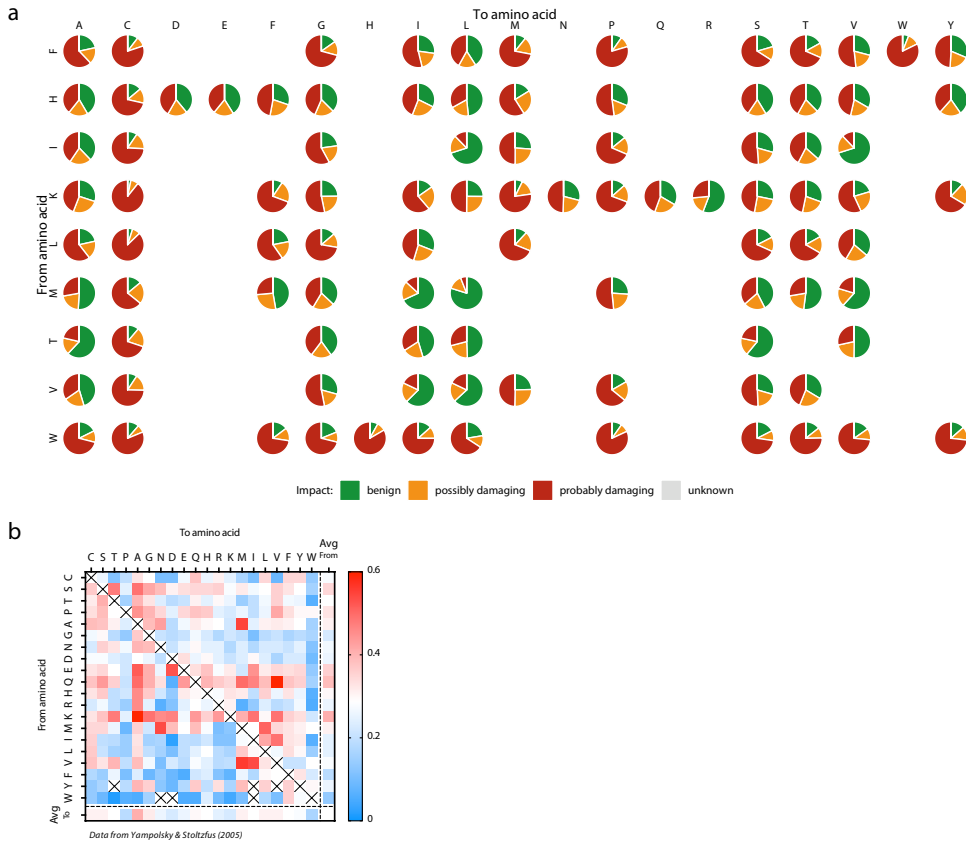
Fig. 4: frequencies of amino acid substitutions in conserved protein and prediction of effect on protein function.

a, PolyPhen-2 HumVar analysis probability of damage scores of all plausible substitutions for essential amino acids. PolyPhen-2 predicts the impact of an amino acid substitution on protein structure and function. Scores from 0.0-0.15 are predicted benign, 0.15-0.85 possibly damaging, and 0.85-1.0 probably damaging.[15] **b**, Heatmap of amino acid exchangeability as calculated by Yampolsky & Stoltzfus (2005).[23]

---

isoleucine (I>L/V), lysine (K>R), methionine (M>A/I/L/T/V), threonine (T>A/S/V), and valine (V>I/L) may support translational and cellular functions. Of these, I>V, K>R, M>I/L, T>A/S and V>I substitutions are indeed common in conserved regions of proteins (> mean + 1 SD; Fig. 4b).[23] Although still requiring confirmation, for these amino acids, tRNA mis-aminoacylation may help to maintain cellular functions in response to

(local) deficiency of essential amino acids and this mechanism may represent a more general mechanism to preserve translation in response to (local) amino acid deficiencies..

With our experiments, we further elucidate the disease mechanism of IARS1 deficiency (Fig. 3d). Autosomal recessive mutations in IARS1 result in decreased aminoacylation of tRNA^{Ile},[1,5] which leads to an increase in uncharged tRNA^{Ile}. Uncharged tRNAs can bind to GCN2 kinase and thereby slow down translation.[24] When an isoleucine codon is not matched by a charged tRNA^{Ile} despite translational slowdown, for example in case of repetitive isoleucine codons or (local) isoleucine deprivation, translation is terminated (Fig. 2b). Abnormal truncated peptides trigger the unfolded protein response (Fig. 3c), thereby generating cellular stress and further reducing cellular proliferation (Fig. 2c). Effects of insufficiency of isoleucine aminoacylation of tRNA^{Ile} in IARS1 deficiency may further be aggravated by additional failure of valine mis-aminoacylation of tRNA^{Ile} as a compensatory response to isoleucine deprivation. This underlines the importance of specific isoleucine supplementation to support tRNA aminoacylation, protein translation and cellular function in patients with IARS1 deficiency.[5]

In conclusion, we show that isoleucine to valine substitutions by IARS1 help to prevent translational termination and maintain cellular function in human primary cells during isoleucine deprivation. We suggest that this is an example of a more general mechanism of preserving translational speed at the cost of translational fidelity to cope with (local) amino acid deficiencies in mammalian cells.

References

1. Fuchs SA, Schene IF, Kok G, et al. Aminoacyl-tRNA synthetase deficiencies in search of commonthemes. *Genet Med*. 2019; 21: 319-330.

2. Griffin LB, Sakaguchi R, McGuigan D, et al. Impaired Function is a Common Feature of Neuropathy-Associated Glycyl-tRNA Synthetase Mutations. *Hum Mutat*. 2014; 35: 1363-1371.

3. Zuko A, Mallik M, Thompson R, et al. tRNA overexpression rescues peripheral neuropathy caused by mutations in tRNA synthetase. *Science*. 2021; 373: 1161-1166.

4. Mendonsa S, von Kuegelgen N, Bujanic L, Chekulaeva M. Charcot–Marie–Tooth mutation in glycyl-tRNA synthetase stalls ribosomes in a pre-accommodation state and activates integrated stress response. *Nucleic Acids Res*. 2021; 49: 10007-10017.

5. Kok G, Tseng L, Schene IF, et al. Treatment of ARS deficiencies with specific amino acids. *Genet Med*. 2021; 23: 2202-2207.

6. Lenz D, Stahl M, Seidl E, et al. Rescue of respiratory failure in pulmonary alveolar proteinosis due to pathogenic MARS1 variants. *Pediatr Pulmonol*. 2020; 55: 3057-3066.

7. Hadchouel A, Drummond D, Pontoizeau C, et al. Methionine supplementation for multi-organ dysfunction in MetRS-related pulmonary alveolar proteinosis. *Eur Respir J*. 2022; 59: 2101554.

8. Mordret E, Dahan O, Asraf O, et al. Systematic Detection of Amino Acid Substitutions in Proteomes Reveals Mechanistic Basis of Ribosome Errors and Selection for Translation Fidelity. *Mol Cell*. 2019; 75: 427-441.e5.

9. Rubio Gomez MA, Ibba M. Aminoacyl-tRNA synthetases. *RNA*. 2020; 26: 910-936.

10. Mohler K, Ibba M. Translational fidelity and mistranslation in the cellular response to stress. *Nat Microbiol*. 2017; 2: 17117.

11. Loftfield RB, Vanderjagt D. The frequency of errors in protein biosynthesis. *Biochem J*. 1972; 128: 1353-1356.

12. Hale SP, Auld DS, Schmidt E, Schimmel P. Discrete Determinants in Transfer RNA for Editing and Aminoacylation. *Science*. 1997; 276: 1250-1252.

13. Schmidt JA, Rinaldi S, Scalbert A, et al. Plasma concentrations and intakes of amino acids in male meat-eaters, fish-eaters, vegetarians and vegans: a cross-sectional analysis in the EPIC-Oxford cohort. *Eur J Clin Nutr*. 2016; 70: 306-312.

14. Juszkiewicz S, Hegde RS. Initiation of Quality Control during Poly(A) Translation Requires Site-Specific Ribosome Ubiquitination. *Mol Cell*. 2017; 65: 743-750.e4.

15. Adzhubei I, Jordan DM, Sunyaev SR. Predicting Functional Effect of Human Missense Mutations Using PolyPhen-2. *Curr Protoc Hum Genet*. 2013; 76.

16. Love MI, Huber W, Anders S. Moderated estimation of fold change and dispersion for RNA-seq data with DESeq2. *Genome Biol*. 2014; 15: 550

17. Xie Z, Bailey A, Kuleshov MV, et al. Gene Set Knowledge Discovery with Enrichr. *Curr Protoc*. 2021; 1: e90.

18. Schmidt E, Schimmel P. Mutational Isolation of a Sieve for Editing in a Transfer RNA Synthetase. *Science*. 1994; 264: 265-267.

19. Zivkovic I, Ivkovic K, Cvetesic N, Marsavelski A, Gruic-Sovulj I. Negative catalysis by the editing domain of class I aminoacyl-tRNA synthetases. *Nucleic Acids Res*. 2022; 50: 4029-4041.

4

20. Pataskar A, Champagne J, Nagel R, et al. Tryptophan depletion results in tryptophan-to-phenylalanine substitutants. *Nature*. 2022; 603: 721-727.

21. Henikoff S, Henikoff JG. Amino acid substitution matrices from protein blocks. *Proc Natl Acad Sci*. 1992; 89: 10915-10919.

22. Kaiser F, Krautwurst S, Salentin S, et al. The structural basis of the genetic code: amino acid recognition by aminoacyl-tRNA synthetases. *Sci Rep*. 2020; 10: 12647.

23. Yampolsky LY, Stoltzfus A. The Exchangeability of Amino Acids in Proteins. *Genetics*. 2005; 170: 1459-1472.

24. Pavlova NN, King B, Josselsohn RH, et al. Translation in amino-acid-poor environments is limited by tRNAGln charging. *eLife*. 2020; 9: e62307.

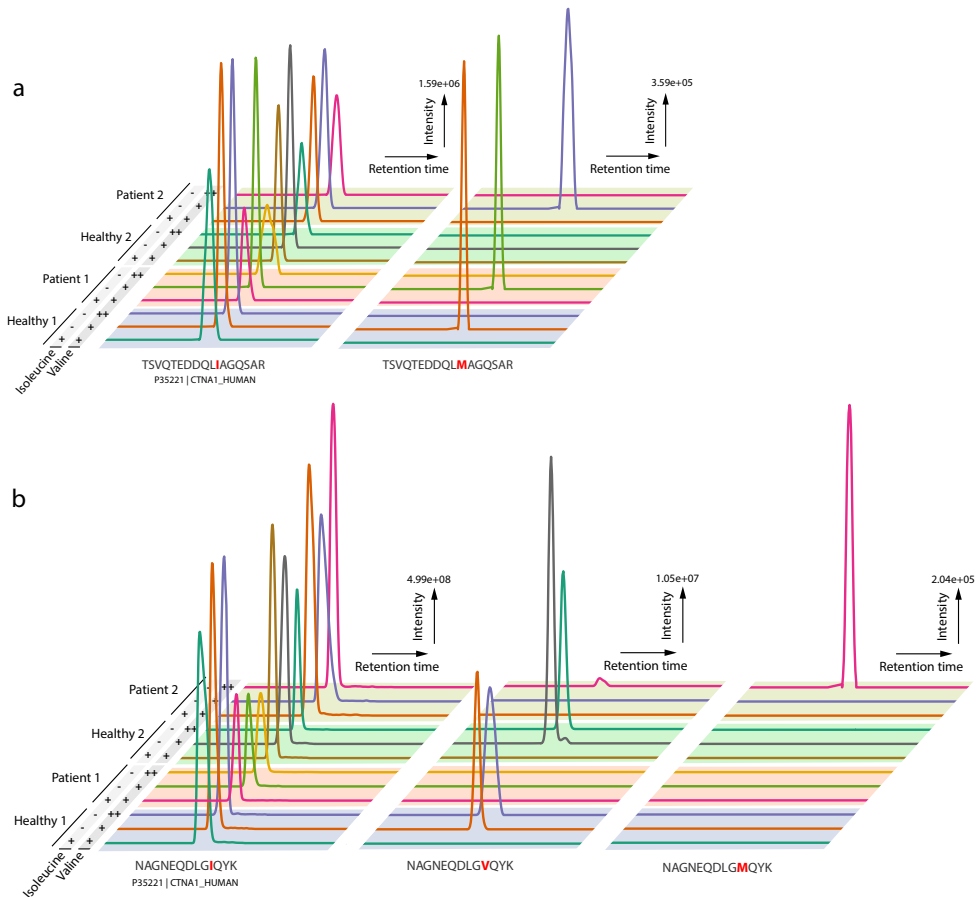## *Acknowledgements*

4

Supplementary figures

Fig S1: **a+b**, Identification of peptides containing a single isoleucine or isoleucine > valine or isoleucine > methionine substitutions in healthy fibroblasts or IARS1 deficient patient fibroblasts.
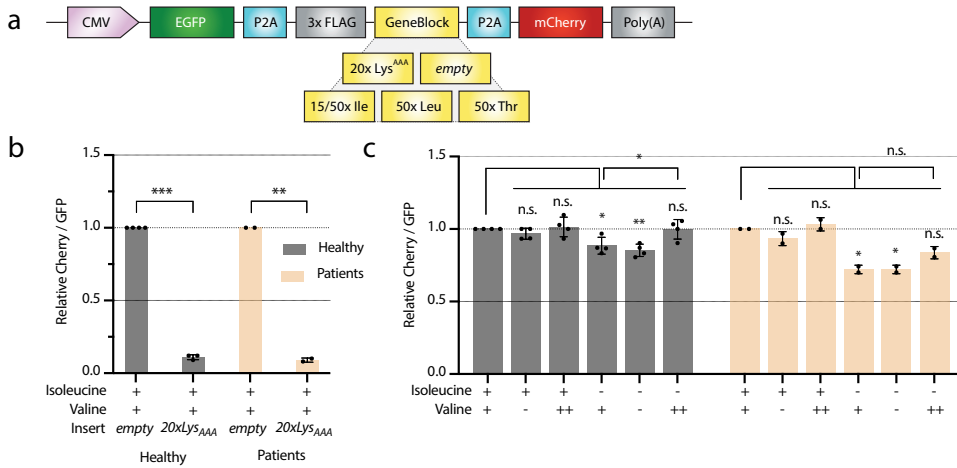
Fig S2: **a**, Design of the ribosomal stalling reporter plasmid, with 20xLys$_{AAA}$ as positive control for ribosomal stalling. **b+c**, relative fluorescence of Cherry / GFP in healthy and IARS1-deficient patient derived fibroblasts using the (**b**) reporter with 20xLys$_{AAA}$ insert and (**b+c**) the reporter without insert ('empty') in (**b**) normal culture media or (**c**) media with varying isoleucine and valine concentrations (**c**; isoleucine: + = 100%, - = 0% | valine: + = 100%, - = 1%, ++ = 1000% of plasma); two-sided unpaired Student's t-test with equal variance: n.s. p ≥ 0.05, * p < 0.05, ** p < 0.01, *** p < 0.001. Bars depict mean ± SD. Note that a decrease of the Cherry/GFP ratio of the empty reporter upon isoleucine restriction can be explained by the presence of 10x Ile in the fluorescent proteins.
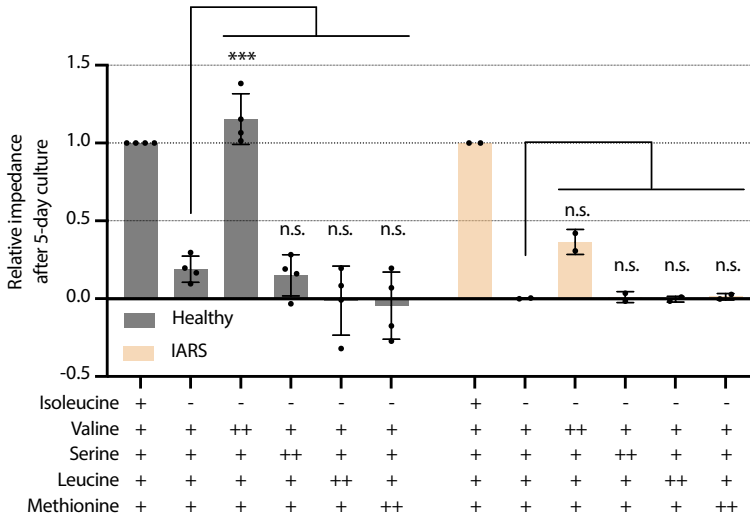
4

Fig S3: normalized impedance on xCELLigence MP real-time-cell-analyzer as measure for proliferation after 5-day culture under varying concentrations of isoleucine, valine, serine, leucine and methionine (+ = 100%, - = 1% of plasma, ++ = 1000% of plasma); two-sided unpaired Student's t-test with equal variance, with Bonferroni correction for multiple testing: n.s. $p \geq 0.05$, * $p < 0.05$, ** $p < 0.01$, *** $p < 0.001$, **** $p < 0.0001$; each dot represents the average of four technical replicates; bars depict mean ± SD.
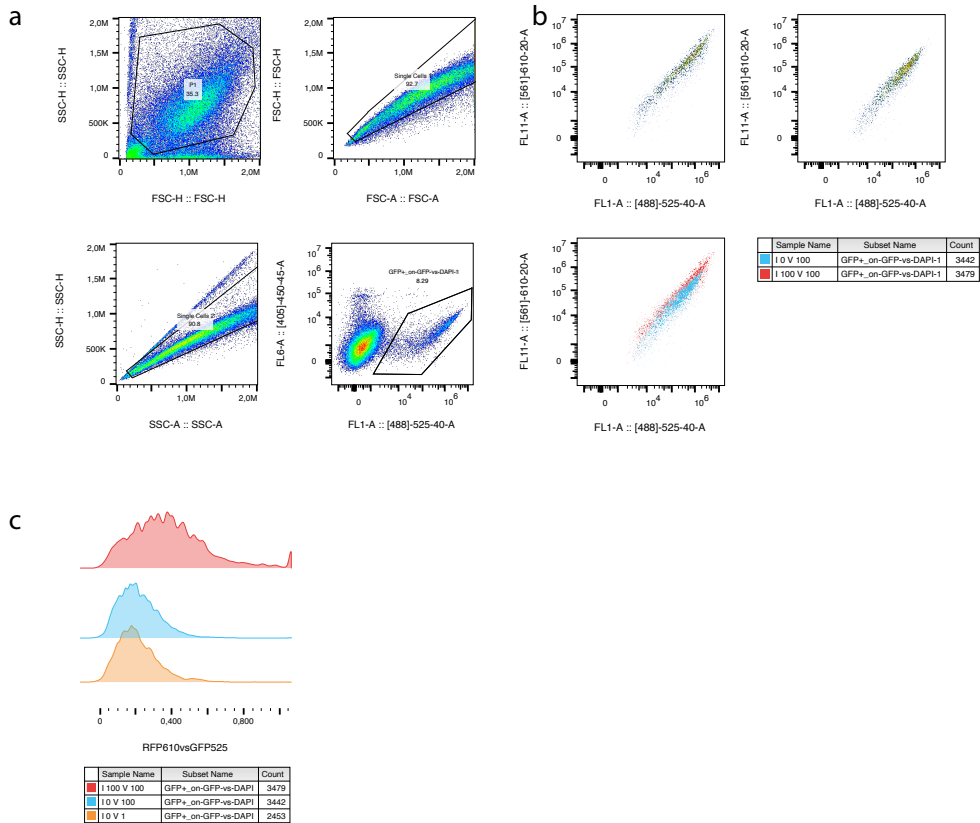
Fig S4: **a**, Gating strategy of dual-fluorescent reporter of terminal translational stalling. **b**, GFP (x-axis) to Cherry (y-axis) signal of IARS1 deficient donor fibroblasts (patient 1: N) with 100% isoleucine (N1) and 0% isoleucine (N2). **c**, Cherry to GFP ratio for IARS1 deficient donor fibroblasts, with 100% isoleucine and valine (N1), 0% isoleucine (N2), 0% isoleucine and 1% valine (N4).

REFINED ANALYSIS OF OPEN PROTEOMICS DATA REVEALS AMINO ACID SUBSTITUTIONS IN HEALTHY TISSUE

Imre Schene*, Gautam Kok*, Edward Nieuwenhuis, Harmjan Vos, Sabine Fuchs

5

I n their article "Tryptophan depletion results in tryptophan-to-phenylalanine substitutants", Pataskar et al. describe how interferon-γ (IFN-γ)-stimulated IDO1 upregulation in tumour cells results in intracellular tryptophan depletion and tryptophan-to-phenylalanine (W>F) substitutions in synthesized proteins.[1] The authors first detect IFN-γ-induced W>F substitutions in rigorous in vitro experiments. Afterward, they search for amino acid substitutions in publicly available proteomes and find that W>F are more common than any other W>X substitution, and that W>F substituent (W>F) peptides occur more often in tumours than control tissue. Initially, we were unable to reproduce this search, resulting from an undescribed filter step. We contacted the authors and they explained how and why filtering was applied for W>X but not for W>F peptides present in more than n proteomes, considering those as noise peptides, as now published in an Author Correction.[2]

In a 'News and Views' item accompanying the original article, this proteomics approach[1] was proposed to discover other examples of amino acid substitutions in freely available data sets.[3] Although we endorse the potential of harnessing the wealth of available proteomic resources to answer new biological questions, we would like to point out some important caveats. We suspect that a substantial fraction of the W>F peptides identified by this approach are false discoveries, leading to an incorrect conclusion that IFN-γ-induced W>F substitutions represent a tumour-specific phenomenon.[1]

We first considered the parameters used to detect W>F peptides in large-scale proteomics data,[1] because we suspected that standard tolerance settings for delta mass (20 ppm) and isotope error (-1, 0, +1, +2, +3) were too high to reliably identify substitutions. This revealed that peptide-spectrum matches (PSMs) identified as W>F peptides displayed the theoretically improbable isotope errors of -1 and +3, which were virtually absent from the wildtype peptide PSM distribution (Fig. 1a). Among the PSMs with an isotope error of zero, those identified as W>F peptides showed a wider delta mass distribution (Fig. 1b). Together, this suggested that a significant fraction of the W>F peptides represent false discoveries.

Since substituent peptides originate from active protein translation, they occur only in expressed proteins. A straightforward filter for misidentified 'W>F peptides' might therefore consist of disregarding peptides in proteins that are not expressed. We discovered that 28% of W>F peptides identified in the LSCC dataset referred to proteins that were not expressed according to the original analysis by Satpathy et al. (Fig. 1c,d, Ta-

——

bles S1A-B).[4] The PSMs of 'W>F peptides' in non-expressed proteins more often had isotope errors of -1 or +3, and a significantly wider delta mass distribution than PSMs of wildtype peptides and W>F peptides in expressed proteins (Fig. 1e,f). This strongly suggested that 'W>F peptides' in non-expressed proteins more often represent misidentified peptides. Concurrently, the increase in W>F peptides identified in LSCC tumour (LSCC) compared with adjacent normal tissue (ANT) samples1 could be fully attributed to W>F peptides in expressed proteins (Fig. 1g).

A considerable portion (57%) of 'W>F peptides' in non-expressed proteins represented immunoglobulin (Ig) variable genes (Fig. 1c, d, Table S1B), which are only expressed in B-cells and not in the LSCC dataset (Table S1D). All 'W>F peptides' in Ig proteins mapped to the conserved tryptophan residue in the FR2 region encoded by IGHV and IHLV genes and were found in LSCC and ANT in equal numbers (Table S1C, Fig. 1g,h).[5] Additional examination of pancreatic ductal adenocarcinoma also revealed identification of 'W>F peptides', but not of wildtype peptides, mapping to IGHV and IHLV. (Extended Data Fig. 1, Table S2A-C).[6] These genes constitute a large homologous set of sequences, sharing highly conserved framework regions interspersed by variable complementary-determining regions (Fig. 1h). This overwhelming homology precludes correct PSM identification, unless strict delta mass thresholds of <1.5 ppm are used.[7] Given the inaccuracy inherent to peptide identification in variable regions of Ig proteins, these regions should be disregarded in substituent peptide analyses.

To further filter out misidentified 'W>F peptides', we considered previously reported methods to detect amino acid substitutions in proteomes. Assuming that mistranslation is a rare event, the substituent variant of a peptide should be less common than its wildtype counterpart. Consequently, Mordret et al. proposed an algorithm that limits the search-space for substitutions in proteomic analyses to peptides with a corresponding wildtype counterpart.[8] We assessed whether this approach could filter misidentified peptides from the dataset of Pataskar, who considered each spectrum that can be matched to a substituent peptide in the human proteome as a genuine substituent.1 We divided the substituent peptides in the LSCC dataset into groups with or without a corresponding wildtype counterpart (Table S3). The delta mass distribution of W>F peptides with corresponding wildtype counterparts better resembled the distribution of wildtype peptides, outperforming the W>F peptides filtered by protein expression only (Fig. 2a, Extended Data Fig. 2a). Still, even the PSMs of W>F peptides with wildtype counterparts contained outliers (±4%) that may represent false discoveries (Fig. 2a). In line with the infrequency of W>F mistranslation, W>F peptides were generally identi-
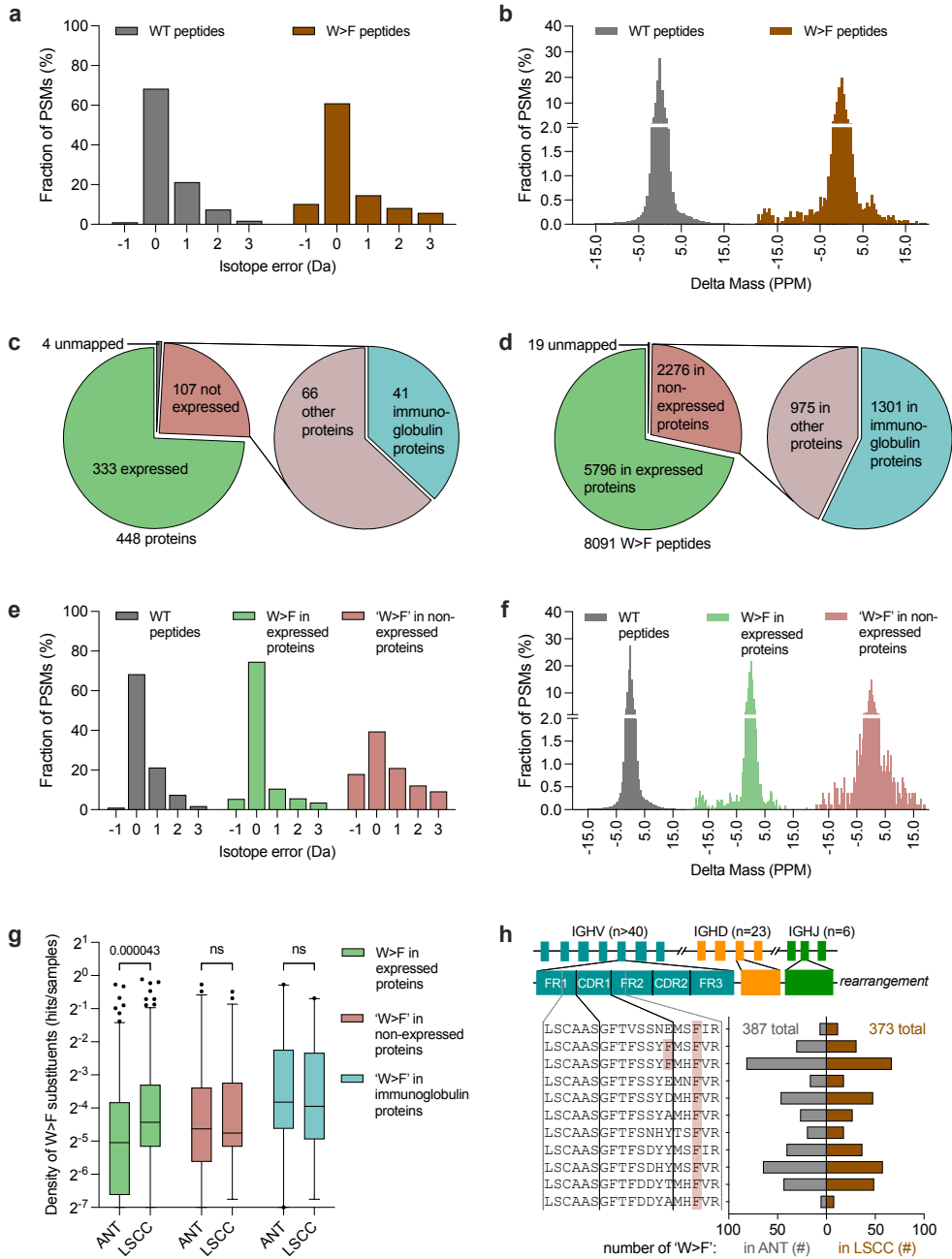
5

Fig. 1: W>F substitutions are frequently misidentified in variable regions of immunoglobulins.

a, Frequency distribution of the isotope error for peptide-spectrum matches (PSM) identified as wildtype (WT) peptides (n>10⁶) and W>F substituent (W>F) peptides (n=5,491). Note that the W>F peptide PSMs contain theoretically improbable -1 and +3 isotope errors. **b,** Frequency distribution of delta mass between the observed peptide and the calculated peptide in parts per million (ppm) for PSMs identified as wildtype peptides (n>10⁶) and W>F peptides (n=3,349) with an isotope error of zero. Note that the W>F peptide PSMs display a significantly broader distribution compared with wildtype peptide PSMs (S.D. = 3.88 vs. 1.91; p=0, F-test). **c**, In LSCC tumour and adjacent normal tissue (ANT) samples combined, 24% of proteins containing W>F peptides in the LSCC analyses of Pataskar et al. were not identified to be expressed in the analysis of the same dataset by Satpathy et al. 41% of these non-expressed proteins were immunoglobulins (Ig). **d**, Based on the same data as **c**: 28% of W>F peptides were found in proteins that were not expressed. 57% of these peptides in non-expressed proteins belonged to Ig proteins. **e**, Frequency distribution of the isotope error for PSMs identified as W>F peptides in expressed (n=3,361) or non-expressed (n=2,130) proteins. Note that the PSMs with theoretically improbable -1 and +3 isotope errors are predominantly identified as peptides in non-expressed proteins. **f**, Frequency distribution of delta mass for PSMs identified as W>F peptides in expressed (n=2,508) or non-expressed (n=841) proteins. Note that the PSMs identified as W>F substituents in non-expressed proteins have a significantly broader distribution than W>F substituents in expressed proteins (S.D. = 5.14 vs. 3.32; p= 2.4 x 10⁻⁶¹, F-test). **g**, Density plots of LSCC tumour and ANT samples showing the chance of a random sample to contain a specific W>F peptide. Mann-Whitney: p = 0.5915 (ns) and 0.6526 (ns) respectively. **h**, Peptides (11/41 examples are shown; see Supplementary Table S1C for the complete list) originating from Ig proteins that are identified as 'W>F substituent peptide' are found in equal numbers in LSCC tumour and ANT samples.

fied less often than their corresponding wildtype variant (Fig. 2b, Extended Data Fig. 2b,c). As expected, the difference in W>F peptides between tumour and ANT samples was predominantly attributable to W>F peptides with a wildtype counterpart (Fig. 2c, Extended Data Fig. 2d,e). Together, this supports that W>F peptides with identified wildtype counterparts mainly represent genuine substituents.

We then searched for protein-expression signatures associated with W>F peptides with or without wildtype counterparts. To this end, we considered protein expression
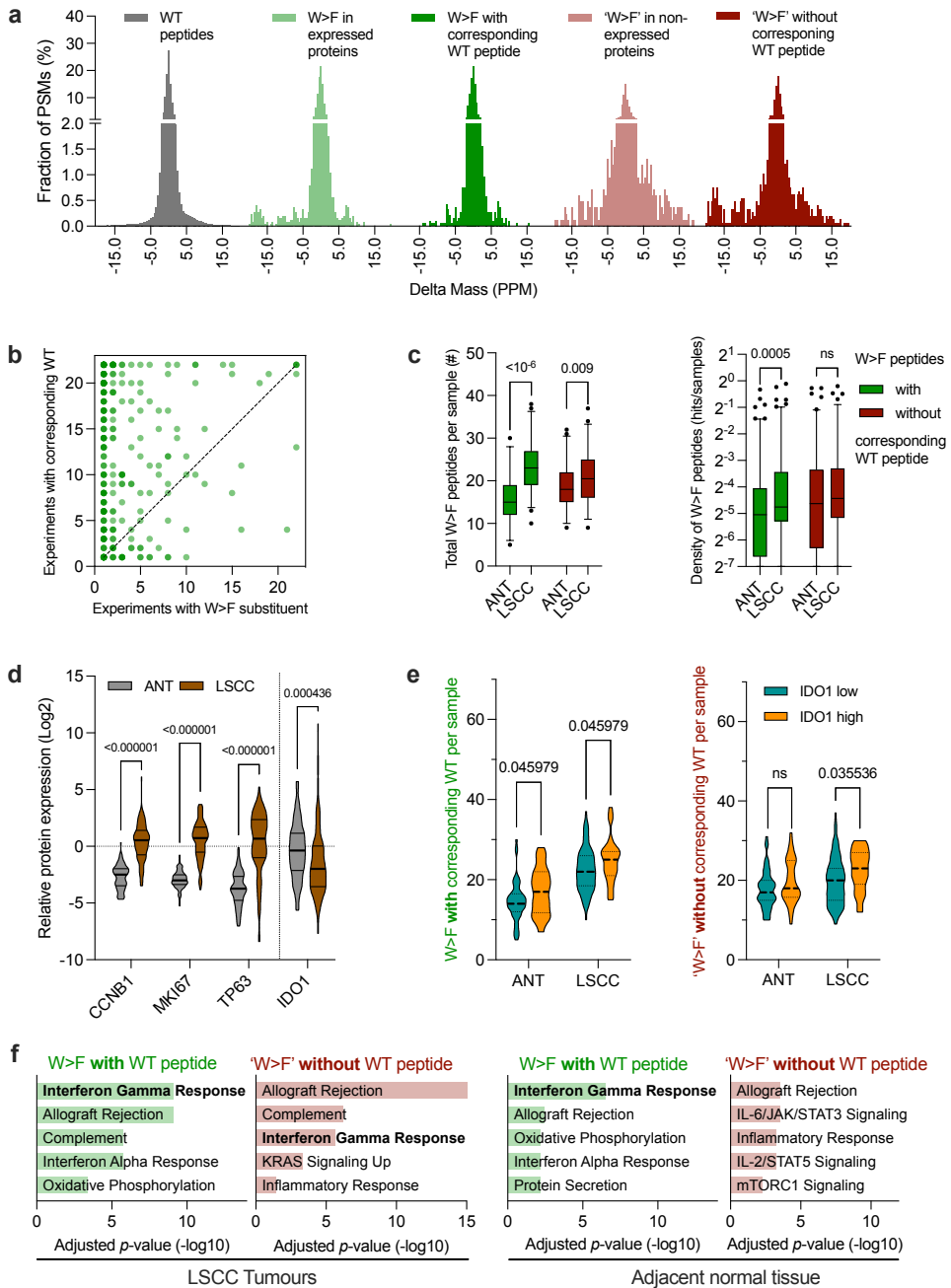
Fig. 2: analysis of reliable, wildtype-matched substituent peptides reveals IFN-γ-related W>F substitution is healthy tissue.

a, Frequency distribution of delta mass for PSMs identified as wildtype (WT) peptides (n>10^6), and PSMs identified as W>F peptides in expressed (n=2,508) or non-expressed (n=841) proteins, and W>F peptides with (n=1,872) or without (n=1,477) an identified corresponding wildtype peptide. Note that PSMs identified as W>F substituents with a corresponding wildtype peptide (dark green) have a narrower delta mass distribution compared with W>F substituents in expressed proteins (light green) (S.D.= 1.98 vs. 3.32; p=7.3 x 10^{-115}, F-test). Also note that the W>F substituents with corresponding wildtype peptides are distributed much more similarly to wildtype peptides (S.D.= 1.98 vs. 1.91; p=0.0164, F-test). **b**, Scatterplot of the number of 11-plex experiments (from a total of 22 experiments) in which a W>F peptide was identified (x-axis) versus the number of experiments in which the corresponding wildtype peptide was identified (y-axis). The dotted line indicates equal experiments with W>F and corresponding wildtype peptides. Note that most W>F substituents, for which a corresponding wildtype peptide was identified, were identified in less or equal experiments when compared with their wildtype counterparts (230/262=88%). **c**, The density (hits/samples) of identification of W>F peptides with and without corresponding wildtype peptide in ANT (n=99) and LSCC tumour (n=108) samples. Note that W>F substituents for which a corresponding wildtype peptide was identified (n=262) are significantly more common in LSCC tumour compared with ANT samples, whereas W>F substituents without an identified corresponding wildtype peptide (n=212) are not (p=0.076 (ns)). Mann-Whitney tests. Boxplot: median with inter-quartile range and 97.5% confidence interval. **d**, Relative expression of tumour markers CCNB, MKI67, and TP63, and of IDO1 in ANT (n=99) and LSCC tumour (n=108) samples from Satpathy et al. (2021). Note that while tumour marker expression is increased in LSCC tumour samples, IDO1 expression is decreased in LSCC tumour compared with ANT samples. Mann-Whitney tests. **e**, The total number of W>F peptides per sample is significantly increased in samples with high IDO1 expression compared with samples with low IDO1 expression. Note that for ANT samples, this difference was only present in W>F peptides for which a wildtype peptide was identified. Mann-Whitney tests: ns: p=0.0779. **f**, Gene set enrichment analyses of LSCC tumour and ANT samples. Genes were ranked on correlation between protein expression and number of W>F substituents with a wildtype counterpart (green) and W>F substituents without a wildtype counterpart (red). Note that in LSCC tumour samples, the interferon-γ (IFN-γ) response is increased predominantly in the group of W>F substituents with wildtype counterparts. Additionally, the IFN-γ response is the Hallmark most associated with W>F substituents in ANT, but this association is absent when W>F substituents without wildtype counterpart are considered.

in the LSCC dataset.[4] Tumour markers were strongly upregulated in LSCC compared with ANT samples. Conversely, IDO1 expression was higher in ANT than LSCC samples, suggesting that non-tumour cells are also deprived of tryptophan (Fig. 2d). Indeed, we found a positive correlation between IDO1 expression and W>F peptides with wildtype counterparts in both LSCC and ANT samples. This relation disappeared when considering 'W>F peptides' without a wildtype counterpart, further negating their biological relevance (Fig. 2e). We then performed gene set enrichment analysis with all proteins associated with W>F substitutions (Table S4A-B). In line with the proposed biological mechanism,[1] W>F substitutions with corresponding wildtype peptides correlated strongly with the IFN-γ response in LSCC samples. Interestingly, the IFN-γ response was also the most significantly associated pathway with W>F substitutions in ANT samples, contradicting the putative tumour-specificity of W>F substitutions and instead suggesting a more general physiological mechanism (Fig. 2f). Again, the IFN-γ response was not correlated with 'W>F peptides' without a corresponding wildtype peptide in ANT samples.

In summary, the proteomics analyses used by Pataskar et al. to detect amino acid substitutions in publicly available datasets are biased by high abundancy of noise peptides, rendering conclusions questionable.[1] It would be best to reduce false discoveries by acquiring mass spectra at higher resolution and identifying peptides using more stringent mass tolerance settings. To limit the impact of the false discoveries in their current approach, we recommend to only consider putative substitutions in peptides of which the wildtype variant is expressed and to exclude 'substitutions' in immunoglobulin peptides, which are inherently resistant to unambiguous interpretation by conventional shotgun proteomics.[7] Application of such filters strengthened the association between W>F substitutions and IFN-γ-induced IDO1 upregulation and revealed that W>F substitutions are not tumour specific, but occur in adjacent normal tissue as well.

Methods

Data acquisition and processing

Supplementary Tables 4 and 7, containing lists of W>F peptide peptides detected in LSCC and PFA, respectively, from Pataskar et al.[1] were downloaded from nature.com. The PDC meta- and proteomics data for LSCC and PDA used by Pataskar et al.[1] were downloaded from pdc.cancer.gov. Supplementary Table 3B from Satpathy et al.[4] was

downloaded from cell.com. Data were merged and processed using R (version 4.0.5) with packages dplyr (version 1.0.9), tidyr (version 1.2.0), and tidyverse (version 1.3.2). Datasheets were further studied using Microsoft Excel (version 16.63.1) and Enrichr on maayanlab.cloud/Enrichr/ (Ma'ayan lab).[9] GraphPad Prism (version 9.4.0) was used to perform statistical analyses and to visualise data.

Identification of wildtype and W>F peptides from large-scale proteomics data

FragPipe (version 18.0) with MSFragger (version 3.5) and Philosopher (version 4.4.0) on a CentOS Linux (version 7.9.2009) based high performance cluster with Java (version 11.0.16) was used to analyse raw LSCC proteomics data (.mzml files) from pdc.cancer.gov, against the UniProt human proteome (UP000005640) fasta from 3 March 2022 with decoys, and the same proteome with all tryptophans (W) replaced by phenylalanines (F). All further settings were equal to those reported by Patasakar et al.[1] Identified peptides (tmt-report/ratio_peptide_None.tsv) were grep-matched (grep -Fwf) against lists of all possible peptides containing a single W or W>F, as created with Cleaver (version 1.28.0) in R (version 4.0.5), allowing 0-2 missed cleavages. It was validated that all W>F peptides identified by Pataskar et al.[1] were also identified by our own FragPipe search; only those W>F peptides were used for further analyses.

Isotope error and delta mass analysis

The PSM.tsv files for every TMT-11-plex experiment, containing PSM characteristics including the absolute observed peptide mass and absolute delta mass in Daltons (Da), were collected and analysed. Relative delta mass in parts per million (ppm) was calculated as 'absolute delta mass' / 'absolute observed peptide mass' $\times$ 10^6. The 'peptide' sequence of PSMs were matched with the W>F substituent peptide list as identified by Pataskar et al.[1] For all PSMs identified as wildtype peptides and W>F peptides, the isotope error was found by binning the absolute delta mass into bins of -1, 0, +1, +2, or +3 Da. For all PSMs with an isotope error of 0 Da, the frequency distribution of the relative delta mass (ppm) was plotted into histograms. The isotope error and delta mass parameters displayed in the frequency distributions are collected in Supplementary Table S5.

Wildtype peptides and distribution over TMT-11-plex experiments

Wildtype peptides were extracted from the PDC LSCC and PDA data and matched with the W>F peptides for LSCC (Table S4) and PDA (Table S7) from Pataskar et al.[1] W>F peptides per sample and per TMT-11 plex experiment were extracted using the same threshold as used by Pataskar et al. (relative Log2 intensity > 0) and categorized to tumour or adjacent normal tissue (ANT) samples using the samples key from PDC. For each W>F peptide, the total number of TMT-11 plex experiments in which the peptide was identified was extracted (samples with NAs refer to experiments in which W>F peptides were not identified). For W>F peptides with matching, corresponding wildtype peptides, the number of TMT-11 plex experiment in which the corresponding wildtype peptides was identified was extracted from the PDC data. For W>F peptides with matching corresponding wildtype peptides, the ratio of 'experiments with W>F peptide' / 'experiments with corresponding wildtype peptide' was calculated and plotted in histograms. The density of specific W>F peptides within groups of tumour and ANT samples was calculated as 'samples with W>F peptide' / 'total samples in group'.

Identification of W>F peptides in expressed and non-expressed proteins

The LSCC protein expression data were extracted from Supplementary Table S3B from Satpathy et al.;[4] the PDA protein expression data was extracted from pdc.cancer.gov. These expression data contained all proteins that comprised of multiple peptides or comprised of a single excellent scoring peptide that was observed in at least 4 TMT-plex experiments. The proteins in which Pataskar et al. identified W>F peptides were matched to the expression data based on gene symbol. For each protein with identified W>F peptides, the presence in the expression data was checked. Based on the presence or absence of the corresponding proteins in the expression data, the number of W>F peptides in expressed vs. non-expressed proteins was calculated (Tables S1A and S2A).

Investigation of W>F peptides in immunoglobulin proteins

All W>F peptides that resided in immunoglobulin (Ig) proteins were identified based on their corresponding gene symbol. The sequence of W>F peptides residing in Ig proteins was blasted against a database of human Ig genes, using IgBLAST.[5] The Ig regions in which W>F peptides occurred according to IgBLAST were collected and noted in Tables S1C and S2C for the LSCC and PDA databases, respectively.

Correlation between W>F peptides and protein expression

The LSCC protein expression data were extracted from Table S3B from Satpathy et al.[4] In case multiple entries (multiple protein isoform) existed for a single gene, the protein isoform with the highest number of spectral counts was selected for further analyses. The reported Log2-expression of proteins was used to plot relative expression of tumour markers and IDO1 in LSCC tumour and ANT samples. The Log2-expresion of IDO1 was used to calculate the number of W>F peptides in the IDO1-high (IDO1 > 0 (log2)) vs. IDO1-low (IDO1 < 0 (log2)) samples. Proteins were ranked by correlation between protein expression and the number of 1) W>F peptides with a wildtype counterpart, 2) W>F peptides without a wildtype counterpart (Supplementary Table 4A).

Enrichment analyses

The top 500 proteins (gene symbols) that correlated most strongly with specific groups of W>F peptides were analysed in Enrichr.[9] The Hallmark pathways (MSigDB Hallmark 2020) that were enriched most significantly (lowest adjusted p-value) for proteins correlating with W>F peptides with and without matching wildtype peptides were collected (Supplementary Table 4B, Fig. 2f).

Statistical analyses

Statistical significance between distributions was determined using Mann-Whitney (Wilcoxon) tests with $\alpha = 0.05$. Statistical significance of equality of variance across groups was determined using two-sample F-tests.

References

1. Pataskar A, Champagne J, Nagel R, et al. Tryptophan depletion results in tryptophan-to-phenylalanine substitutants. *Nature*. 2022*;* 603: 721–727.

2. Pataskar A, Champagne J, Nagel R, et al. Author Correction: Tryptophan depletion results in tryptophan-to-phenylalanine substitutants. *Nature*. 2022; 608: E20.

3. Baranov PV & Atkins JF. Immune cells alter genetic decoding in cancer. *Nature*. 2022: 603; 582-583.

4. Satpathy S, Krug K, Jean Beltran, PM, et al. A proteogenomic portrait of lung squamous cell carcinoma. *Cell*. 2021; 184: 4348-4371.

5. Ye J, Ma N, Madden TL, & Ostell, JM. IgBLAST: an immunoglobulin variable domain sequence analysis tool. *Nucleic Acids Res*. 2013; 41, W34–W40.

6. Cao L, Huang C, Cui Zhou D, et al. Proteogenomic characterization of pancreatic ductal adenocarcinoma. *Cell. 2021;* 184: 5031–5052.e5026.

7. Boutz DR, Horton AP, Wine Y, et al. Proteomic identification of monoclonal antibodies from serum. *Anal Chem*. 2014; 86: 4758–4766.

8. Mordret E, Dahan O, Asraf O, et al. Systematic Detection of Amino Acid Substitutions in Proteomes Reveals Mechanistic Basis of Ribosome Errors and Selection for Translation Fidelity. *Mol Cell* 2019; 75: 427-441.

9. Xie Z, Bailey A, Kuleshov MV, et al. Gene set knowledge discovery with enrichr. *Curr Protoc*. 2021; 1: e90.

Supplementary Figures
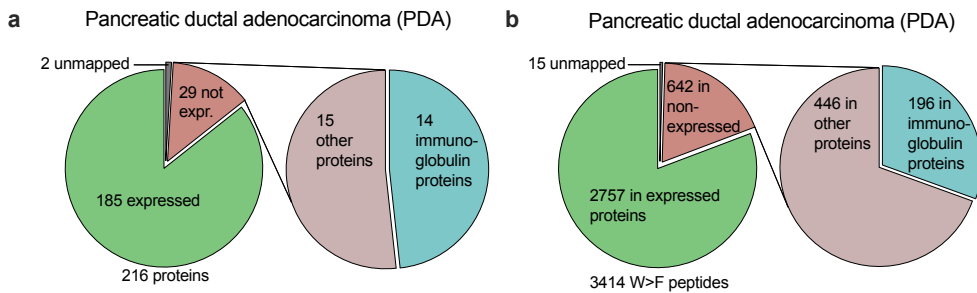
Fig. S1: **a**, In PDA tumour and adjacent normal tissue (ANT) samples combined, 13% of proteins containing W>F peptides in the PDA analyses of Pataskar et al. (2022) were not identified to be expressed in the original analysis of PDA protein expression extracted from pdc.cancer.gov. 48% of these non-expressed proteins were immunoglobulins (Ig). **b**, Based on the same data as **a**: 19% of W>F peptides were found in proteins that were not expressed. 31% of these peptides in non-expressed proteins belonged to Ig proteins.
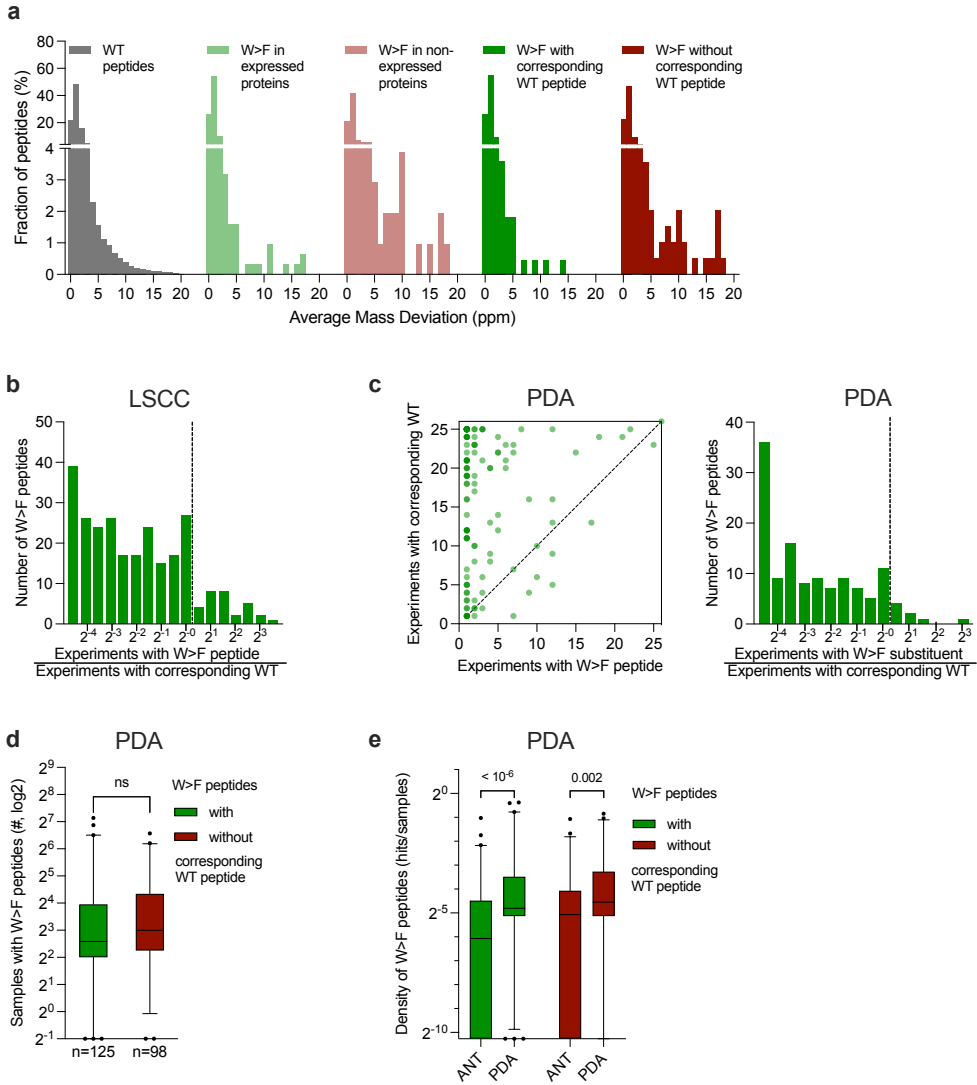
Fig. S2: **a**, Frequency distribution of the average mass deviation (AMD) of peptides in the denoted groups. AMD was calculated for each peptide as the average of the absolute delta mass of all PSMs matching that peptide. **b**, Frequency distribution of the 'number of experiments in which a W>F peptide was identified (x-axis in Fig. 2b)' divided by 'number of experiments in which the corresponding wildtype (WT) peptide was identified (y-axis in Fig. 2b)', for the LSCC dataset. **c**, Left panel: Scatterplot of the number of 11-plex experiments in (from a total of 25 experiments) in which a W>F peptide was identified (x-axis) versus the number of experiments in which the corresponding wildtype peptide was identified (y-axis), for the pancreatic ductal adenocarcinoma (PDA) dataset.[6]

Right panel: Frequency distribution of the 'number of experiments in which a W>F peptide was identified' divided by 'number of experiments in which the corresponding wildtype peptide was identified', for the PDA dataset. Note that most W>F substituents, for which a corresponding wildtype peptide was identified were identified in less or equal experiments when compared with their WT counterparts. **d**, The number of samples in the PDA dataset (tumour and adjacent normal tissue (ANT) samples combined) in which each W>F peptide was identified by Pataskar et al. (2022). Substituents are divided into substituents with (n=125) and without (n=98) an identified corresponding wildtype (WT) peptide. Mann-Whitney tests: p=0.174 (ns). Boxplot: median with inter-quartile range and 97.5% confidence interval. **e**, The density (hits/samples) of identification of W>F peptides with and without corresponding wildtype peptide in ANT and PDA tumour samples.

Supplementary tables

Table S1: W>F peptides identified in the LSCC dataset and the proteins they map to.

Table S2: W>F peptides identified in the PDA dataset and the proteins they map to.

Table S3: W>F peptides identified in the LSCC dataset stratified by identification of their corresponding wildtype counterpart.

Table S4: gene set enrichment analysis with all proteins associated with W>F substitutions.

Table S5: isotope error and delta mass parameters displayed in the frequency distributions.

Will be available for download after publication.

TREATMENT OF ARS-DEFICIENCIES WITH SPECIFIC AMINO ACIDS

Gautam Kok, Laura Tseng, Imre Schene, Monique Dijsselhof, Gajja Salomons, Marisa Mendes, Desiree Smith, Arnaud Wiedemann, Marie Canton, François Feillet, Tom de Koning, Megan Boothe, Joy Dean, Rachel Kassel, Elise Ferreira, Margreet van den Born, Edward Nieuwenhuis, Holger Rehmann, Suzanne Terheggen-Lagro, Clara van Karnebeek*, Sabine Fuchs*

6

Abstract

Purpose

Recessive cytosolic aminoacyl-tRNA synthetase (ARS) deficiencies are severe multiorgan diseases, with limited treatment options. By loading transfer RNAs (tRNAs) with their cognate amino acids, ARS are essential for protein translation. However, it remains unknown why ARS deficiencies lead to specific symptoms, especially in early life and during infections. We set out to increase pathophysiological insight and improve therapeutic possibilities.

Methods

In fibroblasts from patients with isoleucyl-RS (IARS1), leucyl-RS (LARS1), phenylalanyl-RS-beta-subunit (FARSB), and seryl-RS (SARS1) deficiencies, we investigated aminoacylation activity, thermostability, and sensitivity to ARS-specific amino acid concentrations, and developed personalized treatments.

Results

Aminoacylation activity was reduced in all patients, and further diminished at 38.5/40 °C (P^{LARS} and P^{FARSB}), consistent with infectious deteriorations. With lower cognate amino acid concentrations, patient fibroblast growth was severely affected. To prevent local and/or temporal deficiencies, we treated patients with corresponding amino acids (follow-up: $1/2–2^{2/3}$rd years), and intensified treatment during infections. All patients showed beneficial treatment effects, most strikingly in growth (without tube feeding), head circumference, development, coping with infections, and oxygen dependency.

Conclusion

For these four ARS deficiencies, we observed a common disease mechanism of episodic insufficient aminoacylation to meet translational demands and illustrate the power of amino acid supplementation for the expanding ARS patient group. Moreover, we provide a strategy for personalized preclinical functional evaluation.

Introduction

Aminoacyl-tRNA synthetases (ARS) facilitate loading of transfer RNAs (tRNAs) with their cognate amino acids,[1] a pivotal process in translating messenger RNA (mRNA) to protein. ARS function in the cytosol (encoded by *ARS1*), mitochondria (encoded by *ARS2*), or both (encoded by *GARS1*, *KARS1*, *QARS1*). Autosomal recessive *ARS1* variants cause severe symptoms in various organs, especially during the first year of life and infectious episodes, and may lead to premature death,[2] putatively through loss of aminoacylation activity.[3] To improve care for the increasingly recognized group of ARS-deficient patients, we further investigated the disease mechanism for four different ARS deficiencies, and developed a personalized treatment strategy.

Materials and methods

In silico analyses

Protein structure visualizations were based on pdb entries *1ile*, *1ffy*, *3l4g*, *4rge*, and *6lfp*, using molscript, Raster3D, and Bragi.[4-6]

Fibroblast cultures

Fibroblasts were obtained via skin biopsy and cultured in F-12 with 10% FBS and 1% penicillin–streptomycin (PS). For amino acid sensitivity experiments, amino acid free DMEM/F-12 with HEPES and $NaHCO_3$ was supplemented with 1% PS, 1% GlutaMAX, 10% dialyzed FBS, and all amino acids except the tested amino acid. Amino acid concentrations were related to average plasma concentrations (L-isoleucine: 57 µM; L-leucine: 100 µM; L-phenylalanine: 58 µM; and L-serine: 136 µM).

Aminoacylation activity

IARS1, LARS1, FARS1, SARS1, and GARS1 activities were measured in fibroblast lysates, incubated at 37 °C in reaction buffer (50 mM Tris buffer [pH 7.5], 12 mM MgCl, 25 mM KCl, 1 g/l bovine serum albumin, 0.5 mM spermine, 1 mM ATP, 0.2 mM yeast total tRNA, 1 mM dithiothreitol, 0.3 mM [$^{13}C_6$, ^{15}N] isoleucine, 0.3 mM [$^{13}C_2$] leucine, 0.3 mM, [$^{2}H_5$] phenylalanine, 0.3 mM [$^{13}C_3$, ^{15}N] serine, and 0.3 mM [$^{2}H_2$] glycine). Aminoacyl-tRNA was precipitated with trichloroacetic acid (TCA). Labeled amino acids were detached from tRNAs with ammonia. [^{13}C, ^{15}N] glycine was added as in-

ternal standards. Labeled amino acids were quantified by liquid chromatography–tandem mass spectrometry. Analyses were performed in triplicates. To determine thermolability, lysates were incubated at 37 °C, 38.5 °C, and 40 °C.

Amino acid sensitivity

Patient and age-matched control fibroblasts were seeded in triplicates (E-Plate 96 PET, 3,000 cells/well). After 24 hours, medium with the desired L-isoleucine, L-leucine, L-serine, or L-phenylalanine concentrations was applied. Proliferation of fibroblasts was evaluated by continuous impedance analysis over three days using a real-time cell analyzer (xCELLigence MP, ACEA Biosciences). Per donor, impedance at 72 hours was normalized against 100% amino acid concentration.

Medical treatment

Based on the genetic diagnoses and in vitro functional studies, we developed personalized intervention and monitoring protocols for objective safety and outcome parameters (Table S1) as $n = 1$ studies with parents as partners in care.[7,8]

We treated P[IARS] and P[LARS] with high doses of L-isoleucine (35–70 mg/kg/day in three doses), and L-leucine (35–100 mg/kg/day), respectively, and natural protein fortification (2.5 g/kg/day; during illness 3.5 g/kg/day). P[FARSB] and P[SARS] received L-phenylalanine (40–100 mg/kg/day), and L-serine (85.7–97.5 mg/kg/day), respectively (Table S2). Similar amino acid dosages were safely used for other disorders.[8,9]

Results

Patient fibroblasts

We studied fibroblasts from the following:

1. P[IARS] (and P[IARS-2] with similar phenotype): compound heterozygous *IARS1*-variants (NM_002161.5): c.1305G>C p.Trp435Cys and c.3377dup p.Asn1126fs (OMIM 600709),[2,10-12] previously described as P2 and P1, respectively.[2]

2. P[LARS]: compound heterozygous *LARS1*-variants (NM_020117.10): c.1503 + 3A>G p.? and c.1292T>A p.Val431Asp (OMIM 151350).[2]

3. P[FARSB]: compound heterozygous *FARSB*-variants (NM_005687.5): c.3G>T p.-Met1? and c.1118G>C p.Gly373Ala (OMIM 609690).[13-15]

4. P[SARS]: homozygous *SARS1*-variant (NM_006513.3): c.638G>T p.Arg213Leu (OMIM 607529).[16]

In silico analyses

For all variants, we predicted pathogenicity using protein structure analyses (Supplementary Text, Fig. S1).

Fibroblast studies

We confirmed pathogenicity of the variants with decreased aminoacylation activity in patient-derived fibroblasts to 23% and 21% IARS1 activity in P[IARS] and P[IARS-2], respectively, 27% LARS1 activity in P[LARS], 28% FARS1 activity in P[FARSB], and 45% and 50% SARS1 activity in two siblings of P[SARS] with the same homozygous variants (Fig. 1a). Because patients deteriorate during infections,[2] we investigated thermostability of the affected enzymes. At 38.5 °C and 40 °C, LARS1 activity of P[LARS] decreased to 5%, and FARS1 activity of P[FARSB] to 0% at 40 °C (Fig. 1g/h). Corresponding ARS activities in fibroblasts from P[IARS], P[IARS-2], P[SARS], and controls, and GARS1 activity (internal control) were the same at 37 °C, 38.5 °C, and 40 °C (Fig. 1f/i, S2).

Based on severe symptoms at young age and during infections, reflecting periods of increased translation and decreased amino acid availability, we tested if patient fibroblasts were sensitive to ARS-specific amino acid concentrations. Indeed, patient fibroblast proliferation was normal at high concentrations, but decreased in a dose-dependent manner at lower concentrations of isoleucine for P[IARS] and P[IARS-2], leucine for P[LARS], and phenylalanine for P[FARSB] (Fig. 1b-d), when compared to controls. Fibroblasts from P[IARS] and P[LARS] died upon combined amino acid deprivation (data not shown). Serine deprivation did not affect fibroblasts from P[SARS]' two siblings (Fig. 1e). As serine is nonessential, effects may have been compensated by biosynthesis from glycine and glucose in our culture media.

Patient treatment

P[IARS] was an 8-year-old boy with a history of dysmaturity (Fig. 2e), failure to thrive requiring duodenal tube feeding, global developmental delay, autism spectrum disor-
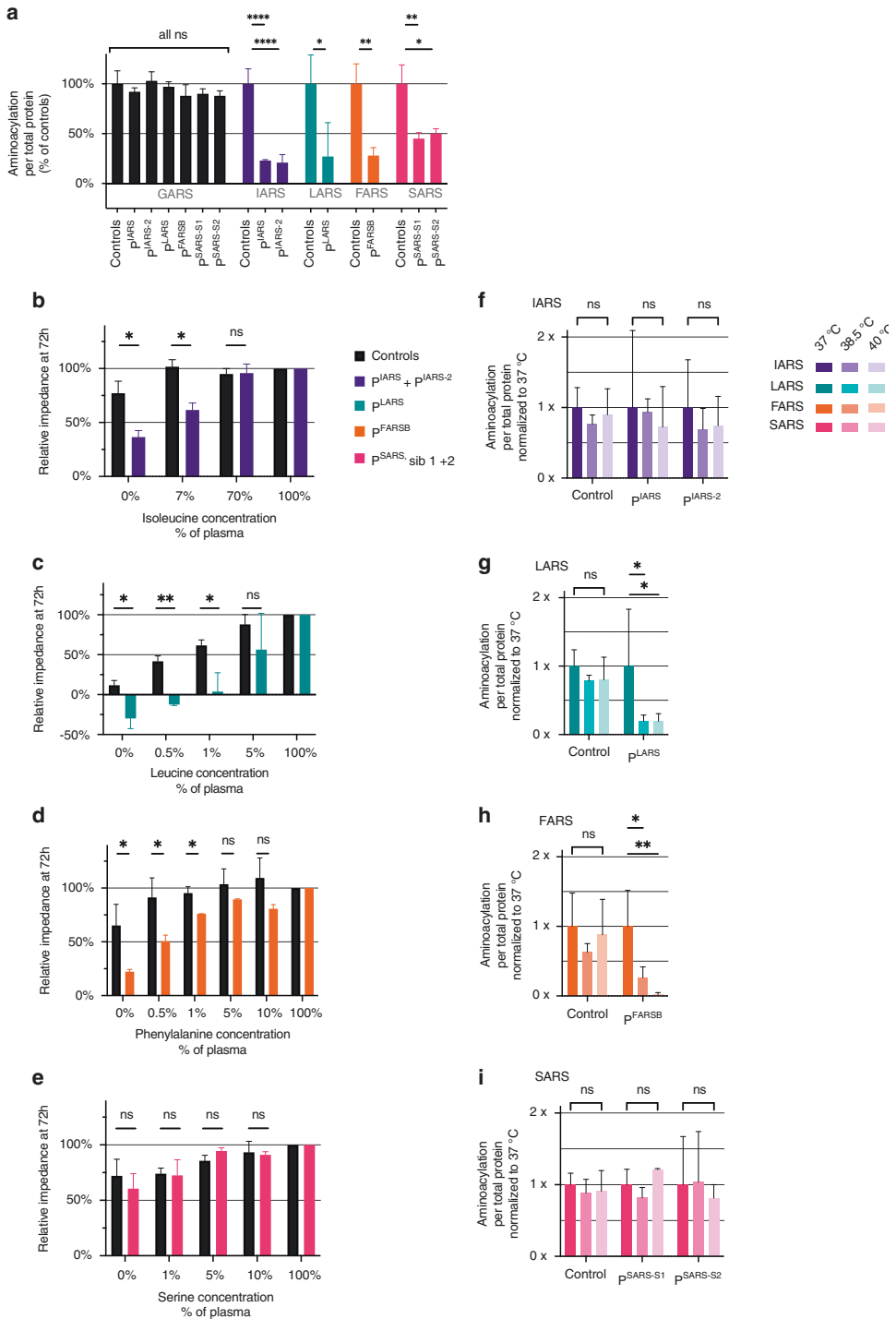
Fig. 1: fibroblast studies: enzyme activity and amino acid sensitivity.

a, Enzyme activity is decreased but not absent in all patients.

Aminoacylation activity in fibroblasts of P^{IARS}, P^{IARS-2}, P^{LARS}, P^{FARSB}, and two siblings with the same homozygous variant as P^{SARS}, presented as percentage of age-matched controls. GARS1-activity was measured as an internal control. All measurements were performed in triplicate (n=3), except IARS controls (n=6) and GARS1 controls (n=12). Error bars show standard deviation. Unpaired t-test: ns p ≥ 0.05, * p < 0.05, ** p < 0.01, *** p < 0.001, **** p < 0.0001.

b-e, IARS1, LARS1 and FARSB1 patient fibroblasts are sensitive to isoleucine, leucine and phenylalanine deprivation, respectively.

72h proliferation of fibroblasts of P^{IARS}, P^{IARS-2}, P^{LARS}, P^{FARSB}, and two siblings with the same homozygous variant as P^{SARS}, compared to age-matched control fibroblasts, exposed to decreasing concentrations of isoleucine (**b**: P^{IARS}/P^{IARS-2}), leucine (**c**: P^{LARS}), phenylalanine (**d**: P^{FARSB}) or serine (**e**: two siblings of P^{SARS}), shown as normalized impedance, measured with an xCELLigence MP. Amino acid concentrations were compared to average plasma concentrations. Every donor was measured once (**a**; n=1 each) or twice (**b-d**; n=2 each). Two (**a-c**) or three (**d**) controls were measured once (n=1 each). Error bars show standard deviation. Unpaired t-test: ns p ≥ 0.05, * p < 0.05, ** p < 0.01, *** p < 0.001.

f-i, LARS1- and FARS1-activity deteriorate in LARS1 and FARSB patient fibroblasts, respectively.

Aminoacylation activity in fibroblasts of P^{IARS} and P^{IARS-2} (**f**), P^{LARS} (**g**), P^{FARSB} (**h**), and two siblings with the same homozygous variant as P^{SARS} (**i**) at 37, 38.5 and 40 °C. Data are presented compared to the enzymatic activity at 37 °C. All measurements were performed in triplicate (n=3). Error bars show standard deviation. Unpaired t-test: ns p ≥ 0.05, * p < 0.05, ** p < 0.01.

der, interstitial lung disease (ILD, Figure S3) requiring oxygen treatment, and repeated (intensive care) admissions for respiratory and circulatory insufficiency during infectious episodes (Fig. 2a). Within weeks after treatment initiation, oral intake increased, vomiting decreased, and pulmonary function improved. After three weeks, isoleucine supplementation was stopped for two weeks due to pharmacy delivery problems. Vomiting, mucus production, and respiratory distress all increased. Upon reinitiation,
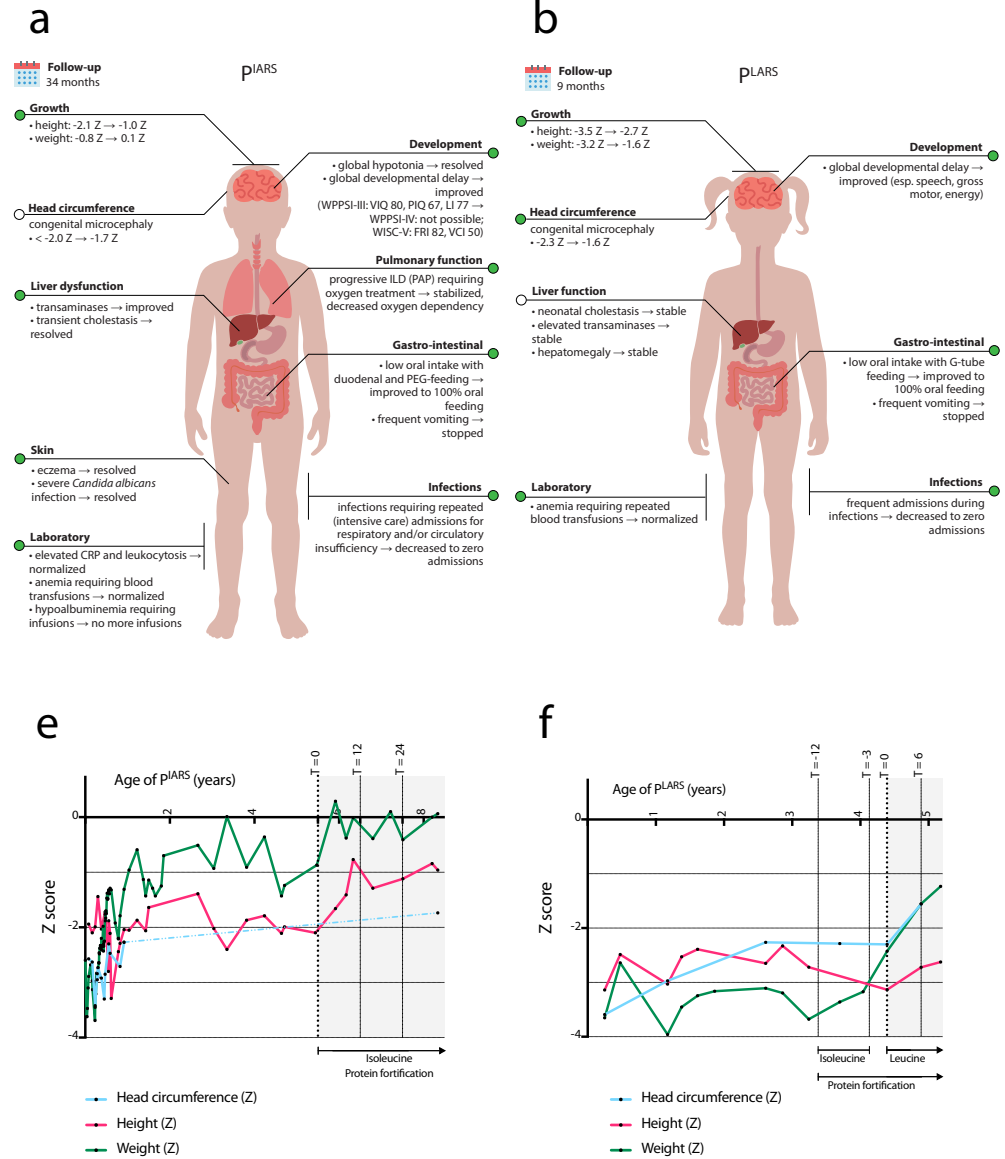
Fig. 2: summary of symptoms and treatment effects in all four patients.

a-d, summary of symptoms and treatment effects.

Summary of the symptoms of P^IARS (**a**), P^LARS (**b**), P^FARSB (**c**), and P^SARS (**d**). Colors indicate the generalized treatment effect on the symptom (green: improved; white: stable or stabilized; red: progressed). Standard deviation scores (Z) for height, weight, and head circumference were calculated using NL reference charts (P^IARS; head circumference of P^LARS), WHO referen-

c

Follow-up
5 months

P^FARSB

Growth
• height: -4.1 Z → -3.4 Z
• weight: -5.0 Z → -4.4 Z

Development & brain
• global developmental delay →
stable
• mild loss of brain parenchyma,
prominent subarachnoid spaces,
mild ventricle dilation → stable

Head circumference
congenital and progressive
microcephaly
• -2.9 Z → -2.4 Z

Pulmonary function
bilateral alveolar airspace
disease → progressive

Liver function
liver failure → progressive
• cholestasis
• elevated transaminases
• portal hypertension

Gastro-intestinal
oral feeding and nasogastric
tube feeding → stable

Laboratory
• hypoalbuminemia requiring
infusions → unchanged
• intermittent asymptomatic
hypoglycemia → stable
• elevated INR, elevated liver
enzymes, cholestasis → stable

Infections
1 episode of bacteremia with
spontaneous bacterial peritonitis
→ no more infections

d

Follow-up
12 months

P^SARS

Growth
• height: -2.2 Z → -0.2 Z
• weight: -2.2 Z → -0.4 Z

Development
global developmental delay →
improved (WPPSI-IV: FSIQ ? → 63,
VCI ? → 50, VSI 69 → 85)

Head circumference
congenital and progressive
microcephaly
• -3.2 Z → -1.4 Z

Hearing
progressive sensorineural
deafness → stable

6

g

h

ce charts (P^FARSB), CDC reference charts (height and weight of P^LARS), and FR reference charts (P^SARS). CRP; C-reactive protein; FSIQ: Full-Scale Intelligence Quotient; G-tube: gastrostomy-tube; ILD: interstitial lung disease; FRI: fluid reasoning index; INR: international normalized ratio; LI: language index; PAP: pulmonary alveolar proteinosis; PEG: percutaneous endoscopic gastrostomy; PIQ: performance intelligence quotient; VIQ: verbal intelligence quotient; VCI: verbal comprehension index; VSI: visual-spatial index; WISC-V: Wechsler Intelligence Scale for Children, fifth edition;WPPSI-III/IV: Wechsler Preschool and Primary Scale of Intelligence, third/fourth edition.

e-h, growth charts: Z-scores of height, weight and head circumference for age.

Growth charts of height, weight, and head circumference in standard deviation score (Z) of **e**: P[IARS] (NL reference charts); **f**: P[LARS] (CDC reference charts for height and weight, NL reference charts for head circumference); **g**: P[FARSB] (WHO reference charts); and **h**: P[SARS] (FR reference charts). T in months from start of treatment.

---

symptoms improved. Similarly, during gastroenteritis and reduced amino acid intake, laboratory markers (albumin, coagulation) deteriorated (Table S3; T = 32 months). During treatment, P[IARS] experienced no infections requiring hospital admission, compared to five admissions two years prior. Growth improved (height: $-2.1Z^{NL}$ to $-1.0Z^{NL}$; weight: $-1.0Z^{NL}$ to $+0.1Z^{NL}$), and tube feeding could be stopped after 16 months (Fig. 2a/e). Periods without oxygen therapy increased in frequency and duration. Upon treatment, progression of ILD ceased as confirmed by computed tomography (CT) scans (Figure S3). P[IARS] became more energetic, interaction increased, and expressive speech and language skills improved according to professionals at school. Behavioral abnormalities became more apparent, and hindered repeat psychological testing. Although incomplete, Dutch Wechsler Intelligence Scale for Children, fifth edition (WISC-V-NL)[17] evaluation showed a disharmonic profile: fluid reasoning and processing speed were stronger (fluid reasoning index [FRI]: 82), compared to verbal understanding and working memory (verbal comprehension index [VCI]: 50).

P[LARS] was a 5-year-old girl with a history of pre/dysmaturity (Fig. 2f), failure to thrive requiring tube feeding, global developmental delay, anemia requiring repeated transfusions, neonatal cholestasis, liver disease, and frequent hospital admissions during infections (Fig. 2b). During nine months of protein fortification and erroneous isoleucine supplementation, she was not admitted to hospital, and was more energetic. Her weight improved, but not height (further deviation), nor head circumference (stable). Within one month after switching to leucine, her oral intake increased. Tube feeding became unnecessary after six months. Height increased from $-3.1Z^{CDC}$ to $-2.7Z^{CDC}$, weight further increased from $-2.4Z^{CDC}$ to $-1.6Z^{CDC}$, and microcephaly resolved from $-2.3Z^{NL}$ to $-1.6Z^{NL}$ (Fig. 2b/f). Liver transaminases, bilirubin, immunoglobulins, and liver ultrasound normalized. Teachers reported more interaction and an accelerated speech/language development; on neurologic examination, gross motor skills normalized, fine motor skills improved and muscle mass, tonus, and strength increased. Re-

cently, she suffered COVID-19 with flu-like symptoms, without derailing. Repeat neuropsychologic testing was delayed due to COVID-19 restrictions.

P$_{FARSB}$ was an 11-month-old boy. Pregnancy was complicated by intrauterine growth restriction and placental abruption. His phenotype was dominated by pre/dysmaturity (Fig. 2g), failure to thrive requiring nasogastric tube feeding and parenteral nutrition, hypoalbuminemia (with edema, ascites) requiring frequent albumin infusions, progressive liver failure, and lung disease (Fig. 2c). After starting treatment, liver function initially improved, as did growth in height (−4.5Z^{WHO} to −3.2Z^{WHO}), head circumference (−2.9Z^{WHO} to −2.4Z^{WHO}), and parental perception of psychomotor development (Fig. 2c/g). After three months, he developed esophageal variceal bleeding. Bleeding was stopped via octreotide and sclerotherapy, but hepatic encephalopathy and respiratory failure shortly ensued. His death was attributed to disease progression.

P$_{SARS}$ was a 5-year-old boy, fourth of five children born to consanguineous parents (first cousins). Symptoms involved dysmaturity (Fig. 2h), progressive sensorineural deafness, and moderate developmental delay (Fig. 2d). Three siblings with the same *SARS1* variants died following infections. One sibling without *SARS1* variants is clinically well. Before treatment, height, weight, and head circumference standard deviations of P$_{SARS}$ gradually decreased with age. After six months of treatment, height improved from −2.2Z^{FR} to −0.2Z^{FR} and microcephaly resolved from −3.2Z^{FR} to −1.4Z^{FR} (Fig. 2d, h). Development improved. Pretreatment, he had significant difficulties in receptive and expressive language, and none of the primary Wechsler Preschool and Primary Scale of Intelligence, fourth edition (WPPSI-IV)[18] subtests could be completed. After one year of treatment, the six primary and five additional subtests of the WPPSI-IV could be completed. While he scored below average on tests requiring sustained attention and working memory and exhibited attentional difficulties in everyday life (CBCL),[19] he scored within normal limits on tasks assessing spatial visualization and constructive skills, as well as logic and perceptual reasoning.

Figure 2a-d summarizes treatment effects. In all patients, treatment was well tolerated, and safety parameters remained stable (Tables S3-6).

Discussion

We report how clinical observations led to targeted studies in patient-derived fibroblasts, providing insight in the disease mechanism and a personalized treatment

strategy. Based on pronounced symptoms during the first year of life and episodes of intercurrent illness, we hypothesized that patient aminoacylation may suffice for cellular functions under normal conditions, but not during periods of increased translation (temporally and spatially controlled tissue formation, rapid growth in early life, illness) or decreased amino acid availability (starvation, vomiting), in particular when the cognate amino acid is essential. Indeed, patient fibroblast studies showed increased sensitivity to ARS-specific amino acid deprivation. Further contributing to deterioration during infections,[2] we evidenced strongly decreased aminoacylation activity for LARS1 and FARSB at feverish temperatures (38.5–40 °C). Variants that decrease protein stability decrease the temperature at which the protein unfolds. It is not possible to predict whether these variants result in unfolding of the protein around body temperature (as for P[LARS] and P[FARSB]). The effect of temperature on proteins with variants affecting dimerization (P[SARS]) and/or specific protein domains (P[IARS]) is even less predictable.

Motivated by these studies and because protein folds typically stabilize when bound to substrates, we initiated supplementation of the ARS-specific amino acid for individual patients with IARS1, LARS1, FARSB, and SARS1 deficiencies, with protein fortification for P[IARS] and P[LARS]. To prevent the ARS proteins from irreversible processes of unfolding, aggregation and degradation, we intensified treatment during infections, and advised strict antipyretic treatment. Furthermore, we provided an emergency protocol for triggers such as fasting, fever, and infections. This approach is radically different from the "high glucose, no protein" emergency treatment to avoid metabolic decompensations for other inherited metabolic diseases.

Overall, we found strikingly beneficial effects and good tolerance and safety. Most consistent was the improvement in growth (including head circumference) quickly after initiation of treatment (Fig. 2), leading to independency from tube feeding, improved development, and coping with infections. In addition, for P[IARS], oxygen dependency decreased and previously progressive pulmonary abnormalities stabilized, and for P[FARSB], liver function improved. The unstable FARS1 protein, as evidenced by severely reduced enzyme activity upon minimal increase over physiological temperature (Fig. 1h), may have contributed to the detrimental disease course in P[FARSB].

Because ARS deficiencies were only recently discovered, it is difficult to relate treatment effects to the natural disease course. One FARSB-, two IARS1-, and two SARS1-deficient patients reached adulthood and retained severe growth retardation, moderate-to-severe intellectual disability (IARS1/SARS1), restrictive lung disease (FARSB), and

liver dysfunction (IARS1/FARSB).[10,14,16] While protein fortification alone caused some improvements, the need for treatment with the corresponding amino acid was evidenced by improved effects after leucine instead of erroneous isoleucine supplementation in P$_{LARS}$, and by transient clinical deterioration during two-week delivery failure of isoleucine in P$_{IARS}$. Concordantly, total parenteral nutrition improved liver function of one MARS1-deficient patient,[20] as did protein fortification in LARS1 deficiency.[21] One IARS1-deficient patient thrived better upon high-caloric feeding, and isoleucine supplementation decreased susceptibility to infections.[10] Recently, protein fortification with methionine supplementation resulted in improved growth, pulmonary function and neurodevelopment in two MARS1-deficient patients.[22] These effects for different ARS deficiencies, and prompt onset after initiation suggest a true treatment effect.

In conclusion, we provide therapeutic recommendations for ARS deficiencies based on in vitro and in vivo evidence of beneficial effects of amino acid and protein supplementation (up to 2$^{2/3rd}$ years) in single patients. This affordable, accessible, and safe strategy holds the potential to improve outcomes for the expanding group of severe, often progressive, multiorgan ARS deficiencies. Although further research and validation for other ARS deficiencies are necessary, our in vitro studies in patient-derived cells may guide personalized therapeutic strategies.

6

References

1. Antonellis A, Green ED. The role of aminoacyl-tRNA synthetases in genetic diseases. A*nnu Rev Genomics Hum Genet*. 2008; 9: 87–107.

2. Fuchs SA, Schene IF, Kok G, et al. Aminoacyl-tRNA synthetase deficiencies in search of common themes. *Genet Med*. 2019; 21: 319–30.

3. Meyer-Schuman R, Antonellis A. Emerging mechanisms of aminoacyl-tRNA synthetase mutations in recessive and dominant human disease. *Hum Mol Genet*. 2017; 26: R114–27.

4. Kraulis PJ. MOLSCRIPT: a program to produce both detailed and schematic plots of protein structures. *J Appl Crystallogr*. 1991; 24: 947–50.

5. Merritt EA, Murphy MEP. Raster3D version 2.0 A program for photorealistic molecular graphics. *Acta Crystallogr D Biol Crystallogr*. 1994; 50: 869–73.

6. Schomburg D, Reichelt J. BRAGI: a comprehensive protein modeling program system. *J Mol Graph*. 1988; 6: 161–5.

7. Tseng LA, Sowerbutt C, Lee JJY, van Karnebeek CDM. P4 medicine for epilepsy and intellectual disability: nutritional therapy for inherited metabolic disease. *Emerg Top Life Sci*. 2019; 3: 75–95.

8. Müller AR, Brands MMMG, van de Ven PM, et al. The power of 1: systematic review of N-of-1 studies in rare genetic neurodevelopmental disorders. *Neurology*. 2021; 96: 529–40.

9. de Koning TJ. Amino acid synthesis deficiencies. *J Inherit Metab Dis*. 2017; 40: 609–20.

10. Kopajtich R, et al. Biallelic IARS mutations cause growth retardation with prenatal onset, intellectual disability, muscular hypotonia, and infantile hepatopathy. *Am J Hum Genet*. 2016; 99: 414–22.

11. Orenstein N, Murayama K, Janecke AR, et al. Bi-allelic IARS mutations in a child with intrauterine growth retardation, neonatal cholestasis, and mild developmental delay. *Clin Genet*. 2017; 91: 913–7.

12. Smigiel R, Biela M, Biernacka A, et al. New evidence for association of recessive IARS gene mutations with hepatopathy, hypotonia, intellectual disability and growth retardation. *Clin Genet*. 2017; 92: 671–3.

13. Zadjali F, Al-Yahyaee A, Al-Nabhani M, et al. Homozygosity for FARSB mutation leads to Phe-tRNA synthetase-related disease of growth restriction, brain calcification, and interstitial lung disease. *Hum Mutat*. 2018; 39: 1355–9.

14. Xu Z, Lo W-S, Beck DB, et al. Bi-allelic mutations in Phe-tRNA synthetase associated with a multi-system pulmonary disease support non-translational function. *Am J Hum Genet*. 2018; 103: 100–14.

15. Antonellis A, et al. Compound heterozygosity for loss-of-function FARSB variants in a patient with classic features of recessive aminoacyl-tRNA synthetase-related disease. *Hum Mutat*. 2018; 39: 834–40.

16. Musante L, Oprescu SN, Griffin LB, et al. Mutations of the aminoacyl-tRNA-synthetases SARS and WARS2 are implicated in the etiology of autosomal recessive intellectual disability. *Hum Mutat*. 2017; 38: 621–36.

17. Kaufman AS, Raiford SE, Coalson DL. Intelligent testing with the WISC-V. Hoboken, NJ, USA: John Wiley & Sons Inc; 2016: 683–702.

18. Wechsler D. Wechsler preschool and primary scale of intelligence. 4th edition. San Antonio, TX, USA: The Psychological Corporation; 2012.

19. Achenbach TM, Rescorla L. Manual for the ASEBA school-age forms & profiles: An integrated system of multi-informant assessment. Burlington, VT: Aseba; 2001.

20. van Meel E, Wegner DJ, Cliften P, et al. Rare recessive loss-of-function methionyl-tRNA synthetase mutations presenting as a multiorgan phenotype. *BMC Med Genet.* 2013; 14: 106.

21. Casey JP, Slattery S, Cotter M, et al. Clinical and genetic characterisation of infantile liver failure syndrome type 1, due to recessive mutations in LARS. *J Inherit Metab Dis.* 2015; 38: 1085–92.

22. Lenz D, Stahl M, Seidl E, et al. Rescue of respiratory failure in pulmonary alveolar proteinosis due to pathogenic MARS1 variants. *Pediatr Pulmonol.* 2020; 55: 3057–66.
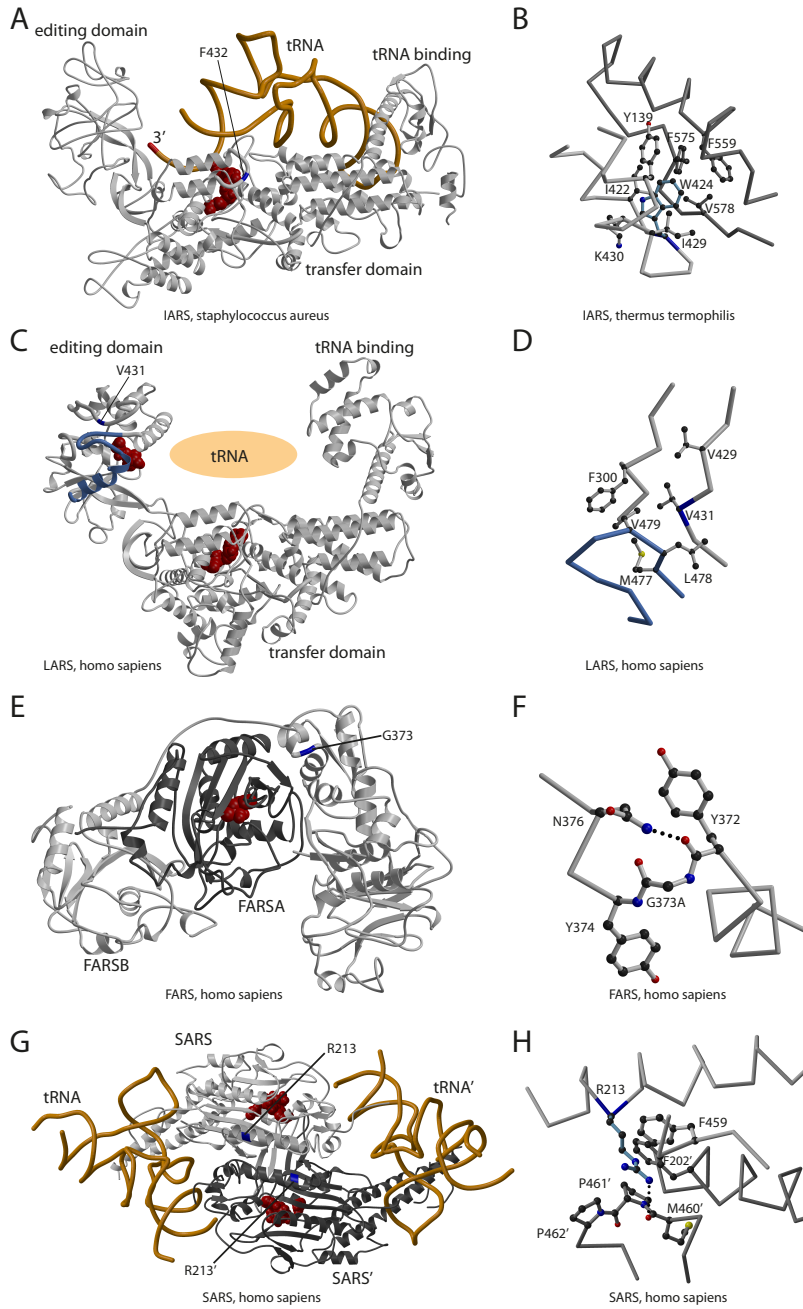
6

Acknowledgments

Supplementary text

Protein structure analyses

It is likely that the IARS1-variant p.Trp435Cys is destabilizing the hydrophobic core of the transfer domain and thereby impacting on catalytic activity. The frameshift variant in the second allele is expected to results in loss of functional protein (Figures S1A-B). The c.1503+3A>G variant in LARS1 is located in a splice site. Abolished splicing could cause an in-frame exon skip, which is incompatible with the normal protein fold. p.Val431 resides in the hydrophobic core of the editing domain and the variant p.Val431Asp is expected to destabilize the protein fold (Figures S1C-D). The variant c.3G>T in FARSB changes the start codon preventing normal initiation of translation. There are six out of frame ATGs prior to the first in frame ATG that codes for p.Met100. It is thus unlikely that the allele results in functional protein. The p.Gly373 forms a turn in the backbone of the protein. The constrains imposed by this turn can principally accommodate for an alanine, though they disfavor it. The stability of the protein fold is thus reduced by the variant p.Gly373Ala (Figures S1E-F). SARS1 forms a dimer, and p.Arg213 is located in the dimer interface. The homozygous variant p.Arg213Leu likely destabilizes dimer formation (Figures S1G-H).

6

Supplementary figures

A

editing domain   F432   tRNA   tRNA binding

3′

transfer domain

IARS, staphylococcus aureus

B

Y139   F575   F559
I422   W424   V578
K430   I429

IARS, thermus termophilis

C

editing domain   V431   tRNA binding

tRNA

LARS, homo sapiens   transfer domain

D

F300   V429
V479   V431
M477   L478

LARS, homo sapiens

E

G373

FARSA

FARSB

FARS, homo sapiens

F

N376   Y372
Y374   G373A

FARS, homo sapiens

G

SARS   R213
tRNA   tRNA′
R213′   SARS′

SARS, homo sapiens

H

R213   F459
F202′
P461′
P462′   M460′

SARS, homo sapiens

Fig. S1: Structural context of the variants.

For each transferase the full structure is shown in ribbon representation on the left and a detailed view of the local environment of the effected residue on the right. Residues effected by single nucleotide variants are highlighted in blue and are labelled. tRNA is shown in orange and bound small molecule ligands are shown as space filling model in red.

A, IARS1 from staphylococcus aureus bound to tRNA with Mupirocin (red) in the transfer domain. Phe432 corresponds to human p.Trp435.

B, IARS1 from thermus termophilis with p.Trp424 to human p.Trp435.

C, LARS1 from homo sapiens with 5'-O-(L-Leucylsulfamoyl)adenosine and 2'-(L-Norvalyl)amino-2'-deoxyadenosine bound to the transfer- and the editing domain, respectively. LARS is shown in the same in the same orientation as IARS in panel A. The binding site for tRNA is indicated. The light blue stretch indicated the missing residues in the c.1503+A>G variant if splicing is assumed to be affected.

D, Local environment of p.Val431.

E, The heterodimeric complex of FARSA and FARSB from homo sapiens shown in dark and light grey, respectively. Phenylalanine bound to FARSA is show in red.

F, Local environment of p.Gly373. The dotted line indicates a hydrogen bond.

G, Dimer of SARS1 from homo sapiens bound to tRNA. Serine and Phoshoaminophosphonic acid-adenylate ester shown in red are bound to the transfer site.

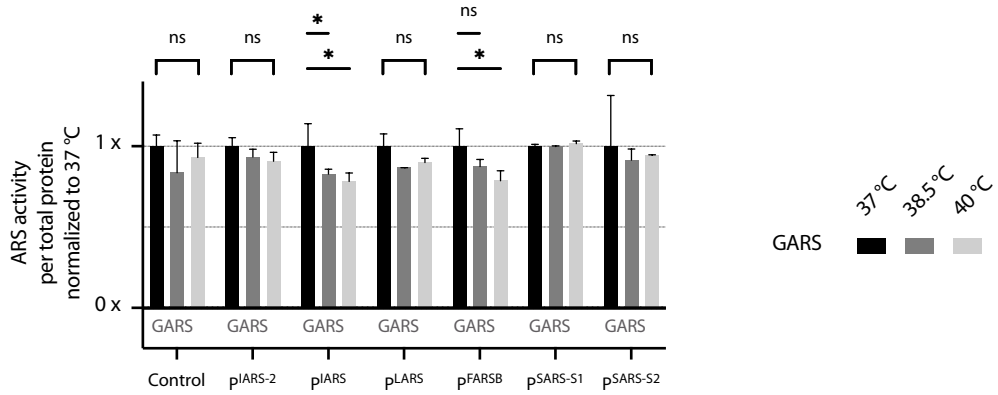**H**, Local environment of p.Arg213. The dotted line indicates a hydrogen bond.

Fig. S2: GARS1 activity is thermostable in patient and control fibroblasts.

GARS1 aminoacylation activity in fibroblasts of P[IARS], P[IARS-2], P[LARS], P[FARSB], and two siblings with the same homozygous variant as P[SARS] at 37, 38.5 and 40 °C. Data are presented compared to the enzymatic activity at 37 °C. All measurements were performed in triplicate (n=3). Error bars show standard deviation. Unpaired t-test: ns p ≥ 0.05, * p < 0.05, ** p < 0.01.

3 months	5 years and 6 months	6 years and 6 months	7 years and 6 months
	T = 0, start treatment	T = 12 months	T = 24 months
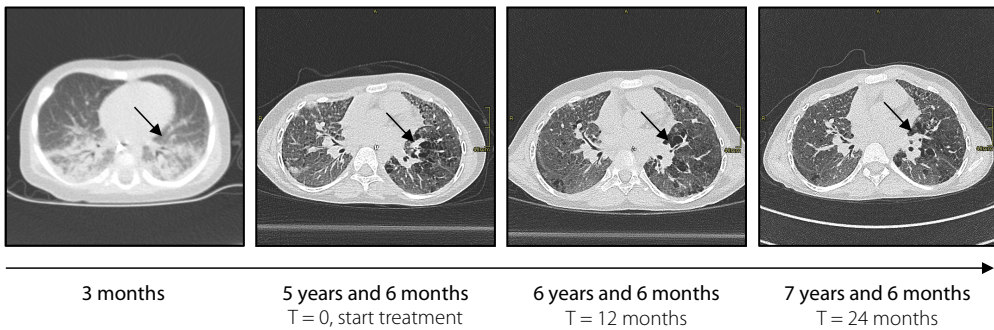
Fig. S3: high-resolution computed tomography (HRCT) chest scans of P[IARS].

From left to right: at age 3 months old, at start of treatment (T = 0), and after 1 year (T = 12), and 2 years (T=24) of treatment. Arrows indicate representative area of abnormalities. The first scan at age 3 months shows bilateral consolidations with some reticulation. The follow-up scans show ground glass changes throughout both lungs with paraseptal and subpleural thin-walled cysts and overall architectural disturbance of the lung. The abnormalities remained stable over the treatment period.

Supplementary tables

Table S1: treatment protocol for isoleucine supplementation and protein fortification (example for IARS-deficiency).

Table S2: clinical symptoms before treatment and treatment response in all treated patients.

Table S3: P^IARS: clinical details and effect of isoleucine and protein fortification treatment on outcome and safety parameters at different timepoints.

Table S4: P^LARS: clinical details and effect of leucine and protein fortification treatment on outcome and safety parameters at different timepoints.

Table S5: P^FARSB: clinical details and effect of phenylalanine supplementation treatment on outcome and safety parameters at different timepoints.

Table S6: P^SARS: clinical details and effect of serine and protein fortification treatment on outcome and safety parameters at different timepoints.

May be downloaded from doi.org/10.1038/s41436-021-01249-z.

SETTING THE STAGE FOR TREATMENT OF OTHER ARS DEFICIENCIES

Gautam Kok, Clara van Karnebeek, Sabine Fuchs

7

Recently, we described our experience with specific amino acid treatment in four patients with IARS1, LARS1, FARSB, and SARS1 deficiency.[1] Aminoacyl–transfer RNA (tRNA) synthetases (ARSs) are responsible for attaching amino acids to their cognate tRNAs. On discerning a common clinical phenotype for different ARS deficiencies, we hypothesized that deficiencies in these enzymes result in a common disease mechanism of insufficiently charged tRNA to keep up with protein synthesis, especially during periods of increased demand, such as infections and rapid growth.[2] We based our treatment strategy on this hypothesis and increased the availability of cognate amino acids to support residual enzymatic function and increase the quantity of amino acid–charged tRNA available for protein translation.

In general, patients benefited from the treatment with most striking effects on growth in height, head circumference, and development. The rapidly growing number of published studies on patients with ARS deficiencies underlines the dire need for a treatment strategy, preferably for all ARS deficiencies. Shen[3] recognized this need and made an attempt at reasoning which ARS deficiencies may and which may not respond to this treatment strategy. First, they speculated on the different classes of ARSs and the different functions of the various ARS enzymes in the multisynthetase complex (MSC). In mammals, the MSC consists of nine synthetases, including IARS1, LARS1, and MARS1 but not FARS(B) and SARS1.[4] Although the exact function of the MSC still requires elucidation, it is thought to have roles in cellular processes such as transcription, translational fidelity and efficiency, cell signaling, and tumorigenesis.[5,6]

Shen[3] proposed that treatment results may be related to MSC effects and may not only depend on the cognate amino acid but also on other amino acids as supplied with additional protein. Indeed, we supplemented the amino acid treatment with natural protein in our patients with IARS1 and LARS1 deficiency. This was also done in a patient with MARS1 deficiency.[6] In our cases, we chose to treat patients with additional protein because we noticed decreased cell viability in fibroblasts derived from patients with IARS1 deficiency on combined isoleucine and leucine deprivation (Fig. 1a). The patient with SARS1 deficiency was started on L-serine treatment and responded so well that further protein fortification was not prescribed. Because the patient with FARSB deficiency had severe liver failure, it was deemed too risky to treat this patient with protein fortification. None of the patients had deficiency of the specific amino acid in plasma before treatment. Similarly, plasma levels of the other amino acids (MSC and non-MSC ARS related) were normal before and after treatment in our patients.
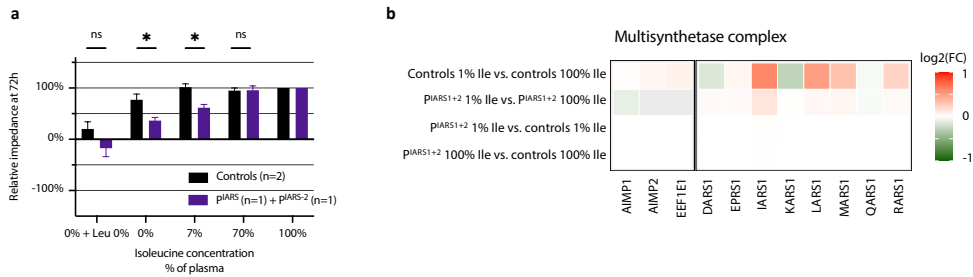
Fig. 1: **a**, IARS1 deficient patient fibroblasts display increased sensitivity to combined isoleucine and leucine deprivation. Proliferation of IARS1 deficient patient (n=2) and control (n=2) fibroblasts measured using an xCELLigence real-time cell analyzer; these data are supplemental to our previously reported Figure 1b.[1]

b, Multisynthetase complex genes are not differentially expressed when comparing IARS deficient patient fibroblasts with controls. mRNA expression of IARS1 deficient patient (n=2) and control (n=4) fibroblasts cultured for 72 hours at 1% or 100% isoleucine concentrations compared to average plasma. Analyses were performed in R (4.0.5) using package DeSeq2 (v1.30.1).

Analysis of messenger RNA sequencing results from dermal fibroblasts of our two patients with IARS1 deficiency and four healthy controls treated for 72 hours with 1% or 100% plasma isoleucine concentrations revealed no differential expression of the MSC genes (Fig. 1b). We previously selected 1% and 100% conditions as deficient and saturating in vivo peripheral tissue intracellular concentrations, respectively.[1] Although we recognize the importance of the MSC, we doubt that MSC is a strong determinant for treatment effects. We based our treatment strategy on a putative common disease mechanism on the basis of a common clinical phenotype that included both MSC ARSs (IARS1, LARS1, MARS1) and non-MSC ARSs (AARS1, YARS1).[2] In addition, we observed similarly beneficial effects of treatment in both patients with MSC deficiency and those with non-MSC synthetase deficiency.

After considering treatment effects for cytosolic ARS deficiencies, Shen[3] speculated on the use of amino acid supplementation for combined cytosolic and mitochondrial ARS deficiencies such as QARS1 deficiency. Although we only described treatment for cytosolic ARS (encoded by *ARS1 genes) deficiencies, we agree that the strategy of amino acid supplementation may also benefit mitochondrial translation. Indeed, we analyzed fibroblasts from 1 of our patients with QARS1 deficiency and detected in-

creased sensitivity of this patient's fibroblasts to glutamine depletion. Consequently, we treated this 8-year-old boy with L-glutamine over the past year with preliminary positive results. Although Shen et al[3,7] warn of potential epileptic effects of L-glutamine treatment in QARS1 deficiency, we observed less epilepsy upon treatment. It remains difficult to directly relate epilepsy severity to the treatment in this patient because he also experienced episodic deteriorations and improvements before the treatment. Nevertheless, after increasing the L-glutamine dosage, the patient was, for the first time in his life, seizure-free for five consecutive weeks. His behavior also changed. He became more alert and open to the environment. Yet, he remains severely disabled. His feeding problems improved with significantly less vomiting, but growth (height, weight, and head circumference) has not improved as of yet. Further follow-up and treatment of other patients will increase our insights in treatment effects, which may vary between patients and pathogenic variants.

Shen[3] further described their experience in treating mitochondrial RARS2 deficiency with arginine. At the time of writing, we were also treating various patients with mitochondrial ARS2 deficiencies and developing in vitro analyses to predict treatment effects. We will soon report our findings separately. Collectively, we hope these studies will improve prospects for the increasingly recognized group of patients with ARS deficiencies.

References

1. Kok G, Tseng L, Schene IF, et al. Treatment of ARS-deficiencies with specific amino acids. *Genet Med*. 2021; 23: 2202-2207.

2. Fuchs SA, Schene IF, Kok G, et al. Aminoacyl-tRNA synthetase deficiencies: in search of common themes. *Genet Med*. 2019; 21: 319-330.
(Published correction appears in *Genet Med*. 2021; 23: 2024))

3. Shen Y-W. Correspondence on "Treatment of ARS deficiencies with specific amino acids" by Kok et al. *Genet Med*. 2022; 24: 503-505.

4. Rubio Gomez MA, Ibba M. Aminoacyl-tRNA synthetases. *RNA*. 2020; 26: 910-936.

5. Perona JJ, Gruic-Sovulj I. Synthetic and editing mechanisms of aminoacyl-tRNA synthetases. in: Aminoacyl-tRNA Synthetases in Biology and Medicine. *Curr Chem*. 2014: 344; 1-41.

6. Lenz D, Stahl M, Seidl E, et al. Rescue of respiratory failure in pulmonary alveolar proteinosis due to pathogenic MARS1 variants. *Pediatr Pulmonol*. 2020; 55: 3057-3066.

7. Shen YW, Zou LP. Correspondence on "Aminoacyl-tRNA synthetase deficiencies: in search of common themes" by Fuchs et al. *Genet Med*. 2021; 23: 587-588.

7

AMINO ACID TREATMENT FOR MITOCHONDRIAL ARS2 AND QARS1 DEFICIENCIES

Irena Muffels, Gautam Kok, Ziqin Tang, Wilbert Vermeij, Marisa Mendes, Gajja Salomons, Desiree Smith, Holger Rehmann, Richard Rodenburg, Kimberly Smit, Richard van Jaarsveld, Marie-José van den Boogaard, Saskia Hopman, Peter van Hasselt, Shanti Balasubramaniam, Shekeeb Mohammad, Annet Bosch, Edward Nieuwenhuis, Klaas Koop, Sabine Fuchs

8

Abstract

Background

Aminoacyl-tRNA synthetases (ARS) facilitate loading of transfer RNAs (tRNAs) with their cognate amino acids in the cytosol (ARS1), mitochondria (ARS2), or both (dual ARS). ARS deficiencies cause heterogeneous, severe and life-threatening disease, although underlying pathophysiological mechanisms may differ. Supplementing corresponding amino acids has proven an effective treatment for several ARS1 deficient patients, but this has not been tested for ARS2, dual ARS and QARS1 deficiencies.

Methods

To mimic treatment response, we challenged fibroblasts derived from ARS2, QARS1 and dual ARS deficient patients with varying amounts of the ARS-specific amino acids. We further performed seven n=1 trials with specific amino acid supplementation in patients with QARS1, AARS2 and VARS2 deficiencies.

Results

Fibroblasts of ARS2, QARS1 and dual ARS – but not ARS1 – deficient patients show mitochondrial dysfunction during amino acid deprivation, illustrated by decreased membrane potential, decreased basal- and maximal respiratory capacity. In QARS1 and dual ARS – but not ARS2 – deficiencies, amino acid deprivation decreased proliferation.

Glutamine treatment in P1[QARS1] decreased seizure frequency and gastrointestinal symptoms, and improved unaided walking ability in P2[QARS1]. Neurological symptoms of P1[QARS1] and P2[QARS1] improved, although both patients remained severely neurologically impaired. During valine treatment, cardiomyopathy resolved in P3[VARS2]. Amino acid treatment was well tolerated.

Discussion

Our in vitro studies reveal that for ARS2, QARS1 and dual ARS deficiencies, mitochondrial function depends on the availability of the ARS-specific amino acids. Treatment of patients with the cognate amino acid could potentially improve clinical symptoms. More extensive clinical studies are required to determine treatment effect.

———

Introduction

Aminoacyl-tRNA synthetases (ARS) are essential for translating messenger RNA (mRNA) to protein by coupling amino acids to their cognate transfer RNAs (tRNAs). ARS1 enzymes work for cytosolic translation, ARS2 enzymes for mitochondrial translation, and glycyl-ARS (GARS1) and lysyl-ARS (KARS1) for both. The clinical phenotype of patients with ARS deficiencies depends on the cellular location and type of ARS that is affected.[1–4]

In ARS1 deficient patients, aminoacylation generally suffices in homeostatic conditions, but falls short during increased translational demands (rapid growth, illness) or decreased amino acid availability (starvation, vomiting).[5] In fibroblasts of ARS1 deficient patients, we found that low cognate amino acid concentrations were detrimental for cellular growth. Therefore, we decided to treat patients with the ARS-specific amino acids,[5] resulting in significant clinical improvements in growth, head circumference, development, gastrointestinal- and pulmonary symptoms.[5–7]

The regulation of mitochondrial translation differs from the regulation of cytosolic translation.[8] Hence, it is expected that the cellular response to amino acid variations is different for patients with cytosolic and mitochondrial ARS deficiencies. For example, mitochondria could use the supplemented amino acids to fuel the TCA cycle instead of supporting mitochondrial translation.

Therefore, motivated by the successful treatment of cytosolic ARS1 deficient patients, we here investigate the effects of amino acid supplementation in dual ARS and mitochondrial ARS2 deficiencies.

Materials and methods

Patient inclusion

Patients with bi-allelic variants in *ARS* genes were recruited from the Wilhelmina Children's Hospital, Utrecht, The Netherlands. Genetic variants were identified using Whole Exome Sequencing, performed as described previously.[10]

Part 2

Amino acid supplementation

Supplementation protocols, including dosing strategy, safety assessment and out-come parameters are available in File S2.

Fibroblast cultures

Fibroblasts were obtained from forearm skin biopsies and cultured in Ham's F-12 supplemented with 10% Fetal Bovine Serum (FBS) and 1% penicillin–streptomycin (PS). For amino acid sensitivity experiments, amino acid free DMEM/F-12 with HEPES and $NaHCO_3$ (US Biological) was supplemented with 1% PS, 1% GlutaMAX (Gibco), 10% dialyzed FBS (ThermoFisher) and amino acids. For amino acid sensitivity tests, patient- and healthy donor derived fibroblasts were treated with the specific amino acid as compared to normal plasma concentrations, indicated as 100% (L-Valine 223 µmol/L, L-Alanine 350 µmol/L, L-Glutamine 541 µmol/L, L-Lysine 129 µmol/L) and in deprivation conditions (1% or 5% of the 100% condition).

Aminoacylation measurements

Aminoacylation measurements were performed as previously described,[5] with $^{13}C_5$ Gln and D_4 Lys as substrates, and D_3 Glu and $^{13}C_6$ Arg as internal standard.

Seahorse MitoStressTest

Cultured fibroblasts were plated at 10.000 cells/well in Seahorse XF24 V7 Cell Cul-ture Microplates (Agilent) and treated with the desired amino acid concentrations for 48 hours. Afterwards, cells were incubated with Seahorse XF DMEM Medium (Agilent) for 1 hour in a non-CO_2 incubator. Mitochondrial respiration was measured as oxygen consumption rate (OCR) using the Seahorse XFe24 Extracellular Flux Assay Kit (Mito Stress Test, Agilent) and XFe24 Seahorse Analyzer (Agilent) with 1 µM oligomycin, 1.5 µM FCCP, 1 µM Rotenone (All MedChemExpress) and 1 µM antimycin A (Sigma) fol-lowing manufacturer's protocol and with three or four technical replicates per condition-on.[11] After analysis, nuclei were stained with Hoechst 33342 (1:1000, Thermo Fisher Scientifics), visualized with Leica Thunder Live Imager (Leica Microsystem) with inten-sive computational clearance method, and counted using ImageJ v1.53o (NIH) for data normalization.

Membrane potential and mitochondrial mass/swelling

Fibroblasts were incubated with Tetramethylrhodamine, methyl ester (TMRM, Sigma) (30 nM) in Hank Balanced Salt Solution (HBSS, Gibco) for 35 minutes. To assess TMRM background, Carbonyl cyanide-p-trifluoromethoxyphenylhydrazone (FCCP, Sigma) (3 μM) was added during the final 5 minutes in 50% of the wells. Cells were harvested using TrypLE and visualized using the Amnis Imagestream Mk II (Luminex).

Cell proliferation

Cell proliferation was measured using a real-time-cell-analyzer (xCELLigence MP) as described previously.[5]

Northern blot

Healthy and QARS1 deficient fibroblasts were cultured in normal media or with 1% glutamine. Mitochondria were isolated as described previously.[12] After isolation, mitochondria were incubated at 70 °C in lysis buffer (1% SDS, 10 mM EDTA,10 mM Tris-HCl (pH 7.4)) and at 37 degrees with proteinase K to inhibit RNase activity. Mitochondrial RNA was isolated using Trizol LS following manufacturer's protocol and stored at -80 °C until use.

RNA isolated from mitochondria was diluted in 2x RNA loading dye (8M urea, 0.1M NaOAc/HOAc pH 4.8, 0.05% bromophenol blue, 0.05% xylene cyanol) and 500 ng was loaded on a 12% acid-urea gel (8M urea, 12% acryl-:bisacrylamide 29:1, 1x TBE, 0.1M NaOAc/HOAc pH 4.8, 0.01% APS, 0.004% TEMED). Gelelectrophoresis was performed in 1x acid TAE (0.1M NaOAc/HOAc pH 4.8) running buffer at 200 V for 30 min. RNA was transferred to a Hybond-XL membrane (GE Healthcare) in 1x electrophoretic transfer buffer (6 mM trisodium citrate, 8 mM sodium phosphate, dibasic (Na_2HPO_4)) at 350 mA for 2 hours. The membrane was crosslinked by baking at 80 °C for 2 hours, pre-hybridised for 5 min with PerfectHyb Plus (Sigma) at 68 °C, then incubated with 3 nM 5'biotin-tRNA$^{Gln(CTG)}$ probe (SEQ) in 5 mL PerfectHyb Plus at 68 °C overnight. The membrane was washed with low stringency wash buffer, incubated with Streptavidin-HRP (1:1000, Genscript) in 5 mL PerfectHyb Plus for 1 hour at room temperature, then washed again in low stringency wash buffer. Chemiluminescence was measured using SuperSignal West Dura (Thermo Fisher) following manufacturer's protocol on a ChemiDoc Imaging System (Bio-Rad).

Statistical analyses

Imagestream data analysis was performed using IDEAS software (version 6.2, Amnis). Seahorse data was analyzed using Agilent Wave software (version 2.6, Agilent). Statistical analyses were performed in Prism (Version 9.3.0, GraphPad Software) with α = 0.05. Welch's T-test was used to compare basal and maximal respiratory capacity between healthy controls and patients. Student's T-test was used to compare membrane potential in healthy controls to patients treated with 1% of amino acid concentrations. Mann Whitney U-test was used to compare relative cellular growth in patients to healthy controls during amino acid deprivation.

Results

Eight patient-derived fibroblast cultures were included in this study (Table S1). We determined pathogenicity of ARS genetic variants prior to inclusion (File S1). For the twins with VARS2 genetic variants, we could not reliably determine pathogenicity.

Amino acid deprivation causes mitochondrial dysfunction in mitochondrial ARS2 deficiencies

Specific amino acid deprivation reduced basal and maximal respiration in fibroblasts of AARS2, VARS2, KARS1 and QARS1 deficient patients but not in controls (Figure 1a-e, File S3). In addition, all patient-derived fibroblasts had significantly decreased mitochondrial membrane potential during amino acid deprivation (Figure 1g).

AARS2 deficient fibroblasts shifted towards glycolytic ATP production during amino acid deprivation, while VARS2 and QARS1 deficient fibroblasts only modestly upregulated glycolytic ATP production. KARS1 deficient fibroblasts had severely reduced oxidative phosphorylation, resulting in increased glycolysis in both normal and deprivation conditions (Figure 1a,f).

Since we could not verify pathogenicity of *VARS2* genetic variants, we assessed whether valine deprivation-induced mitochondrial dysfunction was specific for VARS2 deficient fibroblasts. Indeed, we found no effect on mitochondrial function of valine depletion in fibroblasts from patients with other mitochondrial diseases (Figure 1c, File S3).

QARS1 might aid mitochondrial translation

Glutamine deprivation caused caused mitochondrial dysfunction in QARS1 deficient fibroblasts, but not in other ARS1 deficient fibroblasts (Figure 1a-d, g). We hypothesized that QARS1 might aid mitochondrial translation via import of $tRNA^{Gln}$. To test this, we used northern blotting to determine if cytosolic $tRNA^{Gln}$ was present in mitochondria. We found that in healthy fibroblasts, $tRNA^{Gln}$ was present in mitochondria both in normal and glutamine deprivation conditions, whereas in $P1^{QARS}$ and $P2^{QARS}$ there was no import of $tRNA^{Gln}$ in either condition.

Impaired growth upon amino acid deprivation in QARS1 and dual ARS deficiencies

During amino acid deprivation, proliferation of KARS1 and QARS1 deficient fibroblasts was significantly decreased. However, this was not seen in ARS2 deficient fibroblasts. (Figure 2a).

Clinical outcomes of amino acid supplementation

Five of eight patients received treatment with the ARS-specific amino acids. The KARS1 deficient patient died before treatment initiation, and the AARS2 deficient patients only recently started treatment. Amino acid supplementation was well tolerated in all patients (File S4). Growth parameters in VARS2 deficient patients were between -1 and -2 SD before treatment initiation, and were not affected by treatment (File S5).

VARS2 deficient patients

At the age of one month, twin brothers $P1^{VARS2}$ and $P2^{VARS2}$ were admitted to the hospital due to severe agitation, feeding difficulties and seizures. At the age of five months, their seizures and encephalopathy worsened, resulting in a palliative trajectory. In the weeks following, their symptoms stabilized spontaneously as their seizure frequency decreased. Valine treatment was initiated four months after symptom-stabilization. After valine supplementation, fenobarbital could be stopped, and the patients were less agitated, more comfortable, and made better contact with parents. However, patients did not reach any new developmental milestones, continued to show seizures - albeit decreased in frequency - and still showed severe axial hypotonia and spastic tetraparesis.
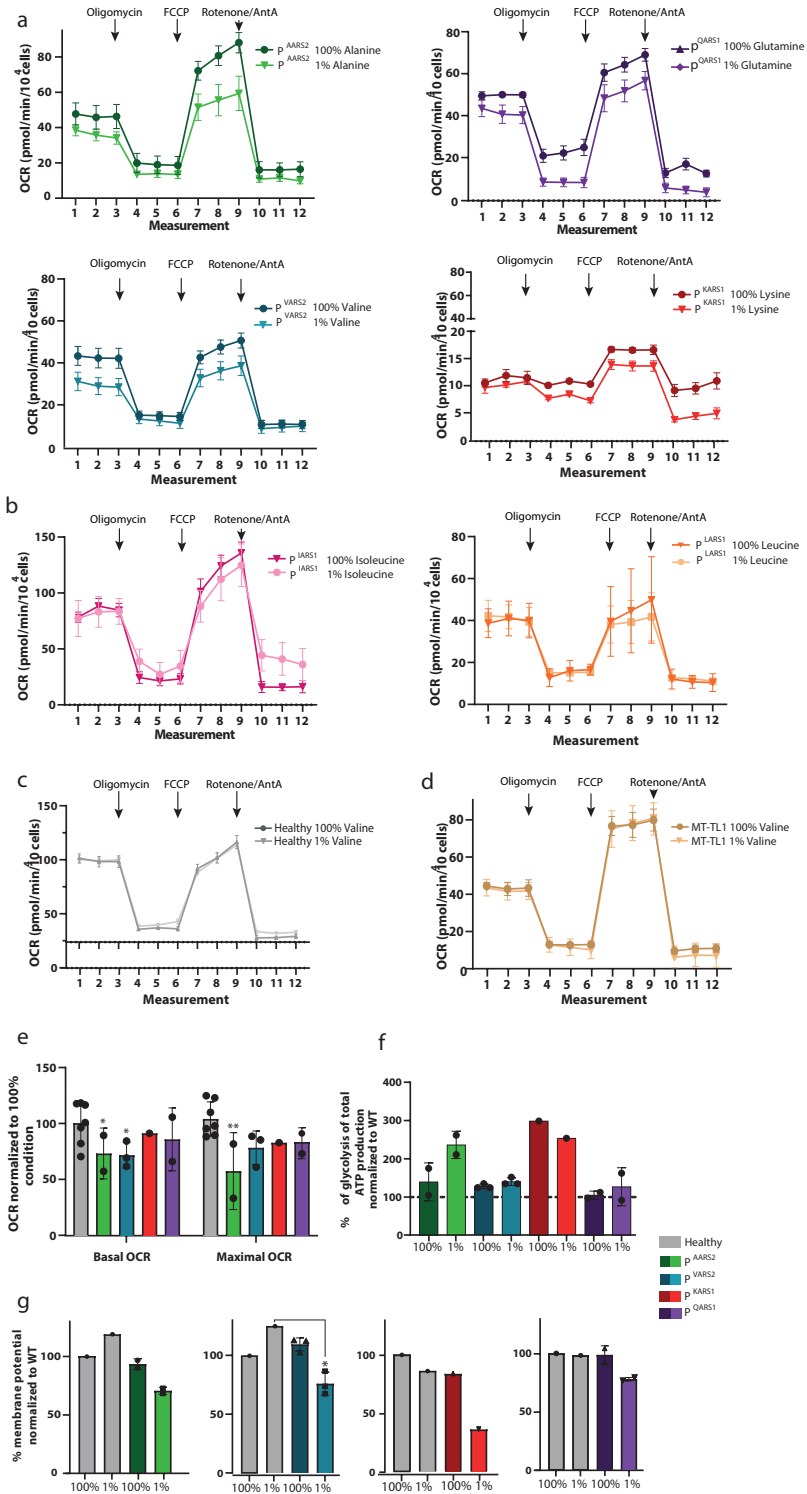
8

Fig. 1: ARS2 and dual ARS deficiency patients show mitochondrial dysfunction during amino acid deprivation (1% of plasma).

a, Oxygen Consumption Rate (OCR; Y-axis) for each measurement (X-axis) with the injection of different compounds (Oligomycin, FCCP, Rotenone/AntimycinA, dotted lines) in ARS2 and dual ARS deficient patient fibroblast lines for blood plasma amino acid concentration (indicated at 100%) and amino acid deprivation (indicated as 1%). All patients show a significant reduction of oxygen consumption rates during deprivation (1%) conditions. The dots represent the average of all donors and technical replicates combined. Error bars represent SEM. **b**, OCR of cytosolic IARS1 and LARS1 deficient fibroblasts with treated with 100% and 1% isoleucine and leucine, respectively, for 2 days. **c**, OCR of healthy fibroblasts lines treated with 100% valine and 1% valine for 2 days. One representative healthy control is shown. **d**, OCR of a mitochondrial disease patient with a MT-TL1 m.3243A>G mutation treated with 100% valine and 1% valine for 2 days. **a-d**, Dots represent the average of technical replicates. The error bars represent SEM. **e**, Bar graphs showing the basal and maximal OCR of healthy controls, ARS2 and dual ARS deficiency patients. The OCR values of the 1% condition are normalized to the 100% condition of the same donor. The bars represent the mean percentage of all donors combined ±SD, the dots represent the mean percentage of all technical replicates per donor. Welsch T-test (ns $p>0.05$, * $p<0.05$, ** $p<0.01$) was used to compare all technical replicates. For the healthy control, the dots represent the mean per donor per individual condition (1% alanine, 1% valine, 1% glutamine and 1% lysine). The bar represents the mean of all healthy donors and all conditions combined. **f**, ATP from glycolysis, compared to healthy donors under similar conditions. ATP produced from glycolysis was calculated using PER. Total ATP production represents mitochondrial plus glycolytic ATP production. Mitochondrial ATP production was calculated using the OCR values derived from the basal respiration (first three) measurements of the experiments in **a**. Bars represent mean percentage of biological replicates compared to healthy controls ± standard deviation (SD). **g**, Mitochondrial membrane potential during 1% and 100% conditions. In the patients, the bars represent membrane potential normalized to healthy controls treated with the same condition. In the healthy control, the 1% condition is normalized to the 100% condition of the healthy control. The 1% condition of healthy controls was compared to the 1% of each group of patients (Students T-test, $p>0.05$ ns, $p<0.05$ *). In the KARS1 patient, a t-test was not applied since there was only one patient.

Two days after birth, P3VARS2 was diagnosed with laryngomalacia, for which she was admitted to the hospital. She developed cardiomyopathy, lactic acidosis and respiratory insufficiency after dexamethasone infusion, requiring mechanical ventilation. Brain MRI showed a thalamic infarction in the right hemisphere. At the age of one month, valine supplementation (25 mg/kg/day) was briefly administered but feeding difficulties limited her intake. As her condition worsened, a palliative trajectory was initiated, and valine supplementation was stopped. At the age of three months, her symptoms stabilized, when her intake improved and her laryngomalacia disappeared. At the age of four months valine supplementation (60 mg/kg/day) was reinitiated. One month later, protein fortification was added (22.5g protein/day). Since then, her condition has significantly improved; her cardiac hypertrophy completely resolved. She never developed microcephaly or epilepsy, and reached all developmental milestones at a normal age.

QARS1 patients

P1QARS1 presented with severe developmental delay, seizures and daily vomiting, possibly of epileptic origin. Glutamine treatment was started at the age of seven years. His vomiting frequency decreased to once a week, and his seizure frequency dropped from 40 to five episodes per day. He experienced his first seizure-free interval of five weeks. He has become more alert, makes better contact, seems happier and laughs more, although his development did not improve significantly. The course of his infections is milder, with less apathy and seizures, and fewer hospital admissions. His constipation improved, and he stopped using laxatives. His growth parameters remained stable with glutamine treatment (Figure S4).

P2QARS1 presented at the age of seven months with focal febrile status epilepticus triggered by viral infections.[13] Additionally, she showed delayed development, short stature, microcephaly and failure to thrive. With carbamazepine treatment she became seizure-free. At four years of age, glutamine supplementation was initiated. Since initiation of glutamine (without any change in carbamazepine dose), she remained seizure-free without epileptiform activity on EEG. Her unaided walking ability improved from 5 to 1000 meters, her axial hypotonia improved, and she makes better eye contact. Her height, weight and head circumference remained stable with glutamine treatment (Figure S4).
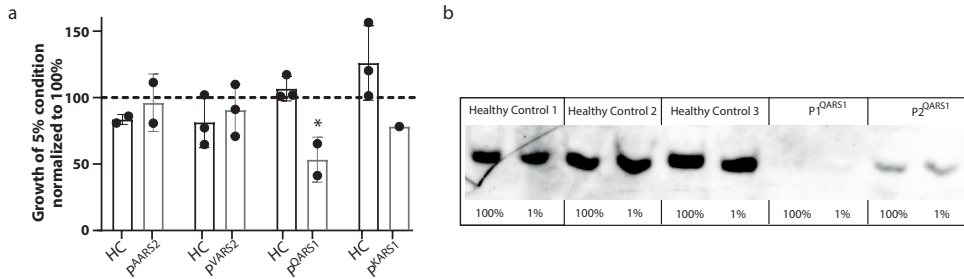
Fig. 2: **a**, Real-time-cell-analyzer results of ARS2 and dual ARS deficiency patients. Relative impedance as measure for cell proliferation after 72 hours of culture with 5% of the ARS specific amino acid. Bars represent mean of biological replicates ± standard deviation (SD). Dots represent mean values of all technical replicates of individual donors. Mann Whitney U test (* p < 0.05). **b**, Northern blot. Each lane was loaded with 500 ng of RNA isolated from mitochondria of healthy and QARS1 deficient fibroblasts treated with 100% or 1% glutamine for 2 days. Bands display cytosolar tRNA$^{Gln(CTG)}$.

Discussion

Specific amino acid deprivation triggers significant mitochondrial dysfunction in fibroblasts of mitochondrial ARS2, dual ARS and QARS1 deficient patients. To prevent mitochondrial dysfunction and subsequent clinical deterioration, we treated VARS2 and QARS1 deficient patients with cognate amino acids. Amino acid supplementation was well-tolerated and safe. Supplementation had variable clinical effects, but was not able to reverse neurological damage.

QARS1 was previously recognized as a dual ARS. However, QARS1 does not have a mitochondrial import sequence and is not present in mitochondria. Therefore, it is now considered a cytosolic ARS1 enzyme.[14] Instead, glutaminyl mt-tRNA (mt-tRNA^{Gln}) in mitochondria is aminoacylated by an indirect pathway, by the glutamyl-tRNA^{Gln} amidotransferase protein complex, that transamidates Glu-mt-tRNA^{Gln} into Gln-mt-tRNA^{Gln}.[15] However, charged cytosolic tRNA^{Gln} has been identified in mammalian mitochondria in vitro,[16] which suggests that under certain conditions, cytosolic tRNA^{Gln} can be imported in mitochondria to aid translation. With northern blot, we found QARS1 deficient patients had significantly decreased import of cytosolic tRNA^{Gln} into their mitochondria, which might explain their mitochondrial dysfunction, as cytosolic

tRNA^{Gln} cannot be used to aid mitochondrial translation. However, cytosolic tRNA^{Gln} import was similar in normal and deprivation conditions, and therefore cannot solely explain the mitochondrial dysfunction that worsens during deprivation conditions. Therefore, additional studies are needed to explore the regulation and mechanism of cytosolic tRNA^{Gln} import into mitochondria, and how that effects mitochondrial function.

All VARS2 deficient patients showed clinical improvement before valine treatment initiation, which made it difficult to distinguish natural course from treatment effects in our cohort. However, while most reported VARS2 deficient patients generally have a progressive disease course,[2] all of our VARS2 deficient patients showed clinical improvements, although P1^{VARS2} and P2^{VARS2} remained severely neurologically impaired. The difference in treatment response may relate to the high variability in valine intake prior to supplementation, the timing of treatment initiation and the primarily affected organ. Additionally, pathogenicity of the VARS2 genetic variant could not be established. Disease severity and exogenous triggers may also affect treatment response. Larger studies are thus needed to identify factors that influence treatment response, and to discriminate treatment effects from natural disease course.

We suspect that the clinical deterioration of all patients was caused by feeding difficulties in combination with high demand for amino acid, leading to a decrease in (local) amino acid availability. Our fibroblast studies confirm this correlation between amino acid availability and mitochondrial function, suggesting that amino acid supplementation could affect mitochondrial translation directly. Amino acid supplementation may thus represent a novel treatment strategy for ARS2, QARS1 and dual ARS deficiencies, to prevent decreased amino acid availability and subsequent mitochondrial dysfunction. For robust treatment effect analysis, amino acid supplementation should be validated on a larger scale and weighed against the natural disease course in a randomized controlled manner. In these studies, it is critical to establish the diagnosis timely and initiate treatment as soon as possible, to prevent the occurrence of (irreversible) damage.

References

1. Konovalova S & Tyynismaa H. Mitochondrial aminoacyl-tRNA synthetases in human disease. *Mol Genet Metab*. 2013; 108: 206-211.

2. Bruni F, Di Meo I, Bellacchio E, et al. Clinical, biochemical, and genetic features associated with VARS2-related mitochondrial disease. *Hum Mutat*. 2018; 39: 563-578.

3. Fuchs SA, Kok G, Schene IF, et al. Aminoacyl-tRNA synthetase deficiencies: in search of common themes. *Genet Med*. 2019; 21: 319-330.

4. Botta E, Theil AF, Raams A, et al. Protein instability associated with AARS1 and MARS1 mutations causes trichothiodystrophy. *Hum Mol Genet*. 2021; 30: 1711-1720.

5. Kok G, Tseng L, Schene IF, et al. Treatment of ARS deficiencies with specific amino acids. *Genet Med*. 2021; 23: 2202-2207.

6. Lenz D, Stahl M, Seidl E, et al. Rescue of respiratory failure in pulmonary alveolar proteinosis due to pathogenic MARS1 variants. *Pediatr Pulmonol*. 2020; 55: 3057-3066.

7. Hadchouel A, Drummond D, Pontoizeau C, et al. Methionine supplementation for multi-organ dysfunction in MetRS-related pulmonary alveolar proteinosis. *Eur Respir J*. 2022; 59: 2101554.

8. Koripella RK, Sharma MR, Haque ME, et al. Structure of Human Mitochondrial Translation Initiation Factor 3 Bound to the Small Ribosomal Subunit. *iScience*. 2019; 12: 76-86.

9. Hewton KG, Johal AS, Parker SJ. Transporters at the interface between cytosolic and mitochondrial amino acid metabolism. *Metabolites*. 2021; 11: 1-28.

10. Muffels IJJ, Wiame E, Fuchs SA, et al. NAA80 bi-allelic missense variants result in high-frequency hearing loss, muscle weakness and developmental delay. *Brain Commun*. 2021; 3: fcab256.

11. Milanese C, Bombardieri CR, Sepe S, et al. DNA damage and transcription stress cause ATP-mediated redesign of metabolism and potentiation of anti-oxidant buffering. *Nat Commun*. 2019; 10: 4887.

12. Preble JM, Pacak CA, Kondo H, et al. Rapid isolation and purification of mitochondria for transplantation by tissue dissociation and differential filtration. *J Vis Exp*. 2014; 91: e51682.

13. Chan DL, Rudinger-Thirion J, Frugier M, et al. A case of QARS1 associated epileptic encephalopathy and review of epilepsy in aminoacyl-tRNA synthetase disorders. *Brain Dev*. 2022; 44: 142-147.

14. Friederich MW, Timal S, Powell CA, et al. Pathogenic variants in glutamyl-tRNA^{Gln} amidotransferase subunits cause a lethal mitochondrial cardiomyopathy disorder. *Nat Commun*. 2018; 9: 4065.

15. Nagao A, Suzuki T, Katoh T, Sakaguchi Y, Suzuki T. Biogenesis of glutaminyl-mt tRNA^{Gln} in human mitochondria. *Proc Natl Acad Sci U S A*. 2009; 106: 16209-16214.

16. Rubio MAT, Rinehart JJ, Krett B, et al. Mammalian mitochondria have the innate ability to import tRNAs by a mechanism distinct from protein import. *Proc Natl Acad Sci U S A*. 2008; 105: 9186-9191.

17. Shen Y-W. Correspondence on "Treatment of ARS deficiencies with specific amino acids" by Kok et al. *Genet Med*. 2022; 24: 503-505.

8

Acknowledgements

The authors thank the Oncode Institute for allowing use of the Seahorse equipment.

Supplementary figures

Figure S1: seahorse and membrane potential measurements in ARS1 deficient patients, healthy controls and patients with mitochondrial disease.

Figure S2: laboratory parameters before and after amino acid treatment in patients.

Figure S3: growth parameters of VARS2 patients before and after amino acid treatment.

Figure S4: growth parameters of QARS1 patients before and after amino acid treatment.

Will be available for download after publication.

Supplementary tables and files

Table S1: clinical characteristics of patients with ARS deficiencies.

File S1: pathogenicity predictions of *VARS2*, *AARS2*, *QARS1* and *KARS1* genetic variants.

File S2: treatment protocol.

Will be available for download after publication.

8

SARS1 VARIANTS IN CHILDREN WITH NEURODEVELOPMENTAL DELAY, DEAFNESS, CARDIOMYO-PATHY, AND DECOMPENSATION DURING FEVER

Jean-Marie Ravel, Natacha Dreumont, Pauline Mosca, Desiree Smith, Marisa Mendes, Arnaud Wiedemann, David Coelho, Emmanuelle Schmitt, Jean-Baptiste Rivière, Frédéric Mau-Them, Julien Thevenon, Paul Kuentz, Marc Polivka, Sabine Fuchs, Gautam Kok, Christel Thauvin-Robinet, Jean-Louis Guéant, Gajja Salomons, Laurence Faivre, François Feillet

Abstract

Aminoacyl-tRNA synthetases (ARS) are ubiquitously expressed enzymes responsible for ligating amino acids to their cognate tRNA molecules through an aminoacylation reaction. The resulting aminoacyl-tRNA is delivered to ribosome elongation factors to participate in protein synthesis. Seryl-tRNA synthetase (SARS1) is one of the cytosolic ARSs and catalyzes serine attachment to tRNA^{Ser}. SARS1 deficiency has already been associated with moderate intellectual disability, ataxia, muscle weakness, and seizure in one family. We describe here a new clinical presentation including developmental delay, central deafness, cardiomyopathy, and metabolic decompensation during fever leading to death, in a consanguineous Turkish family, with biallelic variants (c.638G>T, p.(Arg213Leu)) in *SARS1*. This missense variant was shown to lead to protein instability, resulting in reduced protein level and enzymatic activity. Our results describe a new clinical entity and expand the clinical and mutational spectrum of SARS1 and ARS deficiencies.

A minoacyl-tRNA synthetases (ARS) catalyze an amino acid's esterification onto its cognate tRNA (ligating amino acids to corresponding tRNA molecules).[1,2] Consequently, each proteinogenic amino acid is coupled to its corresponding tRNA by a specific ARS. Since protein translation in eukaryotes occurs in the cytoplasm and the mitochondria, tRNA synthetase activities are generally required for each amino acid in both subcellular locations (ARS1 in the cytosol and ARS2 in the mitochondria. The resulting aminoacyl-tRNA is delivered to ribosome elongation factors to participate in protein synthesis.

ARSs fulfill crucial roles in translation: they provide the essential elements for protein synthesis, but they are also the only enzymes responsible for accurately deciphering the genetic code.[3,4] Beyond these classical functions, these enzymes are also known to have a role in several metabolic and signaling pathways essential for cell viability.[5] The roles of these enzymes are extremely varied in both physiological and pathological conditions and range from RNA processing and trafficking, ribosomal RNA synthesis to cellular processes such as apoptosis, angiogenesis, or inflammation.[6]

Variants in all ARSs have already been associated with various human diseases with both recessive and dominant inheritance patterns.[7–9] As well as many other ubiquitously expressed housekeeping genes, pathogenic variants in ARS have been implicated in intellectual disability and neurological disorders.[10] Autosomal dominant ARS pathogenic variations, such as in *AARS1*, *HARS1*, *GARS1*, *MARS1*, *WARS1*, and *YARS1* result in peripheral neuropathy (CMT2).[11–16] Recessive ARS1 deficiencies result in multiorgan disease associating various but severe symptoms: syndromic intellectual disability,[17] epileptic encephalopathy,[18] leukodystrophy,[19] deafness,[20] and movement disorders.[20] Of note, most of the ARS associated with the dominant transmission have also been associated with recessive transmission mode. Mitochondrial ARS2 deficiencies result in mitochondrial phenotypes: *DARS2* is associated with leukoencephalopathy with brain stem and spinal cord involvement and lactate elevation,[21] whereas *CARS2* pathogenic variations cause combined oxidative phosphorylation deficiency with severe epileptic encephalopathy and complex movement disorder.[22] Bi-functional (GARS1, KARS1) deficiencies result in a combination of mitochondrial and multiorgan disease.[23,24]

The overlap between cytosolic and mitochondrial ARS-associated phenotypes suggested a common pathogenic mechanism. It is probably linked to a shared impossibility to meet the translational need in specific organs.[25]

More specifically, seryl-tRNA synthetase (SARS1) catalyzes serine's attachment to tRNA[Ser] leading to tRNA-amino acid complex binding and then release from SARS1.[3] Moreover, selenocysteine is also incorporated by the ribosome thanks to SARS1.[26] Consequently, SARS1 is vital to selenoprotein synthesis.

Here, we report a Turkish pedigree where the parents were first cousins (Figure S1A) and in which whole-exome sequencing (WES) was carried out in four siblings with neurodevelopmental delay, deafness, cardiomyopathy, and decompensation during fever. The first child (patient 1) was diagnosed with deafness at 12 months of age and received a cochlear implant at 18 months of age (Table 1). He had a developmental delay and acquired independent walking at 23 months. At the age of 4 years, he was transferred to the pediatric intensive care unit (ICU) for sepsis shock in the context of vomiting with erythematous-pultaceous angina. Biologic testing revealed slight hepatic cytolysis and the presence of an increase in creatine phosphokinase (CPK, 900 U/L, reference range: 68–293 U/L) with a slight hyperproteinorachia (1.25 g/L, reference range: <0.3 g/L). Cardiac ultrasonography showed left concentric hypertrophic cardiomyopathy with a collapsed ejection fraction (<10%) not improved by vasopressor, leading to death. Muscle biopsies showed a discrete mitochondrial overload and a discrete lipid overload (Figure S2).

In the second child (patient 2), deafness was diagnosed before the age of 9 months. She died 1 week after her older brother at 30 months of age, following status epilepticus triggered by a febrile episode. Evolution has been towards brain death within 48 h. Moderate hypertrophic cardiomyopathy was detected by cardiac ultrasound. Magnetic resonance imaging (MRI) of the brain showed atrophy of the cerebellum and brain stem with a bilateral inferior dysplastic aspect of the cerebellum. Delayed myelination and a thin corpus callosum were also reported (Figure S3). Lumbar puncture revealed hyperproteinorachia (1.18 g/L, reference range: <0.3 g/L).

Her dizygotic twin sister (patient 3) had moderate dysmorphic features (strabismus, mild midfacial hypoplasia, marked philtrum, bulbous nose, Figure S4), congenital deafness, and severe developmental delay. She acquired walking around 2.5 years of age and had a significant speech delay. MRI showed delayed myelination with strikingly superposing results compared to her twin sister (Figure S3). Cardiological monitoring revealed no cardiomyopathy. At age 9, she was admitted to pediatric intensive care unit for fever, digestive disorders, and inflammatory syndrome. During this febrile episode, she developed a status epilepticus followed by sudden brain death, as shown on

the continuous electroencephalogram (EEG) monitoring recording despite anticonvulsant therapy following recommendation (Figure S5). She had one prior antecedent of convulsion at age 3. As for patient 1, muscle biopsies showed a discrete mitochondrial and lipid overload. The respiratory chain's activity was normal.
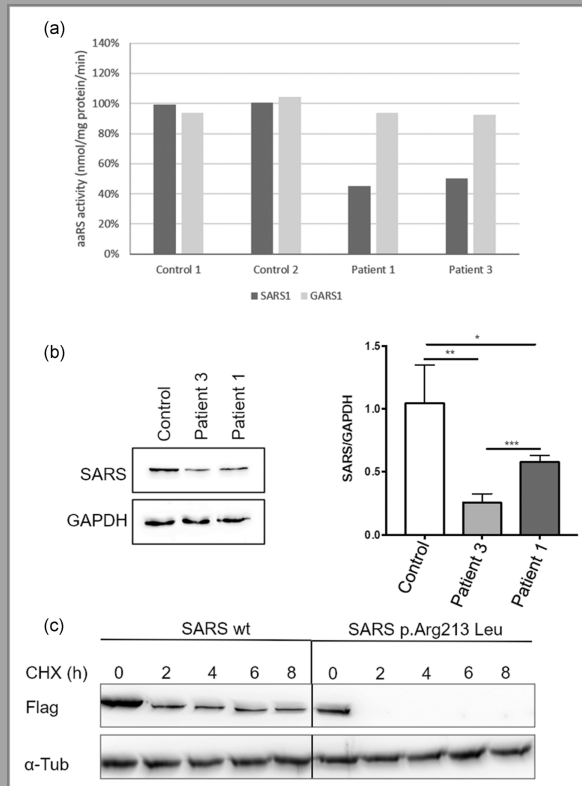
Fig. 1: functional analysis of the p.Arg213Leu variant. **a**, Aminoacylation activity measured in fibroblasts of controls and patients as % of average control (measured in triplicate, a representative experiment is shown). **b**, Quantification of the protein level of SARS1. Left: One representative image of the quantification of the expression level of SARS1 in patient or control fibroblasts by western blot. GAPDH is used as a loading control. Right: Measurement of the SARS1/GAPDH ratio (mean ± standard deviation, $N = 4$, *$p < .05$; ** $p < .01$, *** $p < .005$). **c**, The wild-type and mutant p. Arg213Leu proteins were expressed in HEK-293 cells. Twenty-four hours after transfection, cells were treated with 75 µg/ml cycloheximide (CHX) for the indicated times. Stability of the flag-tagged protein was analyzed by western blot. Alpha-tubulin (Tub) is used as a control. GAPDH, glyceraldehyde 3-phosphate dehydrogenase; SARS1, seryl-tRNA synthetase

The fourth child (patient 4) had congenital deafness, stunted growth, and moderate developmental delay. He had significant oral language difficulties (expression and comprehension) and said a few words at 2 years of age. These symptoms were associated with problems in attention-concentration, agitation, and aggressive behavior. Walking was acquired at 2 years of age. Clinical examination showed dysmorphic features similar to those of his sister (Figure S4). An emergency protocol for fever management was put in place for this child. He presented numerous episodes of hyperthermia, sometimes requiring ICU hospitalization. He is currently 6-year-old and is still being cared for in our unit. Cardiac echography was normal, as well as EEG and MRI. No sign of elevated CPK nor cytolysis was detected. We are currently evaluating l-serine supplementation in this patient.

The fifth child has no symptoms. None of the children presented with neither ataxia, muscle weakness, nor thin body, in contrast to the previous report of Musante and colleagues.[27]

A homozygous NM_006513.3:c.638G>T missense variant in exon 6 of *SARS1* leading to p.(Arg213Leu) was identified in patient 1 by exome sequencing (Figure S1B). The amino acid substitution p.(Arg213Leu) is located in the aminoacylation domain (Figure S1B), and several different pathogenicity predictors (Polyphen2, 0.687; Mut-Pred, 0.663; Mutation Taster, 0.5876) predicted that this variant was deleterious. Moreover, *SARS1* has a pLI of 1, indicating that this gene is susceptible to haploinsufficiency. Besides, it was absent from the gnomAD v2.1.1 database. Two rare variants affecting the same residue are reported in gnomAD (two counts for p.Arg213Cys and four counts for p.Arg213His). That is also consistent with a probable impact of an alteration at this residue on protein function. This position is conserved among species, including *Cnidaria* (Figure S1C).

The other patients were also homozygous for this variant. Both parents are heterozygous as the unaffected brother (Figure S1A).

SARS1 is a dimeric enzyme that belongs to class II tRNA synthetases. Its catalytic domain is composed of 7-stranded antiparallel β-sheets and three conserved motifs. The arginine at position 213 is located in motif 1, which forms the dimer interface, whereas motifs 2 and 3 contain residues of the active site (Figure S1B). According to the crystal structure of human SARS1 dimer complexed with two molecules of tRNA[Sec] (PDB code 4RQE), the lateral chain of arginine at position 213 not only establishes

hydrogen bonds with residues Phe459 and Glu458 (located in motif 3) in one subunit but also with Phe459 of the second subunit.

To evaluate the pathogenicity of the variant, we measured the activity of the SARS1 enzyme. Analysis of patient fibroblasts showed reduced SARS1 activity around 50% (Figure 1A and Table S1). A simultaneously measured enzyme (GARS1) was comparable to controls. In addition, northern blot showed no or only a weak signal for tRNA[Ser](Sec) in patients' fibroblasts compared to control (Figure S6C).

The quantification of protein expression showed a significant reduction in affected patients than in control (Figure 1b). This could be explained by a reduced stability of the p.(Arg213Leu) variant, as a flag-tagged mutant protein was not detected as shortly as 2 h after adding cycloheximide, compared to the wild-type protein (Figure 1b). To further rule out any additional effects of the p.(Arg213Leu) variant, we used constructs expressing either the wild-type or the mutant protein fused to a Flag tag transfected into HEK 293 cells. There was no noticeable change in the mainly cytoplasmic localization of the p.(Arg213Leu) mutated SARS1 compared to the wild-type overexpressed protein (Figure S6A and S6B) and the endogenous protein.[4] The level of wild-type flag-tagged protein was also consistently higher than for the mutant counterpart (Figure 1b and Figure S6). Bioinformatic predictions with ESE finder and Human Splicing Finder suggested the creation of a binding site for SRSF5 (SRp40) with a possible impact on splicing. Still, the analysis of the splicing pattern of the region of exons 5 to 7 by reverse-transcription polymerase chain reaction (RT-PCR) revealed no abnormalities in the splicing profile of patient fibroblasts compared to control fibroblasts (Figure S7A), as exon 6 was fully spliced and no other isoform could not be detected. The messenger RNA level of *SARS1* was also not significantly affected by the variant (Figure S7B). In this study, we demonstrate that rare bi-allelic variants in *SARS1* encoding cytoplasmic SARS1 are a cause of a severe syndrome associating deafness, cardiomyopathy, developmental delay, and febrile decompensation leading to premature death. Muscular puncture also highlighted lipidic and mitochondrial overload with normal mitochondrial activity in two patients. It is, however, unclear if these elements are part of this syndrome.

To date, SARS1 deficiency has only been reported in one publication.[27] They identified a homozygous missense variant (c.514G>A, p.Asp172Asn) in an Iranian family. The patient had an intellectual disability and behavioral disorders (aggressive behavior). The cardiac aspect was not specified. However, our patients display a much

more severe clinical phenotype, despite the similarity in the affected protein domain. The p.Asp172Asn and the p. Arg213Leu variants are localized in the active aminoacylation domain of the SARS1 enzyme (Figure 1b). However, the p.Arg213Leu variant affects protein stability as demonstrated by the cycloheximide chase, whereas the p. Asp172Asn variant mainly affects the catalytic site and leads to impaired serine-activation of the enzyme.[27] Of note, variants in *SARS2*, the gene encoding mitochondrial enzyme, have been associated with the HUPRA syndrome (hyperuricemia, pulmonary hypertension, childhood renal failure, and alkalosis) corresponding to mitochondrial cytopathy.[28] Reported SARS2 deficient patients were born prematurely, had a developmental delay, and died before 14 months.

Fever seems to play an essential role as a trigger for decompensation and death in this family. All deaths were indeed preceded by a severe febrile episode. A temperature rise has been found to induce a decrease in enzymatic activity in mutated LARS1 proteins.[29] Therefore, the deaths of patients 1–3 may be related to decreased SARS1 activity below the minimum threshold necessary for cell survival. Another—but not mutually exclusive—hypothesis may involve failure to meet increased energy demands. Since the rise in temperature during fever is mainly due to increased thermogenesis, fever dissipates a considerable quantity of energy in heat. The metabolic cost of fever is high: a temperature increase of 1°C corresponds to a 15%–50% increase in mitochondrial metabolism.[30,31] Death related to severe febrile episodes has been associated with mitochondrial pathologies. For example, in nicotinamide cofactor repair defects, the accumulation of damaged metabolites likely triggers devastating effects in high-energy consuming tissues such as the brain and heart, eventually leading to death in early childhood.[32] Our patients displayed a clinical phenotype with neurological symptoms, deafness, and cardiomyopathy, suggestive of a mitochondriopathy,[33,34] and received treatment accordingly. The increase in energy metabolism during febrile episodes may thus also have been caused or deteriorated by a failure of the brain (patient 2 and 3) or heart (patient 1) (mitochondrial) metabolism. Functional consequences of the newly identified p.(Arg213Leu) variant in *SARS1* were evidenced by decreased enzymatic activity. The 50%-residual enzyme activity is consistent with the need to integrate serines into protein synthesis and corresponds to enzyme deficiencies reported for other ARS deficiencies. Moreover, the fact that this position is not highly conserved across species supports the hypothesis of an hypomorphic mutation. Variants resulting in absent enzymatic activity are most likely incompatible with embryonic development and thus are lethal. We did not find a relationship between the level of enzyme activity and

protein expression, as patient 1 had higher SARS1 protein expression than patient 3, but similar enzyme activity (45% vs. 50%). Based on clinical observations, considering, in particular, the age of death (4 vs. 9 years), protein level does not seem to correlate with the severity of the disease. It has also been suggested that diet could influence enzyme activity,[35] and other environmental aspects could also be of influence. Alternatively, the age of death may also be determined by the timing or type of febrile exposure since patients 1 and 2 died one week apart.

The p.(Arg213Leu) variation had no impact on cytosolic SARS1 protein localization but resulted in the absence of detectable tRNA[Ser](Sec) in patients' fibroblasts. This observation concurs with the finding that nonaminoacylated tRNAs are degraded and that variants in ARS decrease the amount of both the aminoacylated and the nonaminoacylated tRNAs.[28,36]

SARS1 has several specificities when compared to other tRNA synthetases. For many tRNAs, the anticodon is a significant component determining specificity. That is not the case for serine aminoacylation. In SARS1, a key feature determining specificity is the variable arm, which is positioned between the anticodon arm and the T-arm.[37,38] The presence of an additional UNE-S domain is also remarkable. It contains a nuclear localization domain, which plays a significant role in regulating angiogenesis as a transcriptional repressor of VEGFA.[4,39] Besides, SARS1 is also involved in the synthesis of selenoproteins. Selenocysteyl-tRNA(Sec) is synthesized by converting serine through a multi-step process that depends on tRNA[Ser](Sec). In the first step, the SARS1 enzyme aminoacylates tRNA[Ser](Sec) with serine. Deletion of the tRNA[Ser](Sec) gene in neurons in a murine model leads to cerebellar hypoplasia.[40] This abnormality, also detected by MRI in patient 2, suggests a tRNA Sec deficiency in this patient.

The clinical presentation of other aminoacyl-tRNA deficiencies is very heterogeneous. It can be distinguished into three main groups regarding transmission mode and ARS localization: cytosolic autosomal dominant and recessive, and mitochondrial (see Table S1[9] for a general review).[25,41] Among the recessive group, intellectual disability, developmental delay, and epilepsy are quite common. Similarly, severe forms are common and often progress to an early death. Cardiomyopathy is, however, uncommon and has not been associated yet with another autosomal recessive ARS. Sensitivity to fever has also been described in the case of LARS1 deficiency[29] and urges aggressive antipyretic management.

Since our patients display some residual enzyme activity, supplementation with serine or selenocysteine may be beneficial by saturating enzyme activity.[42] Similar consideration has been made for methionyl-ARS (MARS1) deficiencies.[43] Hadchouel and colleagues have identified biallelic variations in *MARS1* in 26 people from Reunion and neighboring islands and two families from other countries with a specific form of pediatric pulmonary alveolar proteinosis. *In vitro*, MARS1 activity was decreased in methionine-free medium and restored in a methionine-supplemented medium. In patient 4, the surviving patient with SARS1 deficiency we described, we are currently evaluating l-serine supplementation.

In conclusion, we have identified a new clinical presentation associated with biallelic variants in *SARS1*, causing a functional deficiency of SARS1. We here extend the previously described phenotype of developmental delay and behavioral abnormalities to a syndrome with developmental delay, deafness, cardiomyopathy, epilepsy, and severe febrile decompensations. Further identification of *SARS1* variants will contribute to understanding the full clinical spectrum. In terms of treatment, aggressive antipyretic treatment and putatively l-serine or selenocysteine treatment may be considered.

References

1. Ibba M, Söll D. Aminoacyl-tRNA Synthesis. *Annu Rev Biochem*. 2000; 69: 617–650.

2. Pang YLJ, Poruri K, Martinis SA. tRNA synthetase: tRNA aminoacylation and beyond. *WIREs RNA*. 2014; 5: 461–480.

3. Vijayakumar R, Tripathi T. Soluble expression and purification of a full-length asparaginyl tRNA synthetase from Fasciola gigantica. *Prot Expr Purif*. 2018; 143: 9–13.

4. Xu X, Shi Y, Zhang H-M, et al. Unique domain appended to vertebrate tRNA synthetase is essential for vascular development. *Nat Commun*. 2012; 3: 681.

5. Rajendran V, Kalita P, Shukla H, et al. Aminoacyl-tRNA synthetases: Structure, function, and drug discovery. *Int J Biol Macromol.* 2018; 111: 400–414.

6. Ko Y-G, Park H, Kim S. Novel regulatory interactions and activities of mammalian tRNA synthetases. *Proteomics*. 2002; 2: 1304–1310.

7. Antonellis A, Green ED. The Role of Aminoacyl-tRNA Synthetases in Genetic Diseases. *Annu Rev Genom Hum Genet*. 2008; 9: 87–107.

8. Meyer-Schuman R, Antonellis A. Emerging mechanisms of aminoacyl-tRNA synthetase mutations in recessive and dominant human disease. *Hum Mol Genet*. 2017; 26: R114–R127.

9. Manole A, Efthymiou S, O'Connor E, et al. De Novo and Bi-allelic Pathogenic Variants in NARS1 Cause Neurodevelopmental Delay Due to Toxic Gain-of-Function and Partial Loss-of-Function Effects. *Am J Hum Genet*. 2020; 107: 311–324.

10. Najmabadi H, Hu H, Garshasbi M, et al. Deep sequencing reveals 50 novel genes for recessive cognitive disorders. *Nature*. 2011; 478: 57–63.

11. Gillespie MK, McMillan HJ, Kernohan KD, et al. A Novel Mutation in MARS in a Patient with Charcot-Marie-Tooth Disease, Axonal, Type 2U with Congenital Onset. *J Neuromuscul Dis*. 2019; 6: 333–339.

12. Jordanova A, Irobi J, Thomas FP, et al. Disrupted function and axonal distribution of mutant tyrosyl-tRNA synthetase in dominant intermediate Charcot-Marie-Tooth neuropathy. *Nat Genet*. 2006; 38: 197–202.

13. Lee AJ, Nam DE, Choi YJ, et al. Alanyl-tRNA synthetase 1 (AARS1) gene mutation in a family with intermediate Charcot-Marie-Tooth neuropathy. *Genes Genom*. 2020; 42: 663–672.

14. Nan H, Takaki R, Hata T, et al. Novel *GARS* mutation presenting as autosomal dominant intermediate Charcot-Marie-Tooth disease. *J Peripher Nerv Syst*. 2019; 24: 156–160.

15. Wang B, Li X, Huang S, et al. A novel *WARS* mutation (p.Asp314Gly) identified in a Chinese distal hereditary motor neuropathy family. *Clin Genet*. 2019; 96: 176–182.

16. Meyer-Schuman R, Antonellis A. Evidence for a dominant-negative mechanism in *HARS1* -mediated peripheral neuropathy. *FEBS J*. 2021; 288: 91–94.

17. Kuo ME, Theil AF, Kievit A, et al. Cysteinyl-tRNA Synthetase Mutations Cause a Multi-System, Recessive Disease That Includes Microcephaly, Developmental Delay, and Brittle Hair and Nails. *Am J Hum Genet*. 2019; 104: 520–529.

18. Nakayama T, Wu J, Galvin-Parton P, et al. Deficient activity of alanyl-tRNA synthetase underlies an autosomal recessive syndrome of progressive microcephaly, hypomyelination, and epileptic encephalopathy. *Hum Mutat*. 2017; 38: 1348–1354.

19. Mendes MI, Gutierrez Salazar M, Guerrero K, et al. Bi-allelic Mutations in EPRS, Encoding

the Glutamyl-Prolyl-Aminoacyl-tRNA Synthetase, Cause a Hypomyelinating Leukodystrophy. *Am J Hum Genet*. 2018; 102: 676–684.

20. Galatolo D, Kuo ME, Mullen P, et al. Bi-allelic mutations in *HARS1* severely impair histidyl-tRNA synthetase expression and enzymatic activity causing a novel multisystem ataxic syndrome. *Hum Mutat*. 2020; 41: 1232–1237.

21. Scheper GC, van der Klok T, van Andel RJ, et al. Mitochondrial aspartyl-tRNA synthetase deficiency causes leukoencephalopathy with brain stem and spinal cord involvement and lactate elevation. *Nat Genet*. 2007; 39: 534–539.

22. Coughlin CR, Scharer GH, Friederich MW, et al. Mutations in the mitochondrial cysteinyl-tRNA synthase gene, *CARS2,* lead to a severe epileptic encephalopathy and complex movement disorder. *J Med Genet* 2015; 52: 532–540.

23. Itoh M, Dai H, Horike S, et al. Biallelic *KARS* pathogenic variants cause an early-onset progressive leukodystrophy. *Brain*. 2019; 142: 560–573.

24. Oprescu SN, Chepa-Lotrea X, Takase R, et al. Compound heterozygosity for loss-of-function *GARS* variants results in a multisystem developmental syndrome that includes severe growth retardation. *Hum Mutat*. 2017; 38: 1412–1420.

25. Fuchs SA, Schene IF, Kok G, et al. Aminoacyl-tRNA synthetase deficiencies: in search of common themes. *Genet Med*. 2019; 21: 319–330

26. Seeher S, Mahdi Y, Schweizer U. Post-Transcriptional Control of Selenoprotein Biosynthesis. *Curr Protein Pept Sci*. 2012; 13: 337–346.

27. Musante L, Püttmann L, Kahrizi K, et al. Mutations of the aminoacyl-tRNA-synthetases SARS and WARS2 are implicated in the etiology of autosomal recessive intellectual disability: *Hum Mutat*. 2017; 38: 621–63.

28. Belostotsky R, Ben-Shalom E, Rinat C, et al. Mutations in the Mitochondrial Seryl-tRNA Synthetase Cause Hyperuricemia, Pulmonary Hypertension, Renal Failure in Infancy and Alkalosis, HUPRA Syndrome. *Am J Hum Genet*. 2011; 88: 193–200.

29. Lenz D, Smith DEC, Crushell E, et al. Genotypic diversity and phenotypic spectrum of infantile liver failure syndrome type 1 due to variants in LARS1. *Genet Med*. 2020; 22: 1863–1873.

30. Baracos VE, Whitmore WT, Gale R. The metabolic cost of fever. *Can J Physiol Pharmacol*. 1987; 65: 1248–1254.

31. Conti B, Bartfai T. Fever. In: Metabolism of Human Diseases. *Springer (Vienna)*. 2014; pp. 313–317.

32. Van Bergen NJ, Guo Y, Rankin J, et al. NAD(P)HX dehydratase (NAXD) deficiency: a novel neurodegenerative disorder exacerbated by febrile illnesses. *Brain*. 2019; 142: 50–58.

33. Teplova VV, Deryabina YuI, Isakova EP. Mitochondrial cytopathies: Their causes and correction pathways. *Biochem Moscow Suppl Ser A*. 2017; 11: 87–102.

34. Wallace DC, Fan W, Procaccio V. Mitochondrial Energetics and Therapeutics. *Annu Rev Pathol Mech Dis*. 2010; 5: 297–348.

35. Lenz D, Stahl M, Seidl E, et al. Rescue of respiratory failure in pulmonary alveolar proteinosis due to pathogenic *MARS1* variants. *Pediatr Pulmonol*. 2020; 55: 3057–3066.

36. Edvardson S, Shaag A, Kolesnikova O, et al. Deleterious Mutation in the Mitochondrial Arginyl–Transfer RNA Synthetase Gene Is Associated with Pontocerebellar Hypoplasia. *Am J Hum Genet*. 2007; 81: 857–862.

37. Berg MD, Genereaux J, Zhu Y, et al. Acceptor Stem Differences Contribute to Species-Specific Use of Yeast and Human tRNASer. *Genes* 2018; 9: 612.

38. Dock-Bregeon A-C, Garcia A, Giege R, et al. The contacts of yeast tRNASer with seryl-tRNA synthetase studied by footprinting experiments. *Eur J Biochem*. 1990; 188: 283–290.

39. Shi Y, Xu X, Zhang Q, et al. tRNA synthetase counteracts c-Myc to develop functional vasculature. *eLife*. 2014; 3: e02349.

40. Wirth EK, Bharathi BS, Hatfield D, et al. Cerebellar Hypoplasia in Mice Lacking Selenoprotein Biosynthesis in Neurons. *Biol Trace Elem Res*. 2014; 158: 203–210.

41. Rubio Gomez MA, Ibba M. Aminoacyl-tRNA synthetases. *RNA*. 2020; 26: 910–936.

42. Kok G, Tseng L, Schene IF, et al. Treatment of ARS deficiencies with specific amino acids. *Genet Med*. 2021; 23: 2202–2207.

43. 43. Hadchouel A, Wieland T, Griese M, et al. Biallelic Mutations of Methionyl-tRNA Synthetase Cause a Specific Type of Pulmonary Alveolar Proteinosis Prevalent on Réunion Island. *Am J Hum Genet*. 2015; 96: 826–831.

Acknowledgements

Supplementary figures

Figure S1: family trees of reported patients and location of SARS1 mutations.

Figure S2: patient 1 post-mortem muscle biopsies.

Figure S3: cerebral Magnetic Resonance Imaging in SARS1 deficient patients.

Figure S4: dysmorphia was observed in patient 3 and 4.

Figure S5: abrupt cessation of EEG activity in children 3.

Figure S6: the p.Arg213Leu variant dos not affect protein localization but diminishes tRNA[Ser](Sec) levels.

Figure S7: the NM_006513.3:c.638G>T missense variant in exon 6 does not affect SARS1 mRNA processing nor stability.

May be dowloaded from doi.org/10.1002/humu.24285.

Supplementary table

Table S1: Aminoacylation activity. Aminoacylation activity measured in fibroblasts of controls and patients as percentage of average control (measured in triplicate, raw data corresponding to Figure 1A).

May be dowloaded from doi.org/10.1002/humu.24285.

Ad
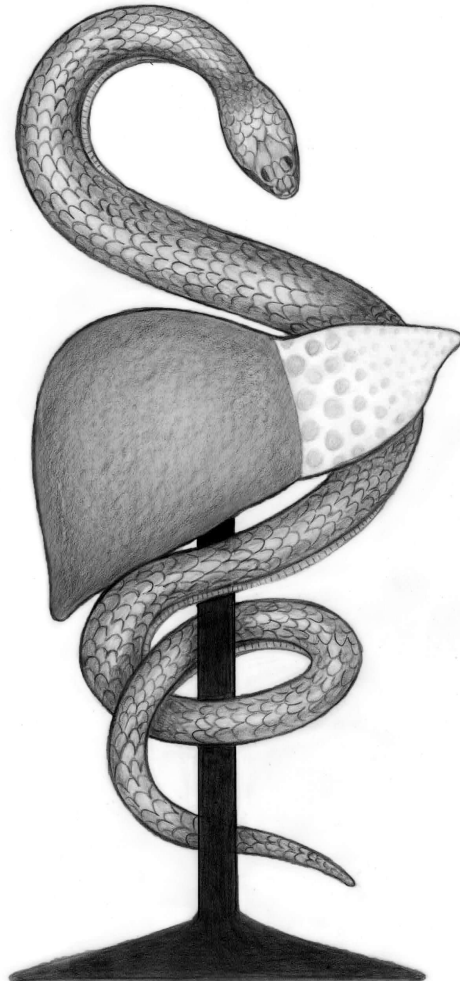
THE NOVEL APPROACH

COMMON TO MANY METABOLIC DISEASES, TARGETING THE LIVER

HLA MATCHING FOR LIVER TRANSPLANTATIONS: A SYSTEMATIC REVIEW AND META-ANALYSIS

Gautam Kok*, Eveline Ilcken*, Roderick Houwen, Caroline Lindemans, Edward Nieuwenhuis, Eric Spierings, Sabine Fuchs

9

Abstract

Objective

To investigate the effects of genetically based HLA matching on patient and graft survival, and acute and chronic rejection after liver transplantation.

Background

Liver transplantation is a common treatment for patients with end-stage liver disease. In contrast to most other solid organ transplantations, there is no conclusive evidence supporting human leukocyte antigen (HLA) matching for liver transplantations. With emerging alternatives such as transplantation of bankable (stem) cells, HLA matching becomes feasible, which may decrease the need for immunosuppressive therapy and improve transplantation outcomes.

Methods

We systematically searched the PubMed, Embase and Cochrane databases and performed a meta-analysis investigating the effect of genetic HLA matching on liver transplantation outcomes (acute/chronic rejection, graft failure and mortality).

Results

We included 14 studies with 2,682 patients. HLA-C mismatching significantly increased the risk of acute rejection (full mismatching: RR=1.90; 95% CI=[1.08-3.33]; P=0.03 | partial mismatching: RR=1.33; 95% CI=[1.07-1.66]; P=0.01). We did not discern any significant effect of HLA mismatching per locus on acute rejection for HLA-A, -B, -DR, and -DQ, nor on chronic rejection, graft failure, or mortality for HLA-DR, and -DQ.

Conclusion

We found evidence that genetic HLA-C matching reduces the risk of acute rejection after liver transplantation, while matching for other loci does not reduce the risk of acute rejection, chronic rejection, graft failure, or mortality.

Introduction

Despite improvement of short-term survival of liver transplantation recipients over the past decades,[1,2] long-term survival has remained suboptimal. With improved immunosuppressant therapies, the main cause of death after liver transplantation shifted from allograft rejection in 1987, to malignancies today. In addition to malignancies, long-term use of immunosuppressants is associated with infections, and renal, neurological, and liver dysfunction.[3–5] Strategies to reduce risks of allograft rejection and immunosuppression use may contribute to improved outcomes.

Allograft rejection is categorized in three subtypes; hyperacute, acute, and chronic rejection. Hyperacute rejection, which is rare among ABO-compatible liver transplantations,[6] occurs during or immediately after transplantation. It results from the presence of preformed anti-donor antibodies that react to vascular endothelium and initiate coagulation and complement activation. Acute rejection develops in the first weeks to months after transplantation. It is characterized by a humoral and/or cellular immune response. The humoral immune response involves presence of donor-specific human leukocyte antigen (HLA) and non-HLA antibodies.[7,8] Sustained acute rejection can lead to tissue damage and is a major risk factor for chronic rejection, which occurs months to years after transplantation.[9,10] Chronic rejection is characterized by obliterative arteriopathy and destruction of biliary duct cells that lead to ductopenia in the liver graft.[11] Risk factors for chronic rejection are frequent and/or severe episodes of acute rejection, an elderly or unrelated donor, and the presence of donor-specific anti-HLA class I and II antibodies.[9,11] Thus, in both acute and chronic rejection, HLA-complexes and alloreactive HLA antibodies play important roles.

HLA matching has improved outcomes for most solid organ transplantations,[12–18] but studies on liver transplantations have reported inconsistent results.[19–24] To date, most studies used serological HLA typing methods. Technological progress has enabled genetic typing of all HLA-loci, which may reveal clinically relevant mismatches that were previously missed.[25] With emerging alternatives such as transplantation of bankable (stem) cells,[26–30] HLA matching becomes feasible, which may decrease the need for immunosuppressive therapy and improve transplantation outcomes. We therefore conducted a meta-analysis to investigate the effects of genetically based HLA matching on patient and graft survival, and acute and chronic rejection after liver transplantation.[31]

9

Methods

We systematically searched the PubMed, Embase and Cochrane databases (Figure 1) up to February 15, 2022, for combinations of search terms: 'liver transplant*/graft', 'HLA/human leukocyte antigen', '(mis)match*/typing', and 'outcome/rejection/survival/recurrence/graft failure'. Duplicates were removed. Article titles and abstracts were screened for description of first liver transplantations with genetic HLA typing. Selected full text articles were screened for eligibility based on the following inclusion criteria: first liver transplantation, genetic HLA typing, specified HLA locus mismatches in at least one locus, specified transplantation outcome with rejection type, patient mortality and/or graft failure, and association of number of HLA mismatches (zero, one or two) to outcomes. Exclusion criteria were: (additional) transplantations other than liver, unspecified HLA loci, re-transplantations, articles not available in English, and unavailable full texts (Table 1).

Quality of included studies was assessed using the Cochrane risk of bias assessment.[32] For the meta-analysis, studies describing all primary liver transplantation indications were combined and the effects of HLA matching on acute and chronic rejection, graft failure, and mortality were analyzed per locus (HLA-A, -B, -C, -DR and -DQ). Risk ratios for these outcomes were determined for zero vs. one, one vs. two and zero vs. two mismatches per HLA locus. Findings of combined loci effects were included when available. Transplantations for autoimmune diseases were also analyzed separately to evaluate a putative favorable effect of mismatching to prevent autoimmune disease recurrence.

All analyses were performed using Cochrane's Review Manager version 5.4. Risk ratios were calculated using a random-effects model.[33] Associations between control and experimental conditions were tested with a Cochran-Mantel-Haenszel test. Overall test effects were estimated using Z-scores and P-values, with $\alpha = 0.05$.

Table 1: inclusion and exclusion criteria.

Inclusion	Exclusion
First liver transplantation	Transplantations other than liver in history, simultaneo
Genetic HLA typing	Serological HLA typing
Specified HLA locus mismatches (at least 1)	Unspecified HLA loci
Specified transplantation outcome (rejection type, pat	Re-transplantations
Outcome association to HLA match (0, 1 and 2)	Article not in English
	Full-text not available

Results

We identified 14 retrospective cohort studies that met the inclusion criteria. These articles were published between 1993 and 2021 and reported a total of 2,682 transplantations (Figure 1a). 13 studies involved liver transplantations for different primary disease types, or did not specify transplantation indication, and one study evaluated liver transplantations for only autoimmune disease (Tables 2 and S1).
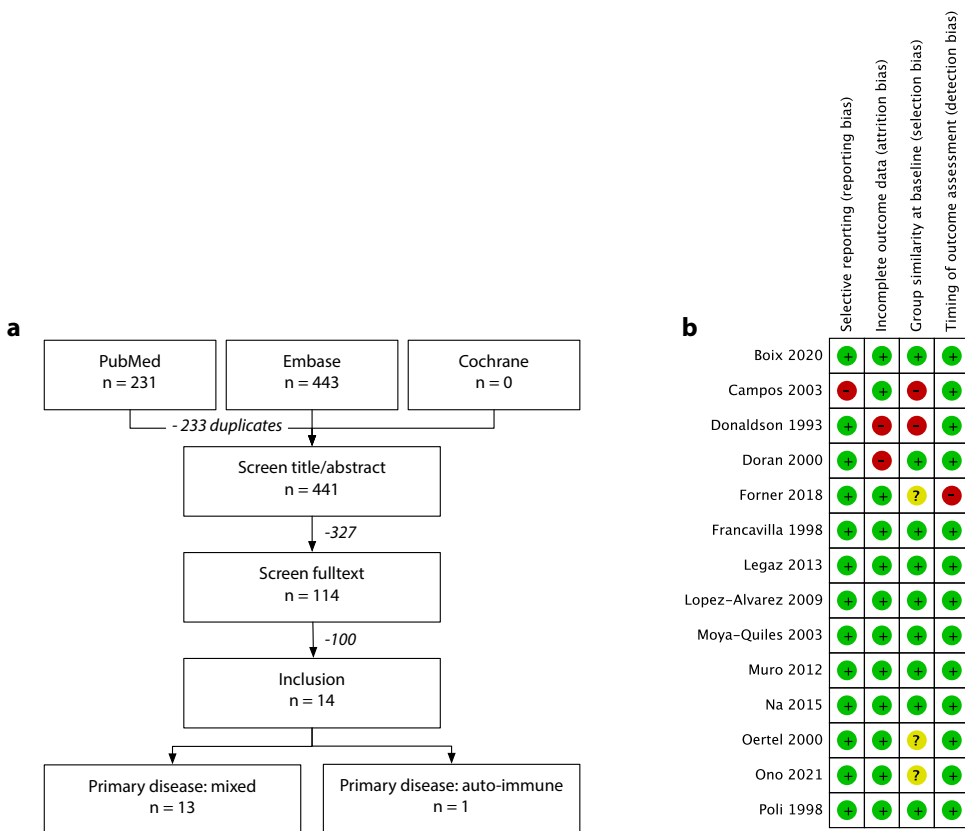

Fig. 1: **a**, Flowchart of the systematic search and literature selection. **b**, Cochrane risk of bias summary for all included studies.

Table 2: characteristics of included articles.

First author[ref]	Year of LTx	Country	No.	HLA Loci	Outcome	Immunosuppression	Follow-up
Doran[46]	1986 to 1998	Australia	71	A, B	AR[e], graft survival in patients with autoimmune diseases	Tacrolimus, mycophenolate	At least 1 year
Donaldson[45]	1984 to 1991	UK	466	DR, DQ	VBDS (CR), graft survival 1 year	Cyclosporine, prednisolone, azathioprine	At least 1 year
Francavilla[43]	1991 to 1996	England	135	DRB1, DQB1	AR, graft survival (1 and 5 years), patient survival (1 and 5 years)	Cyclosporine, methylprednisolone, azathioprine	At least 1 year
Poli[53]	1990 to 1997	Italy	517	DRB1	Graft survival 2 years	Mainly cyclosporine, but 25 tacrolimus with other immunosuppressants	At least 2 years
Oertel[36]	NA	Germany	35	A, B, C, DR, DQ	AR	Cyclosporine, azathioprine, mycophenolate mofetil and prednisolone (22). Tacrolimus, prednisolone (13)	At least 1 year
Campos[44]	2000 to 2002	Spain	20	DRB1, DQB1	AR	Cyclosporine A or tacrolimus with steroids, with or without preconditioning with IL-2 inhibitor	3 to 30 months
Moya-Quiles[42]	1993 to 1999	Spain	100	C	AR	Methylprednisolone, azathioprine, cyclosporine	At least 5 years
Lopez-Alvarez[41]	NA	Spain	300	C	AR	Cyclosporine A or tacrolimus, methylprednisolone and mycophenolate	At least 1 year
Muro[39]	1997 to 2005	Spain	224	A, B, DRB1, DQB1	AR, CR	Cyclosporine A or tacrolimus, methylprednisolone and mycophenolate	At least 5 years
Legaz[38]	NA	Spain	402	A, B, C	AR	Standard triple-immunosuppressive with cyclosporine or tacrolimus	At least 1 year
Na[37]	2008 to 2013	Korea	270	A, B, DR	AR	Tacrolimus or cyclosporin, mycophenolate mofetil and prednisolone, IL-2 inhibitor	Median 31 months (1–68)
Forner[34]	2009 to 2013	Canada	67	A, B, C, DRB1	AR	Calcineurin inhibitor (tacrolimus or cyclosporine), anti-metabolite (CellCept or Myfortic) and prednisolone taper. Also basiliximab, anti-thymocyte globulin and methylprednisolone	Mean 895 days (0-1,911)
Boix[40]	?	Spain	30	A, B, DRB1	AR	Tacrolimus (TRL) with or without mycophenolate mofetil (MMF)	At least 1 year
Ono[35]	2010 to 2019	Japan	45	A, B, C, DRB1, DQB1	AR	FK-506 and methylprednisolone	1 to 5 years

LTx: liver transplantation; AR: acute rejection; CR: chronic rejection; VBDS: vanishing bile duct syndrome as symptom for CR; NA: not available.

The effect of HLA matching on acute rejection

HLA Class I mismatching

To determine the effect of HLA mismatching on acute rejection, we examined the impact of genetic mismatches per class I locus (Table 3). Seven studies explored the effect of HLA-A matching in a total of 1,073 patients with various transplantation indications. One study (n=67) found that two HLA-A mismatches were more frequently associated with acute rejection. 13 (19.4%) patients developed acute rejection, 10 (76.9%) of which had two mismatches for locus HLA-A. All patients were pre-formed donor-specific antibody (DSA) naive before transplantation.[34] Another study (n=45) found that two HLA-A mismatches significantly increased risk of acute rejection over one but not zero HLA-A mismatches.[35] However, the number of patients with one mismatch was very small (n=6).[35] The other studies did not find a significant association between HLA-A mismatching and acute rejection.[36–40] When combining all studies, HLA-A compatibility (partial / full) did not significantly influence acute rejection (Figure 3).

The same seven studies also evaluated the effect of HLA-B matching on acute rejection. No significant associations were found between HLA-B mismatching and acute rejection,[34–40] individually nor when taken together (Figure 2).

For HLA-C, six studies comprising a total of 949 patients showed that full mismatching compared to full matching significantly increased the risk of acute rejection (RR=1.90; 95% CI=[1.08-3.33]; P=0.03), as did full versus partial mismatching for this locus (RR=1.33; 95% CI=[1.07-1.66]; P=0.01, Figure 3). One study found that patients with two HLA-C mismatches had a significantly higher rate of acute rejection (34.7%) than partially (23%) or totally (17.6%) matched patients (OR=1.85; 95% CI=[3.12-1.10]; P=0.02). 84% of all acute rejection episodes happened within the first month after transplantation with a mean of 23.8 ± 4.9 days.[41] Similarly, another study found that higher HLA-C incompatibility increased the incidence of acute rejection (defined as <6 weeks after transplantation): two mismatches: 46.3%; one mismatch: 33.2%, zero mismatches: 16.6%, although not significantly (P=0.12).[42] Lastly, a study reported that specifically recipient HLA-C genotype seemed to influence the risk of acute rejection.[38]

9

Table 3a: results meta-analyses: events and numbers of patients.

Outcome	HLA	No. studies	Events/patients (%)		
			0 MM	1 MM	2 MM
Acute rejection					
	A	7	29/144 (20.1%)	121/486 (24.9%)	133/443 (30.0%)
	B	7	10/63 (17.3%)	101/424 (25.1%)	172/587 (29.3%)
	C	6	10/60 (16.7%)	88/361 (24.4%)	176/528 (33.3%)
	DR	8	16/88 (18.2%)	117/381 (30.7%)	125/355 (35.2%)
	DQ	5	14/53 (26.4%)	96/235 (40.8%)	74/171 (41.8%)
Chronic rejection					
	DR	2	1/14 (7.1%)	24/122 (19.7%)	23/162 (14.2%)
	DQ	2	13/43 (30.2%)	26/154 (16.9%)	11/121 (9.1%)
Graft failure					
1-year	DR	2	26/62 (41.9%)	141/387 (36.4%)	103/340 (30.3%)
	DQ	1	3/8 (37.5%)	20/74 (27.0%)	13/53 (24.5%)
2-year	DR	1	14/50 (28.0%)	84/320 (26.3%)	76/321 (23.7%)
5-year	DR	1	0/1 (0.0%)	21/57 (36.8%)	19/77 (24.7%)
	DQ	1	4/8 (50.0%)	22/74 (29.7%)	14/53 (26.4%)
Mortality					
1-year	DR	1	0/1 (0.0%)	8/57 (14.0%)	10/77 (13.0%)
	DQ	1	2/8 (25.0%)	8/74 (10.8%)	8/53 (15.1%)
5-year	DR	1	0/1 (0.0%)	13/57 (22.8%)	12/77 (15.6%)
	DQ	1	3/8 (37.5%)	12/74 (16.2%)	10/53 (18.9%)

MM: mismatches

HLA Class II mismatching

Of the eight studies that reported the effect of HLA-DR mismatching on acute rejection in 824 patients, none found a significant effect.[34–37,39,40,43,44] One study found an association between HLA-DRB1*13 positive donors and acute rejection. Of the patients with acute rejection, 54% had a donor with this variant, compared to only 5% of patients without rejection (P=0.02).[36] Overall, however, HLA-DR mismatching did not significantly influence acute rejection (Figure 2).

Five studies (n=459) assessed the effect of HLA-DQ matching on acute rejection. None of these studies found any association between HLA-DQ mismatching and acute rejection (Figure 2).[35,36,39,43,44] However, one study (n=135) found a significant increase in the need for high-dose steroids and tacrolimus in patients with one mismatch for HLA-DQ, compared with those without mismatches (P<0.03), independent of the incidence or severity of acute rejection.[43]

Table 3b: results meta-analyses. A positive risk ratio (RR) indicates increased risk of outcome with increased mismatches.

Outcome	HLA	No. studies	0 vs. 1 MM		1 vs. 2 MM		0 vs. 2 MM	
			RR [95% CI]	P	RR [95% CI]	P	RR [95% CI]	P
Acute rejection								
	A	7	0.92 [0.64-1.33]	0.67	1.10 [0.80-1.51]	0.55	1.05 [0.68-1.62]	0.82
	B	7	0.88 [0.44-1.74]	0.71	1.06 [0.85-1.32]	0.61	1.06 [0.52-2.61]	0.88
	C	6	1.40 [0.79-2.49]	0.26	1.33 [1.07-1.66]	0.01	1.90 [1.08-3.33]	0.03
	DR	8	0.93 [0.61-1.41]	0.73	0.99 [0.75-1.31]	0.96	0.98 [0.63-1.53]	0.93
	DQ	5	1.07 [0.68-1.69]	0.77	1.06 [0.86-1.31]	0.59	1.17 [0.67-2.03]	0.56
Chronic rejection								
	DR	2	2.61 [0.56-12.13]	0.22	0.82 [0.40-1.69]	0.59	1.96 [0.42-9.26]	0.40
	DQ	2	0.71 [0.39-1.29]	0.26	0.75 [0.29-1.91]	0.54	0.76 [0.35-1.66]	0.49
Graft failure								
1-year	DR	2	0.87 [0.63-1.20]	0.41	0.84 [0.69-1.04]	0.11	0.75 [0.54-1.06]	0.10
	DQ	1	0.72 [0.27-1.90]	0.51	0.91 [0.50-1.66]	0.75	0.65 [0.24-1.80]	0.41
2-year	DR	1	0.94 [0.58-1.52]	0.79	0.90 [0.69-1.18]	0.45	0.85 [0.52-1.37]	0.50
5-year	DR	1	1.48 [0.13-16.74]	0.75	0.67 [0.40-1.12]	0.13	1.00 [0.09-11.37]	1.00
	DQ	1	0.59 [0.27-1.29]	0.19	0.89 [0.50-1.57]	0.68	0.53 [0.23-1.21]	0.13
Mortality								
1-year	DR	1	0.59 [0.05-7.00]	0.67	0.93 [0.39-2.20]	0.86	0.54 [0.05-6.34]	0.62
	DQ	1	0.43 [0.11-1.70]	0.23	1.40 [0.56-3.48]	0.47	0.60 [0.16-2.35]	0.47
5-year	DR	1	0.93 [0.08-10.74]	0.95	0.68 [0.34-1.38]	0.29	0.64 [0.06-7.46]	0.72
	DQ	1	0.43 [0.15-1.22]	0.11	1.16 [0.54-2.49]	0.70	0.50 [0.18-1.44]	0.20

CI: confidence interval; MM: mismatches; RR: risk ratio

The effect of HLA mismatching on chronic rejection of liver grafts, graft failure and mortality

We found no studies evaluating mismatching of HLA- class I loci in relation to chronic rejection, graft failure or mortality.

Two studies described the effect of HLA-DR (n=298) and -DQ (n=318) mismatching on chronic rejection (Figure 2, Table 3). In the first study (n=95), 31 patients experienced chronic rejection (33%), characterized by vanishing bile duct syndrome
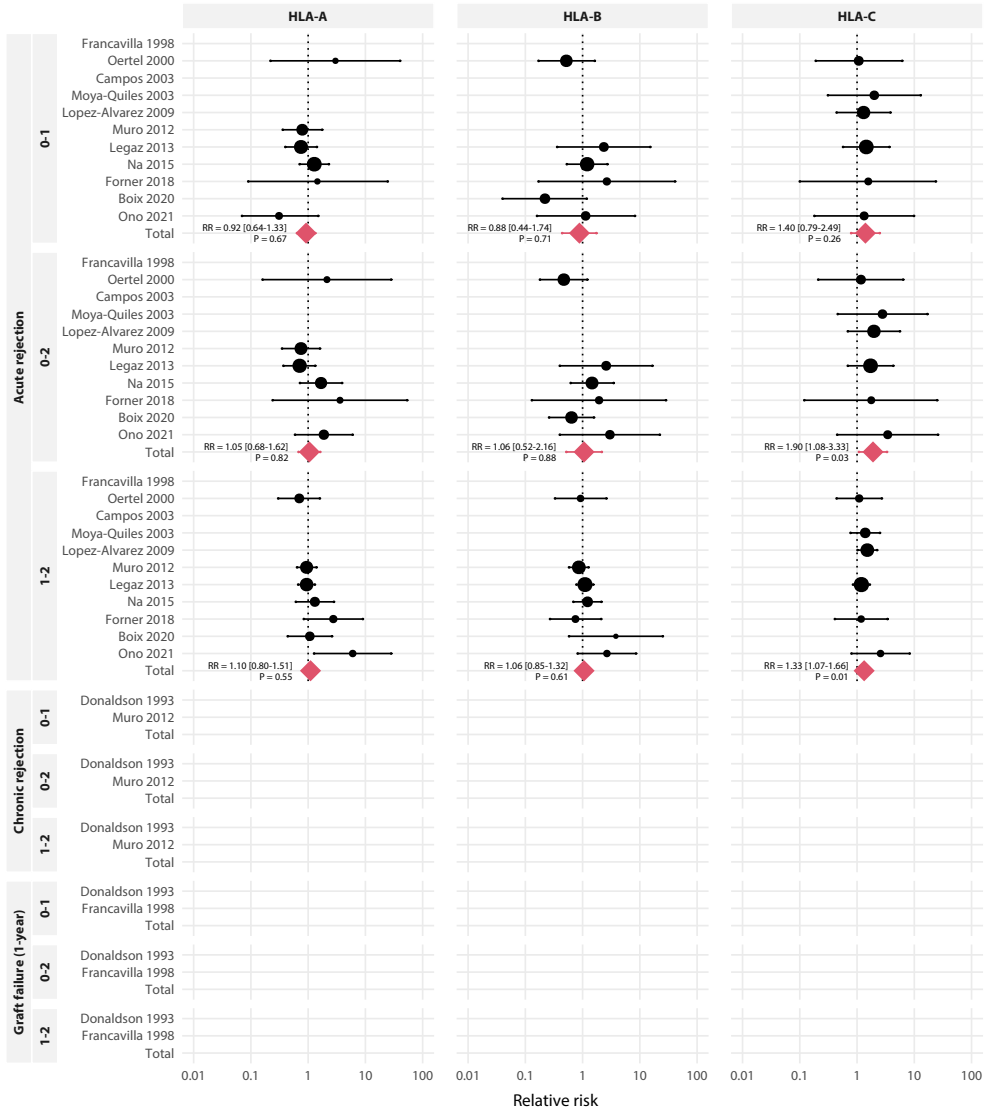
Fig. 3: forest plots of the effect of HLA-A, B, C, DR, and DQ mismatching on acute rejection, chronic rejection and graft failure for patients with mixed primary diseases comparing 0 to 1,

(VBDS). There was no significant association between VBDS and HLA-DR or -DQ mismatching.[45] The other study included 224 patients who received cadaveric liver grafts of whom 20 (9%) developed chronic rejection, characterized by disappearing interlobular bile ducts with mononuclear portal infiltrates that later became fibrotic with enlarged portal tracts. They did not find an association between HLA-DR or -DQ
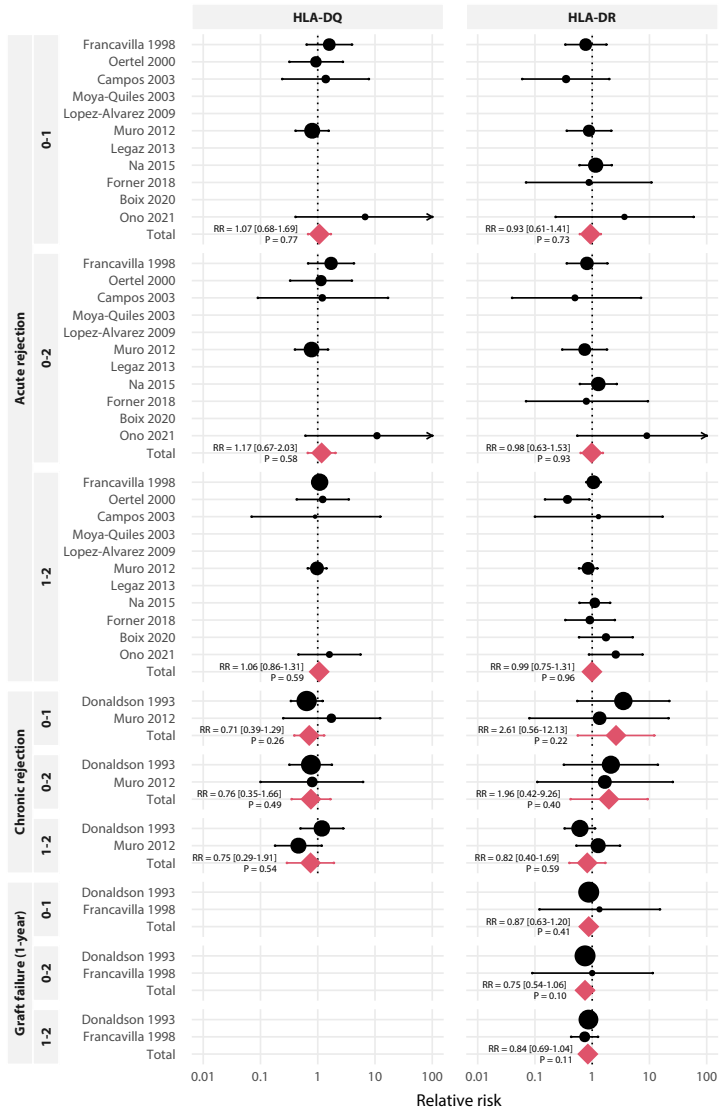
		HLA-DQ	**HLA-DR**

1 to 2, and 0 to 2 mismatches. Positive risk ratio (RR) indicates increased risk of outcome with increased mismatches.

mismatching and chronic rejection.[39] When taken together, HLA-DR and -DQ mismatching did not associate with chronic rejection (Figure 3).

Two studies (n=789) reported effects of HLA-DR mismatching on 1-year graft failure, and neither found an effect (Figure 2, Table 3). Causes of graft failure included

chronic rejection, hepatitis, artery thrombosis, primary non-function, sepsis and recurrent cholangitis, Budd-Chiari syndrome, and primary biliary cirrhosis (PBC).[43,45]

One of the two studies (n=135) also reported the effect of HLA-DR mismatching on 2- and 5-year graft survival, and the effect of HLA-DQ mismatching on 1- and 5-year graft survival. No significant associations were found (Figure S1, Table 3).[43] The same study further reported 1- and 5-year mortality in relation to HLA-DR and -DQ mismatching. 1- and 5-year mortality rates were 13% and 19%, respectively,[43] and no significant associations with HLA-subtype were found (Figure S1, Table 3).

The effect of HLA mismatching for patients with autoimmune diseases

Finally, we examined the role of HLA-A and -B matching in graft failure for patients with autoimmune diseases. A single study reported 63 patients with autoimmune chronic active hepatitis and primary biliary cholangitis, and 287 non-autoimmune diseases. They excluded primary sclerosing cholangitis from all analyses.[46] For patients with autoimmune disease, 1-year graft survival seemed to improve with more mismatches, although this was not statistically significant. Conversely, graft survival of patients without autoimmune disease decreased with more HLA-A or -B mismatches, with a reported statistical significance for HLA-B (0-1 mismatch: 82.8% survival rate; 2 mismatches: 75.0% (P<0.01)). Unfortunately, we could not confirm this nor include their data in our meta-analysis because of the format of their data on acute rejection.

Discussion

Although immune suppressive therapy after liver transplantation has undeniably improved short-term outcomes after liver transplantation, it is a major cause of current long-term complications. Improved insight in the role of HLA-mismatching may improve liver transplantation outcomes. With our meta-analysis of 14 independent studies comprising a total of 2,682 patients, we found a significant effect of HLA-C mismatching on the incidence of acute rejection, both for one vs. two mismatches (RR=1.33; 95% CI=[1.07-1.66]; P=0.01) and zero vs. two mismatches (RR=1.90; 95% CI=[1.08-3.33]; P=0.03). Conversely, we did not discern any significant effect of HLA mismatching per locus on acute rejection for HLA-A, -B, -DR, and -DQ, nor on chronic rejection, graft failure, or mortality for HLA-DR, and -DQ. The possibility exists that such effects were masked by immune suppression use. Associations between mismatching of HLA-DR and 2- and 5-year graft failure, and HLA-DQ and 1-, 2-, and 5-year

graft failure could not be meta-analyzed because data were derived from a single study (Figure S1).

Five of the 14 included articles in our meta-analysis carried a potential risk of bias (Figure 1b). Campos et al. (2003) failed to mention the statistic methodology.[44] Furthermore, Campos et al. (2003), Forner et al. (2018), Oertel et al. (2000), and Ono et al. (2021)[35] did not report the primary transplantation indication (attrition bias).[34,36,44] Donaldson et al. (1993) selected a subgroup of patients to genetically type HLA-DR for analysis of the effect of matching on vanishing bile duct syndrome (VBDS), without providing a reason for this subgroup selection (attrition bias).[45] Forner et al. (2018) failed to accurately report time to rejection (detection bias).[34] Since the data from these studies with a potential risk of bias were usable for our research question, we included them in our analyses. Nevertheless, these studies should be interpreted with more caution. We excluded acute rejection data from Doran et al. (2000), because it was unclear whether biopsy scores were from all patients or from only those with acute rejection.[46]

Whether HLA matching for liver transplantation improves outcomes has long been a topic of debate. The most recent meta-analysis (2010) included 16 articles including serological, not DNA-based HLA typing.[31] The main finding was that combined HLA-A, -B and -DR matching significantly decreased the incidence of acute rejection (0-2 vs. 3-6 mismatches; n=1,268; RR=0.77; 95% CI=[0.61-0.97]; P=0.03). Similar combined data were not available for meta-analysis from the articles included in the current study. Unfortunately, the previous meta-analysis did not provide data on HLA-C mismatching, the only locus we found to be associated with acute rejection (Figure 2). HLA-C eplet mismatching has previously been associated with acute rejection.[47] This may be explained by the interaction of HLA-C with killer immunoglobulin receptors (KIRs) expressed on NK cells and subsets of T-cells. Several other studies suggest that the HLA-C allelic subtype and KIR subtype may interplay to either protect or activate immune responses.[38,41,48]

Not every mismatch has similar consequences. This has stimulated the development of new epitope-based matching algorithms. These algorithms use small polymorphisms on the outer domains of HLA molecules to calculate a mismatch score. For example, HLAMatchmaker uses B-cell epitopes,[49] and has shown to correlate with graft outcome in various solid organ transplantations.[50] PIRCHE (Predicted Indirectly

9

Recognizable HLA Epitopes) uses T-cell epitopes,[51] and matching using this algorithm has shown to reduce formation of dnDSAs after kidney transplantation.[52] A recent study shows that PIRCHE-II mismatching may improve outcomes for young patients transplanted for autoimmune diseases.[50] On the other hand, the use of such algorithms may censor the effect of mismatching of a single-locus (e.g., HLA-C). Conversely, our study relying on aggregation of reported cases in literature made it impossible to study the effects of combined HLA-locus (mis)matching on transplantation outcomes.

In conclusion, we found evidence that genetic HLA-C matching reduces the risk of acute rejection after liver transplantation. Novel techniques to evaluate HLA mismatch-derived peptides may further help to unravel this longstanding liver transplantation paradigm. This is particularly important with the emergence of novel bankable liver cell sources for transplantation, which enable precise matching for clinical practice.

References

1. Feng S & Roayaie K. Liver Transplant. https://transplantsurgery.ucsf.edu/conditions--procedures/liver-transplant.aspx. Accessed: 04-11-2022.

2. Feng S & Bucuvalas J. Tolerance after liver transplantation: Where are we? *Liver Transpl.* 2017; 23: 1601–1614.

3. Ojo AO, Held PJ, Port FK, et al. Chronic Renal Failure after Transplantation of a Nonrenal Organ. *N Engl J Med.* 2003; 349: 931–940.

4. Åberg F, Gissler M, Karlsen TH, et al. Differences in long-term survival among liver transplant recipients and the general population: A population-based nordic study. *Hepatology.* 2015; 61: 668–677.

5. Tasdogan BE, Ma M, Simsek C, Saberi B & Gurakar A. Update on Immunosuppression in Liver Transplantation. *Euroasian J Hepato-Gastroenterol.* 2019; 9: 98–101.

6. Taner T, Stegall MD & Heimbach JK. Antibody-mediated rejection in liver transplantation: Current controversies and future directions. *Liver Transpl.* 2014; 20: 514–527.

7. Halloran PF, Wadgymar A, Ritchie S, et al. The significance of the anti—class i antibody response: I. Clinical and pathologic features of anti—class i—mediated rejection. *Transplantation.* 1990; 49: 85–91.

8. Cheng EY. The Role of Humoral Alloreactivity in Liver Transplantation: Lessons Learned and New Perspectives. *J Immunol Res.* 2017; 1–9.

9. Moreau A, Varey E, Anegon I & Cuturi MC. Effector mechanisms of rejection. *Cold Spring Harb Perspect Med.* 2013; 3: 1–33.

10. Murphy K & Weaver C. Janeway's immunobiology. Garland Science. 2017.

11. Choudhary NS, Saigal S, Bansal RK, et al. Acute and Chronic Rejection After Liver Transplantation: What A Clinician Needs to Know. *J Clin Exp Hepatol.* 2017; 7: 358–366.

12. Opelz G. Effect of HLA matching in 10,000 cyclosporine-treated cadaver kidney transplants. *Transplant Proc.* 1987; 19: 641–646 (1987).

13. Opelz G. Importance of HLA Antigen Splits for Kidney Transplant Matching. *The Lancet.* 1998; 332: 61–64.

14. Anasetti C, Amos D, Beatty PG, et al. Effect of HLA Compatibility on Engraftment of Bone Marrow Transplants in Patients with Leukemia or Lymphoma. *N Engl J Med.* 1989; 320: 197–204.

15. Gjertson DW, Terasaki PI, Takemoto S & Mickey MR. National Allocation of Cadaveric Kidneys by HLA Matching. *N Engl J Med.* 1991; 324: 1032–1036.

16. Opelz G. Effect of HLA matching in heart transplantation. *Transplant Proc.* 1989; 21: 794–796.

17. Doxiadis IIN, Smits JMA, Persijn GG, Frei U & Claas FHJ. It takes six to boogie: Allocating cadaver kidneys in Eurotransplant. *Transplantation.* 2004; 77: 615–617.

18. Eurotransplant. Chapter 10 Histocompatibility Testing. Eurotransplant Manual. 2018; 1–21.

19. Gubernatis G, Kemnitz J, Tusch G & Pichlmayr R. HLA compatibility and different features of liver allograft rejection. *Transpl Int.* 1988; 1: 155–160.

20. Markus BH, Duquesnoy RJ, Gordon RD, et al. Histocompatibility and liver transplant outcome. Does HLA exert a dualistic effect? *Transplantation.* 1988; 46: 372–377.

21. O'Grady JG, Alexander GJ, Sutherland S, et al. Cytomegalovirus Infection and Donor/Recipient HLA Antigens: Interdependent Co-Factors in Pathogenesis of Vanishing Bileduct Syndro-

9

me After Liver Transplantation. *The Lancet*. 1988; 332: 302–305.

22. Chen M, Wade J, Levy GA & Greig PD. Effect of HLA matching and T- and B-cell crossmatch on acute rejection and graft survival following liver transplantation. *Transplant Proc*. 1994; 26: 2695–2696.

23. Nikaein A, Backman L, Jennings L, et al. HLA compatibility and liver transplant outcome: Improved patient survival by HLA and cross-matching. *Transplantation*. 1994; 58: 786–792.

24. Balan V, Ruppert K, Demetris AJ, et al. Long-term outcome of human leukocyte antigen mismatching in liver transplantation: Results of the National institute of diabetes and digestive and kidney diseases liver transplantation database. *Hepatology*. 2008; 48: 878–888.

25. Erlich HA, Opelz G & Hansen J. HLA DNA typing and transplantation. *Immunity.* 2001; 14: 347–356.

26. Fox I, Chowdhury JR, Kaufman SS, et al. Treatment of the Crigler-Najjar Syndrome Type I with hepatocyte transplantation. *N Engl J Med*. 1998; 338: 1422–1426.

27. Puppi J, Tan N, Mitry RR, et al. Hepatocyte Transplantation Followed by Auxiliary Liver Transplantation—a Novel Treatment for Ornithine Transcarbamylase Deficiency. *Am J Transplant*. 2008; 8: 452–457.

28. Stéphenne X, Najimi M, Sibille C, et al. Sustained Engraftment and Tissue Enzyme Activity After Liver Cell Transplantation for Argininosuccinate Lyase Deficiency. *Gastroenterology*. 2006; 130: 1317–1323.

29. Stéphenne X, Debray FG, Smets F, et al. Hepatocyte transplantation using the domino concept in a child with tetrabiopterin nonresponsive phenylketonuria. *Cell Transplant*. 2012; 21: 2765–2770.

30. Kruitwagen HS, Oosterhoff LA, van Wolferen ME, et al. Long-Term Survival of Transplanted Autologous Canine Liver Organoids in a COMMD1-Deficient Dog Model of Metabolic Liver Disease. *Cells*. 2020; 9: 410.

31. Lan X, Zhang M-M, Pu C-L, et al. Impact of human leukocyte antigen mismatching on outcomes of liver transplantation: A meta-analysis. *World J Gastroenterol*. 2010; 16: 3457–3464.

32. Boutron I, Page MJ, Higgins JPT, et al. Considering bias and conflicts of interest among the included studies. in Cochrane Handbook for Systematic Reviews of Interventions. Cochrane. 2021.

33. DerSimonian R & Laird N. Meta-analysis in clinical trials. *Control Clin Trials*. 1986; 7: 177–188.

34. Forner D, Liwski R & Alwayn I. Human leukocyte antigen, allele, and eplet mismatches in liver transplantation; observations from a small, single center cohort. *Hum Immunol*. 2018; 79: 154–159.

35. Ono K, Ide K, Tanaka Y, et al. Molecular Mismatch Predicts T Cell–Mediated Rejection and De Novo Donor-Specific Antibody Formation After Living Donor Liver Transplantation. *Liver Transpl*. 2021; 27: 1592–1602.

36. Oertel M, Berr F, Schröder S, et al. Acute rejection of hepatic allografts from HLA-DR13 (Allele DRB1*1301)-positive donors. *Liver Transpl*. 2000; 6: 728–733.

37. Na GH, Kim EY, Hong TH, You YK & Kim DG. Effects of preoperative positive cross-match and HLA mismatching on early acute cellular rejection and graft survival in living donor liver transplantation. *Ann Transplant*. 2015; 20: 553–560.

38. Legaz I, López-Álvarez MR, Campillo JA, et al. KIR gene mismatching and KIR/C ligands in liver transplantation: Consequences for short-term liver allograft injury. *Transplantation*. 2013; 95: 1037–1044.

39. Muro M, López-Álvarez MR, Campillo JA, et al. Influence of human leukocyte antigen mismatching on rejection development and allograft survival in liver transplantation: Is the relevance of HLA-A locus matching being underestimated? *Transpl Immunol*. 2012; 26: 88–93.

40. Boix F, Legaz I, Minhas A, et al. Identification of peripheral CD154+ T cells and HLA-DRB1 as biomarkers of acute cellular rejection in adult liver transplant recipients. *Clin Exp Immunol*. 2021; 203: 315–328.

41. Lopez-Alvarez MR, Moya-Quiles MR, Minguela A, et al. HLA-C matching and liver transplants: donor-recipient genotypes influence early outcome and CD8+KIR2D+ T-cells recuperation. *Transplantation*. 2009; 88: S54–S61 (2009).

42. Moya-Quiles MR, Torío A, Muro M, et al. Impact of HLA-C on acute rejection in liver transplantation. *Transplant Proc*. 2003; 35: 1892–1893.

43. Francavilla R, Hadzic N, Underhill J, et al. Role of HLA compatibility in pediatric liver transplantation. *Transplantation*. 1998; 66: 53–58.

44. Campos J, Quijano Y, Franco A, et al. Beneficial effects of HLA class II incompatibility in living donor liver transplantation. *Transplant Proc*. 2003; 35: 1888–1891.

45. Donaldson P, Underhill J, Doherty D, et al. Influence of human leukocyte antigen matching on liver allograft survival and rejection: "The dualistic effect". *Hepatology*. 1993; 17: 1008–1015.

46. Doran TJ, Geczy AF, Painter D, et al. A large, single center investigation of the immunogenetic factors affecting liver transplantation. *Transplantation*. 2000; 69: 1491–1498.

47. Guiral S, San Segundo D, Irure J, et al. Number of antibody-verified eplet in HLA-C locus as an independent factor of t-cell-mediated rejection after liver transplantation. *Transplantation*. 2020; 104: 562–567.

48. López-Álvarez MR, Gómez-Mateo J, Ruiz-Merino G, et al. Analysis of KIR2D receptors on peripheral blood lymphocytes from liver graft recipients. *Transpl Immunol*. 2006; 17: 51–54.

49. Duquesnoy RJ. HLAMatchmaker: a molecularly based algorithm for histocompatibility determination. I. Description of the algorithm. *Hum Immunol*. 2002; 63: 339–352.

50. Kok G, Verstegen MMA, Houwen RHJ, et al. Assessment of HLA matching algorithm PIRCHE-II on liver transplantation outcomes. *Liver Transpl*. 2022; 28: 1356–1366.

51. Geneugelijk K, Thus KA & Spierings E. Predicting alloreactivity in transplantation. *J Immunol Res*. 2014.

52. Tafulo S, Malheiro J, Santos S, et al. HLA class II eplet mismatch load improves prediction of dnDSA development after living don or kidney transplantation. *Int J Immunogenet*. 2020; 48: 1–7.

53. Poli F, Scalamogna M, Aniasi A, et al. A retrospective evaluation of HLA-A, B and -DRB1 matching in liver transplantation. *Transpl Int*. 1998; 11: S347–S349.
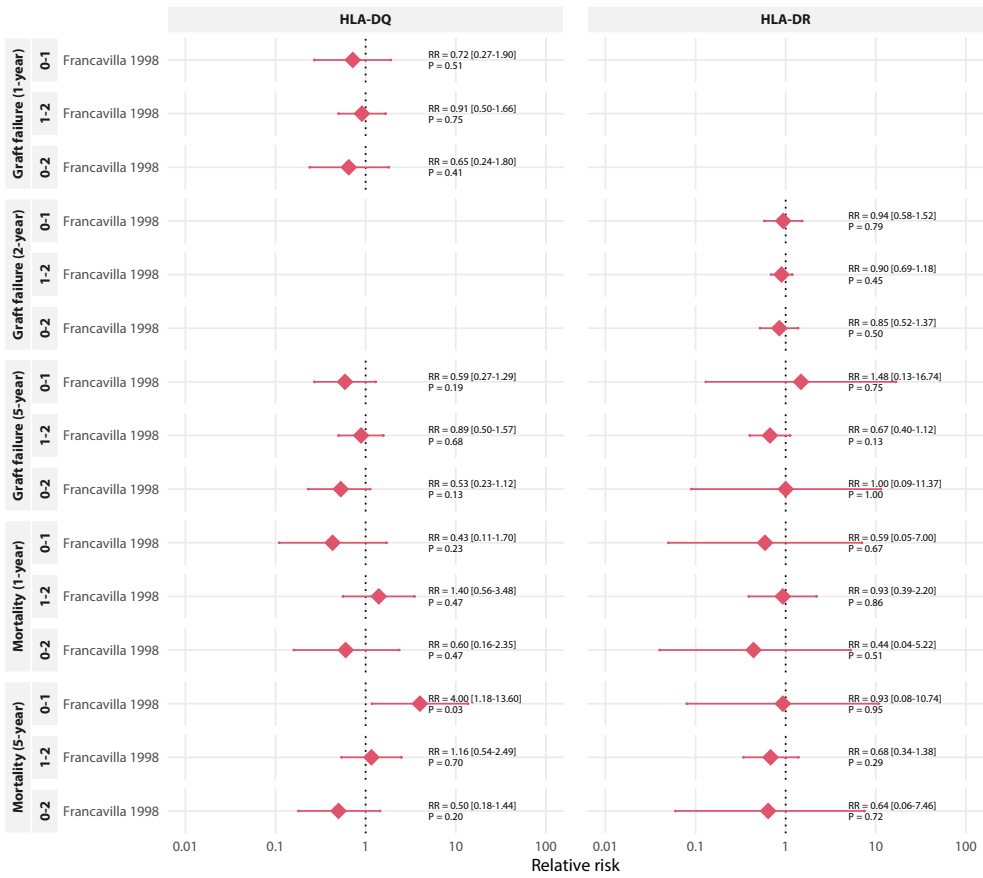
9

Supplementary figure

Fig. S1: Forest plots of the effect of HLA DR, and DQ mismatching on graft failure and mortality for patients with mixed primary diseases comparing 0 to 1, 1 to 2, and 0 to 2 mismatches. Positive risk ratio (RR) indicates increased risk of outcome with increased mismatches. Data are based on a single article and thus not meta analyzed.

Supplementary table

Table S1: characteristics of included studies (continued).

First author[ref] Year	Primary indication for liver transplantation
Doran[46] 2000	Autoimmune diseases: Primary biliary cirrhosis (PBC) (45) and autoimmune chronic active hepatitis (auto-CAH) (26)
Donaldson[45] 1993	Hepatocellular Carcinoma (HCC), Budd-Chiari syndrome, PBC, viral Hepatitis B (HBV), possibly other
Francavilla[43] 1998	Extrahepatic biliary atresia (51), acute hepatic failure (30), α1-antitrypsin deficiency (15), cryptogenic cirrhosis (9); Alagille's syndrome (9); familiar intrahepatic cholestasis (9); tyrosinemia (2); hepatoblastoma (2); hemangioendothelioma (2); autoimmune sclerosing cholangitis (2); and primary sclerosing cholangitis (PSC) (1), autoimmune hepatitis (1), neonatal sclerosing cholangitis (1), cystic fibrosis (1), copper overload (1), fatty acid oxidation defect (1), glycogen storage disease (1), giant cell hepatitis with Coombs' positive hemolytic anemia (1), Wilson's disease (1), and congenital hepatic fibrosis (1)
Poli[53] 1998	Post-hepatitis and alcoholic liver cirrhosis were the underlying diseases in 278 cases (54.7%), other
Oertel[36] 2000	*NA*
Campos[44] 2003	*NA*
Moya-Quiles[42] 2003	Alcoholic cirrhosis (35), alcoholic cirrhosis + (HBV or HCV) (24), malignancies (11), amyloidosis (7), acute hepatic failures (7), wilsons disease (4), chronic active HBV or HCV (4)
Lopez-Alvarez[41] 2009	Alcoholic cirrhosis (103), chronic acive HBV and HCV (61), carcinoma (30), autoimmune diseases (30), alcoholic cirrhosis and HBV and HCV (17), acute hepatic failure (8), other (51)
Muro[39] 2012	Alcoholic cirrhosis (71), cirrhosis after HCV (31), alcoholic cirrhosis HCV/HBV (28), primary hepatic malignancies (24), amyloidosis (17), PBC (13), acute hepatic failure (12), Wilson disease (10), cirrhosis after HBV (7), cryptogenic cirrhosis (7), PSC (3) and autoimmune hepatitis (1)
Legaz[38] 2013	Alcoholic cirrhosis (138), HCV (77), HCC (59), alcoholic cirrhosis plus HCV or HBV (28), autoimmune disease (27), HBV (12), acute hepatic failure (10), viral chronic hepatitis other (1) and others (50)
Na[37] 270	HBV (172), alcoholic cirrhosis (44), autoimmune (17), others (53)
Forner[34] 2018	*NA*
Boix[40] 2020	Alcoholic cirrhosis (viral 6 and non-viral 12), HCV cirrhosis, PBC 6, other (6): Budd-Chiari syndrome, PSC, cholangiocarcinoma
Ono[35] 2021	Alcohol-related liver disease (9), viral (18), HBV/HCV, AIH/PBC/PSC (7), other (11)

9

ASSESSMENT OF HLA MATCHING ALGORITHM PIRCHE-II ON LIVER TRANSPLANTATION OUTCOMES

Gautam Kok, Monique Verstegen, Roderick Houwen, Edward Nieuwenhuis, Herold Metselaar, Wojciech Polak, Luc van der Laan, Eric Spierings*, Caroline den Hoed*, Sabine Fuchs

10

Abstract

For liver transplantations, human leukocyte antigen (HLA) matching is not routinely performed because observed effects have been inconsistent. Nevertheless, long-term liver transplantation outcomes remain suboptimal. The availability of a more precise HLA-matching algorithm, Predicted Indirectly Recognizable HLA Epitopes II (PIRCHE-II), now enables robust assessment of the association between HLA matching and liver transplantation outcomes.

We performed a single-center retrospective cohort study of 736 liver transplantation patients. Associations between PIRCHE-II and HLAMatchmaker scores and mortality, graft loss, acute and chronic rejection, ischemic cholangiopathy, and disease recurrence were evaluated with Cox proportional hazards models. Associations between PIRCHE-II with 1-year, 2-year, and 5-year outcomes and severity of acute rejection were assessed with logistic and linear regression analyses, respectively. Subgroup analyses were performed for autoimmune and nonautoimmune indications, and patients aged 30 years and younger, and older than 30 years.

PIRCHE-II and HLAMatchmaker scores were not associated with any of the outcomes. However, patients who received transplants for autoimmune disease showed more acute rejection and graft loss, and these risks negatively associated with age. Rhesus mismatch more than doubled the risk of disease recurrence. Moreover, PIRCHE-II was inversely associated with graft loss in the subgroup of patients aged 30 years and younger with autoimmune indications.

The absence of associations between PIRCHE-II and HLAMatchmaker scores and the studied outcomes refutes the need for HLA matching for liver (stem cell) transplantations for nonautoimmune disease. For autoimmune disease, the activated immune system seems to increase risks of acute rejection and graft loss. Our results may suggest the benefits of transplantations with rhesus matched but PIRCHE-II mismatched donor livers.

Introduction

Human leukocyte antigen (HLA) matching has reduced incidences of acute and chronic rejection and improved allograft survival for various types of organ transplantations, including kidney,[1-4] heart,[5] and bone marrow transplantation.[6] In contrast, studies on liver transplantation repeatedly demonstrated conflicting results,[7-12] which has resulted in the current clinical practice of matching liver donor and recipients only by blood group and not HLA compatibility. Short-term outcomes of liver transplantation are currently very good, but long-term outcomes remain suboptimal, partially because of the long-term use of immunosuppressants.[13] Better donor–recipient matching holds the potential to improve transplantation outcomes but is hampered by the shortage of donor grafts. With the prospect of biobankable liver cell sources, including human liver organoids and stem cells, the question of whether HLA matching could improve the survival of allogenic cells or tissue constructs is becoming increasingly relevant.[14]

In recent years, more precise methods for HLA matching have been developed. Multiple studies suggest that epitope-based matching algorithms such as HLAMatchmaker[15-17] may predict graft outcome in kidney,[18] lung,[19] cornea,[20] pediatric heart,[21] and pediatric liver transplantation.[22] Epitopes are parts of HLA molecules that may be present on different HLA antigens. Eplets, small polymorphisms on the outer domains of HLA molecules that differ between donor and recipient, are identified by HLA-Matchmaker and presented in a continuous score.[15-17] In addition to the B cell–mediated immune response, T cell–mediated alloreactivity plays a role after solid organ transplantation. The direct pathway comprises T cell recognition of allogeneic HLA molecules on the surface of allogeneic cells. In the indirect pathway, T cells recognize mismatched HLA-derived epitopes processed and presented by nonallogeneic cells. Indirect T cell alloreactivity plays an important role in the humoral response toward HLA. Identification of these indirectly recognizable epitopes provides an alternative to epitope-based matching, which is what the Predicted Indirectly Recognizable HLA Epitopes (PIRCHE-II) algorithm does.[23] This algorithm can estimate the likelihood of HLA-derived peptides to bind HLA class II molecules (HLA-DR, HLA-DQ, and HLA-DP).[24] PIRCHE-II was found to correlate with kidney graft loss[25] and provides a risk classification for the anti-HLA de novo donor-specific antibody (dnDSA) formation after kidney,[26-28] pancreas,[28,29] and liver transplantations.[30,31]

Unfortunately, the results from the aforementioned studies investigating these algorithms for liver transplantation have limited use for clinical practice because they were limited in size and inclusion criteria[22] or only investigated anti-HLA donor-specific antibody (DSA) formation, but no clinical outcomes.[30,31] Also, previous studies generally grouped recipients with immunological (autoimmune) and other transplantation indications. Yet, mismatching may theoretically decrease disease recurrence and improve allograft survival in patients with autoimmune liver disease.[32] In general, the activity of the immune system may play a role in rejection reactions. The interplay between a more active immune system in younger patients and the use of immunosuppressants may influence and/or mask the effects of matching.[33] Therefore, we performed a single-center retrospective cohort study that included 736 patients who underwent primary liver transplantation to evaluate the predictive value of PIRCHE-II scores on liver transplantation outcomes in recipients of varying ages with autoimmune and other liver diseases.

Patients and methods

Study design and patients

We retrospectively included all consecutive adult patients who received a primary liver transplantation in the Erasmus Medical Center, Rotterdam, The Netherlands, between January 1, 2000, and June 30, 2019. Patients for whom HLA typing of donor and recipient were unavailable and patients who received combined liver and kidney transplantation were excluded. We used electronic patient records to collect patient and donor characteristics, including transplantation indication, immune serology, blood group and HLA typing, surgery details, immunosuppressant use, and follow-up markers. The selected timeframe allowed for a minimum follow-up of 1 year. As part of the standard care, all patients were seen at least once a year. The date of the last visit was considered the latest follow-up.

PIRCHE-II and HLAMatchmaker scores

Patients and donors were typed for their HLA by molecular typing methods as per transplant protocol. Typings were reported at the serological split level for all loci following the EuroTransplant guidelines. If HLA-C and/or HLA-DQ were missing (see Table S1), typings for these loci were imputed for epitope calculations as previously reported.[34] PIRCHE-II scores for donor–recipient matches were calculated using the PIR-

CHE-II Matching Service (Pirche AG) in February 2021 as described previously.[25] Because PIRCHE-II and antibody formation are logarithmically correlated,[26] PIRCHE-II scores were transformed by natural logarithm (ln(PIRCHE-II +1)) for further analyses. For comparison, HLAMatchmaker scores were calculated using HLAMatchmaker (Version 2.0).

Outcome measures

Primary outcomes included histology-confirmed acute rejection (defined as rejection activity index [RAI] >2), histology-confirmed chronic rejection, radiology-confirmed ischemic cholangiopathy, graft loss (defined as retransplantation or graft-related death), and mortality (all cause except procedure related). Disease recurrence (except malignancies) was a secondary outcome. Follow-up ended if the patient received another transplantation (e.g., kidney) or a retransplantation, if the patient died or was lost to follow-up, or at the last check of the electronic patient records.

Statistical analyses

All statistical analyses were performed with R (Version 4.0.5; R Foundation for Statistical Computing) packages tableone (0.12.0), survival (3.2–11), survminer (0.4.9), and lmtest (0.9–38). All continuous variables were checked for normal distribution. Kaplan–Meier curves were used to visualize the effect of ln(PIRCHE-II), divided into quartiles, on patient survival and graft survival, and log-rank was used to test for significant differences.

For each of the primary outcomes, univariate Cox proportional hazards models with recipient and donor age and sex, ischemia times, ABO and rhesus mismatches, and ln(PIRCHE-II) as covariates to determine independent risk factors were used. In addition, multivariable Cox proportional hazards models were used, correcting for recipient and donor age and sex, ABO and rhesus mismatches, and autoimmune indication (primary sclerosing cholangitis, primary biliary cirrhosis, acute/chronic autoimmune hepatitis). In these multivariable models, interactions between ln(PIRCHE-II) and the most common individual induction therapies (steroids, mycophenolate mofetil [MMF], tacrolimus, cyclosporin, and basiliximab) were tested. Subgroup analyses were performed for patients with autoimmune indications and nonautoimmune indications and for autoimmune indications in combination with age 30 years and younger. For both univariate and multivariable analyses, adjusted hazard ratios (aHRs) or hazard ratios (HRs) with 95% confidence intervals (95% CIs) were calculated. The likelihood

10

ratio test was used to determine the significance of interactions. Logistic regression analyses were performed to test the associations between ln(PIRCHE-II) and the primary outcomes after 1 year, 2 years, and 5 years of follow-up. Linear regression analysis was used to determine if there was an effect of ln(PIRCHE-II) on the severity of acute rejection (RAI score).

Results

Study population

In the selected timeframe, a total of 873 primary liver transplantations were performed. Of these, 118 patients were excluded because of missing donor or recipient HLA typing, and a further 19 patients were excluded because they received combined liver and kidney transplantations. As a result, a total of 736 patients were included in this study (Figure 1).

The mean age of the recipients was 50.94 ± 12.26 years, and 479 (65.1%) were men. The untransformed PIRCHE-II and HLAMatchmaker scores had means of
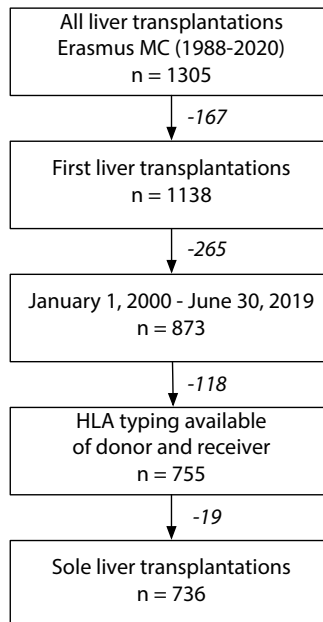

Fig. 1: flowchart of inclusion strategy.

85.88 ± 42.97 and 39.48 ± 12.45, respectively, and were significantly correlated (coefficient = 0.27, $p < 0.001$; Figure S1). Among the most common indications for transplantation were autoimmune diseases (229, 31.1%) followed by viral chronic active hepatitis (156, 21.2%) and alcohol-induced cirrhosis (115, 15.6%). In addition to the primary disease, 215 patients (29.2%) were diagnosed with hepatocellular carcinoma, and 10 (1.4%) with cholangiocarcinoma (of which 8 had primary sclerosing cholangitis). Mean follow-up was 5.98 ± 5.47 years. Most patients retained their donor liver and were alive at the end of follow-up (438, 59.5%). The rest had died (181, 24.6%), received retransplants (86, 11.7%), or received another solid organ transplantation (9, 1.2%). A total of 22 patients (3.0%) were lost to follow-up, with a mean time to loss of follow-up of 6.82 ± 5.27 years. Except ischemia times and perioperative blood loss, all continuous variables were normally distributed. All baseline characteristics are summarized in Tables 1-4. The number of patients analysed (slashed) for each variable may differ from the total number of patients per (sub)group due to missing data or loss to follow-up.

Table 1: general baseline characteristics divided by PIRCHE-II quartiles.

Baseline characteristics, general	PIRCHE-II and ln(PIRCHE-II) quartiles				p
	[0, 55.5] [0, 4.03] n = 184	(55.5, 78.2] (4.03, 4.37] n = 185	(78.2, 108] (4.37, 4.69] n = 183	(108, 273] (4.69, 5.61] n = 184	
Follow-up, years, median [range]	4.01 [0.00, 20.06]	4.85 [0.00, 20.54]	4.32 [0.00, 20.57]	4.24 [0.00, 20.53]	0.52
Reason for end of follow-up, n (%)					0.83
Alive	111 (60.3)	111 (60.0)	99 (54.1)	117 (63.6)	
Deceased	44 (23.9)	44 (23.8)	50 (27.3)	43 (23.4)	
Loss to follow-up	7 (3.8)	6 (3.2)	5 (2.7)	4 (2.2)	
Other Tx	1 (0.5)	4 (2.2)	2 (1.1)	2 (1.1)	
Re-Tx	21 (11.4)	20 (10.8)	27 (14.8)	18 (9.8)	
PIRCHE-II score, mean (SD)	38.98 (11.87)	66.85 (6.67)	92.40 (8.20)	145.44 (31.25)	<0.001
HLAMatchmaker score, mean (SD)	36.34 (18.00)	38.52 (10.64)	39.22 (9.36)	43.84 (8.21)	<0.001

ln(PIRCHE-II), natural logarithm of PIRCHE-II+1; PIRCHE-II, Predicted Indirectly Recognizable HLA Epitopes II; SD, standard deviation; Tx, transplantation.

10

Table 2: donor and recipient baseline characteristics divided by PIRCHE-II quartiles.

Baseline characteristics, donor and recipient	PIRCHE-II and ln(PIRCHE-II) quartiles				p
	[0, 55.5] [0, 4.03] *n* = 184	(55.5, 78.2] (4.03, 4.37] *n* = 185	(78.2, 108] (4.37, 4.69] *n* = 183	(108, 273] (4.69, 5.61] *n* = 184	
Donor					
Age, years, mean (SD)	51.29 (15.65)	46.89 (15.52)	49.53 (15.69)	48.76 (14.82)	0.05
Sex, male, *n* (%)	101/184 (54.9)	88/185 (47.6)	88/183 (48.1)	99/184 (53.8)	0.36
Recipient					
Age, years, mean (SD)	50.03 (13.20)	51.29 (11.67)	51.43 (12.35)	51.01 (11.81)	0.70
Sex, male, *n* (%)	116/184 (63.0)	115/185 (62.2)	124/183 (67.8)	124/184 (67.4)	0.56
BMI, mean (SD)	26.18 (4.65)	25.62 (4.34)	25.76 (4.25)	26.00 (4.46)	0.62
MELD score at Tx, mean (SD)	22.87 (7.23)	23.19 (7.30)	22.25 (6.84)	23.38 (7.28)	0.59
Primary Tx indication, *n(%)*					0.02
Acute liver failure: autoimmune	2 (1.1)	7 (3.8)	0 (0.0)	0 (0.0)	
Acute liver failure: e.c.i.	6 (3.3)	2 (1.1)	4 (2.2)	2 (1.1)	
Acute liver failure: other	1 (0.5)	0 (0.0)	0 (0.0)	1 (0.5)	
Acute liver failure: viral	3 (1.6)	2 (1.1)	3 (1.6)	5 (2.7)	
Biliary atresia	0 (0.0)	0 (0.0)	1 (0.5)	1 (0.5)	
Budd–Chiari syndrome	0 (0.0)	1 (0.5)	2 (1.1)	1 (0.5)	
Chronic-active hepatitis: autoimmune	10 (5.4)	7 (3.8)	6 (3.3)	6 (3.3)	
Chronic-active hepatitis: viral	33 (17.9)	36 (19.5)	35 (19.1)	52 (28.3)	
Cryptogenic cirrhosis	11 (6.0)	13 (7.0)	14 (7.7)	16 (8.7)	
Genetic/metabolic disease	12 (6.5)	13 (7.0)	15 (8.2)	14 (7.6)	
Nonalcoholic steatohepatitis	14 (7.6)	9 (4.9)	4 (2.2)	12 (6.5)	
Polycystic liver disease	2 (1.1)	10 (5.4)	5 (2.7)	6 (3.3)	
Primary biliary cirrhosis	3 (1.6)	10 (5.4)	4 (2.2)	10 (5.4)	
Primary liver tumor, *n* (%)	0 (0.0)	5 (2.7)	1 (0.5)	1 (0.5)	
Primary sclerosing cholangitis, *n* (%)	49 (26.6)	43 (23.2)	43 (23.5)	29 (15.8)	
Secondary biliary cirrhosis, *n* (%)	3 (1.6)	1 (0.5)	2 (1.1)	3 (1.6)	
Toxic: alcohol induced, *n* (%)	29 (15.8)	24 (13.0)	40 (21.9)	22 (12.0)	
Toxic: drug induced, *n* (%)	3 (1.6)	2 (1.1)	3 (1.6)	2 (1.1)	
Other, *n* (%)	3 (1.6)	0 (0.0)	1 (0.5)	1 (0.5)	

BMI, body mass index; e.c.i., et cause ignora; ln(PIRCHE-II), natural logarithm of PIRCHE-II+1; MELD, Model for End-Stage Liver Disease; PIRCHE-II, Predicted Indirectly Recognizable HLA Epitopes II; SD, standard deviation; Tx, transplantation.

Table 3: procedure and matching baseline characteristics divided by PIRCHE-II quartiles.

Baseline characteristics, procedure and matching	PIRCHE-II and ln(PIRCHE-II) quartiles [0, 55.5] [0, 4.03] *n* = 184	(55.5, 78.2] (4.03, 4.37] *n* = 185	(78.2, 108] (4.37, 4.69] *n* = 183	(108, 273] (4.69, 5.61] *n* = 184	p
Procedure					
Graft type n/total	n/179	n/181	n/175	n/178	0.003
Full, *n* (%)	179 (100.0)	172 (95.0)	171 (97.7)	177 (99.4)	
Split, *n* (%)	0 (0.0)	9 (5.0)	4 (2.3)	1 (0.6)	
Donor type n/total	*n*/184	*n*/184	*n*/183	*n*/184	0.55
Deceased, *n* (%)	41 (22.3)	51 (27.7)	48 (26.2)	52 (28.3)	
Living, *n* (%)	142 (77.2)	133 (72.3)	135 (73.8)	132 (71.7)	
Living related, *n* (%)	1 (0.5)	0 (0.0)	0 (0.0)	0 (0.0)	
Cold ischemia time, h, median [range]	6.56 [3.27, 16.47]	6.20 [2.32, 13.92]	6.48 [2.90, 14.90]	6.57 [2.75, 14.80]	0.35
Warm ischemia time, h, median [range]	0.47 [0.25, 1.17]	0.47 [0.18, 1.17]	0.47 [0.23, 1.50]	0.48 [0.27, 1.42]	0.52
Total ischemia time, h, median [range]	6.98 [3.63, 17.63]	6.72 [2.67, 14.68]	7.07 [3.53, 15.38]	7.07 [3.22, 15.60]	0.39
Blood loss, L, median [range]	4.12 [0.00, 62.00]	3.50 [0.00, 39.00]	3.85 [0.50, 34.00]	3.50 [0.00, 58.00]	0.17
Donor–recipient matching, *n/total (%)*					
ABO mismatch	4/184 (2.2)	1/185 (0.5)	1/182 (0.5)	2/184 (1.1)	0.39
Rhesus mismatch	34/184 (18.5)	21/185 (11.4)	11/183 (6.0)	22/184 (12.0)	0.003
HBsAg mismatch	0/182 (0.0)	1/182 (0.5)	0/181 (0.0)	0/183 (0.0)	0.39
HCVAb mismatch	0/182 (0.0)	0/183 (0.0)	0/181 (0.0)	0/183 (0.0)	NA
CMVIgG mismatch	36/182 (19.8)	34/183 (18.6)	33/181 (18.2)	27/184 (14.7)	0.61
EBVIgG mismatch	8/163 (4.9)	3/163 (1.8)	6/156 (3.8)	5/165 (3.0)	0.48
HIVAb mismatch	0/182 (0.0)	0/182 (0.0)	0/180 (0.0)	0/176 (0.0)	NA

ABO, blood group; CMVIgG, cytomegalovirus IgG; EBVIgG, Epstein-Barr virus IgG; HBsAg, hepatitis B surface antigen; HCVAb, hepatitis C virus antibody; HIVAb, human immunodeficiency virus antibody; ln(PIRCHE-II), natural logarithm of PIRCHE-II+1; NA; not available; PIRCHE-II Predicted Indirectly Recognizable HLA Epitopes II

10

Table 4: details of follow-up divided by PIRCHE-II quartiles.

Follow-up	PIRCHE-II and ln(PIRCHE-II) quartiles				p
	[0, 55.5] [0, 4.03] *n* = 184	(55.5, 78.2] (4.03, 4.37] *n* = 185	(78.2, 108] (4.37, 4.69] *n* = 183	(108, 273] (4.69, 5.61] *n* = 184	
Deceased, *n*/total (%)	52/180 (28.9)	57/182 (31.3)	65/179 (36.3)	49/180 (27.2)	0.27
Age of death, years, mean (SD)	55.87 (12.26)	59.26 (10.43)	57.95 (9.29)	57.61 (12.17)	0.45
Cause of death *n*/total	*n*/52	*n*/57	*n*/65	*n*/49	0.64
Postoperative complications, *n* (%)	8 (15.4)	11 (19.3)	14 (21.5)	7 (14.3)	
Graft related, *n* (%)	11 (21.2)	10 (17.5)	11 (16.9)	4 (8.2)	
Medical comorbidity, *n* (%)	18 (34.6)	22 (38.6)	22 (33.8)	24 (49.0)	
Malignancy, de novo, *n* (%)	7 (38.9)	13 (59.1)	9 (40.9)	9 (37.5)	
Infection/sepsis, *n* (%)	5 (27.8)	4 (18.2)	7 (31.8)	7 (29.2)	
Organ failure, excluding liver, *n* (%)	2 (11.1)	0 (0.0)	2 (9.1)	2 (8.3)	
Hemorrhage, excluding cerebral, *n* (%)	3 (16.7)	1 (4.5)	0 (0.0)	1 (4.2)	
Cardiac event, *n* (%)	0 (0.0)	2 (9.1)	1 (4.5)	2 (8.3)	
Stroke, *n* (%)	1 (5.6)	1 (4.5)	2 (9.1)	1 (4.2)	
Other comorbidity, *n* (%)	0 (0.0)	1 (4.5)	1 (4.5)	2 (8.3)	
Procedure related, *n* (%)	5 (9.6)	2 (3.5)	2 (3.1)	2 (4.1)	
Recurrence: malignancy, *n* (%)	7 (13.5)	6 (10.5)	6 (9.2)	7 (14.3)	
Recurrence: primary disease, *n* (%)	0 (0.0)	4 (7.0)	5 (7.7)	2 (4.1)	
Other, *n* (%)	2 (3.8)	1 (1.8)	2 (3.1)	3 (6.1)	
Unknown, *n* (%)	1 (1.9)	1 (1.8)	3 (4.6)	0 (0.0)	
Re-Tx, *n* (%)	21 (11.4)	22 (11.9)	28 (15.3)	20 (10.9)	0.57
Loss to follow-up, *n* (%)	7 (3.8)	6 (3.2)	5 (2.7)	4 (2.2)	0.82
Ischemic cholangiopathy, *n* (%)	11 (6.0)	13 (7.0)	10 (5.5)	13 (7.1)	0.90
Acute rejection, *n* (%)	51 (27.7)	48 (25.9)	53 (29.0)	51 (27.7)	0.94
RAI, mean (SD)	5.00 (1.29)	4.82 (1.21)	4.92 (1.51)	5.25 (1.20)	0.40
Chronic rejection, *n* (%)	6 (3.3)	6 (3.2)	12 (6.6)	5 (2.7)	0.21
Disease recurrence, *n* (%)	18 (9.8)	26 (14.1)	22 (12.0)	24 (13.0)	0.63
Induction therapy regimen, *n* (%)					0.39
Steroids + calcineurin inhibitor	3 (1.6)	4 (2.2)	11 (6.0)	5 (2.7)	
Steroids + calcineurin inhibitor + IL2 inhibitor	49 (26.6)	61 (33.0)	62 (33.9)	63 (34.2)	
Steroids + calcineurin inhibitor + IL2 inhibitor + MMF	5 (2.7)	5 (2.7)	5 (2.7)	8 (4.3)	
Steroids + calcineurin inhibitor + MMF	11 (6.0)	9 (4.9)	14 (7.7)	11 (6.0)	
Steroids + IL2 inhibitor + MMF	99 (53.8)	97 (52.4)	83 (45.4)	89 (48.4)	
None	4 (2.2)	1 (0.5)	2 (1.1)	2 (1.1)	
Other (*n* < 10)	13 (7.1)	8 (4.3)	6 (3.3)	6 (3.3)	

IL2, interleukin 2; ln(PIRCHE-II), natural logarithm of PIRCHE-II+1; MMF, mycophenolate mofetil; PIRCHE-II, Predicted Indirectly Recognizable HLA Epitopes II; RAI, rejection activity index; SD, standard deviation; Tx, transplantation.

Table 5: univariable and multivariable Cox regression analyses for ln(PIRCHE-II) on the primary outcomes mortality (excluding procedure related), graft loss, acute rejection, chronic rejection, and ischemic cholangiopathy.

Cox regression for ln(PIR-CHE-II) versus outcome	Univariable HR (95% CI)	p	Multivariable aHR (95% CI)	p	Events per total n
Mortality	1.03 (0.81–1.31)	0.80	0.99 (0.78–1.26)	0.96	212/710
Graft loss	0.88 (0.65–1.19)	0.40	0.91 (0.67–1.24)	0.56	113/736
Acute rejection	1.10 (0.86–1.41)	0.46	1.17 (0.91–1.51)	0.21	203/726
Chronic rejection	1.11 (0.57–2.14)	0.76	1.11 (0.57–2.16)	0.75	29/736
Ischemic cholangiopathy	0.99 (0.60–1.63)	0.97	1.05 (0.63–1.76)	0.85	46/735

aHR, adjusted hazard ratio; CI, confidence interval; HR, hazard ratio; ln(PIRCHE-II), natural logarithm of PIRCHE-II+1; PIRCHE-II, Predicted Indirectly Recognizable HLA Epitopes II

Table 6: univariable and multivariable Cox regression analyses for HLAMatchmaker scores on the primary outcomes mortality (excluding procedure related), graft loss, acute rejection, chronic rejection, and ischemic cholangiopathy.

Cox regression for HLA-Matchmaker versus outcome	Univariable HR (95% CI)	p	Multivariable aHR (95% CI)	p	Events per total n
Mortality	1.02 (0.92–1.13)	0.72	1.04 (0.93–1.17)	0.44	212/710
Graft loss	1.04 (0.90–1.21)	0.56	1.02 (0.88–1.19)	0.75	113/736
Acute rejection	1.11 (0.99–1.24)	0.07	1.09 (0.98–1.21)	0.13	203/726
Chronic rejection	1.03 (0.77–1.38)	0.83	1.03 (0.76–1.38)	0.86	29/736
Ischemic cholangiopathy	0.99 (0.79–1.26)	0.96	1.01 (0.80–1.27)	0.95	46/735

aHR and HR given per 10-point increase of HLAMatchmaker score. aHR, adjusted hazard ratio; CI, confidence interval; HR, hazard ratio; ln(PIRCHE-II), natural logarithm of PIRCHE-II+1; PIRCHE-II, Predicted Indirectly Recognizable HLA Epitopes II

10

Table 7: logistic regression analyses for ln(PIRCHE-II) on the primary outcomes mortality (excluding procedure related), graft loss, acute rejection, chronic rejection, and ischemic cholangiopathy at the follow-up time points of 1 year, 2 years, and 5 years.

Logistic regression for ln(PIRCHE-II) versus outcome	OR (95% CI)	p	Events per total n
Mortality			
1 year	1.01 (0.65–1.55)	0.98	73/720
2 years	0.96 (0.65–1.40)	0.82	98/719
5 years	0.97 (0.70–1.34)	0.84	146/720
Graft loss			
1 year	0.93 (0.60–1.44)	0.75	70/720
2 years	0.88 (0.60–1.30)	0.54	88/719
5 years	0.87 (0.60–1.25)	0.44	101/719
Acute rejection			
1 year	1.11 (0.81–1.52)	0.50	174/732
2 years	1.05 (0.78–1.42)	0.73	189/731
5 years	1.06 (0.79–1.42)	0.68	199/730
Chronic rejection			
1 year	0.64 (0.31–1.33)	0.24	16/732
2 years	1.02 (0.47–2.19)	0.96	22/731
5 years	1.07 (0.52–2.19)	0.85	26/729
Ischemic cholangiopathy			
1 year	1.08 (0.57–2.08)	0.81	32/730
2 years	1.28 (0.67–2.45)	0.46	35/729
5 years	0.99 (0.56–1.73)	0.96	41/727

CI, confidence interval; OR, odds ratio; PIRCHE-II, Predicted Indirectly Recognizable HLA Epitopes II; ln(PIRCHE-II), natural logarithm of PIRCHE-II+1

Analyses

Patient survival and graft survival did not differ between quartiles of ln(PIRCHE-II) scores (Figure 2A,B) nor did acute and chronic rejection (Figure 2C,D).

In univariable analyses, the continuous ln(PIRCHE-II) and HLAMatchmaker scores were not associated with the primary outcomes mortality, graft loss, acute rejection, chronic rejection, and ischemic cholangiopathy (Tables 5 and 6). Recipient age was independently associated with mortality (HR = 1.03, 95% CI = 1.02–1.05, $p < 0.001$; see Figure S2 for causes of death), graft loss (HR = 0.98, 95% CI = 0.96–0.99, $p = 0.002$), and acute rejection (HR = 0.98, 95% CI = 0.97–0.99, $p = 0.001$). Likewise, an autoimmune transplantation indication was independently associated with mortality (HR = 0.65, 95% CI = 0.48–0.89, $p = 0.008$; see Figure S3 for causes of death), graft loss (HR = 1.47, 95% CI = 1.01–2.14, $p = 0.04$; see Table S2 for causes of graft loss), and acute rejection (HR = 1.74, 95% CI = 1.32–2.30, $p < 0.001$). Both were not inde-
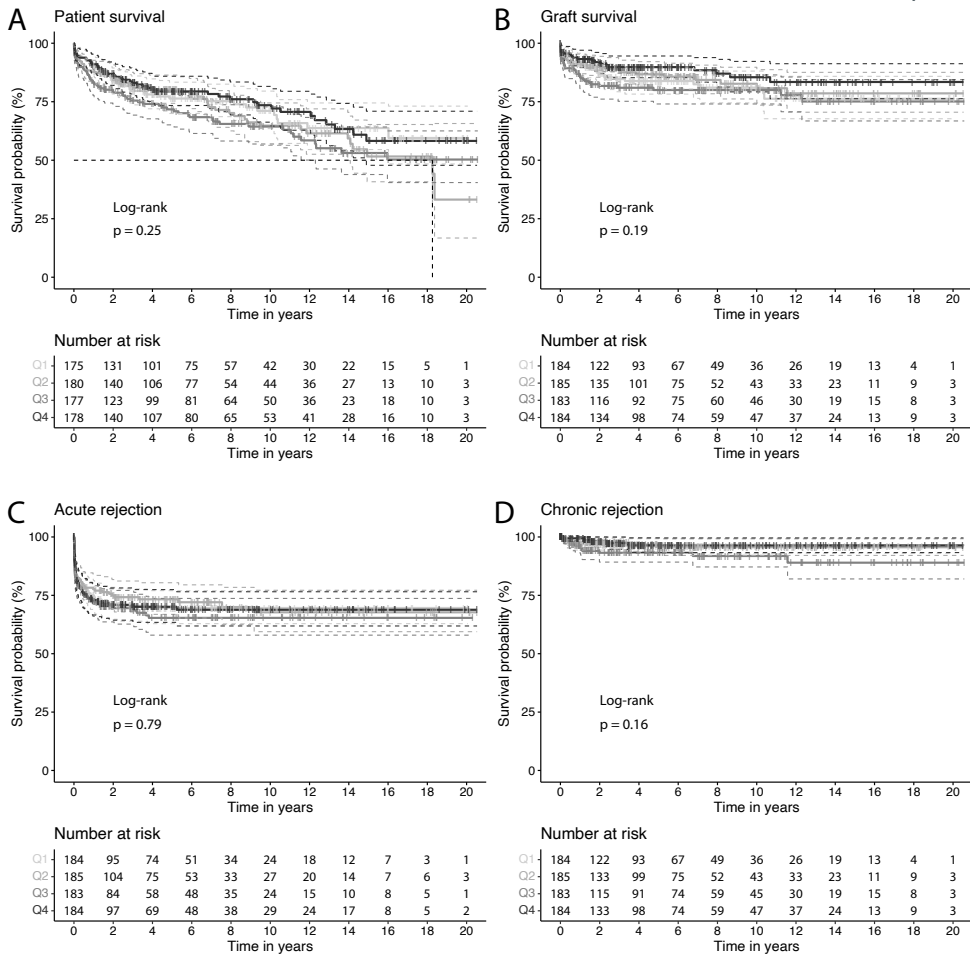
Fig. 2: Kaplan–Meier curves for quartiles of the natural logarithm of PIRCHE-II+1 of **A**, patient survival (excluding procedure-related death), **B**, graft survival, **C**, acute rejection, and **D**, chronic rejection: quartile 1 = [0, 4.03], quartile 2 = (4.03, 4.37], quartile 3 = (4.37, 4.69], and quartile 4 = (4.69, 5.61]

pendently associated with chronic rejection, ischemic cholangiopathy, or disease recurrence.

Logistic regression analyses revealed no associations between ln(PIRCHE-II) and any of the primary outcomes after 1 year, 2 years, and 5 years of follow-up (Table 7). Furthermore, ln(PIRCHE-II) was not correlated with severity of acute rejection, classified as RAI score, as determined by linear regression (coefficient = 0.22, p = 0.23).

Similarly, ln(PIRCHE-II) and HLAMatchmaker scores were not associated with any of the primary outcomes in multivariable analyses. However, in the ln(PIRCHE-II) models, recipient age was correlated with an increased risk of mortality (aHR = 1.03, 95% CI = 1.02–1.05, $p < 0.001$), yet decreased risks of graft loss (aHR = 0.98, 95% CI = 0.97–1.00, $p = 0.01$) and acute rejection (aHR = 0.99, 95% CI = 0.98–1.00, $p = 0.02$). Rhesus mismatch led to an increased risk of ischemic cholangiopathy (aHR = 2.19, 95% CI = 1.11–4.34, $p = 0.03$). Those who received transplants for autoimmune indications were at an increased risk of acute rejection (aHR = 1.63, 95% CI = 1.22–2.19, $p = 0.001$).Subgroup analyses: autoimmune and nonautoimmune indications

Multivariable subgroup analyses revealed no statistically significant associations between ln(PIRCHE-II) and any of the primary outcomes both for transplantations for autoimmune indications ($n = 229$) and transplantations for nonautoimmune indications ($n = 507$). Likewise, no associations between HLAMatchmaker score and any of the primary outcomes were found in these subgroups. Furthermore, ln(PIRCHE-II) and HLAMatchmaker scores were not associated with disease recurrence in either subgroup.

As in the full cohort, the association between age and mortality remained intact in both subgroups (autoimmune: aHR = 1.04, 95% CI = 1.01–1.07, $p = 0.003$; nonautoimmune: aHR = 1.03, 95% CI = 1.01–1.05, $p < 0.001$). However, the association with graft loss remained only in the autoimmune group (aHR = 0.98, 95% CI = 0.95–1.00, $p = 0.04$), and the association with acute rejection was not significant in both subgroups. In addition, a male donor increased the risk of acute rejection in the nonautoimmune subgroup (aHR = 1.66, 95% CI = 1.13–2.44, $p = 0.01$), and an association between rhesus mismatch and disease recurrence was found in the autoimmune subgroup (aHR = 2.43, 95% CI = 1.05–5.62, $p = 0.04$).

Subgroup analyses: young patients with autoimmune indications

There were no formal interactions between PIRCHE-II and age or age 30 years or younger. However, the multivariable subgroup analyses of patients with autoimmune indications and age 30 years or younger ($n = 31$) revealed an inverse association between ln(PIRCHE-II) with graft loss (12 events: aHR = 0.14, 95% CI = 0.03–0.63, $p = 0.01$). No such association was observed for the HLAMatchmaker score. The ln(PIRCHE-II) score was not associated with acute rejection (14 events). Donor age was

associated with decreased graft loss (aHR = 0.95, 95% CI = 0.90–1.00, p = 0.049). Insufficient events occurred to reliably determine associations with mortality (5 events), chronic rejection (3 events), ischemic cholangiopathy (2 events), and disease recurrence (6 events).

Immunosuppressants

Finally, in the full cohort, no statistically significant interactions were found between ln(PIRCHE-II) and the most common individual induction therapy drugs (steroids, basiliximab, MMF, tacrolimus, and cyclosporin) for any of the primary outcomes in the multivariable analyses. Similarly, these interactions were not present for the HLA-Matchmaker score.

Discussion

In this single-center retrospective cohort study of 736 first liver transplantations, we investigated whether the PIRCHE-II score is a predictor of liver transplantation outcomes. For comparison, we also performed all analyses using the HLAMatchmaker score.

We found no associations between PIRCHE-II scores and mortality, graft loss, acute rejection, chronic rejection, ischemic cholangiopathy, or disease recurrence. Furthermore, we found no associations in the subgroups of patients with and without autoimmune indications. Similarly, there were no associations of HLAMatchmaker score with any of the outcomes in the full cohort and subgroups. The finding that both scores overall did not predict transplantation outcomes confirms previous failures to show consistent advantages of HLA matching and is in line with results from a review of different studies on HLA matching and liver transplantation.[35] It also aligns with the current recommendation to not routinely use HLA matching for liver transplantation.

We found an important role for the activated immune system in patients who received transplants for autoimmune indications. These patients had a 74% (univariate) or 63% (multivariable) increase in risk of acute rejection and a 47% (univariate) increase in risk of graft loss, independent of PIRCHE-II or HLAMatchmaker scores. We further found a negative association between age and graft loss, which was most pronounced in the autoimmune group and may well result from decreasing reactivity of the immune system with increasing age. It was previously proposed that HLA matching could have adverse effects for patients with autoimmune diseases.[32] Although we did

10

not find this in the full subgroup of recipients with autoimmune diseases, we observed an inverse association between PIRCHE-II and graft loss, thus a decreased risk of graft loss upon higher mismatch in young patients (30 years and younger). This may be explained by the autoreactivity in this group of patients, where more mismatches lower the risk of a recurring autoimmune reaction. We would also expect an inverse association with disease recurrence, but there were insufficient events in this subgroup to reach statistical significance. We further found that rhesus mismatch more than doubled the risk of autoimmune disease recurrence, putatively through further activation of the immune system. Interestingly, this is not among the known risk factors for autoimmune disease recurrence. To improve transplantation outcomes for autoimmune disease, it may thus be advisable to transplant a donor liver that is PIRCHE-II mismatched but rhesus matched.

Donor preformed and anti-HLA dnDSA have been shown to correlate with rejection in kidney,[36] heart,[37] pancreas,[38] and lung[37] transplantations.[31] Concordantly, it was recently shown that patients with class II anti-HLA dnDSA following liver transplantation had higher PIRCHE-II scores[30] and that PIRCHE-II and HLAMatchmaker scores predict class II anti-HLA dnDSA formation after liver transplantation.[31] In our cohort, we found no association between PIRCHE-II and rejection. Unfortunately, we did not have anti-HLA DSA information for the patients in our study to confirm such an association between PIRCHE-II and anti-HLA dnDSA.

It remains possible that associations between ln(PIRCHE-II) and any of the primary outcomes were masked by drug-induced immune suppression. However, the absence of interactions between ln(PIRCHE-II) and the individual immunosuppressant drugs used suggests that any such influence would be evenly spread over the cohort because most patients received similar combinations of induction therapy. A previous study of 41 patients undergoing calcineurin inhibitor withdrawal found that those with PIRCHE-II scores <68 (or ln(PIRCHE-II) 4.23) had a significantly decreased risk of graft loss compared with those with scores PIRCHE-II ≥68.[39] Because of the retrospective nature of our study, it was not possible to accurately detect changes in (dosage) of medication and therapy withdrawal.

Our study stands out in the inclusion and follow-up of a large number of patients, the length of follow-up, the variety of primary transplantation indications, robustness of outcome parameters, and completeness of the data. Limitations of our study include

the single-center, retrospective design; the absence of anti-HLA DSA information; and limited patient numbers in some of the analyzed subgroups.

In conclusion, we found no associations between PIRCHE-II and HLAMatchmaker scores and mortality, graft loss, acute rejection, chronic rejection, ischemic cholangiopathy, or disease recurrence in our single-center cohort of primary liver transplantations. This implies that HLA matching is not needed for upcoming biobankable liver cell sources, which greatly facilitates the generation of a biobank. Our findings of inverse associations between liver transplantation outcomes and age, especially in patients who received transplants for autoimmune disease, suggest that the activity of the immune system plays an important role and that PIRCHE-II may be an inverse predictor of liver graft loss in younger patients (age 30 years and younger) with autoimmune diseases. Further studies are needed to evaluate whether PIRCHE-II mismatching and rhesus matching should be used to improve outcomes for (young) patients with autoimmune disease.

References

1. Opelz G. Effect of HLA matching in 10,000 cyclosporine-treated cadaver kidney transplants. *Transplant Proc*. 1987; 19: 641-6.

2. Opelz G. Importance of HLA antigen splits for kidney transplant matching. *Lancet*. 1988; 332: 61-4.

3. Anasetti C, Amos D, Beatty PG, et al. Effect of HLA compatibility on engraftment of bone marrow transplants in patients with leukemia or lymphoma. *N Engl J Med*. 1989; 320: 197-204.

4. Gjertson DW, Terasaki PI, Takemoto S, Mickey MR. National allocation of cadaveric kidneys by HLA matching. *N Engl J Med*. 1991; 324: 1032-6.

5. Opelz G. Effect of HLA matching in heart transplantation. *Transplant Proc*. 1989; 21: 794-6.

6. Beatty PG, Anasetti C, Hansen JA, et al. Marrow transplantation from unrelated donors for treatment of hematologic malignancies: effect of mismatching for one HLA locus. *Blood*. 1993; 81: 249-53.

7. Gubernatis G, Kemnitz J, Tusch G, Pichlmayr R. HLA compatibility and different features of liver allograft rejection. *Transpl Int*. 1988; 1: 155-60.

8. Markus BH, Duquesnoy RJ, Gordon RD, et al. Histocompatibility and liver transplant outcome. Does HLA exert a dualistic effect? *Transplantation*. 1988; 46: 372-7.

9. O'Grady JG, Sutherland S, Harvey F, et al. Cytomegalovirus infection and donor/recipient HLA antigens: interdependent co-factors in pathogenesis of vanishing bile-duct syndrome after liver transplantation. *Lancet*. 1988; 332: 302-5.

10. Chen M, Wade J, Levy GA, Greig PD. Effect of HLA matching and T- and B-cell crossmatch on acute rejection and graft survival following liver transplantation. *Transplant Proc*. 1994; 26: 2695-6.

11. Nikaein A, Backman L, Jennings L, et al. HLA compatibility and liver transplant outcome: improved patient survival by HLA and cross-matching. *Transplantation*. 1994; 58: 786-92.

12. Balan V, Ruppert K, Demetris AJ, et al. Long-term outcome of human leukocyte antigen mismatching in liver transplantation: results of the National institute of diabetes and digestive and kidney diseases liver transplantation database. *Hepatology*. 2008; 48: 878-88.

13. Jadlowiec CC, Taner T. Liver transplantation: current status and challenges. *World J Gastroenterol*. 2016; 22: 4438-45.

14. Kruitwagen HS, Oosterhoff LA, van Wolferen ME, et al. Long-term survival of transplanted autologous canine liver organoids in a COMMD1-deficient dog model of metabolic liver disease. *Cells*. 2020; 9: 410.

15. Duquesnoy RJ. HLAMatchmaker: a molecularly based algorithm for histocompatibility determination. I. Description of the algorithm. *Hum Immunol*. 2002; 63: 339-52.

16. Duquesnoy RJ. A structurally based approach to determine HLA compatibility at the humoral immune level. *Hum Immunol*. 2006; 67: 847-62.

17. Duquesnoy RJ. Clinical usefulness of HLA-Matchmaker in HLA epitope matching for organ transplantation. *Curr Opin Immunol*. 2008; 20: 594-601.

18. Wiebe C, Pochinco D, Blydt-Hansen TD, et al. Class II HLA epitope matching—a strategy to minimize de novo donor-specific antibody development and improve outcomes. *Am J Transplant*. 2013; 13: 3114-22.

19. Walton DC, Hiho SJ, Cantwell LS, et al. HLA matching at the eplet level protects against

chronic lung allograft dysfunction. *Am J Transplant*. 2016; 16: 2695-703.

20. Böhringer D, Daub F, Schwartzkopff J, et al. Operational post-keratopasty graft tolerance due to differential HLAMatchmaker matching. *Mol Vis*. 2010; 16: 2362-7.

21. Sullivan PM, Warner P, Kemna MS, et al. HLA molecular epitope mismatching and long-term graft loss in pediatric heart transplant recipients. *J Hear Lung Transplant*. 2015; 34: 950-7.

22. Ekong UD, Antala S, Bow L, et al. HLA, non-HLA antibodies, and eplet mismatches in pediatric liver transplantation: observations from a small, single-center cohort. *Exp Clin Transplant*. 2019; 17: 6-17.

23. Geneugelijk K, Spierings E. PIRCHE-II: an algorithm to predict indirectly recognizable HLA epitopes in solid organ transplantation. *Immunogenetics*. 2020; 72: 119-129.

24. Geneugelijk K, Thus KA, Spierings E. Predicting alloreactivity in transplantation. *J Immunol Res*. 2014; 1-12.

25. Geneugelijk K, Niemann M, Drylewicz J, et al. PIRCHE-II is related to graft failure after kidney transplantation. *Front Immunol*. 2018; 9: 321.

26. Lachmann N, Niemann M, Reinke P, et al. Donor-recipient matching based on predicted indirectly recognizable HLA epitopes independently predicts the incidence of de novo donor-specific HLA antibodies following renal transplantation. *Am J Transplant*. 2017; 17: 3076-86.

27. Sakamoto S, Iwasaki K, Tomosugi T, et al. Analysis of T and B cell epitopes to predict the risk of de novo donor-specific antibody (DSA) production after kidney transplantation: a two-center retrospective cohort study. *Front Immunol*. 2020; 11: 2000.

28. Ladowski JM, Mullins H, Romine M, et al. Eplet mismatch scores and de novo donor-specific antibody development in simultaneous pancreas-kidney transplantation. *Hum Immunol*. 2021; 82: 139-46.

29. Chaigne B, Geneugelijk K, Bédat B, et al. Immunogenicity of anti-HLA antibodies in pancreas and islet transplantation. *Cell Transplant*. 2016; 25: 2041-50.

30. Meszaros M, Dubois V, Niemann M, et al. Class II human leukocyte antigen epitope mismatch predicts de novo donor-specific antibody formation after liver transplantation. *Liver Transpl*. 2019; 25: 184-5.

31. Hamada S, Dumortier J, Thévenin C, et al. Predictive value of HLAMatchmaker and PIRCHE-II scores for de novo donor-specific antibody formation after adult and pediatric liver transplantation. *Transpl Immunol*. 2020; 61: 101306.

32. Neumann UP, Guckelberger O, Langrehr JM, et al. Impact of human leukocyte antigen matching in liver transplantation. *Transplantation*. 2003; 75: 132-7.

33. Colvin MM, Smith CA, Tullius SG, Goldstein DR. Aging and the immune response to organ transplantation. *J Clin Invest*. 2017; 127: 2523-9.

34. Geneugelijk K, Wissing J, Koppenaal D, Niemann M, Spierings E. Computational approaches to facilitate epitope-based HLA matching in solid organ transplantation. *J Immunol Res*. 2017; 2017: 1-9.

35. Reddy MS, Varghese J, Venkataraman J, Rela M. Matching donor to recipient in liver transplantation: relevance in clinical practice. *World J Hepatol*. 2013; 5: 603-11.

36. Terasaki PI, Ozawa M, Castro R. Four-year follow-up of a prospective trial of HLA and MICA antibodies on kidney graft survival. *Am J Transplant*. 2007; 7: 408-15.

37. Morales-Buenrostro LE, Castro R, Terasaki PI. A single human leukocyte antigen-antibody test after heart or lung transplantation is predictive of survival. *Transplantation*. 2008; 85: 478-81.

38. Cantarovich D, De Amicis S, Akl A, et al. Post-transplant donor-specific anti-HLA antibodies negatively impact pancreas transplantation outcome. *Am J Transplant*. 2011; 11: 2737-46.

10

39. Meszaros M, Niemann M, Ursic-Bedoya J, et al. Exploring predicted indirectly recognizable HLA epitopes (PIRCHE-II) in liver transplant recipients on calcineurin inhibitor-free maintenance immunosuppression. A retrospective single center study. *Transpl Immunol*. 2020; 59: 101272.

Acknowledgements

The authors thank Sylvia de Visser-de Vlaming for her significant help with collection of the patient data and Remi Mahmoud and Simone Uniken Venema for guidance with the statistical analyses.

Supplementary figures

Figure S1: distribution of PIRCHE-II and HLAMatchmaker scores and the correlation between then.

Figure S2: density plot of cause of death by transplantation age.

Figure S3: barchart of relative causes of death of patients with non-autoimmune and autoimmune indications.

May be downloaded from doi.org/10.1002/lt.26431.

Supplementary tables

Table S1: HLA typing, divided by PIRCHE-II quartiles.

Table S2: patients for which follow-up ended because of re-transplantation, stratified by autoimmune indication.

May be downloaded from .

10

TRANSCRIPTOMIC COMPARISON OF HEPATOCYTE MODEL SYSTEMS FOR EXPERIMENTAL USE

Ibrahim Ardisasmita*, Imre Schene*, Indi Joore**, Gautam Kok**, Delilah Hendriks, Benedetta Artegiani, Michal Mokry, Edward Nieuwenhuis & Sabine Fuchs

Abstract

The myriad of available hepatocyte in vitro models provides researchers the possibility to select hepatocyte-like cells (HLCs) for specific research goals. However, direct comparison of hepatocyte models is currently challenging. We systematically searched the literature and compared different HLCs, but reported functions were limited to a small subset of hepatic functions. To enable a more comprehensive comparison, we developed an algorithm to compare transcriptomic data across studies that tested HLCs derived from hepatocytes, biliary cells, fibroblasts, and pluripotent stem cells, alongside primary human hepatocytes (PHHs). This revealed that no HLC covered the complete hepatic transcriptome, highlighting the importance of HLC selection. HLCs derived from hepatocytes had the highest transcriptional resemblance to PHHs regardless of the protocol, whereas the quality of fibroblasts and PSC derived HLCs varied depending on the protocol used. Finally, we developed and validated a web application (HLCompR) enabling comparison for specific pathways and addition of new HLCs. In conclusion, our comprehensive transcriptomic comparison of HLCs allows selection of HLCs for specific research questions and can guide improvements in culturing conditions.

Introduction

To accurately study human liver physiology and pathology, in vitro models should faithfully replicate in vivo liver functions. These include elimination of toxins, production and secretion of plasma proteins and bile, and metabolic homeostasis of carbohydrates, amino acids, and lipids. Most of these processes are performed by hepatocytes, epithelial cells that constitute 60% of the number of cells and 80% of the volume of the liver.[1] As such, the pursuit of in vitro models that possess robust hepatocyte functionality remains a major goal of biotechnology.

Freshly isolated primary human hepatocytes (PHHs) represent the gold standard to investigate liver functions. However, standard two-dimensional PHH cultures are difficult to expand and rapidly lose hepatic functions.[2] To overcome these limitations, many groups have attempted to improve long-term PHH culturing methods, stimulating proliferation or minimizing dedifferentiation.[3-7] Additionally, hepatic in vitro models were established from other cell sources, including fetal hepatocytes, intrahepatic cholangiocytes, pluripotent stem cells, fibroblasts, urinary cells, and mesenchymal stem cells.[4,8-56] We here collectively designate these models 'hepatocyte-like cells' (HLCs).

The hepatic phenotype is likely to differ between different HLCs, depending on the cell of origin and culturing protocols. Clarifying these differences and identifying the best performing model is required to select the appropriate HLC model to study a specific biological or clinical question. In this study, we set out to compare hepatocyte functionality between the final stage of each HLC protocol. A systematic search of the literature and analysis of reported functional assays and expression of individual genes of the different HLCs did not allow thorough comparison of the hepatic phenotype between studies. Therefore, we developed a computational algorithm for comparison of whole transcriptome sequencing (RNA-seq) data across different studies and a web application to add additional HLC datasets in the future (HLCompR, https://github.com/iardisasmita/HLCompR). This resource will guide selection of HLCs tailored to a specific research aim and help to improve HLC culturing protocols.

Results

Reported hepatocyte functions are insufficient for HLC comparison

We searched the literature for articles that described HLC culture protocols and characterized hepatic functions. As cross-study comparison of HLCs requires a universal standard, we only considered studies that tested HLCs alongside PHHs. This strategy yielded 53 studies describing HLCs derived from pluripotent stem cells (PSCs), fibroblasts, mesenchymal stem cells, urinary cells, intrahepatic cholangiocytes, and PHHs (Fig. 1a and Supplementary Fig. 1). For our quantitative comparison, we considered hepatic functional assays that were performed in more than 10 studies, the expression of associated genes, and genes commonly used as hepatic markers (Supplementary Data 1).

Some functions, including albumin secretion and CYP3A4 activity were assessed in most (>50%) studies, while other important liver functions, including bile secretion, cholesterol metabolism, and gluconeogenesis were generally left unaddressed (Fig. 1a and Supplementary Data 1). Moreover, many studies did not include PHHs in all functional assays. Similarly, only the RNA expression of *ALB*, *CYP3A4*, *CYP1A2*, and *CYP2C9* were reported in the majority (>50%) of studies while other important hepatic markers were lacking.

For cross-study comparison of liver functionality we considered functional activity of HLCs, calculated as a percentage of the PHH control included in the same study (Fig. 1a). Using this method, different hepatic functions seemed to evolve independently from each other. For example, high albumin secretion correlated with high CYP3A4 activity in PSC-derived HLCs of Wang et al.,[46] but not in PSC-derived HLCs of Boon et al.[30] This suggests that it is impossible to predict overall hepatocyte maturation using only a single hepatic function.

Importantly, different studies did not specify the culture time of PHH controls. This may have caused significant variability in control PHH functionality, as specific hepatic functions, including CYP3A4 activity, are rapidly lost during PHH culturing (Fig. 1b).[12,57] As such, minor variations in culture duration and assay procedures of control PHHs may have profound effects on the relative activity of liver functions in HLCs.

Together, the frequent omission of PHH controls, the narrow range of functional assays performed, and the possible variability of PHH controls made it impossible to compare the hepatic phenotype between HLCs based on reported assays.

Transcriptomic comparison reveals distinct liver-specific molecular signatures in HLCs

To allow transcriptome-wide and standardized comparison of HLCs, we developed a computational algorithm to analyze raw bulk RNA-seq data from different HLC studies, that included PHHs or liver tissue as universal controls (Fig. 2a). This yielded 11 studies describing HLCs derived from hepatocytes, intrahepatic cholangiocytes, fibroblasts, and PSCs (Fig. 2b and Supplementary Data 2). In addition, protocols developed by Huch et al.[17] and Hu et al.[4] are commonly used in our laboratory and elsewhere to generate intrahepatic cholangiocyte-derived organoids and (fetal) hepatocyte-derived organoids, respectively. Since both studies did not provide bulk RNA-seq data, we generated RNA-seq data of HLCs derived from intrahepatic cholangiocytes (Huch-Chol-HLCs) and fetal hepatocytes (Hu-FHep-HLCs) using the corresponding protocols.[4,17,58] We did not include the adult hepatocyte-derived organoids because we were not able to culture them over long periods of time and, to the best of our knowledge, nor were other groups.[58,59] The protocols used to generate the different HLCs are represented in Supplementary Fig. 2. In addition to the HLCs and their respective PHH controls, we included fetal hepatocytes, PSCs, fibroblasts, hepatoma cell line HepG2, and common bile-duct tissue (CBD,[60] i.e., extrahepatic cholangiocytes; Supplementary Data 2).

Principal component analysis (PCA) showed that samples clustered by cell type rather than by study, confirming that our computational approach allows cross-study comparison (Fig. 2c). This also confirmed transcriptional homogeneity of PHH/liver samples from different studies, which can collectively serve as a common hepatic benchmark. Most HLCs clustered closely to their respective cells of origin, with hepatocyte-derived HLCs (Hep-HLCs) clustering most closely to PHHs and liver tissue (Fig. 2c). Fibroblast-derived HLCs (Fib-HLCs) from Xie and Du clustered strikingly close to Hep-HLCs, while Fib-HLCs from Gao grouped closer to fibroblasts. Du and Gao used similar media compositions but different transcription factors (TFs) for transdifferentiation (Fig. 2b), showing better hepatic reprogramming using the TF combination of Du. The protocols differentiating intrahepatic cholangiocytes towards hepatocytes (Chol-HLCs) resulted in HLCs that clustered with CBDs. Interestingly, the PSC-derived HLCs (PSC-HLCs) from Mun, which underwent a final maturation step according to the intrahepa-
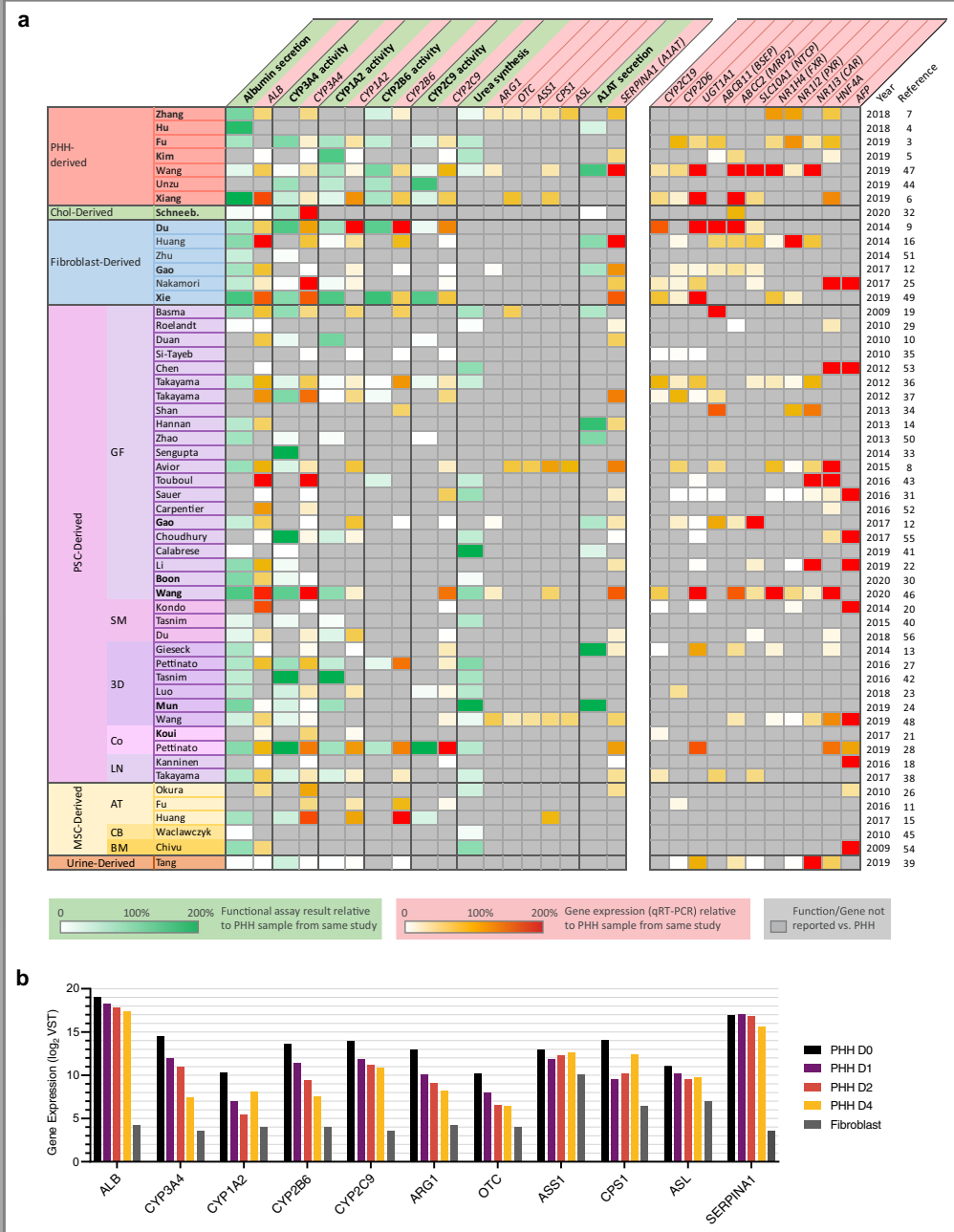
Fig. 1: reported hepatic functional assays and gene expression are insufficient for HLC comparison. **a**, The most commonly reported hepatic functions and gene expression are presented. The value in each cell represents the activity or expression level of an HLC as a percentage of the PHH control in the same study. HLCs are grouped based on the type of

cells they were generated from. Pluripotent stem cell (PSC) derived HLCs are further grouped into: GF, standard protocols employing growth factors; SM, protocols solely using synthetic molecules; 3D, protocols utilizing 3D matrices; Co-cult, protocols combining multiple cell types; and LN, protocols focusing on the effect of laminin coating. Mesenchymal stem cell (MSC) derived HLCs are categorized into the tissue of origin: AT adipose tissue, CB cord blood, BM bone marrow. **b**, mRNA expression (log2) of genes relevant to the commonly reported hepatic functions in PHHs cultured for 0, 1, 2, and 4 days and cultured dermal fibroblasts, from the study of Gao et al.[12] Note that expression of some genes (e.g. CYP3A4, CYP1A2, OTC) decreases >4-fold within the first 24 h of culturing, whereas expression of other genes (ALB, ASS1, SERPINA1) remains relatively stable.

---

tic cholangiocyte culture protocol of Huch et al. (Supplementary Fig. 3),[17,24] also clustered closer to CBDs than to either PSCs or PHHs. This suggests that the culture protocol of Huch et al.[17] directs differentiation towards cholangiocytes rather than hepatocytes. Considering other PSC-derived HLCs (PSC-HLCS), we observed that the HLCs from Wang, which were derived from PSCs with the ability to form extra-embryonic tissues,[61] clustered closer the Hep-HLCs than the HLCs derived from standard PSCs (Gao, Mun, Boon, Koui; Fig. 2c).

We established a general hepatic fingerprint, by considering the top-expressed genes in the liver from the Genotype-Tissue Expression (GTEx) database. Hierarchical clustering showed that only Hep-HLCs clustered with PHHs and liver tissue based on these top-expressed liver genes (Fig. 2d). To quantify the overall resemblance of HLCs to PHHs according to a given gene set, we calculated distance-based similarity scores (DBS) (Fig. 2e). Hep-HLCs showed the highest DBS based on top-expressed liver genes, followed by Wang-PSC-HLCs, Fib-HLCs, other PSC-HLCs, and finally Chol-HLCs (Fig. 2e).

Next, we considered several gene sets related to specific hepatic functions. HLCs derived from hepatocytes, fibroblasts from Xie, and extended PSCs from Wang were generally most similar to PHHs, but clear differences could be observed when considering particular gene sets (Fig. 2f and Supplementary Figs. 4 and 5). For example, expression of most gene sets was higher in Hep-HLCs than in Fib-HLCs, except for the gluconeogenesis gene set. Among all Hep-HLC samples, Xiang-Hep-HLC-D15 was generally most similar to PHHs and liver tissue (Fig. 2f), which may result from the relatively short culture time (15 days) of this HLC sample compared to other HLCs (>3
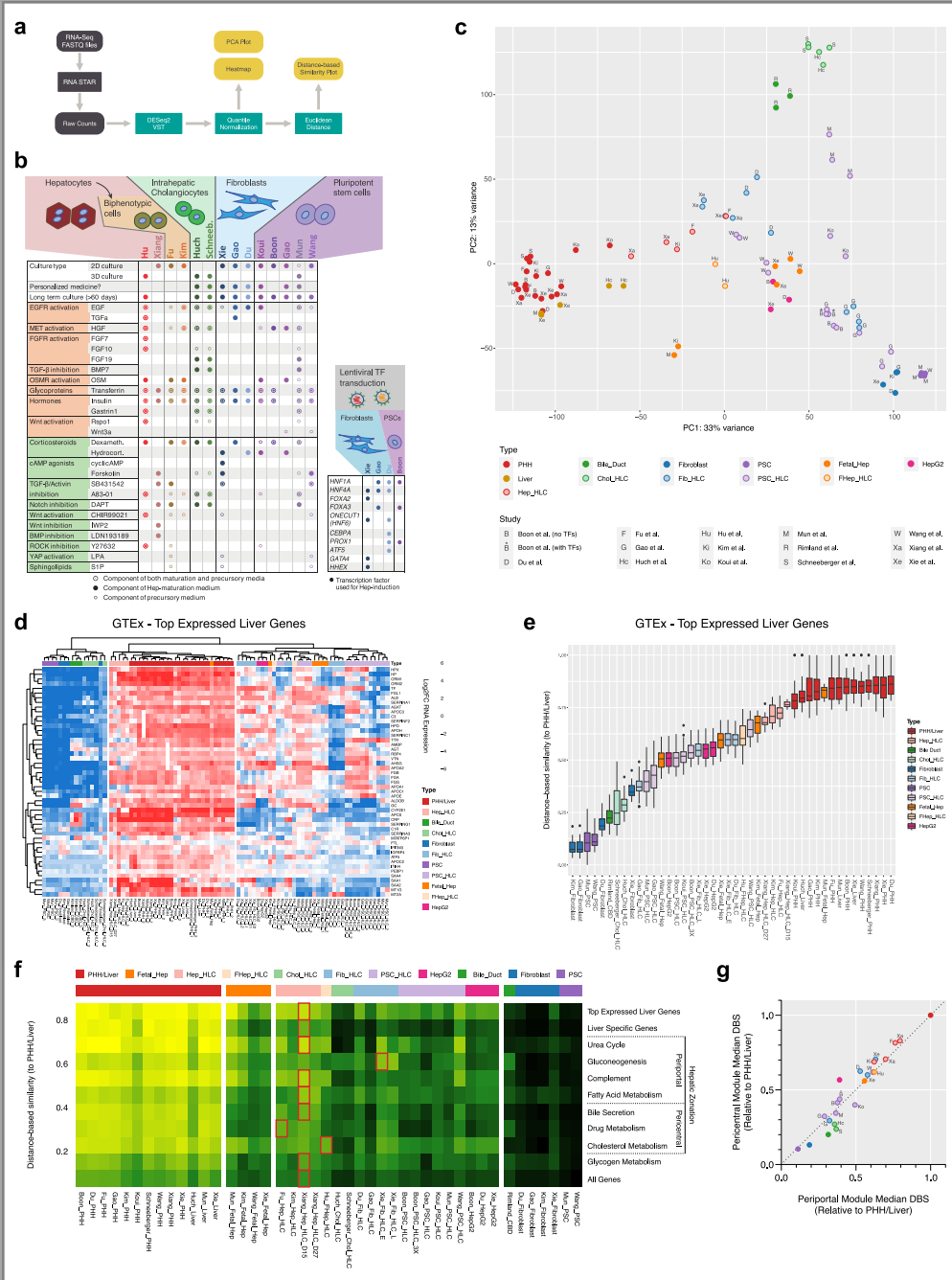
Fig. 2: transcriptomic comparison reveals distinct liver-specific molecular signatures in HLCs. **a**, Schematic of the algorithm employed to conduct the transcriptomic comparison analysis. All steps in gray were performed on the Galaxy web platform. **b**, Summary of pro-

tocols used to generate HLCs that were included in the transcriptomic comparison analysis. Precursory medium is any medium that was used directly prior to the final maturation medium, including progenitor/expansion medium (hepatocyte-, cholangiocyte-, and fibroblast-derived HLCs) and hepatocyte differentiation medium (PSC-derived HLCs). **c**, Principal component analysis created using 5000 genes with the highest variance among all samples from different studies. **d**, Heatmap of top- expressed liver genes according to the Genotype-Tissue Expression (GTEx) project. Hierarchical clustering was performed using Euclidean distance. **e**, Distance-based similarity score (DBS) calculated using Euclidean distance describing the resemblance between each sample to all PHH/Liver samples based on the top-expressed liver gene set. Box-and-whisker plots are shown as median (line), interquartile range (box), and data range or 1.5x interquartile range (whisker). **f**, Heatmap showing the median DBS of all samples using various liver function associated gene sets. Red outlines indicate the HLC with the highest DBS for each gene set. **g**, The median DBS of all samples relative to PHH/Liver based on the pericentral and periportal modules (see Fig. 2c for legend).

---

weeks).[3,5,6] We also observed that Chol-HLCs remained highly similar to CBDs in overall gene expression (Fig. 2c), with a slight increase in expression of genes involved in cholesterol metabolism and bile secretion (Fig. 2f). In HepG2 cells, specific gene sets including cholesterol and glycogen metabolism and complement production were relatively well expressed.

We then evaluated whether the expression of gene sets related to specific liver functions reflected differences in zonation between HLCs. To this end, we extracted periportal and pericentral gene from the single-cell analysis of human hepatocytes performed by Aizarani and colleagues.[62] To ensure that these modules assessed hepatic specific genes associated with hepatocyte zonation, we only included zonation genes that were enriched (>2-fold) in PHH/liver samples compared to other HLC cell sources (Fib, PSC, Chol) (Supplementary Fig. 6). This approach revealed that most HLCs expressed periportal and pericentral modules in a linear manner (Fig. 2g). This may suggest that either there are no strong zonation patterns in most HLCs (assuming homogenous gene expression profiles in all cells) or there are zonation patterns that cannot be discerned due to the nature of bulk sequencing analysis. Single-cell RNA sequencing analysis is needed to fully address zonation in HLCs. Interestingly, Chol-HLCs and HepG2 cells deviated most from this general linear pattern. Chol-HLCs displayed a

predominant periportal identity (Fig. 2g) which corresponded to relatively high expression of gluconeogenic genes (Fig. 2f). In contrast, HepG2 cells exhibited a more pericentral identity (Fig. 2g), corresponding to higher expression of genes involved in cholesterol metabolism (Fig. 2f).[63]

By considering HLCs from all available studies, our approach also revealed the relative magnitude of hepatic differences between HLCs generated using various protocols within individual studies. For instance, the HLCs in the study of Gao were either directly transdifferentiated from fibroblasts (Fib-HLCs) or generated through an intermediate iPSC step (PSC-HLCs). Gao et al.[12] observed that their Fib-HLCs performed better at Phase I and II reactions, whereas their PSC-HLCs modeled hepatic fatty acid metabolism better. Our analysis confirmed these findings (Fig. 2f and Supplementary Figs. 4e and 5a) but also demonstrated that both the Fib-HLCs and PSC-HLCs from the Gao study displayed relatively weak hepatic phenotypes compared to HLCs from other studies. Furthermore, Boon et al.[30] attempted to enhance the maturation of PSC-derived HLCs with TF transduction (*HNF1A, FOXA3, PROX1*) and showed that this approach resulted in higher albumin secretion and CYP3A4 activity. However, in relation to other HLCs, TF transduction only resulted in a slight improvement of hepatocyte differentiation (Fig. 2c,f,g). Moreover, TF transduction not only increased (e.g., *ALB* and *HPX)* but also decreased (e.g., *APOA2* and *TTR*) the expression of some specific liver markers in the PSC-HLCs of Boon et al. (Fig. 2d).[30]

HLCs display different cell/tissue identities

The quality of hepatocyte in vitro models should not only be defined by the presence of hepatocyte identity (Fig. 2) but also by the absence of unwanted cell/tissue identities. We therefore analyzed the HLCs using CellNet,[64,65] a platform that quantifies resemblance to a larger variety of human cell and tissue types (cell/tissue classification score) based on establishment of tissue-specific gene regulatory networks (GRN status).

CellNet classified most HLCs as liver but only the (fetal) hepatocyte-derived HLCs attained a pure liver classification. The HLCs derived from PSCs, fibroblasts, and cholangiocytes were either classified as multiple cell/tissue types or non-liver tissues (Fig. 3a). The unwanted cell identities of these HLCs can be attributed to incomplete loss of their original cell identity or undesired gain of non-liver identity.

The incomplete loss of original cell identity could be observed in all PSC-HLCs, which showed a higher embryonic/pluripotent stem cell (ESC) GRN status compared to PHHs (Fig. 3b and Supplementary Fig. 7). Interestingly, despite retaining discernible ESC GRN status, the PSC HLCs from Wang displayed similar liver GRN status to Hep-HLCs (Fig. 3b). For Fib-HLCs, only the samples from Gao failed to fully extinguish their fibroblast GRN status (Fig. 3b and Supplementary Fig. 7). This incomplete loss of fibroblast GRN and partial gain of liver GRN in Fib-HLCs from Gao resulted in low classification scores for all specific cell/tissue types (Fig. 3a). This heterogeneity in cell identity between HLCs starting from the same cell source (Wang-PSC-HLCs vs. other PSC-HLCs and Gao-Fib-HLCs vs. other Fib-HLCs) reflects the effects of different culture protocols applied in each study.

All non-hepatocyte-derived HLCs manifested undesired gain of intestine/colon identity (Fig. 3a). Additionally, PSC-HLCs from Koui also gained lung identity possibly due to their protocol involving differentiation towards multiple lineages (Fig. 3a and Supplementary Fig. 2). This gain of non-liver identity may occur in all cells or only in a subpopulation of cells, resulting from heterogeneous differentiation. Regardless, this suggests that all HLC generation protocols are still imperfect and fine-tuning the cell fate specification of these HLCs may improve hepatic (trans-) differentiation.[66] Surprisingly, the Chol-HLCs from Huch and Schneeberger and PSC-HLCs from Mun bore higher resemblance to the intestine/colon than to the liver (Fig. 3a). Furthermore, our CBD control samples had lower intestine/colon classification than the Huch protocol-cultured HLCs (Fig. 3a). Nevertheless, PCA-analysis showed that the Huch protocol-cultured HLCs were more similar to CBD than to intestine/colon samples (Supplementary Fig. 3b), suggesting that the Huch protocol not only promotes CBD but also intestinal gene expression. This is in line with the finding of Aizarani et al. that intrahepatic cholangiocytes upregulates intestinal marker genes when cultured as organoids in Huch expansion medium.[62]

Besides unwanted adult cell/tissue identities, HLCs may also display immature hepatic identity, resembling fetal hepatocytes.[67] Since CellNet was trained to only distinguish between adult tissue identities, we created a classification algorithm based on the transcriptome of adult and fetal hepatocytes. Corresponding with the CellNet results, the Hep-HLCs of Fu and Xiang best resembled the adult hepatocyte transcriptome (Fig. 3a,c). Interestingly, none of the HLCs displayed fully mature hepatocyte fingerprints, resulting from absence of adult markers or presence of fetal markers (Fig. 3c). The Chol-HLCs were not classified as either adult or fetal hepatocytes (Fig. 3c), under-
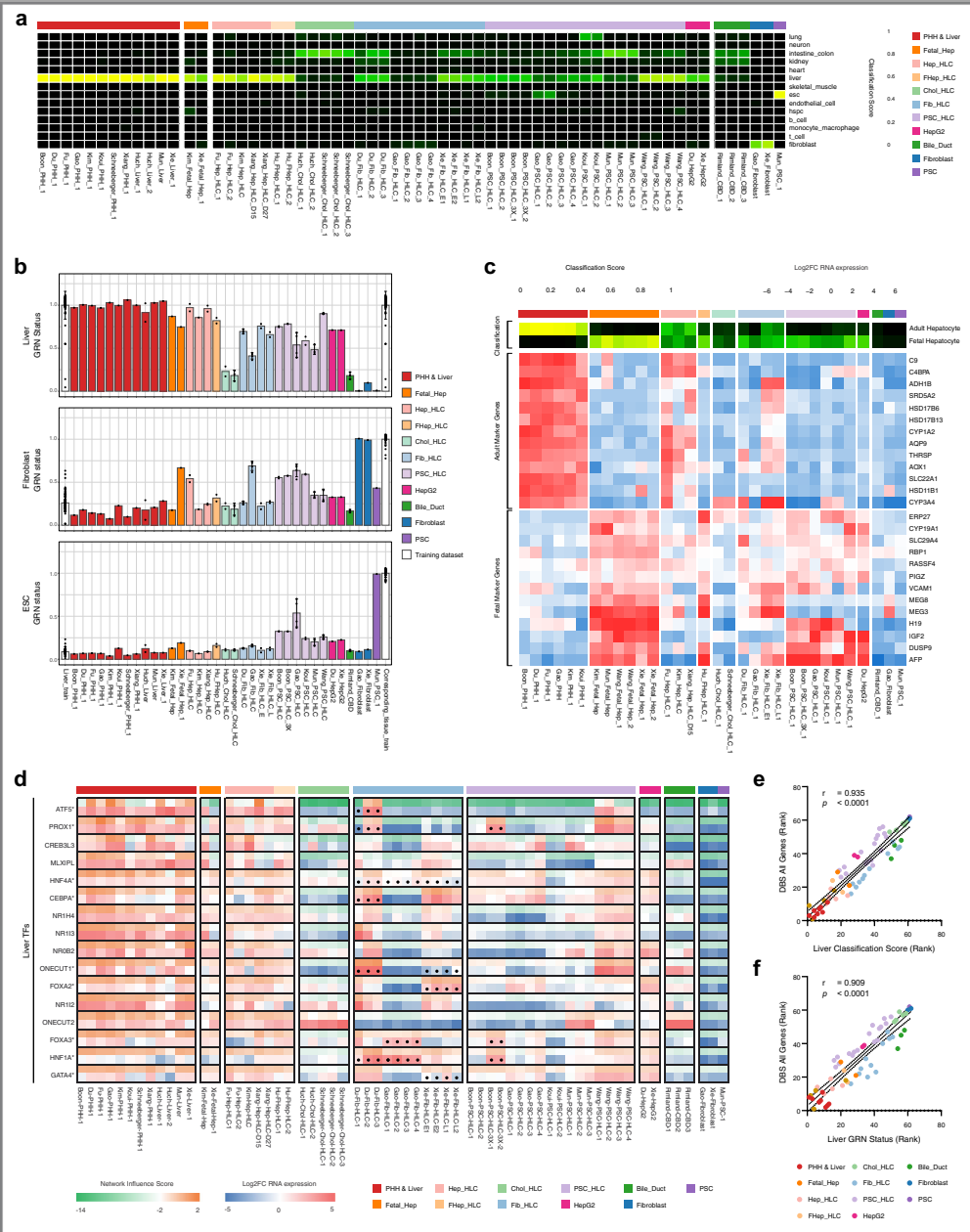
Fig. 3: HLCs display different cell/tissue identities. **a**, Cell/tissue classification heatmap showing different cell/tissue identities of various HLCs. The classification scores represent the probability that the samples express indistinguishable gene regulatory networks (GRN) from the training dataset. **b**, Liver, fibroblast, and embryonic stem cell (ESC) GRN status of HLCs and CellNet training datasets expressed as mean values. Each dot and error bar repre-

sents an individual sample and the standard deviation, respectively. **c**, Heatmaps showing the adult/fetal hepatocyte classification score and expression of representative marker genes for the adult and fetal hepatocyte identities. **d**, Heatmap showing the network influence scores (NIS) and expression values of liver-associated transcription factors (TFs). Asterisks and dots indicate the TFs used for transductions. **e**, Spearman correlation between the rank of CellNet liver cell/tissue classification score or **f**, CellNet liver GRN status and the rank of the DBS for all genes. Lower ranks represent higher liver classification, GRN status, and DBS. Spearman's correlation coefficient (r) and P value (p) are shown on the top left of the graphs (n = 62 biologically independent samples). Dotted lines represent the 95% confidence interval.

---

lining their weak hepatic differentiation. Among all fibroblast- and PSC-derived HLCs, only the Fib-HLCs of Xie attained a strong adult identity, expressing mature hepatocyte markers including *ADH1B* and *SRD5A2*. Despite convincing liver GRN status in the CellNet analysis, the PSC-derived HLCs from Wang still demonstrated a fetal identity (Fig. 3b,c).

For HLC protocols using TF transduction, the extent of hepatic (trans-) differentiation is determined in part by the effectiveness of the TF combinations used. This effectiveness can be assessed using the network influence scores from CellNet analysis. Network influence scores indicated that TF transduction in Fib-HLCs of Gao (*HNF4A, FOXA3, HNF1A*) and PSC-HLCs of Boon (*PROX1, FOXA3, HNF1A*) increased TF expression and activation of associated TF networks, without resulting in activation of other liver TF networks (Fig. 3d). In contrast, the additional TFs used in the Fib-HLCs of Du (*ATF5, PROX1, CEBPA, ONECUT1* (also known as *HNF6*)) and Xie (*ONECUT1, FOXA2, GATA4*) yielded widespread activation of other liver TF networks. Of note, low RNA expression and low network influence scores suggested ineffective transduction of *ATF5* and *PROX1* in one of the Du samples (Du-Fib-HLC-1), but effective transduction of *ONECUT1*, which still resulted in broad hepatic TF network activation. Together, this suggests that *ONECUT1* is an important factor in the hepatic transdifferentiation cocktail.

Additionally, we used CellNet to validate our computational algorithm and found that the PHH/liver, fibroblast, and PSC samples included in our analysis showed high similarity to their corresponding CellNet training datasets (Fig. 3a,b). Furthermore, both the ranked CellNet liver classification score and liver GRN status correlated well with
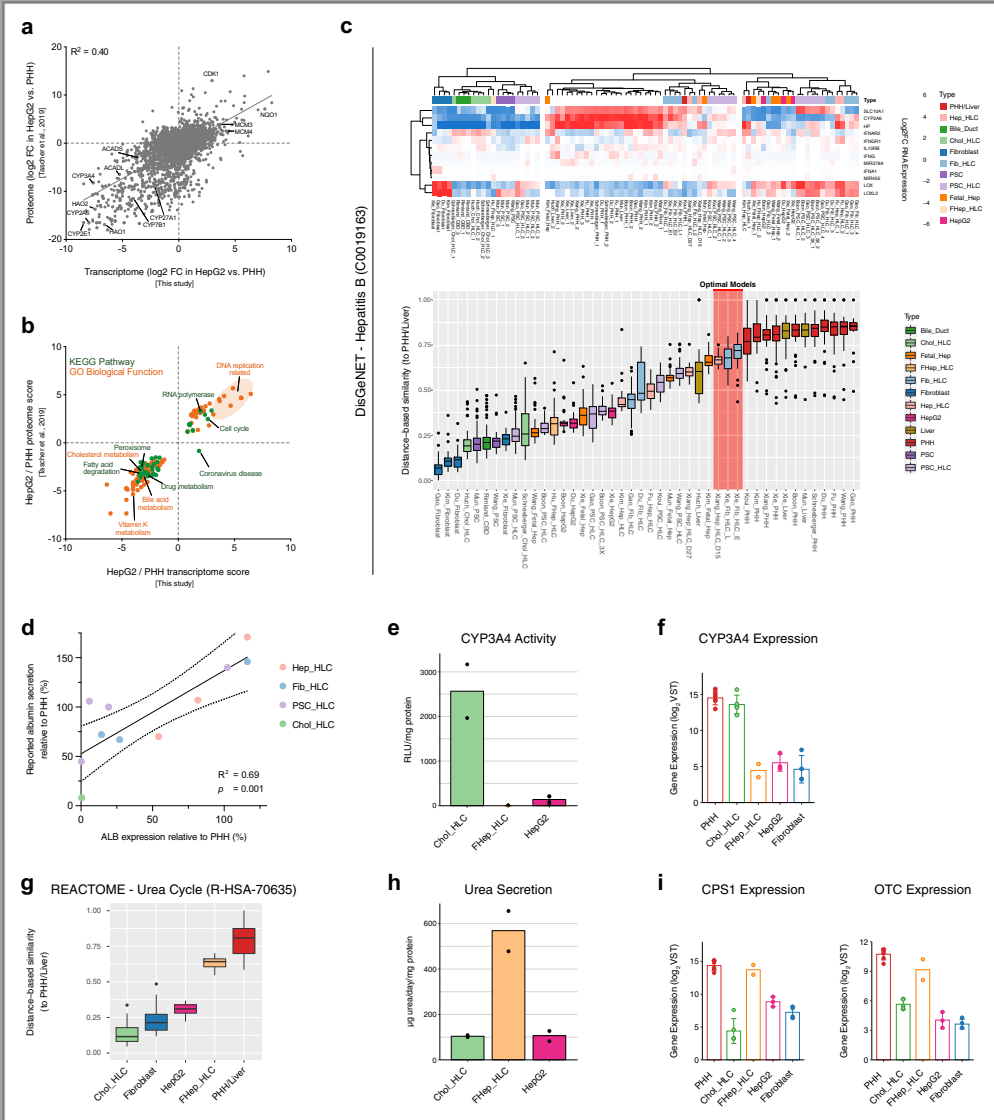
Fig. 4: transcriptomic comparison allows prediction of HLC functionality. **a**, Scatter plot of protein abundance ratios against corresponding mRNA ratios in HepG2 cells vs. PHHs for proteins/genes that are detected in both transcriptome (from our transcriptomic comparison) and proteome (from Tascher et al.[68]). Pearson's coefficient of determination (R^2) is shown at the top left of the plot. **b**, Scatter plot of enriched pathways based on transcriptome and proteome. Only pathways that are enriched on both the transcriptomic and proteomic levels are shown. **c**, Heatmap and DBS of hepatitis B associated genes according to the DisGeNET database. Red highlight indicates the predicted optimal hepatocyte in vitro

models. **d**, Correlation plot of the gene expression levels of ALB from the transcriptomic comparison data (x-axis) and the reported relative albumin secretion (y-axis) in included HLCs. Pearson's coefficient of determination (R^2) and P value (p) are shown on the bottom right of the graph (n = 11 biologically independent samples). Dotted lines represent the 95% confidence interval. **e**, CYP3A4 activities presented as mean. **f**, Gene expression level of CYP3A4 from the transcriptomic comparison data presented as mean ± standard deviation. **g**, The DBS of urea cycle genes according to the Reactome database. The combined values of Chol-HLC, fibroblast, HepG2 cell, FHep-HLC, and PHH/liver samples from different studies are presented. **h**, Urea secretion level presented as mean. **i**, Gene expression level of CPS1 and OTC from the transcriptomic comparison data presented as mean ± standard deviation. Box-and-whisker plots are shown as median (line), interquartile range (box), and data range or 1.5x interquartile range (whisker).

the DBS score (using all genes) obtained through our own approach (Fig. 3e,f). This confirmed that our transcriptomic analysis accurately quantified liver resemblance.

Transcriptomic comparison allows prediction of HLC functionality

Our transcriptomic comparison indicated substantial variability in the expression of liver-related gene sets between included HLCs (Fig. 2f). To determine if our comparison could predict the ability of specific HLCs to model liver functions, we assessed whether transcriptomic differences translate into proteomic and ultimately functional differences.

We first considered publicly available proteomes of HepG2 cells and PHHs[68] and found that the transcriptomes of HepG2 cells and PHHs from our dataset correlated very well ($R^2 = 0.40$, $p < 0.0001$; Fig. 4a) to the proteomes from this independent study.[68] In fact, this correlation was comparable to within-study transcriptome-proteome correlations ($R^2 = 0.41$).[69] Transcriptomic and proteomic enrichment analyses concurrently indicated that HepG2 cells display higher expression of cell cycle pathways and lower expression of liver-related pathways, compared to PHHs (Fig. 4b).

We next assessed if transcriptional differences translate into functional differences by considering Hepatitis B virus (HBV) infection. This disease has been successfully modeled using Hep-HLCs from Xiang and Fib-HLC form Xie.[6,49] Accordingly, the expression of the genes associated with HBV infection and propagation was best recapi-

Fig. 5: HLCompR web application for HLC selection. **a**, The HLCompR web application allows filtering for HLCs based on various properties and enables easy selection of gene sets relevant to hepatic functions and diseases. **b**, Heatmap showing the relative expression of SERPINA1 and G6PC between samples. **c**, Boxplot showing DBS of non-alcoholic fatty liver disease-associated genes according to the DisGeNET database. Box-and-whisker plots are shown as median (line), interquartile range (box), and data range or 1.5x interquartile range (whisker).

tulated by these two HLCs (Fig. 4c). This confirms that for HBV, our transcriptomic comparison could predict suitability for in vitro modeling.

We further validated the predictive power of our transcriptomic comparison by considering reported albumin secretion (Fig. 1a) because the gene expression of *ALB* remains stable for several days in cultured PHHs (Fig. 1b). As such, the relative albumin secretion of different HLCs is reasonably unaffected by the variability of the PHH controls, and can therefore be compared across studies. The expression of *ALB* in our transcriptomic comparison was a good predictor ($R^2 = 0.69$; $p = 0.001$) of reported albumin secretion for the 11 included HLCs (Fig. 4d).

Finally, we validated that our transcriptomic comparison can also predict the activity of functions that are highly affected by the freshness of the internal PHH controls, such as CYP3A4 and urea cycle activity (Fig. 1b). To ensure comparability, we performed assays of these functions in a uniform setup using HLCs that are well-established in our group (Chol-HLCs, FHep-HLCs, and HepG2 cells). We found that the enzymatic activity of CYP3A4 was highest in Chol-HLCs (Fig. 4e), which was correctly predicted by the transcriptomic comparison (Fig. 4f). Considering urea cycle gene expression, FHep-HLCs resembled PHH/Liver most, followed by HepG2 cells and Chol-HLCs (Fig. 4g). In line with this, FHep-HLCs displayed highest urea secretion among these HLCs (Fig. 4h). The smaller expressional difference between Chol-HLCs and HepG2 cells (Fig. 4g) did not result in differences in urea secretion levels (Fig. 4h), possibly because two essential enzymes of the urea cycle (*CPS1* and *OTC*) are lowly expressed in both Chol-HLCs and HepG2 cells (Fig. 4i). In fact, both HLCs had expression levels similar to fibroblasts (Fig. 4g,i), which also poorly convert ammonia to urea.[70] Together, these findings supported that our cross-study transcriptomic comparison predicts HLC protein abundance and functionality.

HLCompR web application for HLC selection

To allow other researchers to examine the expression of an important gene or an entire gene set to select appropriate HLC models, we created HLCompR, a web application for easy exploration of the relative expression of any gene (set) of interest (https://github.com/iardisasmita/HLCompR). Additionally, HLCompR allows researchers to filter HLCs by specific characteristics, including culture duration, expandability, and cell source, and easily select function- or disease- associated gene sets (Fig. 5a).

To illustrate how HLCompR can help to select the optimal HLCs for specific research purposes, we considered liver diseases associated with a single gene defect (Fig. 5b). This showed that multiple HLCs express the *SERPINA1* gene on a similar level
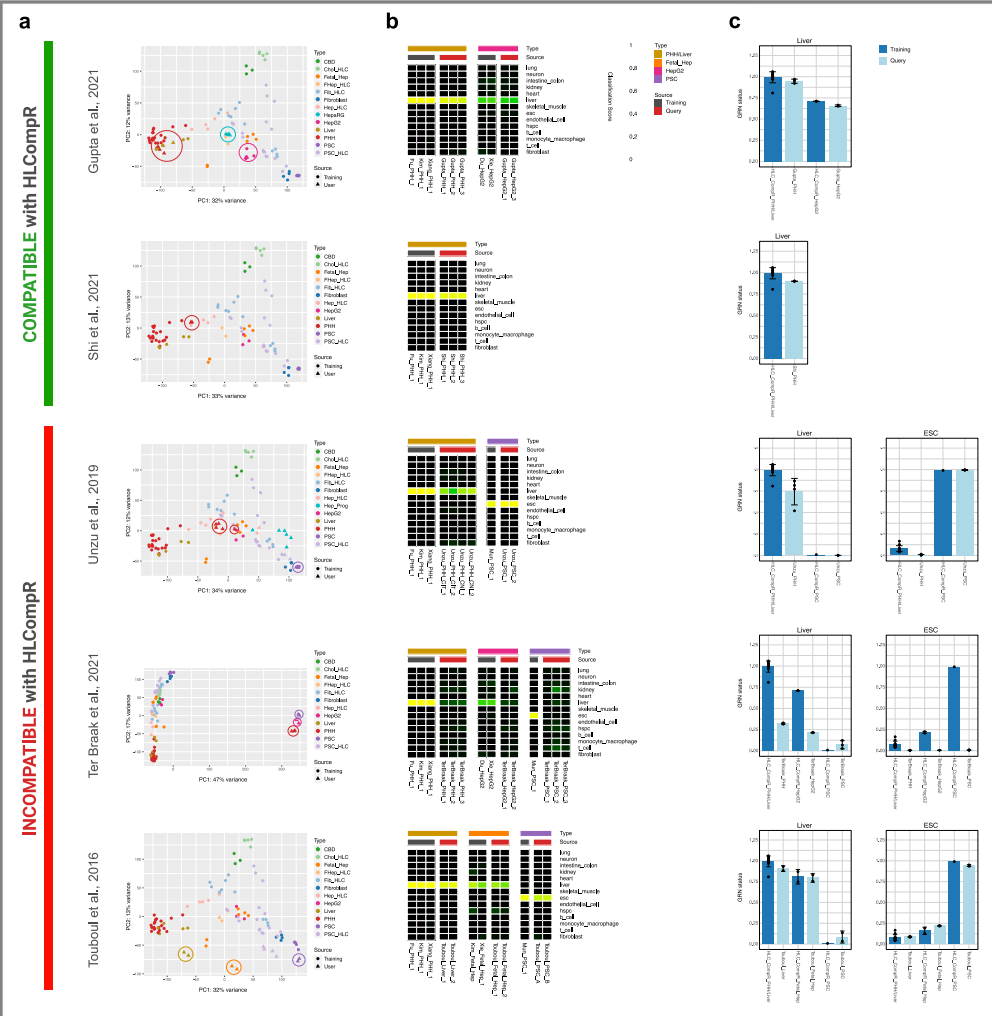
Fig. 6: Addition of new HLC transcriptomes to the HLCompR web application. **a**, Principal component analysis on query datasets. Circles indicate the cell or tissue types in the query datasets that are also present in the training dataset (e.g., PHH, liver, HepG2, fetal hepatocyte, and PSC) or the HepaRG samples in Gupta[74] dataset. HLCompR compatibility is categorized based on the comparability of PHHs and liver tissue between the query and training datasets. **b**, Cell/tissue classification heatmap of representative training samples and query samples. **c**, Gene regulatory network status of liver and embryonic stem cells (ESCs) of all PHH, liver, HepG2, and PSC samples from training dataset and query dataset presented as mean ± standard deviation.

to PHHs, and might therefore be appropriate to study protein secretion and activity in alpha-1-antitrypsin deficiency. In contrast, only a few HLCs may optimally model the function of the enzyme affected in glycogen storage disease type 1a (*G6PC*; Fig. 5b). The optimal choice for modeling this disease would be the Fib-HLCs from Xie.

For more complex liver diseases associated with multiple genes, the distance-based similarity score of the disease-associated gene set provides a better overview of the modeling capabilities of various HLCs. For example, Hep-HLCs better resembled the hepatic expression of genes related to non-alcoholic fatty liver disease (NAFLD) compared to HepG2 cells, which are commonly used to model NAFLD (Fig. 5c).[71] In addition to transcriptional resemblance to PHH, NAFLD modeling requires long-term culturing of fully matured HLCs. Therefore, Hep-HLCs from Xiang, which can be maintained in a differentiated state for 1 month, may represent the optimal in vitro model for this disease.

Addition of new HLC transcriptomes to the HLCompR web application

Given the technical challenges and variability inherent to HLC protocols, replication of such protocols might not yield phenotypically identical HLCs. In addition, new HLC protocols are continually developed. We therefore supported addition of new RNA-seq data to the HLCompR analysis using read counts processed according to our pipeline as inputs (https://github.com/iardisasmita/HLCompR).

To determine whether new datasets can be compared using HLCompR, we tested publicly available RNA-seq datasets of PHH or liver tissue samples in the application.[72-76] We also included several studies that did not meet our RNA-seq inclusion criteria (query dataset) (Supplementary Fig. 1).[43,44] The samples included in Fig. 2 served as the training dataset for HLCompR.

The query dataset from Gupta et al.[74] was compatible with HLCompR because their PHH and liver samples clustered together with the training samples (Fig. 6a). Accordingly, these samples acquired high liver classification and liver GRN status scores in CellNet (Fig. 6b,c). Query datasets of Shi et al.[75] and Vieyres et al.[76] were also compatible with HLCompR, even though their PHH clustered in between the training PHH/liver samples and hepatocyte-derived HLCs (Fig. 6a and Supplementary Fig. 8a). CellNet classified their PHH samples as liver, but their liver GRN status was slightly lower than training PHH/liver samples (Fig. 6b,c and Supplementary Fig. 8b,c).

The query dataset from Unzu et al.[44] was incompatible with HLCompR, because the PHHs from their dataset did not cluster with the training data, but the PSCs did (Fig. 6a). Concurrently, analysis with CellNet showed incorrect classification of PHHs and correct classification of PSCs (Fig. 6b,c). Similarly, PHHs included in the query datasets from ter Braak et al.,[72] Wang et al.,[48] and Guan et al.[73] did not cluster with the training dataset (Fig. 6a and Supplementary Fig. 8a), which was also reflected by low CellNet liver scores (Fig. 6b,c and Supplementary Fig. 8b,c). Samples from Touboul et al.[43] clustered close to the respective training samples on principal component 1 (PC1) but were separated by principal component 2 (PC2) (Fig. 6a). Still, CellNet analysis showed classification scores similar to those of training samples (Fig. 6b,c). Interestingly, when changing the number of genes considered for PCA or reducing the number of samples included (Supplementary Fig. 8d), the samples of Touboul et al.[43] clustered together with the training samples. Nevertheless, we considered the samples from Touboul et al.[43] incompatible with HLCompR. We recommend use of HLCompR only when control PHH/liver samples are comparable to the training PHH/liver samples. We added a Random Forest classifier that automatically reports compatibility of a new dataset based on this parameter.

Since standardized mapping and RNA-seq processing may still result in incompatibility with HLCompR, we hypothesized that the type of RNA-seq library preparation or sequencer might influence compatibility (Supplementary Data 2). Based on this possibility, we suggest that libraries should be prepared using standard Illumina TruSeq RNA sample preparation kit and sequenced with Illumina sequencing machines. As we cannot guarantee compatibility, new datasets should always include PHH/liver control samples.

When a dataset is compatible with HLCompR, new HLC samples can be compared to the other HLCs in the training dataset. For example, in the query dataset from Gupta et al.,[74] the hepatically differentiated hepatoma cell line HepaRG showed better resemblance to PHHs than HepG2 cells (Fig. 6a). Correspondingly, HepaRG cells have also been reported to perform better at hepatic functional assays than HepG2 cells.[77]

Discussion

The availability of myriad hepatocyte model systems gives researchers the option to select one that best suits their study, but an educated choice is hampered by the absence of standardized evaluation. We addressed this by performing a comprehensive

cross-study comparison of HLCs, derived from various cell sources. Our literature search showed that only a small subset of hepatic functions is routinely tested in direct comparison to PHH controls, precluding cross-study comparison of HLCs. Furthermore, as cultured PHHs rapidly lose specific hepatic functions, a major determinant of the relative activity of these functions in HLCs is the culture time of control PHHs. Since various HLC studies use control PHHs cultured for different durations, the relative activities of most reported hepatic functions cannot be reliably compared across studies. Therefore, we not only recommend that protocols describing new HLCs report a set of minimal hepatic characteristics,[78] but we also stress the importance of using standardized assays and inclusion of control PHHs that are cultured for a standardized duration.

Using currently available RNA-seq data, we developed a computational algorithm for in-depth cross-study comparison of HLCs with minimal study-specific batch effects. This allowed evaluation of genes that are rarely investigated in individual studies but may be important for specific hepatic functions or liver disease models. Our analysis revealed that the transcriptomic profile of HLCs is determined by the cell of origin and the protocol used, with hepatocyte-derived HLCs most closely resembling PHHs. In addition, we identified hepatic marker genes that are lowly expressed in most HLCs, including *CYP2E1*, *ADH1A*, *F9*, and *SERPINC1*. These genes may serve as important indicators of mature hepatic differentiation, besides common markers such as *ALB*, *CYP3A4*, and *SERPINA1*.

We found that hepatic genes are differentially expressed between different HLCs. This underlines the importance of selecting the most appropriate HLC for a specific research question. We validated that our transcriptomic HLC comparison allows functional performance prediction in well-established models in our laboratory. The strong correlation between transcriptional and functional profiles supports the use of our transcriptomic comparison as a resource to select HLCs for specific research goals. Choosing the optimal HLCs is accommodated by our web application (HLCompR), which allows filtering by HLC properties and selecting custom gene sets. This functionality sets HLCompR apart from other comparison platforms such as CellNet, which are focused on evaluating the general cell identity of HLCs. The HLCompR web application also allows researchers to test HLCs generated in their own laboratories, including replications of HLC protocols included in this study or development of novel HLC protocols, if the PHH control is comparable to the training dataset. Therefore, we advise that protocols describing new HLCs provide publicly available transcriptomic data alongside PHH controls that serve as a benchmark for cross-study comparability.

Besides transcriptional and functional similarity to PHHs, other characteristics may be important when selecting the optimal liver in vitro model, including the ability to derive HLCs from small biopsies for personalized medicine. This can be achieved by using skin-derived fibroblasts that are directly transdifferentiated (Xie, Gao, Du) or reprogrammed to induced-PSCs (iPSCs) that are subsequently differentiated to HLCs (Koui, Gao, Mun). Using a specific combination of TFs, direct transdifferentiation of fibroblasts resulted in HLCs that are transcriptionally closer to PHHs than most PSC-derived HLCs. Our approach specifies the effects of these TFs. The combination of TFs used by Xie, for example, not only induced activation of gene networks regulated by the transduced TFs, but also of other networks (Fig. 3d). Addition of *ATF5* and *PROX1*, which were relatively poorly established in the Fib-HLCs of Xie may further improve hepatic differentiation.

Hepatocyte maturity cannot be solely defined by the transcriptome, but should also be determined by the proteome and ultimately the functionality. However, reliable comparison of hepatic functionality between HLCs requires complete standardization of methodology and PHH controls. In practice, this entails performing the assays in all HLCs simultaneously using the same experimental setup. Given the difficulties in reproducing all HLCs, this would be highly challenging. Therefore, transcriptomic comparison may represent the most compelling solution to ensure standardization of multiple samples from various studies. Indeed, this allows evaluation of HLCs using a common benchmark of PHH controls from multiple studies, preventing over- or underestimation of hepatic characteristics caused by suboptimal PHH controls in individual studies. Additionally, transcriptomic comparison enables comprehensive characterization based on more than a handful of reported marker genes. This includes assessment of multiple cell/tissue identities and the extent of hepatocyte maturation (Fig. 3).

In summary, this study provides a method and a web application (HLCompR) to compare and evaluate HLCs from multiple studies. We found that the transcriptome of hepatocyte-derived HLCs is currently most similar to primary hepatocytes. For personalized medicine purposes however, dermal fibroblasts are more readily available and improvements in direct transdifferentiation of fibroblasts have resulted in excellent HLCs. Importantly, our strategy allows identification of individual TFs or culturing conditions that might improve hepatic differentiation. Moreover, evaluation of HLCs alongside relevant control tissues provides insight into their tissue identity. These insights will guide improvement of HLC culture protocols, thereby advancing hepatic in vitro modeling and supporting regenerative strategies. Finally, although we focused on

in vitro models of hepatocytes, the same method may be applied to evaluate in vitro models of other cell types or organs.

Methods

Data collection

The PubMed database was systematically searched for studies that mention the development or evaluation of HLC culturing protocols. Search terms were selected to include studies performing long-term culturing of human primary hepatocytes or (trans)differentiation of human somatic or stem cells into HLCs, including functional or transcriptomic evaluation (Supplementary Fig.1). The titles and/or abstracts of all hits were screened, including studies describing and evaluating new HLC protocols, and excluding studies using previously described HLC protocols. During subsequent full-text screening, only studies that functionally evaluated new HLC protocols alongside PHH as a common standard were selected for functional and expressional comparison in Fig. 1. Finally, from selected studies, only those providing publicly available bulk RNA-seq datasets with the inclusion of PHH/liver controls were included for analysis in our computational algorithm (Supplementary Fig. 1).

Functional and expressional comparison of HLCs using reported data

Quantification of functional assays and mRNA expression by qPCR was estimated based on the figures and graphs provided in the original studies. Functional and ex-pressional data of HLCs were normalized to the corresponding PHH data from the same study and represented as a percentage. Pearson correlation between assays and/or gene expression was calculated and visualized using GraphPad Prism 8.

Study approval and human subjects

The study was approved by the responsible local ethics committees (Institutional Review Board of the University Medical Center Utrecht (STEM: 10-402/K; TcBio 14-008; Metabolic Biobank: 19–489), Erasmus MC Medical Ethical Committee (MEC-2014-060), and the Dutch Ethical Medical Council (Leiden University MC)). Tis-sue biopsies from livers of healthy donors were obtained during surgery in the Erasmus MC, Rotterdam. Human fetal livers were obtained from Leiden University Medical Centre (MC). All patient materials were used after written informed consent.

Organoid establishment and culture

Cholangiocyte-derived organoids were established and cultured as described previously.[17] To obtain the cells, liver biopsies were cut into small pieces and digested using 10 mg/ml Collagenase D (Sigma, 11088866001) for 20 min at 37 °C. The samples were then washed with cold Advanced DMEM/F12 (Gibco, 12634028) supplemented with 2 mM GlutaMAX (Gibco, 35050061), 10 mM HEPES (Gibco, 15630080), 100 U/ml PenStrep (Gibco, 15140122), and spun at 1500 rpm for 5 min. Cell pellet was plated in matrigel (Corning, 356231) and culture medium was added. Culture media was based on Advanced DMEM/F12 supplemented with 2 mM GlutaMAX, 10 mM HEPES, 100 U/ml PenStrep, 2% B27 without vitamin A (Gibco, 12587010), 10 mM Nicotinamide (Sigma, N0636), 1.25 mM *N*-Acetylcysteine (Sigma, A9165), 10% RSPO1 conditioned media (homemade), 10 nM Gastrin (Tocris, 3006/1), 50 ng/ml EGF (Peprotech, AF-100-15), 100 ng/ml FGF10 (Peprotech, 100-26), 25 ng/ml HGF (Peprotech, 100-39), 50 µg/ml Primocin (Invivogen, ant-pm-2), 5 µM A83-01 (Tocris, 2939/10), and 10 µM Forskolin (Tocris, 1099/10). For the first 3 days after isolation from biopsies, the medium was supplemented with 30% Wnt conditioned media (homemade), 25 ng/ml Noggin (Peprotech, 120-10C), and hES cell cloning recovery solution (Stemgent, 010014500). The medium was changed every 3–4 days and organoids were passaged 1:4–1:8 each week. Differentiation towards hepatocyte was initiated by culturing the organoids in culture medium supplemented with 25 ng/ml BMP7 (Peprotech, 120-03) for 5–7 days. The medium was then changed to Advanced DMEM/F12 supplemented with 2 mM GlutaMAX, 10 mM HEPES, 100 U/ml PenStrep, 2% B27 without vitamin A, 1.25 mM *N*-Acetylcysteine, 10 nM Gastrin, 50 ng/ml EGF, 25 ng/ml HGF, 100 ng/ml FGF19 (Peprotech, 100-32), 50 µg/ml Primocin, 500 nM A83-01, 25 ng/ml BMP7, 10 µM DAPT (Sigma, D5942), and 30 µM Dexamethasone (Sigma, D4902) for 8 days.

Fetal hepatocyte-derived organoids were established and cultured as described previously.[58] Human fetal liver tissue was chopped and digested using 100 µg/ml Collagenase Type IV (Sigma, C5138) for 5 min. Cells were washed with Advanced DMEM/F12 supplemented with 2 mM GlutaMAX, 10 mM HEPES, 100 U/ml PenStrep, filtered through 100-µm filter, and plated in matrigel. After matrigel had solidified, HEP medium was added. HEP medium consisted of Advanced DMEM/F12 supplemented with 2 mM GlutaMAX, 10 mM HEPES, 100 U/ml PenStrep, 2% B27 without vitamin A, 15% RSPO1 conditioned media, 2.5 mM Nicotinamide, 1.25 mM *N*-Acetylcysteine, 3 µM CHIR-99021 (Sigma, SML1046), 50 µg/ml Primocin, 50 ng/ml FGF7 (Peprotech,

AF-100-19), 50 ng/ml FGF10, 50 ng/ml HGF, 50 μM Y-27632 (Abmole Bioscience, M1817), 1 μM A83-01, 20 ng/ml TGFα (Peprotech, 100-16 A), 50 ng/ml EGF, and 10 nM Gastrin. Medium was refreshed every 2–3 days and organoids were passaged 1:2–1:5 every week.

RNA sequencing of intrahepatic cholangiocyte- and fetal hepatocyte-derived organoids

For RNA sequencing analysis, we included liver samples, intrahepatic cholangiocyte-derived organoids, and fetal hepatocyte organoids that were cultured as described above. RNA was isolated using Trizol LS reagent (Invitrogen) and stored at –80 °C until further processing. mRNA was isolated using Poly(A) Beads (NEXTflex). RNA integrity was assessed using the Agilent RNA 6000 Nano kit and concentrations were determined using the Qubit RNA HS Assay Kit. Only RNA samples with RIN > 8.0 were used for sequencing. Sequencing libraries were prepared using the Rapid Directional RNA-Seq Kit (NEXTflex) and sequenced on a NextSeq500 (Illumina) to produce 75 base long reads (Utrecht Sequencing Facility).

Raw read processing and normalization pipeline

Raw reads from the RNA-seq data were obtained from the European Nucleotide Archive (ENA, https://www.ebi.ac.uk/ena). Raw reads were processed using Galaxy (https://usegalaxy.eu/) web-based platform.[79] Sample quality was assessed using FastQC tool (Galaxy Version 0.72). Low quality reads and adapter sequences were trimmed using Cutadapt (Galaxy Version 1.66.6). Alignment of the raw reads and quantification of gene expression were performed using RNA STAR tool (Galaxy Version 2.7.2b). Reads were mapped to Gencode human reference genome sequence release 33 (GRCh38.p13) and Gencode comprehensive gene annotation v33, using default parameters. Read counts were obtained using the "–quantMode GeneCounts" option in the RNA STAR tool. Normalized counts were obtained by applying the DESeq2 variance-stabilizing transformation (VST) to the read counts using the 'DESeq2' R package[80] followed by quantile normalization using the 'preprocessCore' R package.[81] Additional information regarding our normalization pipeline is provided in Supplementary Note 1 and Supplementary Fig. 9.

Principal component analysis

Principal component analysis (PCA) was performed using normalized counts and plotted using the 'ggplot2' R package by adopting the R function 'plotPCA' (including top 5,000 highest variance genes) from the 'DESeq2' R package.

Euclidean distance and distance-based similarity

The Euclidean distance was calculated by applying the R function 'dist' (method=euclidean) to the normalized counts. Distance-based similarity score (DBS) was defined so that a DBS of '1' signifies perfect similarity to PHH controls and '0' signifies the sample least similar to PHH controls. The DBS for each sample was obtained using the following formula:

$$DBS = (Max_{PHH} - Dist_{PHH}) / Max_{PHH}$$

Max_{PHH}: *the maximum distance value to PHH in the sample matrix of a certain gene set.*
$Dist_{PHH}$: *the distance value of a sample to PHH.*

Gene expression heatmaps

To visualize gene expression, normalized counts were mean-centered per row or gene (Log2FC RNA Expression) and plotted in heatmaps using the 'pheatmap' R package. When cluster trees were absent in heatmaps, columns were ordered by the type of cell source.

CellNet analysis

The bulk RNA-Seq CellNet pipeline was employed to quantify gene expression estimates as previously described,[65] using the 'cn_salmon' function for alignment to reference genome GRCh38. Classification and gene regulatory network (GRN) status analysis were performed using the 'cn_apply' function, based on the human cn-Proc_HS_RS_Jun_20_2017 object trained by 14 types of cells and tissues from 97 studies. Tissue classification scores were exported and plotted in heatmaps using the 'pheatmap' R package. GRN status scores were exported and plotted in bar graphs using the 'ggplot2' R package. Network influence scores of tissue-specific transcription factors were calculated using the 'cn_nis_all' function for 'liver'. Network influence

scores were exported and plotted in heatmaps alongside the normalized expression of corresponding genes, using the 'pheatmap' R package.

Classification of adult vs. fetal hepatocyte identity

Top 5000 genes with the highest variance across different cell types (primary human hepatocytes, fetal hepatocytes, common bile duct, fibroblasts, and pluripotent stem cells) were used to build a Random Forest classifier using the "randomForest" R package. Samples used to train the classifier are listed in Supplementary Data 2. Performance of the classifier was evaluated using the out-of-bag error rate.

Comparison of transcriptomic analysis to proteomes

The gene expression of various HepG2 cells, relative to the control PHH/livers, was compared to the publicly available proteomic data of HepG2 cells and PHHs from Tascher et al.[68] Of the 3995 identified proteins, 3703 (93%) could be matched to a unique gene included in the transcriptomic analysis. Enrichment analysis was performed in ernichR[82] using differentially abundant proteins (Tukey p value < 0.05, lfc > 1; data from Tascher et al.[68]) and differentially expressed genes (padj <0.05, lfc >1) as separate inputs. Proteome and transcriptome enrichment scores were defined as log2 of the odds ratio and log2 of the inverse odds ratio for upregulated and downregulated genes in HepG2 vs. PHH samples, respectively.

Functional assays

Urea secretion was measured using a urea assay kit (Abcam, ab83362) according to the manufacturer's instructions. Briefly, 1 mM ammonium chloride was added to the culture medium. After 24 h, urea concentration in the medium was measured. CYP3A4 activity was measured using a P450-Glo CYP3A4 assay kit (Promega, V9001) according to the manufacturer's recommendations. All data were normalized to total protein content measured using Pierce BCA Protein Assay Kit (Thermo Fisher Scientific, 23225).

PHH/liver quality control for HLCompR inclusion

Quality of new PHH/liver data was assessed using the Random Forest classifier. The RNA-seq data used in Fig. 2 served as a training dataset to build the classifier. A dataset

is not recommended to be used when the new PHH/liver samples have PHH/liver classification probability below 45%.

Statistics and reproducibility

Statistical analyses (Pearson's and Spearman's correlation) were performed using GraphPad Prism 8. Results were considered significant when $p < 0.05$. Sample sizes are generally indicated in the figures. For transcriptomic studies we included a minimum of two samples per type of hepatocyte-like cell (HLC) model, if available. In experiments designed to compare the functional capabilities of HLCs, we included at least two biological replicates for each HLC model. Unless stated otherwise, bar graphs are shown as mean ± standard deviation and box-and-whisker plots are shown as median (line), interquartile range (box), and data range or 1.5x interquartile range (whisker).

References

1. Kmiec Z. Cooperation of Liver Cells in Health and Disease. *Adv Anat Embryol Cell Biol*. 2001; 161: 1–151.

2. Pek NMQ, Liu KJ, Nichane M & Ang LT. Controversies surrounding the origin of hepatocytes in adult livers and the in vitro generation or propagation of hepatocytes. *Cell Mol Gastroenterol Hepatol*. 2021; 11: 273–290.

3. Fu GB, Huang W-J, Zeng M, et al. Expansion and differentiation of human hepatocyte-derived liver progenitor-like cells and their use for the study of hepatotropic pathogens. *Cell Res*. 2019; 29: 8–22.

4. Hu H, Gehart H, Artegiani B, et al. Long-term expansion of functional mouse and human hepatocytes as 3D organoids. *Cell*. 2018; 175: 1591–1606.e19.

5. Kim Y, Kang K, Lee SB, et al. Small molecule-mediated reprogramming of human hepatocytes into bipotent progenitor cells. *J Hepatol*. 2019; 70: 97–107.

6. Xiang C, Du Y, Meng G, et al. Long-term functional maintenance of primary human hepatocytes in vitro. *Science*. 2019; 364: 399–402.

7. Zhang K, Zhang L, Liu W, et al. In vitro expansion of primary human hepatocytes with efficient liver repopulation capacity. *Cell Stem Cell*. 2018; 23: 806–819.e4.

8. Avior Y, Levy G, Zimerman M, et al. Microbial-derived lithocholic acid and vitamin K2 drive the metabolic maturation of pluripotent stem cells-derived and fetal hepatocytes. *Hepatology*. 2015; 62: 265–278.

9. Du Y, Wang J, Jia J, et al. Human hepatocytes with drug metabolic function induced from fibroblasts by lineage reprogramming. *Cell Stem Cell*. 2014; 14: 394–403.

10. Duan Y, Ma X, Zou W, et al. Differentiation and characterization of metabolically functioning hepatocytes from human embryonic stem cells. *Stem Cells*. 2010; 28: 674–686.

11. Fu Y, Deng J, Jiang Q, et al. Rapid generation of functional hepatocyte-like cells from human adipose-derived stem cells. *Stem Cell Res Ther*. 2016; 7: 1–12.

12. Gao Y, Zhang X, Zhang L, et al. Distinct gene expression and epigenetic signatures in hepatocyte- like cells produced by different strategies from the same donor. *Stem Cell Rep*. 2017; 9: 1813–1824.

13. Gieseck RL, Hannan NRF, Bort R, et al. Maturation of induced pluripotent stem cell derived hepatocytes by 3D-culture. *PLoS ONE*. 2014; 9: e86372.

14. Hannan NRF, Segeritz CP, Touboul T & Vallier L. Production of hepatocyte-like cells from human pluripotent stem cells. *Nat Protoc*. 2013; 8: 430–437.

15. Huang J, Guo X, Li W & Zhang H. Activation of Wnt/β-catenin signalling via GSK3 inhibitors direct differentiation of human adipose stem cells into functional hepatocytes. *Sci Rep*. 2017; 7: 1–12.

16. Huang P, Zhang L, Gao Y, et al. Direct reprogramming of human fibroblasts to functional and expandable hepatocytes. *Cell Stem Cell*. 2014; 14: 370–384.

17. Huch M, Gehart H, van Boxtel R, et al. Long-term culture of genome-stable bipotent stem cells from adult human liver. *Cell*. 2015; 160: 299–312.

18. Kanninen LK, Harjumäki R, Peltoniemi P, et al. Laminin-511 and laminin-521-based matrices for efficient hepatic specification of human pluripotent stem cells. *Biomaterials*. 2016; 103: 86–100.

19. Basma H, Soto-Gutiérrez A, Yannam GR, et al. Differentiation and transplantation of human

embryonic stem cell-derived hepatocytes. *Gastroenterology*. 2009; 136: 990–999.e4.

20. Kondo Y, Iwao T, Yoshihashi S, et al. Histone deacetylase inhibitor valproic acid promotes the differentiation of human induced pluripotent stem cells into hepatocyte-like cells. *PLoS ONE*. 2014; 9: 1–11.

21. Koui Y, Kido T, Ito T, et al. An in vitro human liver model by iPSC-derived parenchymal and non-parenchymal cells. *Stem Cell Rep*. 2017; 9: 490–498.

22. Li Z, Wu J, Wang L, et al. Generation of qualified clinical-grade functional hepatocytes from human embryonic stem cells in chemically defined conditions. *Cell Death Dis*. 2019; 10: 763.

23. Luo Y, Lou C, Zhang S, et al. Three-dimensional hydrogel culture conditions promote the differentiation of human induced pluripotent stem cells into hepatocytes. *Cytotherapy*. 2018; 20: 95–107.

24. Mun SJ, Ryu J-S, Lee M-O, et al. Generation of expandable human pluripotent stem cell- derived hepatocyte-like liver organoids. *J Hepatol*. 2019; 71: 970–985.

25. Nakamori D, Akamine H, Takayama K, Sakurai F & Mizuguchi H. Direct conversion of human fibroblasts into hepatocyte-like cells by ATF5, PROX1, FOXA2, FOXA3, and HNF4A transduction. *Sci Rep*. 2017; 7: 16675.

26. Okura H et al. Properties of hepatocyte-like cell clusters from human adipose tissue-derived mesenchymal stem cells. *Tissue Eng Part C Methods*. 2010; 16: 761–770.

27. Pettinato G, Ramanathan R, Fisher RA, et al. Scalable differentiation of human iPSCs in a multicellular spheroid-based 3D culture into hepatocyte-like cells through direct Wnt/β-catenin pathway inhibition. *Sci Rep*. 2016; 6: 1–17.

28. Pettinato G, Lehoux S, Ramanathan R, et al. Generation of fully functional hepatocyte-like organoids from human induced pluripotent

stem cells mixed with Endothelial Cells. *Sci Rep*. 2019; 9: 1–21.

29. Roelandt P, Pauwelyn KA, Sancho-Bru P, et al. Human embryonic and rat adult stem cells with primitive endoderm-like phenotype can be fated to definitive endoderm, and finally hepatocyte-like cells. *PLoS ONE*. 2010; 5: e12101.

30. Boon R, Kumar M, Tricot T, et al. Amino acid levels determine metabolism and CYP450 function of hepatocytes and hepatoma cell lines. *Nat Commun*. 2020; 11: 1393.

31. Sauer V, Tchaikovskaya T, Wang X, et al. Human urinary epithelial cells as a source of engraftable hepatocyte-like cells using stem cell technology. *Cell Transpl*. 2016; 25, 2221–2243.

32. Schneeberger K, Sánchez-Romero N, Ye S, et al. Large-scale production of LGR5-positive bipotential human liver stem cells. *Hepatology*. 2020; 72: 257–270.

33. Sengupta S, Johnson BP, Swanson SA, et al. Aggregate culture of human embryonic stem cell-derived hepatocytes in suspension are an improved In Vitro model for drug metabolism and toxicity testing. *Toxicol Sci*. 2014; 140: 236–245.

34. Shan J, Schwartz RE, Ross NT, et al. Identification of small molecules for human hepatocyte expansion and iPS differentiation. *Nat Chem Biol*. 2013; 9: 514–520.

35. Si-Tayeb K, Noto FK, Nagaoka M, et al. Highly efficient generation of human hepatocyte-like cells from induced pluripotent stem cells. *Hepatology*. 2010; 51: 297–305.

36. Takayama K, Inamura M, Kawabata K, et al. Generation of metabolically functioning hepatocytes from human pluripotent stem cells by FOXA2 and HNF1α transduction. *J Hepatol*. 2012; 57: 628–636.

37. Takayama K, Inamura M, Kawabata K, et al. Efficient generation of functional hepatocytes from human embryonic stem cells and induced

pluripotent stem cells by HNF4α transduction. *Mol Ther*. 2012; 20: 127–137.

38. Takayama K, Akita N, Mimura N, et al. Generation of safe and therapeutically effective human induced pluripotent stem cell-derived hepatocyte-like cells for regenerative medicine. *Hepatol Commun*. 2017; 1: 1058–1069.

39. Tang W, Guo R, Shen S-J, et al. Chemical cocktails enable hepatic reprogramming of human urine-derived cells with a single transcription factor. *Acta Pharmacol Sin*. 2019; 40: 620–629.

40. Tasnim F, Phan D, Toh YC & Yu H. Cost-effective differentiation of hepatocyte-like cells from human pluripotent stem cells using small molecules. *Biomaterials*. 2015; 70: 115–125.

41. Calabrese D, Roma G, Bergling S, et al. Liver biopsy derived induced pluripotent stem cells provide unlimited supply for the generation of hepatocyte-like cells. *PLoS ONE*. 2019; 14: 1–27.

42. Tasnim F, Toh Y-C, Qu Y, et al. Functionally enhanced human stem cell derived hepatocytes in galactosylated cellulosic sponges for hepatotoxicity testing. *Mol Pharm*. 2016; 13: 1947–1957.

43. Touboul T, Chen S, To CC, et al. Stage-specific regulation of the WNT/β-catenin pathway enhances differentiation of hESCs into hepatocytes. *J Hepatol*. 2016; 64: 1315–1326.

44. Unzu C, Planet E, Brandenberg N, et al. Pharmacological induction of a progenitor state for the efficient expansion of primary human hepatocytes. *Hepatology*. 2019; 69, 2214–2231.

45. Waclawczyk S, Buchheiser A, Flögel U, Radke, TF & Kögler G. In vitro differentiation of unrestricted somatic stem cells into functional hepatic-like cells displaying a hepatocyte-like glucose metabolism. *J Cell Physiol*. 2010; 225: 545–554.

46. Wang Q, Sun D, Liang Z, et al. Generation of human hepatocytes from extended pluripotent stem cells. *Cell Res*. 2020; 30: 810–813.

47. Wang Z, Li W, Jing H, et al. Generation of hepatic spheroids using human hepatocyte-derived liver progenitor-like cells for hepatotoxicity screening. *Theranostics*. 2019; 9: 6690–6705.

48. Wang S, Wang X, Tan Z, et al. Human ESC-derived expandable hepatic organoids enable therapeutic liver repopulation and pathophysiological modeling of alcoholic liver injury. *Cell Res*. 2019; 29: 1009–1026.

49. Xie B, Sun D, Du Y, et al. A two-step lineage reprogramming strategy to generate functionally competent human hepatocytes from fibroblasts. *Cell Res*. 2019; 29: 696–710.

50. Zhao D, Chen S, Duo S, et al. Promotion of the efficient metabolic maturation of human pluripotent stem cell-derived hepatocytes by correcting specification defects. *Cell Res*. 2013; 23: 157–161.

51. Zhu S, Rezvani M, Harbell J, et al. Mouse liver repopulation with hepatocytes generated from human fibroblasts. *Nature*. 2014; 508: 93–97.

52. Carpentier A, Nimgaonkar I, Chu V, et al. Hepatic differentiation of human pluripotent stem cells in miniaturized format suitable for high-throughput screen. *Stem Cell Res*. 2016; 16: 640–650.

53. Chen YF, Tseng C-Y, Wang H-W, et al. Rapid generation of mature hepatocyte-like cells from human induced pluripotent stem cells by an efficient three-step protocol. *Hepatology*. 2012; 55: 1193–1203.

54. Chivu M, Dima SO, Stancu CI, et al. In vitro hepatic differentiation of human bone marrow mesenchymal stem cells under differential exposure to liver-specific factors. *Transl Res*. 2009; 154: 122–132 (2009).

55. Choudhury Y, Toh YC, Xing J, et al. Patient-specific hepatocyte-like cells derived from induced pluripotent stem cells model pazopanib-mediated hepatotoxicity. *Sci Rep*. 2017; 7: 41238.

56. Du C, Feng Y, Qiu D, et al. Highly efficient and expedited hepatic differentiation from human

pluripotent stem cells by pure small-molecule cocktails. *Stem Cell Res Ther*. 2018; 9: 58.

57. Ulvestad M, Nordell P, Asplund A, et al. Drug metabolizing enzyme and transporter protein profiles of hepatocytes derived from human embryonic and induced pluripotent stem cells. *Biochem Pharmacol*. 2013; 86: 691–702.

58. Hendriks D, Artegiani B, Hu H, Chuva de Sousa Lopes S & Clevers H. Establishment of human fetal hepatocyte organoids and CRISPR–Cas9-based gene knockin and knockout in organoid cultures from human liver. *Nat Protoc*. 2021; 16: 182–217.

59. Peng WC, Kraaier LJ & Kluiver TA. Hepatocyte organoids and cell transplantation: What the future holds. *Exp Mol Med*. 2021; 53: 1512–1528.

60. Rimland CA, Tilson SG, Morell CM, et al. Regional differences in human biliary tissues and corresponding in vitro–derived organoids. *Hepatology*. 2021; 73: 247–267.

61. Yang Y, Liu B, Xu J, et al. Derivation of pluripotent stem cells with in vivo embryonic and extraembryonic potency. *Cell*. 2017; 169: 243–257.e25.

62. Aizarani N, Saviano A, Sagar, et al. A human liver cell atlas reveals heterogeneity and epithelial progenitors. *Nature*. 2019; 572, 199–204.

63. Cunningham RP & Porat-Shliom N. Liver zonation – revisiting old questions with new technologies. *Front Physiol*. 2021; 12, 1–17.

64. Cahan P, Li H, Morris SA, et al. CellNet: network biology applied to stem cell engineering. *Cell*. 2014; 158: 903–915.

65. Radley AH, Schwab RM, Tan Y, et al. Assessment of engineered cells using CellNet and RNA- seq. *Nat Protoc*. 2017; 12: 1089–1102.

66. Morris SA, Cahan P, Li H, et al. Dissecting engineered cell types and enhancing cell fate conversion via CellNet. *Cell*. 2014; 158, 889–902.

67. Baxter M, Withey S, Harrison S, et al. Phenotypic and functional analyses show stem cell-derived hepatocyte-like cells better mimic fetal rather than adult hepatocytes. *J Hepatol*. 2015; 62, 581–589.

68. Tascher G, Burban A, Camus S, et al. In-depth proteome analysis highlights heparg cells as a versatile cell system surrogate for primary human hepatocytes. *Cells*. 2019; 8: 1–25.

69. Schwanhäusser B, Busse D, Li N, et al. Global quantification of mammalian gene expression control. *Nature*. 2011; 473: 337–342.

70. Häberle J, Boddaert N, Burlina A, et al. Suggested guidelines for the diagnosis and management of urea cycle disorders. *Orphanet J Rare Dis*. 2012; 7: 0–1.

71. Müller FA & Sturla SJ. Human in vitro models of nonalcoholic fatty liver disease. *Curr Opin Toxicol*. 2019; 16: 9–16.

72. ter Braak B, Niemeijer M, Boon R, et al. Systematic transcriptome-based comparison of cellular adaptive stress response activation networks in hepatic stem cell-derived progeny and primary human hepatocytes. *Toxicol In Vitro*. 2021; 73: 105107.

73. Guan Y, Xu D, Garfin PM, et al. Human hepatic organoids for the analysis of human genetic diseases. *JCI Insight*. 2017; 2: e94954.

74. Gupta R, Schrooders Y, Hauser D, et al. Comparing in vitro human liver models to in vivo human liver using RNA-Seq. *Arch Toxicol*. 2021; 95, 573–589.

75. Shi Y, Jiang C-F, Chen Y, et al. Identification of accessible hepatic gene signatures for interindividual variations in nutrigenomic response to dietary supplementation of omega-3 fatty acids. *Cells*. 2021; 10: 467.

76. Vieyres G, Reichert I, Carpentier A, Vondran F WR & Pietschmann T. The ATGL lipase cooperates with ABHD5 to mobilize lipids for hepatitis C virus assembly. *PLoS Pathog*. 2020; 16: 1–41.

77. Stanley LA & Wolf CR. Through a glass, darkly? HepaRG and HepG2 cells as models of human phase I drug metabolism. *Drug Metab Rev*. 2022; 54: 46–62.

78. Rombaut M, Boeckmans J, Rodrigues RM, et al. Direct reprogramming of somatic cells into induced hepatocytes: cracking the Enigma code. *J Hepatol*. 2021; 75: 690–705.

79. Afgan E, Baker D, Batut B, et al. The Galaxy platform for accessible, reproducible and collaborative biomedical analyses: 2018 update. *Nucleic Acids Res*. 2018; 46: W537–W544.

80. Love MI, Huber W & Anders S. Moderated estimation of fold change and dispersion for RNA-seq data with DESeq2. *Genome Biol*. 2014; 15, 1–21.

81. Bolstad BM, Irizarry RA, Åstrand M & Speed TP. A comparison of normalization methods for high density oligonucleotide array data based on variance and bias. *Bioinformatics*. 2003; 19: 185–193.

82. Chen EY, Tan CM, Kou Y, et al. Enrichr: interactive and collaborative HTML5 gene list enrichment analysis tool. *BMC Bioinform*. 2013; 14: 128.

Acknowledgements

Supplementary figures

Supplementary Fig. 1: strategy and results of systematic literature search and data collection.

Supplementary Fig. 2: summary of HLC generation protocols.

Supplementary Fig. 3: principal component analysis of samples using/adopting Huch protocol.

Supplementary Fig. 4: heatmaps and distance-based similarity scores (DBS) of various liver function associated gene sets.

Supplementary Fig. 5: heatmaps and distance-based similarity scores (DBS) of various liver function associated gene sets.

Supplementary Fig. 6: liver zonation analysis.

Supplementary Fig. 7: evaluation of fibroblast and ESC identities.

Supplementary Fig. 8: testing the HLCompR web application using additional studies.

Supplementary Fig. 9: normalization method for cross-study RNA-seq analysis.

May be downloaded from doi.org/10.1038/s42003-022-04046-9.

Supplementary data

Supplementary Data 1: Summary table of reported functional assays and gene expression.

Supplementary Data 2: detailed information on RNA-seq data used in the study.

Supplementary Data 3: reported functional and expression data.

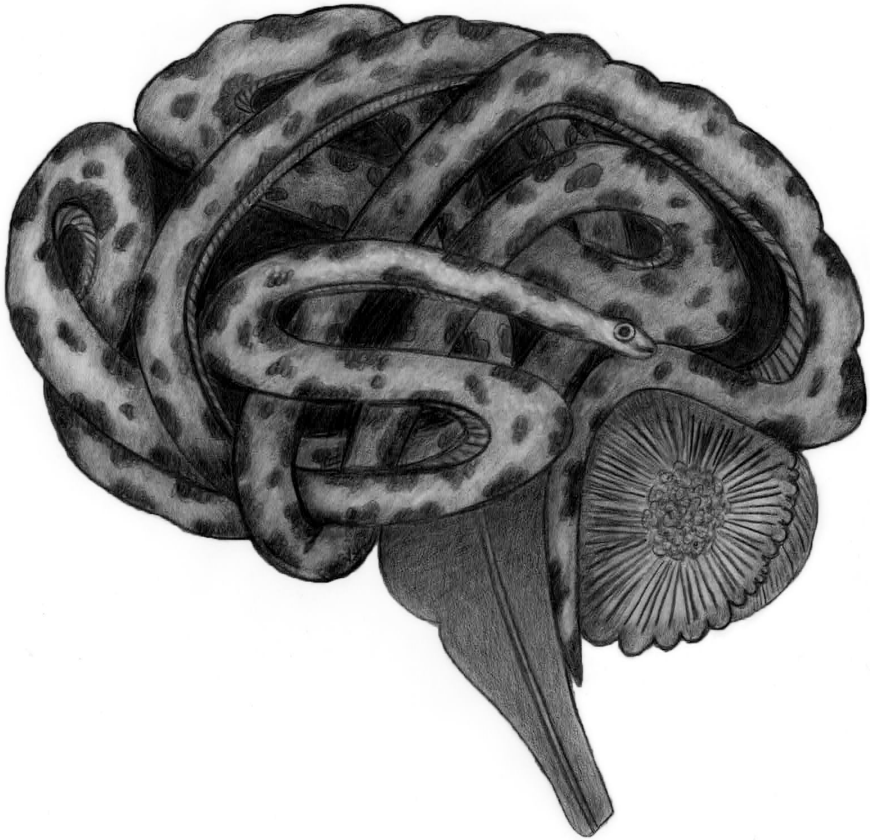**Supplementary Data 4**: count matrices of the RNA-seq data.

Supplementary Data 5: median DBS based on hepatocyte functions and liver zonation gene sets.

Supplementary Data 6: HLC identity analysis.

Supplementary Data 7: validation of transcriptomics.

Supplementary Data 8: additional HLC samples.

May be downloaded from doi.org/10.1038/s42003-022-04046-9.

THE FUTURE APPROACH

COMMON TO ALL METABOLIC DISEASES, TARGETING THE GENETIC ORIGIN OF THE DISEASE

PRIME EDITING TO REPAIR POLG-RELATED DISEASE

Gautam Kok, Remi Stevelink, Eline Kormelink, Maaike Lenderink, Irena Muffels, Indi Joore, Imre Schene, Eveline Ilcken, Bobby Koeleman, Ewart Kuijk, Kees Braun, Sabine Fuchs

11

Project goal

We aim to develop prime editing for *in vivo* genetic repair of *POLG*-mutations as the first potentially curative treatment of *POLG*-related disease. We will first optimize *in vitro* effectiveness and safety of prime editing in patient-specific organ and cell models. Next, we will perform *in vivo* prime editing in mouse models of *POLG*-related disease to optimize *in vivo* distribution and activity and establish functional repair of the disease phenotype. As such, our project aims to prepare for the first-in-human trial of a disease modifying therapy directly correcting the root cause of *POLG*-related disease.

Introduction

Autosomal recessive point mutations in the *POLG*-gene cause a range of severe symptoms, including developmental delay, intractable epilepsy, hypotonia, gastrointestinal problems, and liver failure.[1] *POLG* encodes DNA polymerase subunit gamma, the only polymerase responsible for replication and maintenance of mitochondrial DNA (mtDNA). Around 1% of the population carries pathogenic *POLG* variants, suggesting a 1:10.000 prevalence of the disease.[1] The majority of patients harbors the same single disease-causing *POLG* point mutation (p.A467T), leading to a 96% decrease in enzyme function.[2] This causes depletion of mitochondrial DNA, defects in the respiratory energy chain and symptoms prominently affecting organs with high energy demand such as the brain and liver. Patients with this common *POLG* variant often have detrimental epilepsy, which usually manifests in infancy or in childhood with an explosive onset of intractable seizures. There is currently no causative treatment; conventional antiepileptic drugs are commonly ineffective, and children typically die within months to years after symptom onset due to status epilepticus, sepsis and/or liver failure.[3]

Gene therapy holds promise to directly correct the root cause of *POLG*-related disease. The potential of gene therapy has already been shown for another detrimental neurological disease: spinal muscular atrophy type 1 (SMA1). Until several years ago, there was no therapy for SMA1 and those affected died in infancy. With a single intravenous injection of a virus containing a healthy copy of the affected gene, children can now be treated before they develop symptoms.[4] Sometimes these children now even develop normally.[4,5] Similar therapies may also cure other genetic diseases.[6] Unfortunately, for most diseases this relatively simple method of viral delivery of an entire healthy gene is not possible, for the simple reason that most genes, like *POLG*, are too large to fit in a virus. Moreover, the gene that is virally injected is continuously active and lacks normal physiological control, rendering the treatment suboptimal for some conditions.

These shortcomings are overcome by targeted repair in the host genome with the CRISPR-Cas9 system. This field progresses rapidly, and the first clinical trials have already shown potential to permanently cure human diseases.[7,8] However, efficiency and safety of gene correction strongly depends on the mutation and gene editing strategy. The most versatile and safe CRISPR-Cas9-derived technique is the recently devel-
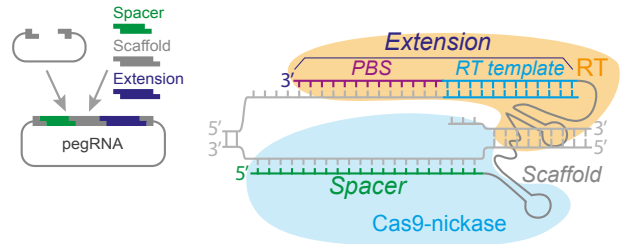
11

Fig. 1: Schematic representation of the prime editing technology. A prime editing guide RNA (pegRNA) guides a Cas9-nickase to the target DNA location. The Cas9-nickase creates a nick in the targeted DNA strand. A reverse transcriptase uses the pegRNA encoded template containing the desired edit for transcription. Image reproduced with permission from Schene et al. (2020).[12]

oped "prime editing" strategy.[9,10] The versatility and precision of prime editing is provided by the combination of a Cas9-nickase with a reverse transcriptase protein, and a prime editing guide RNA (pegRNA). This pegRNA can target almost any location in the genome, and simultaneously provides a template for genetic repair (Figure 1). The genetic location and genomic context of the most common *POLG* mutation (c.1399G>A; p.A467T in exon 7 (Figure 2a) are favorable for prime editing and allow for numerous options to design pegRNAs for optimal editing efficacy and safety.[11]

Our research group was the first in the world to use prime editing to efficiently repair disease-causing mutations in patient-derived organoids and demonstrate functional repair of the disease phenotype without unwanted off-target effects.[12] Our group is now developing a prime editing program to treat children with inherited metabolic diseases targeting the liver. The liver is a crucial metabolic organ in which almost all metabolic pathways are expressed at least to some extent. Moreover, the liver is a feasible target, because restoration of only 5% of the liver function is thought to reverse the clinical phenotype of many metabolic diseases. Furthermore, delivery strategies for gene products predominantly target the liver.

For *POLG*-related disease, the brain is the most important organ that needs to be treated. However, delivery of the gene editing machinery to the brain is complicated by the need to pass the blood brain barrier and reach sufficient affected cell types in the relevant functional brain areas. We aim to build on current technological advances to address these challenges and target the brain. The most promising method to deliver
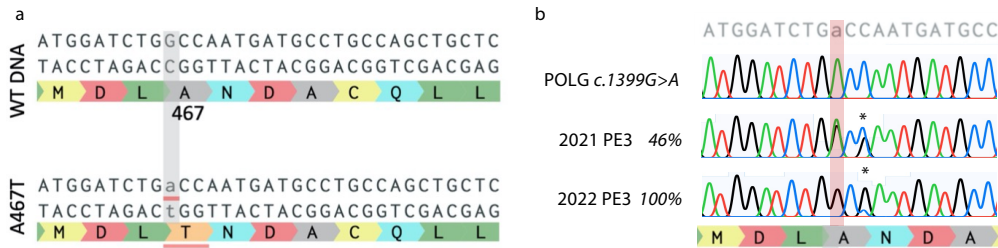
Figure. Prime editing strategy for the POLG c.1399G>A (p.A467T) mutation, and successful repair thereof. **a**, The c.1399G>A mutation in exon 7 of the POLG-gene, leading to the p.A467T change at position 467 in the POLG-protein. **b**, Successful repair of the c.1399G>A mutation in a subset of patient-derived fibroblasts. Sanger sequencing before and after prime editing. EditR was used to quantify the percentage of gene editing, which shows 26% of repair of the p.A467T point mutation using prime editing in 2021 and 81-100% using prime editing in 2022. Efficiency still varies between attempts. We did not find any unwanted editing of other nucleotides. *Intended silent mutation in PAM-site to increase editing efficiency without affecting the resulting amino acid.

gene products to the brain employs adeno associated viruses (AAV). Because the CRISPR-Cas based gene editing machinery is too large to fit in one AAV, 'split intein' AAVs were developed, in which two separate AAVs carry half of the machinery, which is reassembled inside the cell after delivery.[13,14] This method was successfully used to genetically correct up to 59% of brain cells (and 38% of liver cells) with base editing (a technique similar to prime editing) in mice with genetic Niemann–Pick disease type C.[13] At the moment, AAVs targeting brain cells are being developed and tested for use in primates.[15,16]

Our hospital is a well renowned tertiary referral center where we regularly diagnose and treat patients with *POLG*-related disease as well as other metabolic disorders. We are a nationally accredited expertise center for metabolic disorders and for refractory epilepsy. Furthermore, we are ERN accredited for pediatric metabolic diseases (MetabERN), and epilepsy (EpiCARE). We routinely combine fundamental research with translational approaches to directly benefit the treatment of patients with metabolic diseases. We have established a large metabolic biobank, allowing access to primary cells and organoids from patients with metabolic diseases, including *POLG*-related disease. We can build on our prime editing expertise and translational prime editing

program targeting the liver. This specific expertise and embedding makes our group particularly suited to prepare prime editing for *in vivo* treatment of *POLG*-related disease.

All in all, we believe that the current technological progress in genetic correction techniques and delivery methods makes *in vivo* prime editing a *timely and feasible* strategy to address the enormous unmet clinical need associated with *POLG*-related disease. Our collaborative expertise in pediatric metabolic diseases and pediatric epilepsy, our experience with prime editing, and current program to develop treatments for metabolic diseases and pediatric epilepsy puts our group at the frontline to develop the first treatment strategy for *POLG*-related disease.

Aims and objectives

We aim to prepare prime editing for the first *in vivo* repair of human disease-causing *POLG* mutations. We plan to reach the following objectives:

1. Develop a safe and efficient *in vitro* gene repair strategy
2. Generate patient-specific brain and liver models for validation of prime editing
3. Test and optimize genetic and functional correction in different target organ models
4. Generate AAV vectors for delivery to the brain and liver
5. *In vivo* gene repair of *POLG*-related disease in mouse model

With this approach, we aim to pave the way towards eventual causal treatment of patients suffering from *POLG*-related disease as well as provide an overall approach for causal treatment of other severe monogenic diseases affecting the brain and liver.

Detailed workplan

Develop a safe and efficient *in vitro* gene repair strategy

We have already designed and tested editing efficiency of several pegRNAs for the p.A467T substitution, one of which resulted in highly efficient repair of the p.A467T mutation in fibroblasts from a patient treated in our center (Figure 2b). We will further test these pegRNAs for editing reproducibility and editing efficiency in various cell types, including patient-derived fibroblasts, and brain and liver cells derived from induced pluripotent stem cells (iPSC, *see further*). Furthermore, we will use whole-genome

and amplicon sequencing to determine both desired and undesired gene editing effects in these cell types. In case of presence of off-target effects, we will design and test further pegRNAs. In addition, we will keep testing the most recent prime editors, which are published at high frequency. We aim to select the best performing combination of prime editor and pegRNA in terms of efficiency, reproducibility, absence of off-target effects and minimal undesired on-target effects. This way, we will select the strategy with the best efficacy balanced with the best safety-profile for further experiments.

Generate patient-specific cell and organoid models

After establishing efficacy and safety in fibroblasts, we will generate disease-relevant organoids and cells, which are required to establish functional repair. We already have access to liver organoids from one patient. We have fibroblasts from two patients (one homozygous, one compound heterozygous for p.A467T), and have access to additional patient fibroblast cultures through our clinical network. We will reprogram patient-derived fibroblasts from at least 2 homozygous donors into iPSCs using an adapted lentiviral transduction protocol.[17] In short, we will transduce these fibroblasts with reprogramming vectors Oct4, Sox2, Klf4, c-Myc, and a dTomato fluorescent reporter to track reprogramming factor expression and pick reprogrammed colonies. iPSCs will be validated by analyzing morphology and staining for pluripotency markers (SSEA4, Oct4). We will differentiate the iPSCs into neural stem cells and neurons[18] (dual SMAD inhibition protocol) and validate differentiation by analyzing morphology and staining for PAX6, FoxG1, Otx1, and Otx2. Furthermore, we will differentiate the iPSCs into liver organoids (endoderm differentiation by Activin A, FGF2, BMP4, hepatoblast differentiation by FGF2 and BMP4, hepatic maturation by HGF and oncostatin M)[19] and validate differentiation by analyzing morphology and validating expression of hepatocyte markers (HNF4a, ALB). We will use these syngeneic iPSC derived brain and liver cells to test prime editing efficacy, reproducibility, safety (also with AAV vectors, *see further*), and function (*see further*).

Test and optimize genetic and functional correction in liver and brain models.

We have developed functional readouts for fibroblasts and organoids with *POLG* mutations to evaluate functional effects of gene repair (Figure 3). Concurrent with the putative *POLG*-related disease mechanism of mtDNA depletion and consequential respiratory energy chain deficiency, we found that *POLG*-deficient fibroblasts had decreased mtDNA concentrations compared to healthy controls, which we were able to
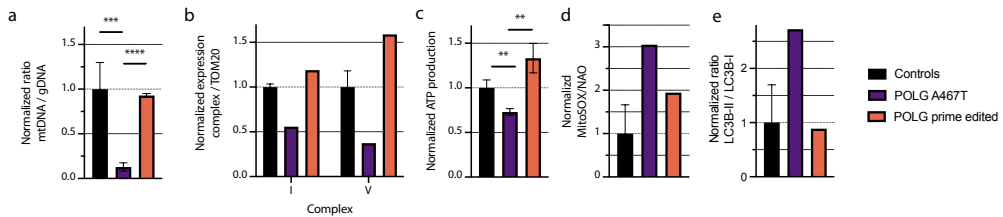
11

Fig. 3: Functional evaluation of POLG deficiency (homozygous p.Ala467Thr) and correction with prime editing (data from single experiments, prime editing experiment from 2021). **a**, POLG-deficient fibroblasts have a significantly lower amount of mitochondrial DNA than controls, as determined using quantitative PCR (qPCR) of mitochondrial and nuclear DNA. Correction of the POLG-variant with prime editing restores the mitochondrial DNA levels. **b**, POLG-deficient fibroblasts have decreased protein expression of mitochondrial complexes I and V. These complexes are responsible for production of ATP. Correction of the POLG-variant with prime editing restores the complex protein expression. **c**, POLG-deficient fibroblasts have decreased ATP production. Correction of the POLG-variant with prime editing restores ATP production. **d**, POLG-deficient fibroblasts have increased production of mitochondrial reactive oxygen species (ROS), as measured using MitoSOX and corrected for total mitochondrial mass. Correction of the POLG-variant decreased the mitochondrial ROS production. **e**, POLG-deficient fibroblasts have increased autophagy ('recycling' of damaged cellular components). Autophagy is represented by the ratio between proteins LC3B-II and LC3B-I. Correction of the POLG-variant with prime editing restores the increased autophagy.

restore following genetic correction with prime editing with our pilot constructs. We further observed decreased expression of mitochondrial complex proteins and ATP production, which normalized following genetic correction. Moreover, we found increased mitochondrial reactive oxygen species (ROS) and increased autophagy, which both normalized following genetic correction. We have experience with various other methods to determine mitochondrial function, including Seahorse XF mitochondrial flux analysis and imaging flowcytometry (Imagestream) analyses. We aim to evaluate whether fibroblasts, organoids, and iPSC-derived liver and brain cells from the same patients exhibit a normalization of their phenotypes after successful repair of the p.A467T *POLG* mutation. As such, we will measure functional repair of various relevant molecular defects associated with POLG-deficiency, because direct measures of the neurological phenotype, including electrical recordings, cannot be evaluated in NSCs.[20]

Generate AAV vectors for delivery to the brain and liver

We aim to use AAV viral vectors for the delivery of the gene editing machinery to enable *in vivo* gene editing of the *POLG* p.A467T mutation. AAV viral vectors do not cause human disease and can efficiently and safely cross the blood-brain barrier to transfect human brain cells. This is the same viral vector that is efficiently and safely used to treat patients with SMA1.[5] Unfortunately, one AAV viral vector is too small to carry all components necessary for prime editing. With a new technique called 'split inteins',[21] two different viral vectors can both deliver half of the required gene product, which reassemble within the transduced cells. It was recently shown in mice that a single systemic injection of such dual AAV viral vectors encoding the base editing machinery can genetically repair up to 59% of brain cells and 38% of cells in the liver, resulting in functional repair of the disease phenotype.[13] We will produce dual-AAV viral vectors optimized for *in vivo* repair of the common p.A467T *POLG* mutation. More efficient AAVs to target brain cells are continuously being developed,[15,22] and if better alternatives arise, we will explore using these. If delivery by AAV vectors proves insufficient for functional *in vivo* gene repair, we will explore alternative delivery options that are currently being developed (including those investigated in our group: lipid nanoparticles which may be administered intravenously and/or intrathecally, and virus-like particles).[23]

***In vivo* gene repair of mouse model**

After validating our approach in patient-derived cells and organs, we will test our approach in a mouse model of *POLG*-related disease to test *in vivo* distribution, genetic and functional effects and safety. The *POLG*-gene, and especially the mutation-containing region, is highly conserved between humans and mice (98.1% amino acids matching), making mice ideal for both generation and repair of human mutations.

Various mouse models ($POLG^{A449T/A449T}$, $POLG^{Y933C/A449T}$) have already been developed and characterized in collaboration with the POLG Foundation. Phenotypical characterization of the $POLG^{A449T/A449T}$ mice showed only a mild reduction in mtDNA in various tissues and no reduction in lifespan or any obvious age-related phenotypes.[24] Unfortunately, the mice did not have epilepsy, liver failure and were resilient to valproic acid.[24] If the compound heterozygous mouse model (e.g., $POLG^{Y933C/A449T}$, unpublished) displays a phenotype that is more representative of human *POLG*-related disease, we will use that model.

Depending on practical issues such as availability of the mouse model, we will preferentially perform the experiments in our own animal facility. If that is not possible, we will collaborate with the external research group that developed the mouse models. In six phenotypically characterized mice, we will inject the dual AAV gene-editing vectors intravenously and we will use non-targeting pegRNAs in six control mice. Previous studies using dual AAV injections of the related CRISPR-Cas9 base editing system have shown that systemic injection of 1 µl of AAV mix (containing $4×10^9$ vg of each split) in three to six mice per group was sufficient to obtain robust and statistically significant results.[13,25] We anticipate that systemic injection of AAV gene editing vectors enables sufficient targeting of the brain and the liver. In case we do not manage to reach sufficient editing, defined as less than 50% of alleles edited, or a lack of neurological improvement in a mouse model with a clear neurological phenotype, we will consider intrathecal or intraventricular injection of the AAV to increase bioavailability in the brain. If we still do not reach the desired efficiency, we may test alternative delivery methods (e.g., modified RNA prime editing constructs encapsuled in lipid nanoparticles, see *risks and mitigation*). For these alternatives, we will use groups and conditions similar to the original experiments. We will perform extensive phenotypic characterization to assess whether any *POLG*-related disease phenotype is functionally repaired. Post sacrifice, we will perform genotyping of all organs, with specific focus on the brain and liver, to evaluate gene editing efficiency and assess potential off-target gene editing. We will assess liver transaminases and platelets to evaluate potential hepatotoxicity associated with AAV treatment.[4] Furthermore, we will use our previously developed functional assays to test for repaired function *in vitro* in relevant tissues and organs.

Risks and mitigation

We do not expect substantial risks associated with the first half of the project. We have ample experience with genetic correction in various cell types, including fibroblasts and intestinal- and liver organoids. Moreover, we have already developed prime editing constructs with which we can efficiently correct the *POLG* p.A467T variant. We have previously performed whole genome sequencing analyses to determine off-target effects in liver organoids after prime editing, and we did not find any. We will build on the results from developing an *in vivo* gene editing strategy for metabolic liver diseases, which our group is currently actively working on. This includes production of

modified RNA (modRNA) of the prime editor and pegRNAs and microfluidic encapsulation in lipid nanoparticles (LNP).

The main risks we foresee for this project involve (1) the differentiation of iPSCs into neurons, (2) *in vitro* gene editing using AAV vectors, and (3) the availability of a mouse model with a clear *POLG*-related disease phenotype.

Differentiation of iPSCs into neurons which can be genetically edited.

While we have experience with culturing induced pluripotent stem cells, we have not yet transdifferentiated them into neuronal cells. For this, we will build on the experience from within our group and/or other scientists in our Utrecht Science Campus. If the arising neurons cannot be gene edited, we will perform the gene editing in the pluripotent state prior to differentiation and evaluate the functional effects. In case we do not manage to transdifferentiate the iPSCs into neurons, we may use other (commercially) available neuronal cell lines, in which we may induce the common POLG variant with prime editing (using regular transfection methods of DNA prime editing constructs).

***In vitro* gene editing using AAV vectors.**

We will use the protocols employed for efficient AAV mediated gene editing in brain cells in mice,[13,15] and test and optimize the resultant vectors in the different cell types. In case we do not reach efficient gene editing (>50% cells) using AAV delivery methods, we may use other methods currently explored in our group for *in vivo* editing of metabolic liver disease. Recent literature suggests that the Cas9 nickase and reverse transcriptase do not necessarily need to be fused, but may also be delivered separately.[26] We will also test this strategy to improve AAV delivery. Furthermore, we are developing LNPs which carry the prime editing constructs as stable modRNA. In case of insufficient targeting of the brain with AAV vectors, we may test intrathecal or intraventricular instead of systemic injection with AAVs or LNPs to genetically correct the common POLG mutation in the *in vivo* mouse studies.

Mouse model with a *POLG*-related disease phenotype.

Fortunately, mouse models for *POLG*-related disease have already been developed in collaboration with the POLG Foundation. However, the mouse model homozygous for A449T (human A467T) shows a molecular phenotype, but no gross developmental,

metabolic or neurological phenotype to test functionally therapeutic effects.[24] It is currently unknown what fraction and which cell types need to be genetically repaired to cure the neurological and liver phenotype of POLG-related disease. Therefore, we hope that a compound heterozygous mouse model with the common variant shows a disease phenotype comparable to humans. Even without a functional disease phenotype, the mouse studies will allow us to determine *in vivo* gene editing efficiency (on a genetic level). Irrespective of the phenotype, safety can be established by assessing unwanted on- and off-target effects, systemic toxic effects and organ-specific effects.

Future prospects

Our project aims to lay the foundation for the first-in-human clinical trial of gene repair for *POLG*-related disease and provide the basis for a risk/benefit analysis to evaluate if and/or what still needs to be done prior to clinical application. Upon developing a clinical therapy, the systems and strategies developed in this project can also be used to target other organs (e.g. muscles or the gastrointestinal tract) by adapting the delivery gene-vectors. Since prime editing techniques are versatile and easily adaptable, the application developed in this project can easily be translated to target almost any other mutation that causes an untreatable genetic disease in the brain or liver. Although such diseases are all individually rare, together they affect a large proportion of patients for whom currently no causative treatment exists.

References

1. Rahman S & Copeland WC. POLG-related disorders and their neurological manifestations. *Nat Rev Neurol*. 2019; 15: 40–52.

2. Chan SSL, Longley MJ, Copeland WC. The Common A467T Mutation in the Human Mitochondrial DNA Polymerase (POLG) Compromises Catalytic Efficiency and Interaction with the Accessory Subunit. *J Biol Chem*. 2005; 280: 31341–31346.

3. Hikmat O, Tzoulis C, Chong WK, et al. The clinical spectrum and natural history of early-onset diseases due to DNA polymerase gamma mutations. *Genet Med*. 2017; 19 :1217–1225.

4. Strauss KA, Farrar MA, Muntoni F, et al. Onasemnogene abeparvovec for presymptomatic infants with two copies of SMN2 at risk for spinal muscular atrophy type 1: the Phase III SPR1NT trial. *Nat Med*. 2022; 28: 1381–1389.

5. Mendell JR, Al-Zaidy S, Shell R, et al. Single-Dose Gene-Replacement Therapy for Spinal Muscular Atrophy. *N Engl J Med*. 2017; 377: 1713–1722.

6. Bulaklak K & Gersbach CA. The once and future gene therapy. *Nat Commun*. 2020; 11: 5820.

7. Arnold C. What's new in clinical CRISPR? *Nat Med*. 2021; 27: 184–185.

8. Gillmore JD, Gane E, Taubel J, et al. CRISPR-Cas9 In Vivo Gene Editing for Transthyretin Amyloidosis. *N Engl J Med*. 2021; 385: 493–502.

9. Anzalone AV, Randolph PB, Davis JR, et al. Search-and-replace genome editing without double-strand breaks or donor DNA. *Nature*. 2019; 576: 149–157.

10. Porto EM, Komor AC, Slaymaker IM, et al. Base editing: advances and therapeutic opportunities. *Nat Rev Drug Discov*. 2020; 19: 839–859.

11. Kim HK, Yu G, Park J, et al. Predicting the efficiency of prime editing guide RNAs in human cells. *Nat Biotechnol*. 2021; 39: 198–206.

12. Schene IF, Joore IP, Oka R, et al. Prime editing for functional repair in patient-derived disease models. *Nat Commun*. 2020; 11: 5352.

13. Levy JM, Yeh W-H, Pendse N, et al. Cytosine and adenine base editing of the brain, liver, retina, heart and skeletal muscle of mice via adeno-associated viruses. *Nat Biomed Eng*. 2020; 4: 97–110.

14. Truong D-JJ, Kühner K, Kühn R, et al. Development of an intein-mediated split–Cas9 system for gene therapy. *Nucleic Acids Res*. 2015; 43: 6450–6458.

15. Stanton AC, Lagerborg KA, Tellez L, et al. Systemic administration of novel engineered AAV capsids facilitates enhanced transgene expression in the macaque CNS. *Med*. 2022; S2666634022004561.

16. Yao Y, Wang J, Liu Y, et al. Variants of the adeno-associated virus serotype 9 with enhanced penetration of the blood–brain barrier in rodents and primates. *Nat Biomed Eng*. 2022; 6: 1257–1271.

17. Warlich E, Kuehle J, Cantz T, et al. Lentiviral Vector Design and Imaging Approaches to Visualize the Early Stages of Cellular Reprogramming. *Mol Ther*. 2011; 19: 782–789.

18. Galiakberova AA, Dashinimaev EB. Neural Stem Cells and Methods for Their Generation From Induced Pluripotent Stem Cells in vitro. *Front Cell Dev Biol*. 2020; 8: 815.

19. Olgasi C, Cucci A, Follenzi A. iPSC-Derived Liver Organoids: A Journey from Drug Screening, to Disease Modeling, Arriving to Regenerative Medicine. *Int J Mol Sci*. 2020; 21: 6215.

20. Liang KX, Kristiansen CK, Mostafavi S, et al. Disease-specific phenotypes in iPSC-derived

11

neural stem cells with POLG mutations. *EMBO Mol Med*. 2020; 12: e12146.

21. Liu P, Liang S-Q, Zheng C, et al. Improved prime editors enable pathogenic allele correction and cancer modelling in adult mice. *Nat Commun*. 2021; 12: 2121.

22. Goertsen D, Flytzanis NC, Goeden N, et al. AAV capsid variants with brain-wide transgene expression and decreased liver targeting after intravenous delivery in mouse and marmoset. *Nat Neurosci*. 2022; 25: 106–115.

23. Saha K, Sontheimer EJ, Brooks PJ, et al. The NIH Somatic Cell Genome Editing program. *Nature*. 2021; 592: 195–204.

24. Silva-Pinheiro P, Pardo-Hernández C, Reyes A, et al. DNA polymerase gamma mutations that impair holoenzyme stability cause catalytic subunit depletion. *Nucleic Acids Res*. 2021; 49: 5230–5248.

25. Koblan LW, Erdos MR, Wilson C, et al. In vivo base editing rescues Hutchinson–Gilford progeria syndrome in mice. *Nature*. 2021; 589: 608–614.

26. Liu B, Dong X, Cheng H, et al. A split prime editor with untethered reverse transcriptase and circular RNA template. *Nat Biotechnol*. 2022; 40: 1388–1393.

11

MUTATION-SPECIFIC REPORTER FOR OPTIMIZATION AND ENRICHMENT OF PRIME EDITING

Imre Schene*, Indi Joore*, Jan Baijens, Remi Stevelink, Gautam Kok, Sawsan Shehata, Eveline Ilcken, Eva Nieuwenhuis, Dian Bolhuis, Rosalie van Rees, Sascha Spelier, Hubert van der Doef, Jeffrey Beekman, Roderick Houwen, Edward Nieuwenhuis, Sabine Fuchs

Abstract

Prime editing is a versatile genome-editing technique that shows great promise for the generation and repair of patient mutations. However, some genomic sites are difficult to edit and optimal design of prime-editing tools remains elusive. Here we present a fluorescent prime editing and enrichment reporter (fluoPEER), which can be tailored to any genomic target site. This system rapidly and faithfully ranks the efficiency of prime edit guide RNAs (pegRNAs) combined with any prime editor variant. We apply fluoPEER to instruct correction of pathogenic variants in patient cells and find that plasmid editing enriches for genomic editing up to 3-fold compared to conventional enrichment strategies. DNA repair and cell cycle-related genes are enriched in the transcriptome of edited cells. Stalling cells in the G1/S boundary increases prime editing efficiency up to 30%. Together, our results show that fluoPEER can be employed for rapid and efficient correction of patient cells, selection of gene-edited cells, and elucidation of cellular mechanisms needed for successful prime editing.

Introduction

Prime editing is a precise genome-editing technique able to generate any moderately sized genetic variation without the need for double-strand DNA breaks.[1] This technique allows repair of patient mutations, generation of disease models, and in vivo editing.[2,3] The prime editor protein consists of a modified Cas9 protein creating single-strand DNA breaks (nicking Cas9) fused to a reverse transcriptase. This fusion protein forms a complex with a prime editing guide RNA (pegRNA). The pegRNA consists of a spacer defining the target site, a single-guide RNA (sgRNA) scaffold, and an extension encoding the intended edit (Fig. 1a). More specifically, the spacer region of the pegRNA is homologous to the genomic target region and guides the prime editor to create a single-strand DNA break (nick) at the specified location. The pegRNA extension consists of a primer binding site (PBS) and a reverse transcriptase template (RTT). The PBS is homologous to the target region and binds to the nicked DNA strand, priming the reverse transcriptase to elongate the nicked DNA strand based on the sequence encoded by the RTT. The elongation of the nicked strand forms a 3′ DNA flap containing the intended edit. Finally, the 3′ flap is resolved by cellular DNA repair pathways, resulting in genomic incorporation of the intended edit (Fig. 1a).

The technology of prime editing undergoes rapid optimization, including adaptations to the pegRNA to increase degradation resistance (epegRNAs[4]), improvements to the prime editor to increase editing efficiency[5] and to increase the flexibility to allow editing in different genomic contexts.[6] Specifically, the increase in flexibility of prime editors has improved employability beyond the original prime editor (PE2), which requires a protospacer adjacent 'NGG' motif (NGG-PAM) to edit DNA. On average, the pathogenic mutations described in the ClinVar database have only one nearby NGG-PAM (Supplementary Fig. 1). This limits pegRNA design to often suboptimal spacers and PBSs and thereby reduces gene-editing efficiency. Prime editor variants with flexible PAM recognition[6-8] provide at least nine additional PAM sites to target the pathogenic mutations described within the ClinVar database and thereby greatly improve gene-editing potential (Supplementary Fig. 1).

With the rise of new prime editing machinery and the complex mechanisms underlying editing efficiency of (e)pegRNAs, designing optimal prime editing strategies remains largely elusive. A number of pegRNA design tools have been developed, but these are not data-driven and lack extensive validation.[9-11] For the original NGG-PAM-dependent prime editor protein, a deep learning strategy was developed to specify pe-

Part 4

gRNA characteristics relevant to editing efficiency.[12] Although informative, this deep learning algorithm failed to predict a pegRNA efficiency score for >80% of the mutations in the ClinVar database and does not support non-NGG-pegRNA prediction (Supplementary Fig. 2a,b). As expected, for those pathogenic mutations within the scope of the prediction algorithm, a higher number of available PAMs per mutation resulted in a higher predicted maximum pegRNA efficiency (Supplementary Fig. 2c).

To address the shortcomings of current prediction methods and harness the strength of next-generation prime editing machinery, we present fluoPEER: a fluorescent prime editing and enrichment reporter. Previously developed genome editing reporters for cutting Cas9 and base editors are not applicable to prime editing.[13-17] Furthermore, pegRNAs designed to repair patient mutations can currently only be tested in patient cells. FluoPEER can be tailored to any genomic target site and allows high-throughput analysis of pegRNA designs and prime editors in the cell line of choice using fluorescence-activated cell sorting (FACS) within 7 days from the start of cloning. Moreover, fluoPEER provides a selection method to enrich for genomic editing up to 3-fold relative to conventional selection of transfected cells.

Results

FluoPEER guides pegRNA design for efficient genomic editing

To test the efficiency of various pegRNA and prime editor combinations, we cloned genomic target regions (45–100 nucleotides) into the fluoPEER plasmid. Specifically, the target region was inserted between an (e)GFP and an (m)Cherry cassette under constitutive expression (Fig. 1a). If the genomic target mutation results in a premature stop codon (nonsense) or a frameshift, the unmodified genomic target site can be inserted into the fluoPEER plasmid, resulting in a construct that only expresses GFP. Successful prime editing of the fluoPEER plasmid results in activation of Cherry expression. If the genomic target mutation is not a nonsense or frameshift mutation, either one is added to the target insert in the fluoPEER plasmid (Fig. 1a). We hypothesized that this adaptation would not limit the predictive power of fluoPEER since the substitution or insertion of single nucleotides in the RTT-region has minor effects on prime-editing efficiency (Supplementary Fig. 3). Importantly, this system allows targeting of the reporter and the corresponding genomic locus with the same pegRNA design.

We transfected fluoPEER together with prime editing machinery into HEK293T cells and analyzed reporter editing using FACS after 3 days (Fig. 1b). Based on the ratio of Cherry to GFP signal, an efficiency score was established for each editing condition, enabling ranking of prime editor variants and pegRNAs (Fig. 1c). To verify the reliability of this reporter system, we tested combinations of prime editor variants and pegRNAs to convert a genomically integrated GFP gene to BFP. The same prime editor-pegRNA combinations were used to edit a GFP-derived target region that was inserted into the fluoPEER plasmid (Fig. 1d and Supplementary Fig. 4a). When ranking the editing conditions based on efficiency for both strategies, the correlation between genomic editing and reporter prediction was strong ($R = 0.94$, Fig. 1d and Supplementary Fig. 4b,c). This correlation further confirms that insertion of a 1-nucleotide frameshift mutation in the reporter does not affect the predictive capacity. Importantly, Sanger sequencing only detected genomic editing in conditions with >10% BFP+ cells (Supplementary Fig. 4c), supporting the need for a sensitive reporter system when targeting difficult-to-edit loci. Next, we tested the ability of fluoPEER to predict the efficiency of prime editor-pegRNA combinations for three different genomic mutations, including a substitution, insertion, and deletion mutation. Again, we found strong correlations between the fluoPEER efficiency score and genomic editing as quantified by next-generation sequencing (Fig. 1e).

We also compared fluoPEER to the DeepPE pegRNA efficiency prediction algorithm, which only supports pegRNA prediction on NGG-PAM sites. Testing combinations of NGG-PE2 with three to four different pegRNAs for six genomic target regions, we found that fluoPEER outperformed the DeepPE algorithm on all targets (Supplementary Fig. 5). Furthermore, we confirmed the robustness of the Cherry over GFP ratio as a read-out for efficiency by varying the input reporter plasmid concentration (Supplementary Fig. 6a,b). By varying the time point of read-out, we further corroborated that the ratio-based ranking was stable over a period of 6 days (Supplementary Fig. 6c). Finally, we confirmed that fluorescent activity disappears from fluoPEER-transfected cells within around 2–3 weeks (Supplementary Fig. 6d).

Using the reporter system, we tested pegRNAs and prime editor variant combinations for various genomic loci. Using available knowledge of characteristics influencing editing efficiency,[12,18] we designed pegRNAs containing spacers with high Cas9 single guide RNA (sgRNA) binding scores, PBSs of 9–15 nucleotides length containing at least 5 guanine or cytosine (G/C) nucleotides, and RTTs of 10–20 nucleotides length (Supplementary Fig. 7). Selection of the pegRNA-prime editor condition with the hig-
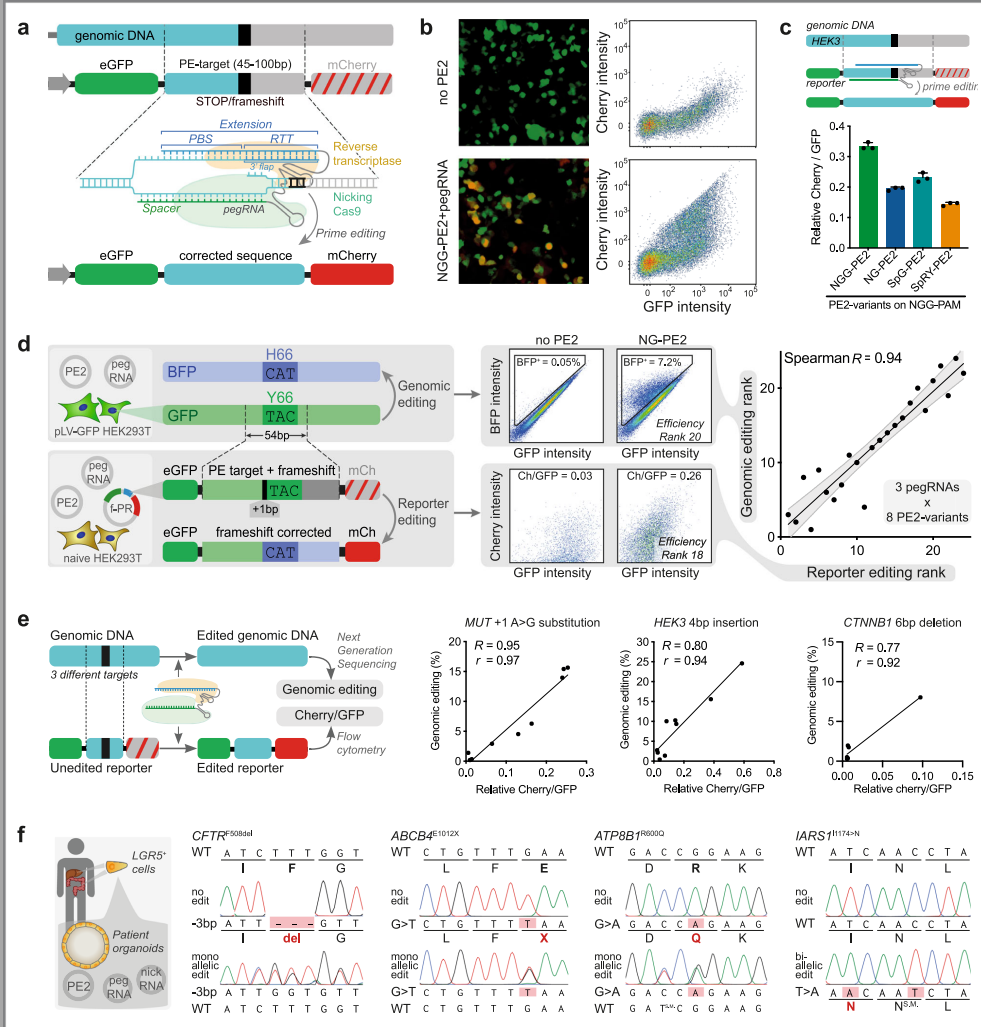
Fig. 1: fluoPEER instructs pegRNA design for genomic editing. **a**, The fluoPEER plasmid uses a 45–100 nucleotide genomic region containing a stop codon or frameshift between sequences encoding two fluorescent proteins (eGFP and mCherry). In case the genomic region does not contain a naturally occurring stop codon or frameshift, one is added. The prime edit machinery targets and edits the genomic insert, removing the insertion or stop codon, leading to expression of mCherry in addition to eGFP. The same prime edit machinery, including the same pegRNA design, can edit the genomic DNA. A finished fluoPEER plasmid contains CMV-GFP-P2A-Genomic insert-P2A-Cherry. See method section for more details. **b**, Editing of the genomic insert is visualized by Cherry signal and quantified using flow cytometry. **c**, FluoPEER distinguishes between the efficiency of different prime editor

(PE2) variants. This is quantified as the average ratio of Cherry signal over GFP signal of each transfected HEK293T cell, which gives a measure of editing per transfected plasmid. n = 3 biologically independent replicates. d Comparison between GFP to BFP conversion using prime editing on genomic DNA and the fluoPEER plasmid. HEK293T cells containing a lenti-virally integrated genomic GFP cassette were transfected with prime editing machinery to convert GFP to BFP in 24 conditions. The same conditions were applied to HEK293T cells co-transfected with the fluoPEER plasmid containing the sequence encoding the GFP to BFP conversion. R = Spearman correlation. Gray area represents 95% confidence interval of the linear regression line. e For three different genomic targets, various pegRNA designs to in-stall either a substitution, deletion, or insertion mutation were tested in HEK293T cells and editing outcomes were measured using next-generation sequencing (NGS). Corresponding genomic targets were inserted into fluoPEER and the efficiency ratio was extracted. R = Spearman correlation and r = Pearson correlation. f Using the optimal pegRNA-prime editor combination based on fluoPEER ranking (Supplementary Fig. 7), several pathogenic mutati-ons in patient-derived organoids were genetically corrected and organoids with biallelic IARS1 mutations were generated in wildtype liver organoids. Error bars represent standard deviations from the mean.

hest reporter prediction score enabled quick and efficient repair of disease-causing mutations in patient-derived organoids (Fig. 1f). These included common mutations causing cystic fibrosis (*CFTR^F508del* and *CFTR^G542X*) that are difficult to edit without the use of prime editors with flexible PAM recognition. In addition, we corrected mutati-ons causing progressive familial intrahepatic cholestasis (PFIC) type 3 (*ABCB4^E1012X*), and PFIC type 1 (*ATP8B1^R600Q*). Furthermore, we used fluoPEER ranking to efficiently mutate the gene coding for cytosolic isoleucyl-tRNA synthetase (*IARS1*) in liver-derived organoids, generating both biallelic and monoallelic clones (Supplementary Fig. 7b). In these disease models, we confirmed that biallelic, but not monoallelic, *IARS1^I1174N* mutations impaired organoid expandability, reflecting the failure to thrive observed in patients with biallelic *IARS1* mutations[19,20] (Supplementary Fig. 7b,c). Importantly, pe-gRNAs targeting a difficult-to-edit locus (low GC-content) to repair a common me-thylmalonic acidemia mutation (*MUT^R369H*) failed to edit the reporter (Supplementary Fig. 7a) and also failed in organoids, demonstrating accurate negative prediction (Sup-plementary Fig. 7d).
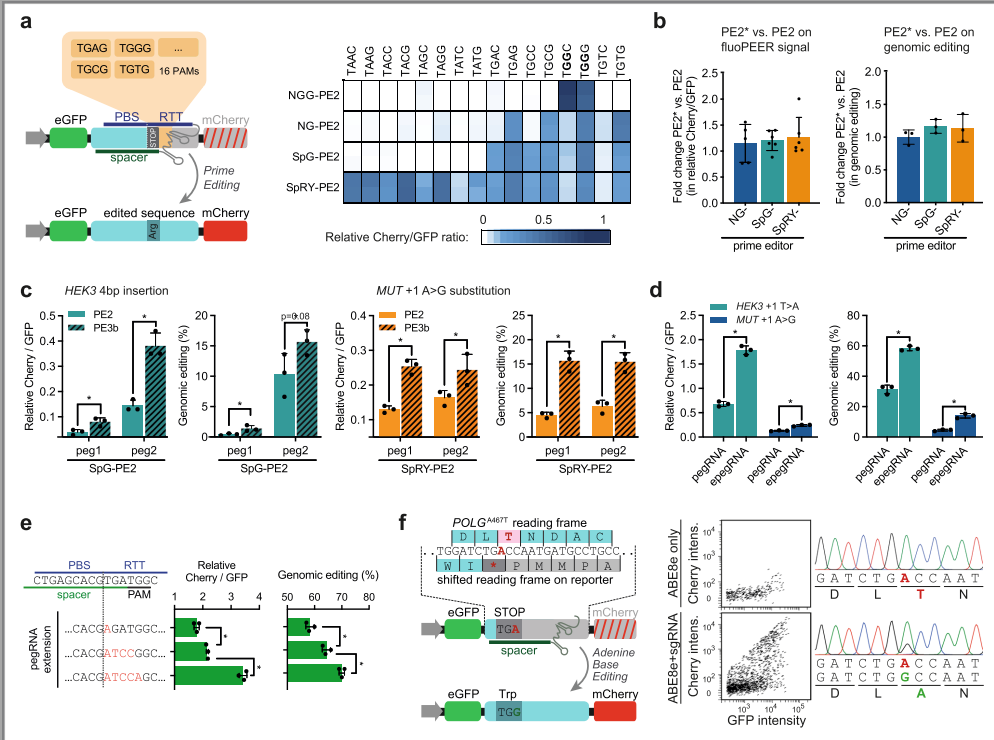
Fig. 2: FluoPEER enables characterization of various genome editing techniques. **a**, 16 fluo-PEER plasmids were constructed to contain the same pegRNA spacer binding site (*HEK3*) including a stop codon, followed by 16 different 4-nucleotide PAM sequences. Prime editing using a pegRNA that converts this stop codon to an arginine-encoding codon results in Cherry signal. The heatmap shows the fluoPEER signal for these 16 plasmids, four prime editor (PE2) variants, and replicates (*n* = 2) per condition in HEK293T cells. **b**, Prime editor variants with adapted nuclear localization sequences (PE2*) were tested in HEK293T cells. Graphs show a summary of all fluoPEER scores (left panel) and of the conversion efficiency of the genomic mutation (right panel), expressed as the fold change (FC) of the PE2* variants relative to the corresponding PE2 variants. See also Supplementary Fig. 8. *n* = 2–3 biologically independent replicates. **c**, FluoPEER was used to evaluate nicking sgRNAs for the PE3b technique in HEK293T cells. PE3b designs increased fluoPEER scores (Cherry/GFP ratios) as well as genomic editing as measured by NGS. **d**, Improved prime editing using epegRNAs was measured on fluoPEER. Cherry over GFP was measured on fluoPEER; genomic editing was measured using NGS. **e**, Increased mismatches between the pegRNA RTT and the target sequence resulted in higher prime editing efficiency on fluoPEER and the geno-

me. Three pegRNAs with varying mismatches with the genome were adopted from Chen et al.[5] More mismatches resulted in higher editing efficiency on the genome and fluoPEER. Significance was analyzed using a two-tailed unpaired Student's t test (*$P < 0.05$) for $n = 3$ biologically independent replicates for **c-e. f**, FluoPEER can report base editing when editing of the target nucleotide resolves a stop codon in any possible reading frame. The genomic region of the $POLG^{A467T}$ mutation was inserted into fluoPEER with a shifted reading frame to create a stop codon (left). This fluoPEER was transfected into fibroblasts with biallelic $POLG^{A467T}$ mutations to show base editing on the reporter (middle) and the genome (right). Error bars represent standard deviations from the mean.

FluoPEER enables characterization of various genome editing techniques

To better characterize PE2 protein variants with flexible PAM recognition, we adapted the genomic target region of fluoPEER to test PAM specificities. We found that SpG-PE2 and NG-PE2 have comparable flexible PAM preferences, but that SpG-PE2 has higher efficiency scores overall (Fig. 2a). SpRY-PE2 was most flexible in PAM recognition, essentially functioning as a PAM-less prime editor. Interestingly, a guanine nucleotide on the 4th PAM position led to higher editing efficiency compared to cytosine (Fig. 2a). Overall, the NG-, SpG-, and SpRY-PE2 protein variants displayed PAM-specificity patterns highly similar to their corresponding cutting Cas9 proteins.[8] We also tested PE2* protein variants with improved nuclear localization,[3] but these variants did not display higher efficiency of reporter editing and genomic editing compared to standard PE2 protein variants in HEK293T cells for the tested mutations (Fig. 2b and Supplementary Fig. 8a,b).

We continued to characterize the ability of the fluoPEER system to report genome editing techniques beyond the standard prime editing strategy of combining a pegRNA and a prime editor. The addition of a nicking sgRNA that only binds on the unedited strand after successful editing of the edited strand is known as PE3b and can increase prime editing efficiency.[1] Indeed, fluoPEER accurately predicted PE3b conditions to increase genomic editing efficiency (Fig. 2c). Next, we tested the recently reported degradation-resistant epegRNAs[4] and found higher editing efficiency compared to the original pegRNAs, both on the fluoPEER system and genomic DNA (Fig. 2d). Recently, DNA mismatch repair (MMR) was found to inhibit the installment of substitution mutations by prime editing. By increasing the number of mismatches between the RTT and the genome, MMR may be evaded and editing efficiency enhanced.[5] We confirmed
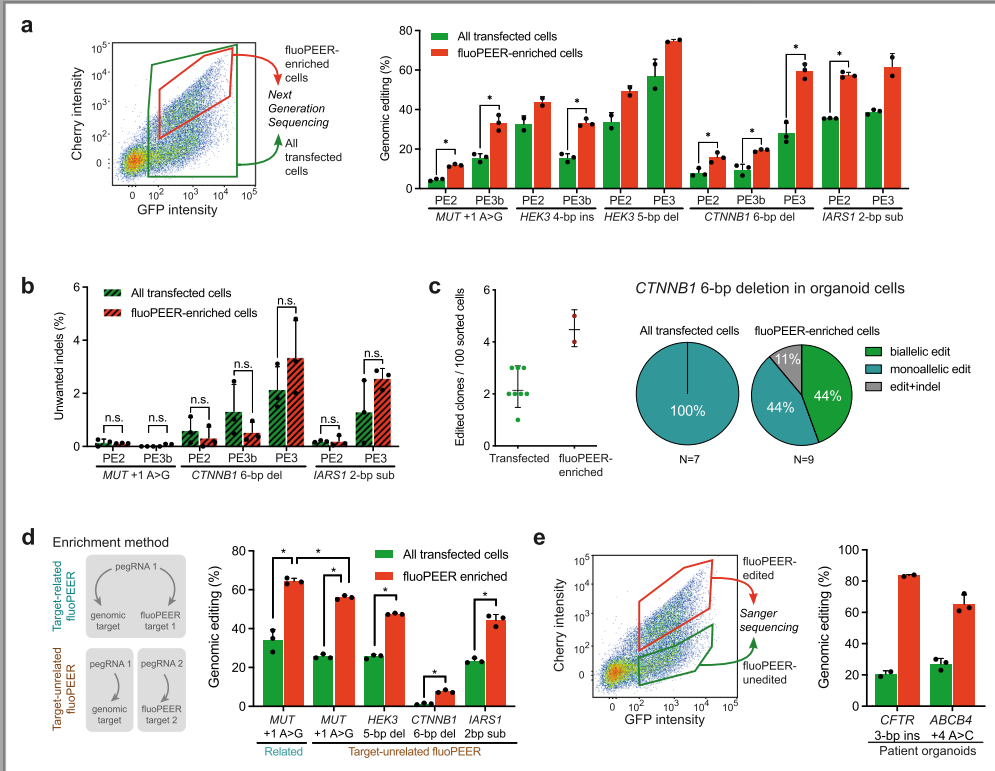
Fig. 3: FluoPEER enriches for genomic editing. **a**, FACS sorting based on transfection of the reporter plasmid (GFP+) and presence of reporter editing (GFP+Cherry+) shows enrichment for genomic editing of various genes for PE2 and PE3(b) in the reporter-edited HEK293T cells. Successful editing was quantified by NGS. Note that the *HEK3* 4-bp insertion PE2 condition was performed with NGG-PE2, while the corresponding PE3b condition was performed with SpG-PE2, resulting in lower editing. **b**, FluoPEER-enrichment of genomic editing does not increase unwanted indels in HEK293T cells, as quantified by NGS. Significance was analyzed using a two-tailed unpaired Student's *t* test (*$P < 0.05$) for $n = 3$ biologically independent replicates for **a** and **b**. **c**, Activating *CTNNB1* mutations in liver-derived organoid cells allow sustained organoid growth despite removal of Wnt-activator Rspo1 from the culture medium.[2] When creating an activating 6-bp deletion in *CTNNB1* by prime editing, fluoPEER-enrichment resulted in outgrowth of more Rspo1-independent liver organoid clones, compared to regular transfection sorting. From the clones with activating *CTNNB1* mutations, only the clones obtained by fluoPEER-enrichment contained biallelic *CTNNB1* mutations. **d**, Use of an unrelated fluoPEER allows enrichment for a genomic edit. Either HEK293T cells were transfected with the fluoPEER corresponding to the genomic mutation

or transfected with a fluoPEER unrelated to the genomic mutation. It should be noted that enrichment with the 'related' fluoPEER still yields the highest editing percentage. Significance was analyzed using a two-tailed unpaired Student's *t* test (*$P < 0.05$) for $n = 3$ biologically independent replicates. **e**, Pathogenic mutations in patient colon (*CFTR*^F508del^) and liver (*ABCB4*^E1012X^) organoids were targeted by PE3 and sorted 72 h after transection based on fluoPEER editing. Reporter-edited organoid cells were enriched for genomic editing compared to reporter-unedited organoid cells. Error bars represent standard deviations from the mean of $n = 2$–3 biologically independent replicates.

---

this mechanism, which increased editing efficiency both on the reporter and the genome (Fig. 2e). To evade MMR, a new prime editor construct was developed, expressing a dominant negative MMR-disrupting MLH1, called PE4max.[5] Interestingly, we found no significant differences in editing efficiency between PE3 (PE2 + nicking sgRNA) and PE5 (PE4max + nicking sgRNA) for two edits on the genome and fluoPEER in HeLa cells (Supplementary Fig. 8c). This confirms that the effect of suppressing MMR differs greatly between edits.[5]

Finally, we tested fluoPEER for base editing, which is possible when base editing resolves a stop codon in any of the six possible reading frames of the genomic target region. We integrated the genomic region of the common *POLG*^A467T^ mutation into the fluoPEER plasmid with a reporter-shifted (+1) reading frame that resulted in a stop codon (Fig. 2f). Adenine base editing (ABE8e-TadA) corrected this mutation on both the plasmid and the genomic DNA of patient-derived fibroblasts (Fig. 2f), showing that fluoPEER could be used for testing base editing gRNA design as well.

FluoPEER enriches for genomic editing

The selection of cells with a detectable edit has been shown to enrich for a simultaneously introduced edit at another locus.[21,22] To test whether fluoPEER allows such enrichment, we sorted HEK293T cells that were plasmid-edited (GFP+Cherry+, fluoPEER-enriched population) and found that these cells showed up to 3-fold increases in genomic editing compared to the complete transfected cell population (GFP+) (Fig. 3a). This enrichment of genomic editing did not result in an increase of unwanted insertion and deletion mutations (indels) in the target region (Fig. 3b). In line with previous findings,[1] no mutations could be detected at off-target sites in either transfected or fluoPEER-enriched cell populations (Supplementary Table 1). FluoPEER enrichment of liver-derived organoid cells yielded higher numbers of edited organoid clones. Strikingly,
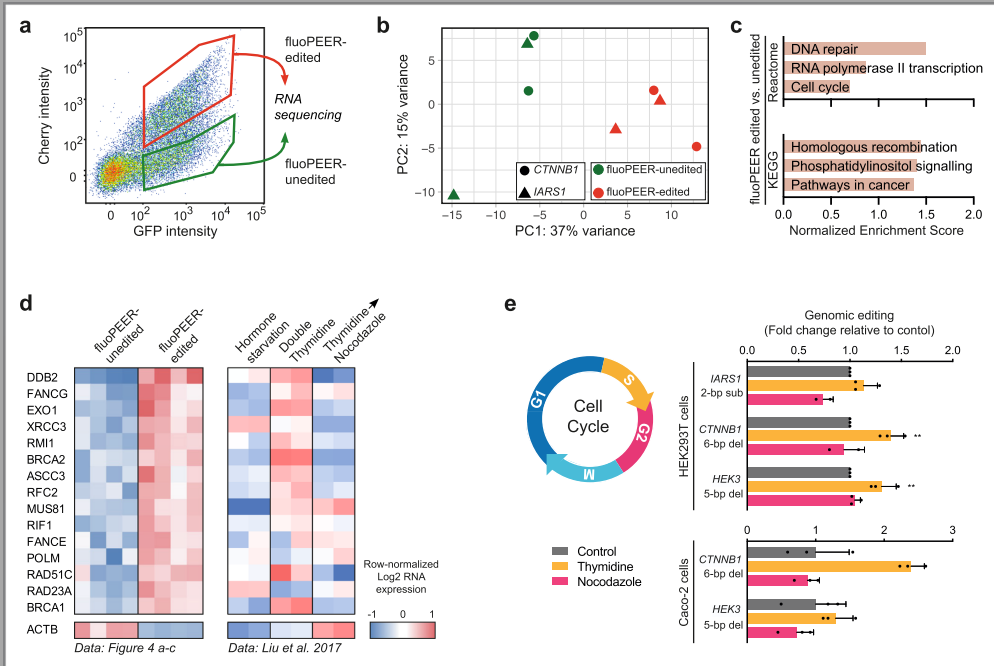
Fig. 4: Endogenous DNA repair proteins and the cell cycle affect prime editing outcomes. **a**, Schematic overview of RNA-sequencing set-up. FluoPEER-edited and -unedited HEK293T cells were sorted separately and RNA was sequenced. **b**, PCA plot and **c**, gene set enrichment analysis of RNA sequencing of the fluoPEER-edited and -unedited cell populations show expression-based differences in DNA repair- and cell cycle-associated genes. **d**, Left panel shows a heatmap of the expression of DNA-repair-associated genes which were enriched in the transcriptome of fluoPEER-edited vs. fluoPEER-unedited HEK293T cells from **a**–**c**. Right panel shows expression of the same genes in publicly available transcriptome profiles (GSE94479) of MCF-7 cells stalled in different cell cycle phases.[49] For both transcriptomic datasets, log2-transformed expression values were mean centered per gene for visualization. **e**, Cell cycle synchronization at the G1/S boundary (double thymidine block) or G2/M phase (nocodazole block) affects genomic prime editing efficiency in HEK293T and Caco-2 cells. HEK293T replicates were normalized to the average editing of the control condition for each of three repeated, independent experiments; Caco-2 replicates ($n = 3$) were normalized to the average editing of the control condition for a single representative experiment with three biological replicates. Error bars represent standard deviations from the mean.

enrichment also enabled generation of clonal organoid lines with biallelic edits (Fig. 3c), which may facilitate in vitro modeling of recessive genetic disorders.

We hypothesized that enrichment of a genomic mutation does not require the use of a 'related' fluoPEER with an insert of the corresponding genomic target region. To test this, we transfected cells with a mix of (1) a pegRNA that targets the genomic DNA, (2) a second pegRNA that targets, (3) an unrelated fluoPEER plasmid, and (4) a prime editor. Indeed, we found that editing of the 'unrelated' fluoPEER plasmid by the second pegRNA enriched for genomic editing by the first pegRNA (Fig. 3d). Importantly, enrichment using a 'related' fluoPEER resulted in slightly higher genomic editing than using a second, unrelated pegRNA-fluoPEER combination (Fig. 3d). Finally, we used the mechanism of fluoPEER enrichment to efficiently generate gene-corrected patient-derived organoids (Fig. 3e). These results establish fluoPEER as a highly dynamic prime-editing read-out, enabling enrichment of genomic editing based on plasmid co-editing.

Endogenous DNA repair proteins and the cell cycle affect prime editing outcomes

We considered whether enrichment of genomic editing was caused by higher co-transfection rates of all prime editing plasmids in fluoPEER-edited cells.[23] We therefore transfected a mix of up to four fluorescent plasmids (mTurq2, eGFP, mKO2, mCherry) and tested co-transfection efficiency using FACS. We found that >90% of the cells receiving one fluorescent plasmid also received the three other fluorescent plasmids (Supplementary Fig. 9). This suggests that variance in editing efficiencies within the transfected cell population is not due to unequal co-transfection. In order to investigate differences between reporter-edited and -unedited cells, we compared the transcriptomes of these two populations (Fig. 4a). The transcriptome of reporter-edited cells was enriched for genes associated with DNA repair, specifically homologous recombination, and cell cycle progression (Fig. 4b,c and Supplementary Fig. 10a-d, and Supplementary Data file 1). To further elucidate the association between expression of reporter-enriched DNA repair genes and the cell cycle, we compared our data to publicly available transcriptomes of cells stalled in different cell cycle phases. Interestingly, DNA repair genes upregulated in edited cells were generally higher in cells stalled at the G1/S boundary using a double thymidine treatment (Fig. 4d). We stalled cells at the G1/S and G2/M boundary through application of a double thymidine or nocodazole block, respectively. Directly after releasing cells, we introduced the prime editing machinery and tested genomic editing two days later. For both HEK293T and Caco-2

cells, we observed a general increase in editing efficiency in cells stalled at the G1/S boundary but not in the G2/M phase (Fig. 4e). Using Hoechst staining and fluoPEER, we evaluated prime editing in cycling cells. We found a >40% increase of Cherry signal in cells that were in G2 one day after transfection of prime editing plasmids (Supplementary Fig. 10e). This further confirms an important effect of cell cycle-associated mechanisms, but in this experiment, the precise cell cycle stages that benefit prime editing are difficult to infer due to the delay in Cherry expression. Taken together, successful prime editing was associated with higher expression of DNA repair genes, specifically those expressed at the G1/S boundary. As such, thymidine treatment of cells increased editing efficiency.

Discussion

We developed fluoPEER as a customizable tool to guide pegRNA design, and to select and optimize prime editor proteins for almost any mutation in patient-derived cells. Furthermore, fluoPEER provides a transient selection method to enrich for genomic editing up to 3-fold compared to conventional selection of transfected cells. Given near-complete co-transfection in our experiments (Supplementary Fig. 9), we used a separate GFP-expressing plasmid and not a prime editor plasmid containing a GFP cassette for this comparison. In contrast to previously developed base-editing reporter and enrichment systems,[21,22] this versatile tool is only transiently active, does not require transfection of a second pegRNA, does not rely on genomic integration of a selection cassette, nor requires generation of an additional genomic edit. Moreover, we use fluoPEER to gain insight in the cellular mechanisms underlying prime editing and find cell cycle-related effects on editing efficiency.

Several tools and strategies have been developed to support pegRNA design. DeepPE is a data-driven pegRNA efficiency prediction algorithm, which yielded important insights in general characteristics for pegRNA design.[12] However, the algorithm lacks predictive capacity beyond the NGG-PAM PE2 version of the prime editor. Furthermore, the DeepPE algorithm performs in silico predictions, based on experimentally derived parameters, and can be unreliable in predicting the in vitro efficiency of new pegRNA designs (Supplementary Fig. 5). An in vitro strategy to evaluate pegRNA designs in high throughput is the use of lentiviral libraries of pooled pegRNAs paired to a DNA target sequence. These pegRNA-target pairs are transduced into cells after which a prime editor is transfected and editing efficiency can be assessed through deep sequencing.[12,24] However, this method only allows testing of pegRNAs with a

single prime editor. Conversely, we uncovered optimal combinations by testing peg-RNA designs with various (flexible) prime editors.

One proposed method to test combinations of pegRNAs and various prime editors is the Prime Edit Activity Reporter (PEAR). The PEAR depends on the removal of a dysfunctional splice site by prime editing, resulting in activation of GFP expression.[25] It was reported that PEAR can be adjusted to test different pegRNA spacers and PBSs. However, the same splice site-restoring RTT has to be used in all PEAR-targeting peg-RNAs, making it impossible to test actual genome-targeting pegRNAs in this system. A more straightforward, but less high-throughput method of testing pegRNA-prime editor combinations is targeting the native genomic site in an easily transfectable cell line, followed by quantification of editing using Sanger sequencing or NGS. However, San-ger sequencing lacks sensitivity, missing sequence variants consisting of up to 15% of total reads (Supplementary Fig. 11). This may lead to underestimation of pegRNA effi-ciency. Furthermore, although NGS is much more sensitive and reliable than Sanger sequencing in quantifying sequence variants, it is more expensive and time-consu-ming. Finally, cell lines have wild-type genomes and might therefore be inadequate to test designs that correct pathogenic mutations, such as the *CFTR^{F508del}* mutation targe-ted in this work.

Because fluoPEER is more flexible than pooled pegRNA screens, more truthful in pegRNA design than PEAR, more sensitive than Sanger sequencing, and quicker and cheaper than NGS, fluoPEER forms an attractive alternative for optimization of prime editing strategies. Although fluoPEER requires an additional cloning step, this can be performed simultaneously with pegRNA cloning, thereby not requiring additional time. Nevertheless, the preferred method for prime editing optimization might differ bet-ween projects and groups, depending on the application and availability of techniques and resources.

The cellular mechanisms underlying successful prime editing are an active topic of research. Our data suggest that the activity of DNA repair mechanisms, specifically homologous recombination, and the cell cycle may influence the outcome of prime editing. A role for the cell cycle has recently been confirmed, with ±1.5 times more efficient prime editing in cycling compared to non-cycling cells.[26] Our results indicate that prime editing is most efficient in cells that are released after stalling in G1/S, which can be linked to the activity of homologous recombination during late S/early G2.[27] Still, while homology directed repair is restricted to dividing cells, prime editing

is also active in non-dividing cells.[1,26,28] Furthermore, a large CRISPR interference screen elucidated the effect of 476 DNA repair-related genes on prime editing outcomes.[5] Interestingly, genes involved in homologous recombination were found to mainly prevent indel formation by prime editing, whereas inhibition of mismatch repair-associated genes increased successful editing.

To conclude, fluoPEER is a straightforward and versatile tool that facilitates effective prime editing in various relevant cell types and increases our understanding of cellular processes underlying this genome editing technique.

Methods

Study approval and human subjects

The study was approved by the responsible local ethics committees (Institutional Review Board of the University Medical Center Utrecht and University Medical Center Groningen (STEM: 10-402/K; TcBio 14-008; Metabolic Biobank: 19-489)). For cystic fibrosis organoids, collection of patient tissue and data was performed following the guidelines of the European Network of Research Ethics Committees (EUREC). Tissue biopsies from the liver of a patient with ABCB4 deficiency (PFIC3) were obtained during a liver transplant procedure in the UMCG, Groningen. Rectal biopsies used for intestinal organoid culture from a patient with ATP8B1 deficiency (PFIC1) and skin biopsies used for fibroblasts culture from a patient with homozygous *POLG*[A467T] mutations were obtained at the outpatient clinic in the UMCU, Utrecht. Biobanked intestinal organoids are stored and cataloged (https://huborganoids.nl/) at the foundation Hubrecht Organoid Technology (http://hub4organoids.eu). All biopsies were used after written informed consent.

ClinVar database computational analysis

Information for all pathogenic mutations shorter than 51 bp was obtained from the ClinVar database,[29] accessed October 2020. Genomic sequences flanking these mutations were obtained from RefSeq[30] accessed October 2020, using the SPDI data model[31] and a custom python script. The −10 to +4 bp region around the target sites were searched for NGG, NAN, or NGN PAMs. The efficiency of prime editing using NGG PAMs was predicted using PE_Position and PE_type random forest models, provided by

Kim et al.[12] Figures were made in python using Matplotlib.[32] The code used for this analysis is available on GitHub (https://github.com/JBaijens/PE_prediction).

Plasmid cloning

FluoPEER plasmids were cloned using the backbone of the pmGFP-P2A-K0-P2A-RFP (Addgene #105686) stalling reporter (SR) plasmid, which was a gift from Ramanujan Hegde. This plasmid was cut directly upstream of the K0-SR domain with SalI and Acc65I for 16 hours at 37 °C, creating 'TCGA' and 'GTAC' overhangs, after which the 6 kb fragment was isolated from gel. Genomic insert oligos containing 5′ 'TCGACC' and 3′ 'G' overhangs on the top oligo, and 5′ 'GTACC' and 3′ 'GG' overhangs on the bottom oligo were annealed and inserted using a conventional ligation protocol (see Supplementary Note 1). Note that a finalized fluoPEER plasmid still contains the K0-SR domain, which is not shown in the schematic representations in Figs. 1a,d,e and 2a,f as it is not important for the working mechanism of fluoPEER. Cloning of pegRNA and epegRNA plasmids was performed according to previously described protocols.[1,4] In brief, the pU6-pegRNA-GG-Vector (Addgene #132777) or the pU6-tevopreq1-GG-acceptor (Addgene #174038) was digested for 16 h with BsaI-HFv2 (NEB), after which the 2.2 kb fragment was isolated from gel. Oligonucleotide duplexes of the pegRNA spacer, pegRNA extension, and pegRNA scaffold sequences were ordered containing the appropriate overhangs and subsequently annealed. The annealed pegRNA duplexes were ligated into the pU6-pegRNA-GG-Vector using Golden Gate assembly with BsaI-HFv2 (NEB) and T4 DNA ligase (NEB) in a protocol of 12 cycles of 5 min at 16 °C and 5 min at 37 °C. For cloning of sgRNAs used for PE3, we replaced the BsmBI restriction sites of the BPK1520 plasmid with BbsI restriction sites using PCR, which allowed direct ligation of sgRNA-spacer duplexes.[33] All fluoPEER insert, pegRNA, and sgRNA sequences used in this work are listed in Supplementary Data file 2 and were synthesized by Integrated DNA Technologies (IDT). pCMV-PE2 (Addgene #132775), pU6-pegRNA-GG-acceptor (Addgene #132777), and pU6-tevopreq1-GG-acceptor (Addgene #174038) were gifts from David Liu; BPK1520 (Addgene #65777) was a gift from Keith Joung.

Cloning of flexible PE2s, flexible PE2*, and SpRY-PE4max

Using PCR and In-Fusion cloning (Takara Bio), the NGG PAM-recognition domain of the prime editor protein (PE2) was replaced with the corresponding domains in NG-ABEmax,[34] SpG-ABEmax, or SpRY-ABEmax,[8] to create NG-, SpG-, and SpRY-PE2, res-

pectively. NG-ABEmax was a gift from David Liu (Addgene #124163). SpG- and SpRY-ABEmax were gifts from Benjamin Kleinstiver (Addgene plasmids #140002 and #140003). PE2* variants with improved nuclear localization sequences (NLSs) were adapted from the NGG-PE2* developed by Liu et al.[3] and were cloned by PCR and In-Fusion cloning (Takara Bio). Successful cloning of all plasmids was confirmed by Sanger sequencing. Using PCR and In-Fusion cloning (Takara Bio), SpRY-PE4max was created by replacing the PAM-recognition domain of PE4max[5] (#174828) with the corresponding domain of SpRY-ABEmax (#140003).[8] pCMV-PEmax-P2A-hMLH1dn (PE4max, Addgene #174828) was a gift from David Liu.

Organoid culture

Liver and intestinal organoids were grown under standard culture conditions according to previously described protocols.[35,36] In short, liver organoids were plated in matrigel (Corning) and maintained in human liver expansion medium (hL-EM), consisting of AdDMEM/F12 (Gibco) supplemented with, GlutaMAX (1x, Gibco), HEPES (1x, Gibco), PenStrep (1x, Gibco), 2% B27 without vitamin A (Gibco), 1.25 mM N-Acetylcysteine (Sigma), 10 mM Nicotinamide (Sigma), 10 nM gastrin (Sigma), 10% RSPO1 conditioned media (homemade), 50 ng/ml EGF (Peprotech), 100 ng/ml FGF10 (Peprotech), 25 ng/ml HGF (Peprotech), 5 mM A83-01 (Tocris), and 10 mM FSK (Tocris). Small intestine and colon organoids were plated in matrigel and maintained in human small intestine expansion medium (hSI-EM), consisting of AdDMEM/F12 (Gibco) supplemented with, GlutaMAX (1x, Gibco), HEPES (1x, Gibco), PenStrep (1x, Gibco), 50% WNT3A-, 20% RSPO1-, and 10% NOG(gin)-conditioned medium (all homemade), 2% B27 with vitamin A (Gibco), 1.25 mM N-Acetylcysteine, 10 mM Nicotinamide, 50 ng/ml murine-EGF (Peprotech), 500 nM A83-01, and 10 mM SB202190 (Sigma). The medium was changed every 2–4 days and organoids were passaged 1:4–1:8 each week. After thawing, organoids were passaged at least once before electroporation.

Cell culture, lentiviral production, and lentiviral transduction

HEK293T, Caco-2 and HeLa cells were obtained from the ATCC.

Fibroblasts were maintained and split every 7 days in standard medium, consisting of F-12 Nut Mix (Ham) (Gibco), 10% FBS (Gibco), and PenStrep (1x, Gibco). HEK293T, Caco-2, and HeLa cells were maintained and split every 4-5 days in standard medium, consisting of DMEM + GlutaMAX (1x, Gibco), 10% FBS (Gibco), and PenStrep (1x, Gibco). For production of lentivirus, HEK293T cells were plated in a 145 mm CELL-

STAR dish (Corning) in standard medium without PenStrep and transfected 24 hours later (at 50–60% confluence) with a mix of 10 µg of the pLenti-CMV-GFP-Hygro plasmid, 5 µg of psPAX2, 5 µg of pMD2.G, and 60 µl of polyethylenimine (1 mg/ml). pLenti-CMV-GFP-Hygro was a gift from Eric Campeau & Paul Kaufman (Addgene #17446). psPAX2 and pMD2.G were gifts from Didier Trono (Addgene plasmids #12260 and #12259). 24 h after transfection, the medium was replaced with standard medium with PenStrep, and virus-containing medium was harvested at 48 and 96 hours after transfection. Medium was centrifuged at $400 \times g$ for 5 min and supernatants were filtered through a 0.22-µm filter, after which virus particles were concentrated by ultracentrifugation at $50,000 \times g$ for 2 hours and resuspension in 1 ml DMEM. HEK293T cells were transduced at an MOI of 2 for 24 h in the presence of polybrene (8 µg/µl) and analyzed by FACS 14 days after transduction to confirm stable GFP expression.

Transfection of HEK293T cells

HEK293T cells were plated in standard medium at a density of 50,000 cells per well in a 96-well plate 1 day prior to transfection. HEK293T cells were transfected with 0.1 µg fluoPEER plasmid, 0.25 µg prime editor plasmid, 0.1 µg pegRNA plasmid, and optionally 0.05 µg nicking-gRNA plasmid in a mix of 25 µl OptiMEM and 0.5 µl lipofectamine 2000 for each well.

Electroporation of organoid cells

Before electroporation, organoids were grown under standard culture conditions. Four wells containing organoids were then dissociated for each condition using TrypLE (Gibco) for 4–5 min at 37 °C, after which mechanical disruption was applied through pipetting. Cells were washed once using Advanced DMEM/F12, resuspended in 80 µl OptiMEM containing Y-27632 (10 µM), and 20 µl DNA mixture was added. For prime editing, the DNA mixture contained 4 µg fluoPEER, 12 µg prime editor plasmid, 4 µg pegRNA plasmid, and 2 µg nicking sgRNA plasmid. The cell-DNA mixture was transferred to an electroporation cuvette and electroporated using a NEPA21 electroporator (NEPA GENE) with 2× poring pulse (voltage: 175 V, length: 5 ms, interval: 50 ms, polarity: +) and 5× transfer pulse (voltage: 20 V, length: 50 ms, interval: 50 ms, polarity ±), as previously described.[37] Cells were removed from the cuvette and transferred into 500 µl OptiMEM containing Y-27632 (10 µM). After 20 minutes, cells were plated in 120 µl matrigel divided over four wells. Upon polymerization of the Matrigel, hl-EM or hSI-EM was added containing Y-27632 (10 µM).

Transfection of fibroblast and HeLa cells

Skin-derived fibroblasts were grown under standard culture conditions and plated on 12-well plates 3 days prior to transfection so that confluency was 60–70% at transfection. HeLa cells were grown under standard culture conditions and plated on 24-well plates 1 day prior to transfection so that confluency was 60–70% at transfection. For prime editing experiments, fibroblasts and HeLa cells were transfected with 0.12 μg fluoPEER plasmid, 0.19 μg prime editor plasmid, 0.05 μg pegRNA plasmid and 0.05 μg nicking-gRNA plasmid in a mix of 8.4 μl OptiMEM, 0.6 μl lipofectamine 3000, and 0.4 μl P3000 reagent. For base editing experiments, the DNA mix consisted of 0.14 μg fluoPEER plasmid, 0.2 μg ABE8e-TadA (V106W) plasmid, and 0.06 μg sgRNA. ABE8e (TadA-8e V106W) was a gift from David Liu (Addgene #138495).

FACS

Organoids and cell lines were harvested and dissociated to single cells using TrypLE (Gibco) or Trypsin (Gibco), respectively, after which cells were resuspended in FACS buffer (phosphate-buffered saline with 2 mM ethylenediaminetetraacetic acid and 0.5% bovine serum albumin). Prior to FACS, cells were filtered through a 5 ml Falcon polystyrene test tube (Corning). Flow cytometry was performed on the FACS Fortessa (BD) and sorting was performed on the FACS FUSION (BD) using FACS Diva software (BD). Sorted cells were collected in culture medium and spun down. Gating strategy for cells included for fluoPEER analysis is shown in Supplementary Fig. 12a. The ratio was calculated by dividing the average measured Cherry signal by the average measured GFP signal for all GFP+ cells.

Genotyping

Sorted cells were harvested using the Quick-DNA microprep kit (Zymogen) according to manufacturer's protocols. PCR was performed on the genomic region of interest using the Phusion polymerase (ThermoFisher) or Q5 polymerase (NEB) and purified using the QIAquick PCR Purification Kit (Qiagen) according to manufacturer instructions. The PCR product was sent for Sanger sequencing to EZSeq Macrogen Europe. All PCR and sequencing primers used are listed in Supplementary Data file 2.

High-throughput DNA sequencing of genomic DNA samples

Genomic sites of interest were amplified from genomic DNA samples and sequenced on an Illumina iSeq 100 as previously described.[38] In short, PCR primers containing Illumina forward and reverse adapters (Supplementary Data file 2) were used in a first amplification reaction (PCR1) of 25 µl using Q5 polymerase (NEB) to amplify the genomic region of interest. In a second round of PCR (PCR2, 25 µl), 1 µl of each PCR1 was barcoded with unique Truseq DNA Index primers (Illumina) and isolated from gel. DNA concentration was measured by fluorometric quantification (Qubit, ThermoFisher Scientific) and sequenced on an Illumina iSeq 100 instrument according to the manufacturer's protocols to create 2 × 150 bp paired-end reads. The resulting FASTQ files were analyzed with the RGEN PE-analyzer, using the unedited sequence as the reference sequence and the prime-edited sequence as the intended sequence.[39] Prime editing efficiency was calculated as the percentage of (RGEN PE-reads/RGEN more than minimum frequency reads). For unwanted byproduct analysis at the pegRNA or nickase sgRNA site, a comparison range (R) of 30 bp or 70 bp was used so that 60 bp or 140 bp flanking the predicted nicking site were considered. Frequency of indels was calculated as the percentage of (RGEN reads with unwanted inserts and deletions/RGEN more than minimum frequency reads).

RNA sequencing

HEK293T cells were transfected with fluoPEER, PE2, pegRNA, and nicking sgRNA plasmids and FACS sorted after 48 h. Total RNA was isolated using Trizol LS reagent (Invitrogen) and stored at –80 °C until further processing. mRNA was isolated using Poly(A) Beads (NEXTflex). Sequencing libraries were prepared using the Rapid Directional RNA-Seq Kit (NEXTflex) and sequenced on a NextSeq500 (Illumina) to produce 75 base long reads (Utrecht DNA Sequencing Facility). Sequencing reads were mapped against the reference genome (hg19 assembly, NCBI37) using BWA[40] package (mem –t 7 –c 100 –M –R). Raw reads were further analyzed as described under 'Data analysis'.

Chemical cell cycle synchronization

Chemical cell cycle synchronization using thymidine and nocodazole was performed as described previously.[41,42] In short, 50,000 HEK293T cells or 10,000 Caco-2 cells were plated in 24-well plates. After 8 h, 2 mM thymidine was added to the cells. 17 h later, cells were washed twice and medium was replaced with standard culture

medium. 8 h later, 2 mM thymidine was readded to the cells. At the same time point, 200 ng/ml nocodazole was added for the nocodazole treatment. 20 h later, cells were washed twice, medium was replaced with standard culture medium, and prime editing was performed by transfection of 0.25 µg prime editor plasmid and 0.1 µg pegRNA plasmid in a mix of 100 µl OptiMEM and 0.3 µl lipofectamine 2000 for each well. 48 h later, transfected cells were sorted using flow cytometry and genotyping was performed as described above.

fluoPEER cell cycle analysis

200 ng/ml nocodazole was added to HEK293T cells 20 h before FACS analysis as a control for cells in G2 phase. 24 h before fluoPEER read-out and genomic Sanger sequencing, HEK293T cells were transfected. 60 min before harvesting for FACS analysis, 10 µg/ml Hoechst 33342 (ThermoFisher) was added to the culture medium. Gating strategy for G1, S, and G2 phases of the cell cycle is shown in Supplementary Fig. 12b.

Data analysis

Flow cytometry data were analyzed using FlowJo™ Software. RNA sequencing was analyzed using DESeq2 in RStudio,[43] gene set enrichment analysis,[44] and enrichR.[45] All figures were made in Prism (GraphPad Software) or GGPlot2[46] in RStudio. Sanger sequencing was quantified using EditR[47] or Tide.[48] Sanger sequencing chromatograms were made in Benchling. NGS data were quantified and analyzed using RGEN PE-analyzer.[39]

Statistics and reproducibility

No pre-specified effect size was calculated, and no statistical method was used to predetermine sample size. For comparisons of multiple groups, an ordinary one-way ANOVA with Holm–Sidak correction for multiple comparisons was used and performed in Prism (GraphPad Software). Statistical tests were appropriate for comparisons being made; assessment of variation was carried out but not included. Experiments were not randomized. Reproducibility: Fig. 1c representative of three biologically independent replicates from one experiment. In Fig. 1d, each point in the dot-plot represents the mean of three (reporter rank) or two (genomic rank) replicates in two independent experiments. Each point in graphs of Fig. 1e represents the mean of at least two biologically independent replicates for each prime editing condition in a single experiment. Figure 1f representative of (1) 14/20 clonally picked intestinal organoids

from two different patients with biallelic *CFTR^F508del* mutations, that showed swelling after addition of 1 µM forskolin to the medium, (2) 2/10 clonally picked liver-derived organoids from a patient with biallelic *ABCB4^E1012X* mutations, (3) 3/10 clonally picked intestinal organoids from a patient with biallelic *ATP8B1^R600Q* mutations, and (4) 2/10 clonally picked liver-derived organoids from a healthy control, in which biallelic *IARS1^I1174N* were created; 4/10 clonally picked organoids from the same experiment showed monoallelic *IARS1^I1174N* mutations.

Figure 2a is representative of two replicates in two independent experiments. In Figure 2b each dot represents the ratio of two bars (PE2* vs. PE2) in Supplementary Figures 8a,b. In Supplementary Figures 8a,b, each bar represents the mean of 2–3 biologically independent replicates. Figures 2c,d,e are representative of three biologically independent replicates from one experiment. Figure 2f shows representative data from one experiment. Figures 3a,b are representative of at least two biologically independent replicates from one experiment. Data from Figure 3c is based on one transfection, of which 8 conditions of 100 GFP + cells and 2 conditions of 100 GFP+RFP+ cells were sorted. Figure 3d is representative of three biologically independent replicates from one experiment. Figure 3e is representative of two or three biologically independent replicates from one experiment. Figure 4b–d are data from RNA sequencing of two biologically independent replicates for both conditions (GFP+RFP-/GFP+RFP+) for each edit (*CTNNB1/IARS1*) from one experiment. In Figure 4e HEK293T, each dot represents the mean of three biologically independent replicates, three independent experiments were performed. In Figure 4e Caco-2, each dot represents a biologically independent replicate from one experiment.

Supplementary Figure 4 is representative of two replicates from two independent experiments. The fluoPEER data in Supplementary Figures 5a,b are representative of three biologically independent replicates in one experiment; fluoPEER data in supplementary Figure 5c is representative of two biologically independent replicates in one experiment that was characteristic of two repeated experiments. Supplementary Figures 6a-c are representative of two biologically independent replicates per condition in one experiment; for representation of the percentage of GFP+ cells, data from different conditions were pooled. Supplementary Figure 6d is based on data from three biologically independent replicates of sorted cells to seed 100% GFP+ conditions. Each pegRNA-PE2-fluoPEER combination from Supplementary Figure 7 was tested in at least two independent transfection experiments. Supplementary Figure 7 is representative of two or three biologically independent replicates from one characteristic experiment.

Supplementary Figures 7b,c are representative of clonally picked liver organoids with monoallelic (two clones) or biallelic (two clones) $IARS1^{I1174N}$ mutations. Supplementary Fig. 7d representative of 20 clonally picked liver-derived organoids from a patient with biallelic MUT^{R329H} mutations. Supplementary Figure 8c is representative of three biologically independent replicates from one experiment. Supplementary Figure 9 shows FACS plots of single conditions that are representative of two independent transfection experiments. Supplementary Figure 10a-d represent data from two biologically independent replicates for each experimental group. Supplementary Figure 10e represents data from three biologically independent replicates for two independent biological replicates. Supplementary Figure 11 data is representative of three biologically independent replicates from NGS. Supplementary Figure 12 is representative FACS data for all FACS experiments shown.

References

1. Anzalone AV, Randolph PB, Davis JR, et al. Search-and-replace genome editing without double-strand breaks or donor DNA. *Nature. 2019;* 576: 149–157.

2. Schene IF, Joore IP, Oka R, et al. Prime editing for functional repair in patient-derived disease models. *Nat Commun.* 2020; 11: 5352.

3. Liu P, Liang S-Q, Zheng C, et al. Improved prime editors enable pathogenic allele correction and cancer modelling in adult mice. *Nat Commun.* 2021; 12: 2121.

4. Nelson JW, Randolph PB, Shen SP, et al. Engineered pegRNAs improve prime editing efficiency. *Nat Biotechnol.* 2022; 40: 402-410.

5. Chen PJ, Hussmann JA, Yan J, et al. Enhanced prime editing systems by manipulating cellular determinants of editing outcomes. *Cell.* 2021; 184: 5635–5652.

6. Kweon J, Yoon J-K, Jang A-H, et al. Engineered prime editors with PAM flexibility. *Mol Ther.* 2021; 29: 2001–2007.

7. Nishimasu H, Shi X, Ishiguro S, et al. Engineered CRISPR-Cas9 nuclease with expanded targeting space. *Science.* 2018; 361: 1259–1262.

8. Walton RT, Christie KA, Whittaker MN & Kleinstiver BP. Unconstrained genome targeting with near-PAMless engineered CRISPR-Cas9 variants. *Science.* 2020; 368: 290–296.

9. Hsu JY, Grünewald J, Szalay R, et al. PrimeDesign software for rapid and simplified design of prime editing guide RNAs. *Nat Commun.* 2021; 12: 1034.

10. Standage-Beier K, Tekel SJ, Brafman DA & Wang X. Prime editing guide RNA design automation using PINE-CONE. *ACS Synt Biol.* 2021; 10: 422–427.

11. Chow RD, Chen JS, Shen J & Chen S. A web tool for the design of prime-editing guide RNAs. *Nat Biomed Eng.* 2021; 5: 190–194.

12. Kim HK, Goosang Y, Park J, et al. Predicting the efficiency of prime editing guide RNAs in human cells. *Nat Biotechnol.* 2021; 39: 198–206.

13. Certo MT, Ryu BY, Annis JE, et al. Tracking genome engineering outcome at individual DNA breakpoints. *Nat Methods.* 2011; 8: 671–676.

14. Coelho MA, Li S, Pane LS, et al. BE-FLARE: a fluorescent reporter of base editing activity reveals editing characteristics of APOBEC3A and APOBEC3B. *BMC Biol.* 2018; 16: 150.

15. Standage-Beier K, Tekel SJ, Brookhouser N, et al. A transient reporter for editing enrichment (TREE) in human cells. *Nucleic Acids Res.* 2019; 47: e120.

16. Martin AS, Salamango DJ, Serebrenik AA, et al. A panel of eGFP reporters for single base editing by APOBEC-Cas9 editosome complexes. *Sci Rep.* 2019; 9: 497.

17. Wang P, Xu L, Gao Y & Han R. BEON: a functional fluorescence reporter for quantification and enrichment of adenine base-editing activity. *Mol Ther.* 2020; 28: 1696–1705.

18. Lin Q, Jin S, Zong Y, et al. High-efficiency prime editing with optimized, paired pegRNAs in plants. *Nat Biotechnol.* 2021; 39: 923–927.

19. Kopajtich R, Murayama K, Janecke AR, et al. Biallelic IARS mutations cause growth retardation with prenatal onset, intellectual disability, muscular hypotonia, and infantile hepatopathy. *Am J Hum Genet.* 2019; 99: 414–422.

20. Fuchs SA, Schene IF, Kok G, et al. Aminoacyl-tRNA synthetase deficiencies in search of common themes. *Genet Med.* 2019; 21: 319–330.

21. Katti A, Foronda M, Zimmerman J, et al. GO: a functional reporter system to identify and enrich base editing activity. *Nucleic Acids Res.* 2020; 48: 2841–2852.

22. Li S, Akrap N, Cerboni S, et al. Universal toxin-based selection for precise genome engineering in human cells. *Nat Commun.* 2021; 12: 497.

23. Adikusuma F, Lushington C, Arudkumar J, et al. Optimized nickase-and nuclease-based prime editing in human and mouse cells. *Nucleic Acids Res.* 2021; 49: 10785–10795.

24. Ioannidi EI, Yarnall MTN, Schmitt-Ulms C, et al. Drag-and-drop genome insertion without DNA cleavage with CRISPR-directed integrases. *bioRxiv.* 2021.

25. Simon DA, Tálas A, Kulcsár PI & Welker E. PEAR: a flexible fluorescent reporter for the identification and enrichment of successfully prime edited cells. *bioRxiv.* 2021.

26. Wang Q, Liu J, Janssen JM, et al. Broadening the reach and investigating the potential of prime editors through fully viral gene-deleted adenoviral vector delivery. *Nucleic Acids Res.* 2021; 49: 11986–12001.

27. Zhao X, Wei C, Li J, et al. Cell cycle-dependent control of homologous recombination. *Acta Biochim Biophys Sin.* 2017; 49: 655–668.

28. Böck S, Rothgangl T, Villiger L, et al. Treatment of a metabolic liver disease by in vivo prime editing in mice. *bioRxiv.* 2021.

29. Landrum MJ, Lee JM, Benson M, et al. ClinVar: improving access to variant interpretations and supporting evidence. *Nucleic Acids Res.* 2018; 46: D1062–D1067.

30. Pruitt KD, Tatusova T & Maglott DR. NCBI Reference Sequence (RefSeq): a curated non-redundant sequence database of genomes, transcripts and proteins. *Nucleic Acids Res.* 2005; 33: D501–D504.

31. Holmes JB, Moyer E, Phan L, Maglott D & Kattman B. SPDI: data model for variants and applications at NCBI. *Bioinformatics.* 2020; 36: 1902–1907.

32. Hunter JD. Matplotlib: a 2D graphics environment. *IEEE Ann Hist Comput.* 2007; 9: 90–95.

33. Ran FA, Hsu PD, Wright J, et al. Genome engineering using the CRISPR-Cas9 system. *Nat Protoc.* 2013; 8: 2281–2308.

34. Huang TP, Zhao KT, Miller SM, et al. Circularly permuted and PAM-modified Cas9 variants broaden the targeting scope of base editors. *Nat Biotechnol.* 2019; 37: 626–631.

35. Huch M, Gehart H, van Boxtel R, et al. Long-term culture of genome-stable bipotent stem cells from adult human liver. *Cell.* 2015; 160: 299–312.

36. Sato T, Vries RG, Snippert HJ, et al. Single Lgr5 stem cells build crypt-villus structures in vitro without a mesenchymal niche. *Nature.* 2009; 459: 262–265.

37. Fuji M, Matano M, Nanki K, et al. Efficient genetic engineering of human intestinal organoids using electroporation. *Nat Protoc.* 2015; 10: 1474–1485.

38. Chen L, Park JE, Paa P, et al. Programmable C: G to G: C genome editing with CRISPR-Cas9-directed base excision repair proteins. *Nat Commun.* 2021; 12: 1384.

39. Hwang GH, Jeong YK, Habib O, et al. PE-Designer and PE-Analyzer: web-based design and analysis tools for CRISPR prime editing. *Nucleic Acids Res.* 2021; 49: W499–W504.

40. Li H & Durbin R. Fast and accurate short read alignment with Burrows – Wheeler transform. *Bioinformatics.* 2009; 25: 1754–1760.

41. Chen G & Deng X. Cell synchronization by double thymidine block. *Bio Protoc.* 2018; 8: e2994.

42. Lin S, Staahl BT, Alla RK & Doudna JA. Enhanced homology-directed human genome engineering by controlled timing of CRISPR/Cas9 delivery. *Elife.* 2014; 3: e04766.

43. Love MI, Huber W & Anders S. Moderated estimation of fold change and dispersion for RNA-seq data with DESeq2. *Genome Biol.* 2014; 15: 550.

44. Subramanian A, Tamayo P, Mootha VK, et al. Gene set enrichment analysis: a knowledge-based approach for interpreting genome-wide expression profiles. *Proc Natl Acad Sci USA.* 2005; 102: 15545–15550.

45. Chen EY, Tan CM, Kou Y, et al. Enrichr: interactive and collaborative HTML5 gene list enrichment analysis tool. *BMC Bioinformatics.* 2013; 14: 128 .

46. Wickham H. ggplot2: Elegant Graphics for Data Analysis. 2016 (Springer-Verlag New York).

47. Kluesner MG, Nedveck D, Lahr WS, et al. EditR: a method to quantify base editing from Sanger sequencing. *CRIPSR J.* 2018; 1: 239–250.

48. Brinkman EK, Chen T, Amendola M & van Steensel B. Easy quantitative assessment of genome editing by sequence trace decomposition. *Nucleic Acids Res.* 2014; 42: e168.

49. Liu Y, Chen S, Wang S, et al. Transcriptional landscape of the human cell cycle. *Proc Natl Acad Sci USA.* 2017; 114: 3473–3478.

Acknowledgements

Supplementary figures

Supplementary Figure 1: analysis of the targeting scope of (NGG-)PE2 and flexible PE2 variants within the ClinVar database.

Supplementary Figure 2: evaluation of reparable mutations in the ClinVar database within the scope of the PE_prediction machine learning algorithm.

Supplementary Figure 3: correlation of prime-editing efficiency of 1-bp deletions versus 1-bp insertions.

Supplementary Figure 4: comparison of genomic editing of GFP→BFP to editing on the corresponding fluoPEER plasmid.

Supplementary Figure 5: comparison of fluoPEER ranking with predictions by the DeepPE algorithm.

Supplementary Figure 6: dynamics of fluoPEER under various transfection conditions and read-out times.

Supplementary Figure 7: testing various pegRNAs and prime editor variants for seven genomic loci and fluoPEER-predicted editing in organoids.

Supplementary Figure 8: characterization of prime editor NLS adaptations and PE4max using fluoPEER.

Supplementary Figure 9: dynamics of cotransfection of four fluorescent plasmids.

Supplementary Figure 10: RNA sequencing analysis of fluoPEER-edited versus -unedited cells.

Supplementary Figure 11: Sanger sequencing is unable to quantify <15% editing of total reads.

Supplementary Figure 12: flowcytometry gating strategies.

May be downloaded from doi.org/10.1038/s41467-022-28656-3.

Supplementary data

Supplementary Data 1: differentially expressed genes in fluoPEER-edited vs. -unedited cells.

Supplementary Data 2: oligos used in this study.

May be downloaded from doi.org/10.1038/s41467-022-28656-3.

THE FINISH

GENERAL DISCUSSION

Inborn errors of metabolism, also known as metabolic diseases, affect the body's ability to properly process or produce cellular metabolites. These diseases have significant impact on a child's health, development, and overall quality of life. Current treatment options are often limited and may include dietary modifications and enzyme replacement therapy. There are thousands of different metabolic diseases, and many of them are ultra-rare, which makes it difficult if not impossible to develop new treatments for each disease individually. Consequently, there is a critical unmet need for the development of new therapeutic strategies that target multiple diseases.

Doing the right research right

Many years ago, I decided to dedicate my scientific career to address unmet needs. I wanted my research to be translational and have a positive impact on patient care (**prologue**).[1] In this thesis, I explore various approaches to develop new therapeutic strategies for metabolic diseases, all initiated for patients from our hospital. First, for cytosolic isoleucyl-ARS1 (IARS1) deficiency, I gained insight into the molecular mechanism (adaptive translation) and tested substrate therapy with isoleucine. To use this conventional approach beyond a single disease, I then further expanded this treatment to patients with various other ARS1 deficiencies and studied the mitochondrial ARS2 deficiencies. Next, I briefly explored a new approach to treat various metabolic liver diseases, by investigating if matching for human leukocyte antigen (HLA) would improve transplantation outcomes. Liver stem cell transplantations, with or without *ex vivo* genetic correction, could potentially treat children with a large variety of metabolic liver diseases. During my research, genetic editing techniques rapidly improved, and *in vivo* genetic editing became more feasible. With the potential to cure almost all metabolic diseases, I propose a plan to use *in vivo* genetic editing of the brain and liver for a mitochondrial disease caused by a common pathogenic *POLG* variant.

Protein synthesis: aminoacyl-tRNA synthetases, and their role in disease

Any error in decoding DNA to RNA (transcription) or RNA to protein (translation) can result in wrongly synthesized proteins. For example, errors in transcription (or splicing) can lead to exon skipping, causing synthesis of incomplete and nonfunctional proteins. Errors in the decoding of mRNA can lead to the incorporation of incorrect amino acids. Similarly, charging tRNAs with the wrong amino acids can lead to the incorporation of wrong amino acids into proteins. Many years ago, it was calculated

that an error rate of no higher than 1 in 3,300 is required for sufficient translational fidelity to be compatible with life.[2]

Fortunately, nature has found ways to cope with translational errors. The most established translational 'mistake' is codon wobbling. Ribosomes translate mRNA to proteins at a speed of 4-22 amino acids per second at 37 °C.[3] To safeguard this speed, ribosomes may sometimes allow an incorrect tRNA in their A-site to bind to a codon to prevent ribosomal stalling, ribosomal collision, and +1 frameshifting.[4,5] This usually concerns a codon with a single nucleotide mismatch, often the third, but sometimes also the first.[6] Fortunately, most amino acids are encoded by multiple codons, mostly differing by a single nucleotide. This decreases the risk of incorrect amino acid incorporation following incorrect codon pairing.

Similarly, computational analyses revealed that various amino acids are interchangeable without a negative effect on protein function (**chapter 4**). Many of these interchangeable amino acids have highly similar codons, often only different in the first or last nucleotide. For example, the codons of isoleucine (AU[A/C/U]) and valine (GU[A/C/G/U]) are highly similar. Likewise, codons of methionine (AUG) are very similar to those of isoleucine and leucine (UU[A/G]). Thus, mistakes at this level could then still result in a functional protein.

Table 1. Editing function of cytosolic aminoacyl-tRNA synthetases (ARS1) and their currently known target amino acids. Summarized data from Gomez et al.[13] Classes are defined by enzymatic features.

Class 1		Class 2	
ARS	**Editing: amino acid**	**ARS**	**Editing: amino acid**
MARS1*	Yes: ncaa	SARS1	Yes: Thr, Cys, ncaa
VARS1	Yes: Thr, Cys, Ala,	TARS1	Yes: Ser
LARS1	Yes: Ile, Met, ncaa	AARS1	Yes: Ser, Gly
IARS1*	Yes: Val, Cys, Thr, ncaa	GARS1	No
CARS1	n.d.	HARS1	No
RARS1*	n.d.	DARS1*	No
EPRS1*	Yes: Ala, Cys	NARS1	No
QARS1*	n.d.	FARS1	Yes: Tyr, Ile
YARS1	n.d.	KARS1*	Yes: ncaa
WARS1	n.d.		

ncaa: non-coding amino acids, may include any of: homocysteine, norvaline, 4-hydroxyproline, homocysteyine thiolactone, serine hydroxamate, ornithine, homoserine, γ-hydroxyleucine, δ-hydroxyleucine, γ-hydroxyisoleucine, δ-hydroxyisoleucine, α-aminobutyrate; n.d.: not determined. Members of the multisynthetase complex are marked with an asterix (*).

12

Protein mistranslation

Yet, our observation of isoleucine to valine substitutions caused by cytosolic IARS1 challenges the basic principles of aminoacylation. There are two variants of misacylation: a cognate amino acid on a noncognate tRNA, and a noncognate amino acid on a cognate tRNA. Regarding the first form, ARS are highly selective for their tRNAs through multiple minor and major recognition sites. There is one known exception: methionyl-ARS1 (MARS1) misacylation of noncognate tRNAs under oxidative stress is thought to be a protective response to oxidative damage, by allowing oxidation of the highly reactive sulphur in methionine.[7] There are no other known examples of incorrect binding and charging of tRNAs by ARS enzymes.[8,9] Regarding the second form of misacylation, ARS can bind and activate structurally similar but smaller amino acids.[9] Hence, it is known that bacterial IARS1 can bind and misactivate tRNA^{Ile} with valine instead of isoleucine with an error rate of 1 in 180.[10] Subsequent pre- and post-transfer editing activity safeguard translational fidelity, decreasing the error rate to 1 in 50,000 in rabbits.[2] Despite this editing function, we found that by decreasing the availability of isoleucine in the medium, healthy isoleucyl-ARS1 (IARS1) charged tRNA^{Ile} with valine at a higher rate, leading to amino acid substitutions in proteins (**chapter 4**). Putatively, the editing function of IARS1 was overwhelmed and unable to correct for the continuous mischarging of valine instead of isoleucine onto tRNA^{Ile}, which would follow basic enzyme kinetics. Misacylation may be explained by the evolutionary desire to preserve translational speed at the cost of translational fidelity, as exemplified by the beneficial effects on protein translation and cellular survival of isoleucine to valine substitutions during isoleucine deprived conditions.[11] Not all amino acid substitutions are expected to be beneficial for cellular function. A good example is the recent finding of tryptophan to phenylalanine substitutions caused by tryptophanyl-ARS1 (WARS1) misacylation under tryptophan depletion in tumor cells.[12] In contrast to IARS1, WARS1 does not have known editing function (**Table 1**).[13] Our *in silico* experiments show that tryptophan to phenylalanine substitutions would be detrimental to protein function. Indeed, the authors describe that these substitutions both follow and promote a T-cell-mediated response and are potentially harmful to the tumorous cells. After repeating their computational analyses,[14] we found that such substitutions also occur in healthy tissue (**chapter 5**). Whereas we did find an association with the interferon-gamma (IFN-γ) pathway in the datasets we analyzed, we cannot rule out such substitutions occurring in normal or other inflammatory conditions as well. Unfortuna-

tely, the publicly available data were of insufficient resolution to draw any definitive conclusion. In an editorial accompanying the original publication, Baranov and Atkins were surprised that similar substitutions were not yet discovered by other scientists.[15] I indeed believe they exist and that we will find more examples once identification methods become more refined.

Charged tRNA fraction and ribosomal stalling

Despite our efforts, some ARS1-related questions remain unanswered. We hypothesized that deficiency of IARS1 would result in a decreased fraction of charged tRNA^{Ile}. To quantify this, I wanted to perform an acid-denaturing northern blot of tRNA isolated under acidic conditions to retain the amino acid-tRNA bond. The deprecated technique using radioactive probes was no longer in use in our proximity, so I developed a biotin-based protocol. Despite countless twenty-four-hour attempts and several successful northern blots without two bands (one for charged, one for uncharged tRNA), I gave up. Nevertheless, we are still able to use my protocol to test other hypotheses (**chapter 8**). In recent years, sequencing techniques have been developed to accurately determine tRNA charge status.[16] These methods make use of the periodate resistant 3'-ends of the charged tRNAs, allowing for quantification of charged versus uncharged tRNA by sequencing and calculating tRNA's with 3' CCA (charged) and 3' CC (uncharged) tRNAs.[17] These techniques are complex and require further improvements before they can be successfully employed by other labs. I hope that in the near future these will help to finally determine the charged fraction in our patient fibroblasts under various conditions.

We further hypothesized that a decrease in charged tRNA^{Ile} would result in a translational problem at isoleucine codons. Indeed, using a dual-fluorescent reporter, we found that IARS1-deficient cells were less efficient in translating an isoleucine-rich region than IARS1-proficient cells (**chapter 4**). To investigate whether this was caused by translational stalling on isoleucine codons, we took various attempts at ribosome sequencing. In this technique, we pause the ribosomes using a selective translation elongation inhibitor, digest all mRNA except the ribosome protected fragments and sequence these fragments. This relatively new technique thus allows for sequencing of a snapshot of the actively translated mRNA strands.[18] From the 28 or 29 nucleotide ribosome protected fragments, it is possible to deduct the location of the ribosomal A-site.[19] We expected to find an increase in abundancy of isoleucine codons in the ribo-

12

somal A-sites in actively translating fibroblasts derived from patients with IARS1-deficiency. Unfortunately, we were not able to confirm this, despite various attempts. In our first attempt, we snap froze the isolated ribosomes, which may have caused ribosomal shifting. We then skipped the freezing step, but did not find any increase of isoleucine codons in the A site, despite including isoleucine deficient conditions. Recent literature suggested that a ribosomal conformational change upon stalling could result in smaller 21 nucleotide ribosome protected fragments that were removed in processing steps prior to sequencing.[19,20] In a final attempt, we used a variant of ribosome sequencing optimized for single-cell analyses which also takes the smaller fragments into account.[21] However, we remained unable to identify an overrepresentation of isoleucine codons in these smaller fragments. Based on our experiments demonstrating failure to translate isoleucine rich regions and an increased sensitivity to isoleucine depletion for expansion, we expect that ribosomes in IARS1 deficient cells are unable to fill all isoleucine codons, especially in isoleucine deprived conditions (**chapter 4**). Putatively, ribosomal stalling occurs, but our analytical strategy is not optimal yet. Alternatively, there is no ribosomal stalling due to 1) binding of alternative(ly charged) tRNAs; 2) ribosomal frameshifting, or 3) a change of translational speed.

There are more intriguing ARS1 characteristics that require further research. For example, I do not yet understand what causes the organ-specific symptoms associated with the various ARS1-deficiencies. I can imagine that different amino acid composition of proteins, differential amino acid utilization or expression of the different ARS1 enzymes or tRNAs in each specific organ could be of importance. Alternatively, loss of noncanonical function plays a role. Since the main symptom of ARS1 deficiency is growth failure, we were unable to expand organoids from ARS1 deficient patients. Therefore, we performed all experiments in patient derived fibroblasts, while ARS1 deficient patients seldom have skin symptoms. Development and use of other organ models may help to answer the intriguing open questions related to ARS1 enzymes.

The role of noncanonical functions in disease

The canonical functions of ARS1 enzymes are now relatively well-established. In addition to the essential role in protein translation, ARS1 enzymes have increasingly been associated with noncanonical functions, making use of domains and active sites that are involved in (regulation of) other pathways, and cellular processes including gene expression.[22] This noncanonical signal transduction may be activated by 1) ARS1 post-translational modifications following cytokine or growth factor stimulation, 2)

altered cellular localization following stimulation, 3) interaction to form new functional protein complexes, and 4) binding of DNA. For example, glutamyl-prolyl-ARS1 (EPRS1) is rapidly phosphorylated upon stimulation with IFN-γ in human macrophages, releasing it from the multisynthetase complex (MSC) to function in anti-inflammatory, anti-viral, pro-adiposity, and pro-fibrosis pathways. With other proteins, EPRS1 may form the tetrameric gamma-interferon activated inhibitor of translation (GAIT) complex, which inhibits translation of various inflammation-related transcripts.[22] Another example is leucyl-ARS1 (LARS1). Besides its canonical function, it serves as a sensor for starvation by sensing leucine. Independent of tRNA charging activity, the C-terminus of LARS1 binds the GTPase of the mTORC1 complex only in the presence of leucine, which is required for activation of mTORC1. Other known noncanonical functions include roles in allergy response (lysyl-ARS1: KARS1), vascular development (seryl-ARS1: SARS1), stress transduction (tyrosyl-ARS1: YARS1; and tryptophanyl-ARS1: WARS1).[22] Unfortunately, the noncanonical functions of IARS1 remain unknown.[23] I expect that further understanding of these noncanonical functions may help us better understand ARS1-related diseases.

Deep phenotyping

When we started our investigation into the ARS1 deficiencies, we tried to determine the cellular problems at the molecular level to understand and if possible, treat the clinical symptoms. Because of the rarity of these diseases, it is crucial to register all reported patients. To simplify this, I designed a prototype web application that allows you to keep track of all reported patients and their symptoms as classified by Human Phenotype Ontology (HPO). The extracted symptoms can then be rapidly analyzed. In this prototype, I included the gene occurrence ratio, which can distill the most distinctive features per gene.[24] Other analyses, such as comparing various genes and diseases, may be added in the future. Advances in artificial intelligence may one day allow the tool to automatically scan scientific literature for patients and extract their symptoms into the tool. The tool is available freely at www.hpodp.nl.

Amino acid treatment for cytosolic ARS1 deficiencies

For autosomal recessive ARS deficiencies, we translated the combination of basic phenotypical features (symptoms related to growth and fast-growing tissues such as dysmaturity, failure to thrive, microcephaly, hypoalbuminemia, and anemia) and increased symptom severity during periods of high translational demands such as

growth, infections, and the first year of life; **chapter 2**)[25] with basic laboratory findings (decreased aminoacylation activity, decreased translation of isoleucine rich regions, decreased cellular viability upon isoleucine restriction; **chapter 4**) into a specific amino acid treatment. While initially designed primarily for one of our own patients, we were able to successfully test this treatment in three other patients, and we are currently asked for advice by physicians from all over the world.[26] We aim to determine the optimal dosage for the various deficiencies. We are currently working on an international registry of all ARS1 deficient patients, including their genotype, phenotype, treatment, and reaction to treatment. Furthermore, we are considering a large-scale (> 20 patients), multi-center randomized clinical cross-over study for LARS1, IARS1, and MARS1 deficiencies, which could be expanded to other ARS1 deficiencies. If the results from this trial confirm a strong treatment effect, I believe we should proceed to introduce the cytosolic ARS1 deficiencies into (genetic) neonatal screening programs. In this way, we might be able to treat ARS1 deficiencies before severe symptoms arise.

Treatment of mitochondrial ARS2 deficiencies

Based on the beneficial effects of the treatment of ARS1 deficiencies, we questioned whether we could also treat mitochondrial ARS2 deficiencies. Despite their mitochondrial function, the ARS2 enzymes are encoded by nuclear genes. All 17 ARS2 genes have been associated with disease.[27] Unsurprisingly, autosomal recessive variants in these genes present with a typical mitochondrial phenotype, affecting primarily organs with high energy demand, such as the brain (e.g., leukoencephalopathy, Alpers syndrome, ataxia), heart (e.g., cardiomyopathy), and liver.[28] Interestingly, there is quite some heterogeneity in symptoms between patients with variants in the different ARS2 genes. This may be explained by highly varying percentages of amino acids in mitochondrial proteins.[28] Amino acid variation in proteins may be worth to further explore for both ARS1 and ARS2 deficiencies. However, clinical phenotypes may also strongly vary between patients with mutations in the same ARS2-gene.

Unfortunately, most of the laboratory assays we used to characterize the cytosolic ARS1 deficiencies did not work for ARS2 deficiencies. Most importantly, we are still unable to quantify aminoacylation activity in mitochondria (despite collaboration with the Amsterdam UMC). Patient-derived fibroblasts did not show any proliferation defects upon amino acid restriction, but they did show mitochondrial defects. Based on our experience with patients with ARS1 deficiencies and the beneficial safety profile of amino acid treatment, we decided to start treating patients with ARS2 deficiency

(**chapter 8**). We are still uncertain about the treatment effects, and it is difficult to relate the disease course to the natural disease evolution. In addition, maybe treatment is able to prevent further deterioration but is unable to repair damage. Moreover, cells and mitochondria may metabolize supplemented amino acids, decreasing bioavailability for mitochondrial translation.[29] In addition, amino acid treatment may well fail to compensate for the loss of noncanonical function.[28] Further research into the mechanism of disease and well-designed trials combined with careful observation and follow-up of patients will hopefully help us differentiate treatment effects from the natural disease course.

QARS1: cytosolic and mitochondrial, or not?

Based on the absence of a QARS2 enzyme, QARS1 was long regarded as an enzyme needed for both cytosolic and mitochondrial translation.[30] Indeed, patients with QARS1 deficiency, including our own patients, have a severe neurological, putatively mitochondrial phenotype (**chapters 2, 3, and 7**). However, QARS1 is not expressed in mitochondria, nor does it have a mitochondrial transfer sequence. It is therefore unlikely that it exhibits a direct mitochondrial function. Instead, mitochondrial glutamyl-ARS (EARS2) misacylates mt-tRNA^{Gln} to mt-Glu-tRNA^{Gln}, which is then transamidated by glutamyl-tRNA amidotransferase (GAT) to the correct mt-Gln-tRNA^{Gln}. Interestingly, studies of in vivo human and rat liver mitochondria showed that nucleus-encoded cytosolic tRNA^{Gln} can be imported into mitochondria.[31] In vitro, this process was shown to be ATP-dependent, and independent of the import of other factors.[31] This combination suggests that there is use for cytoplasmic tRNA^{Gln} in mitochondria. Indeed, in absence of QARS2, this may represent some form of backup for mitochondria. Indeed using northern blotting we found high levels of cytosolic tRNA$_{CUG}^{Gln}$ in mitochondria from healthy fibroblasts but not in mitochondria from two QARS1 deficient patient-derived fibroblast lines (**chapter 8**). Putatively, deficiency of cytosolic tRNA$_{CUG}^{Gln}$ in mitochondria from QARS1 patients contributes to the mitochondrial dysfunction.

In short, our work on the molecular mechanism of IARS1 deficiency led to development of an amino acid treatment, which we were able to expand to various other ARS1 deficiencies. We continue to investigate other ARS1, and ARS2 deficiencies. More or improved strategies to target more different metabolic diseases are deeply needed. We have been working on two such strategies.

12

Liver stem cells transplantations for metabolic liver diseases

Liver stem cell transplantations form a potential treatment strategy for many different metabolic liver diseases. It aims to reintroduce the deficient enzymatic function in the liver. The liver stem cells putatively differentiate into various liver cell types, including hepatocytes and cholangiocytes, which can then produce the deficient enzyme. For many metabolic diseases, it is estimated that only 5% restitution of the enzymatic function in the liver is sufficient to treat the symptoms of the patient.[32]

Undeniably, one of the main challenges in the liver field involves identifying and culturing the optimal liver stem cells. For many years, we have been using liver organoid models,[33] which expand very well, yet do not represent all liver functionalities optimally. Using an extensive transcriptomic comparison method, my colleagues discovered that the "liver organoids" we generally use rather resemble cholangiocytes than hepatocytes (**addendum to part 4**).[34] Based on their progeny from a bipotent cholangiocyte progenitor, we now refer to these organoids as intrahepatic cholangiocyte organoids, or ICOs.[35] To allow other researchers to compare their own hepatocyte models to cellular systems, I developed a free online application of the aforementioned comparison method, named HLCompR (utrecht-university.shinyapps.io/HLCompR).

This rather cholangiocyte than hepatocyte phenotype may well explain the poor engraftment in the liver upon transplantation in animal models.[33,36,37] Various research groups, including our own, try to improve insights into factors that regulate hepatic differentiation and function, not only to improve in vitro modeling but potentially also to enhance engraftment upon transplantation. Yet, even upon engraftment cell survival is not secure, as illustrated by immunological rejection following liver transplantations. To gain insight into potential rejection mechanisms, I focused on the role of HLA compatibility between donors and recipients of a transplant liver (**chapters 9 and 10**). This is one of the potential determinants of rejection that we would be able to control in liver stem cell transplantations, where we can set up a biobank of healthy liver stem cell donors, which can be rapidly matched and expanded to the required amounts before allogeneic transplantation.

For many other solid organ transplantations, mismatching between donor and recipient HLA may cause rejection, increasing the need for immunosuppressive treatment. For liver transplantation, however, study outcomes have remained contradictory. For

this reason, we performed a large meta-analysis on the effect of genetic HLA mismatching on liver transplantation outcomes. We found an effect of HLA-C mismatching on acute rejection (**chapter 9**). Additionally, we wanted to determine whether HLA matching algorithms including HLAMatchmaker and PIRCHE-II performed better for predicting negative outcomes following liver transplantation, which was generally not the case (**chapter 10**).[38]

Based on the results of our meta-analysis, it may be advisable to match liver stem cell transplantations for HLA-C to reduce the chance of developing an acute rejection. Additionally, when concerning a young patient with autoimmune liver disease, one may consider transplanting cells from a PIRCHE-II mismatched donor to reduce the risk of graft loss,[38] as more mismatches may lower the risk of a recurring autoimmune reaction in the autoreactive environment.[39] Unfortunately, the limited number of patients in this subgroup in our cohort did not support the expected inverse correlation with disease recurrence.[38] Hence, before mismatching for this subgroup is applied in a clinical setting, further validation in a larger cohort is required.

Since all patients receive extensive immunosuppressant therapy following transplantation, it is possible that this treatment concealed rejection reactions. Our interest would be to minimize immunosuppressant therapy. In our retrospective study cohort, only a minority of patients was without immunosuppressant therapy, and all but one showed signs of rejection.[38] Furthermore, it is important to note that all data were obtained from adults only and that the situation in children may be different. It would be interesting to perform similar studies in cohorts of pediatric liver transplantation patients.

Ex vivo genetic correction of autologous liver stem cells

In recent years, rapid advances have been made in gene editing technology. CRISPR/Cas9 was first discovered in bacteria, where it functions as part of the immune system, protecting against viral infections.[40] While the repeating DNA sequences and virus-derived 'spacers' were already identified in 1987,[41] it wasn't until 2005 that their function was discovered. In 2012, it became clear that these spacers could be combined with a Cas9 nuclease to make precise cuts in the genome of any organism.[42,43] Since then, new variants of the system have been developed. These expanded the genomic locations that could be targeted and allowed for single- instead of double-strand

12

breaks, reducing unwanted and potentially harmful effects – one of the major risks involved with using these technologies.

Correction of the genetic cause of disease holds the promise to revolutionize outcomes for patients with metabolic diseases. We have successfully used most of these techniques on our liver organoids. We then considered autologous transplantation with patients' own cells following *ex vivo* genetic correction. As this transplantation would involve the patient's own cells, this would eliminate the need for matching for any parameter, ultimately reducing or eliminating the need for immunosuppressive therapy.

While our work on improving liver organoid differentiation and enhancing engraftment could still provide an interesting treatment, I now believe that *in vivo* gene editing directly in the liver of patients is more promising. However, I still see potential in liver stem cell transplantations, either using allogenic, or autologous *ex vivo* genetically corrected cells. This may be particularly relevant for (metabolic and non-metabolic) liver diseases in which the damage has progressed to a stadium where *in vivo* genetic repair would no longer be a feasible option.

In vivo genetic correction is the future

The latest gene editing technology, prime editing, was published in 2019.[44] It allows for the editing of DNA at nearly any genomic location with extreme specificity. In a recent study, we show that there were no off-target effects in both human intestinal and liver organoid systems after prime editing.[45] Combined with the versatility, high efficiency, high reproducibility, and our tool to select the most efficient prime editing strategy,[46] this technology holds the potential to revolutionize treatments for genetic diseases.

Before clinical translation, several challenges of *in vivo* genetic correction need to be addressed. One of the most significant challenges is the delivery of genetic editing components to the correct target tissues in the body. For *in vivo* genetic correction to be effective, the gene editing components must be delivered to the correct cells in the body in sufficient quantities, and without causing harm to the patient.[47] This may require innovative delivery methods and technologies, like for example packaging the editing components in lipid droplets (lipid nanoparticles), that are readily taken up by liver cells. It may, however, prove challenging to target other organs specifically. A second important challenge is the (long-term) safety of *in vivo* editing. Both the genetic

editing and the delivery approach pose potential risks of unwanted off-target effects or genomic integration of vehicle nucleic acids.[47] Fortunately, we did not see any off-target effects with prime editing *in vitro*,[45] and with carefully selecting the delivery method, we may be able to avoid any unwanted effects in the first *in vivo* trials. When proven effective and safe, *in vivo* genetic correction may be considered controversial and may raise ethical concerns. These ethical concerns include the potential long-term consequences of genetic modifications, the risk/benefit determination for a new therapy, the possibility to give informed consent in the context of severely affect patients and/or children, the effects on justice and equity, and the possibility of editing in embryos and the germ-line.[48] It will be important to address these issues to ensure the responsible and ethical development of this new therapeutic strategy. Some may be addressed by thorough experimental work (e.g., long-term consequences and risks and benefits), others by engaging in extensive public and political discussions, nationally and internationally (informed consent, embryos, germ-line editing).

With *in vivo* editing, it may become possible to treat genetic diseases in patients before symptom onset. After the onset of symptoms, gene correction may stop the progression or even permanently cure the disease. This will likely eliminate the need for *ex vivo* editing and liver stem cell transplantations and open the avenue to potentially cure many more diseases. In addition, it may prove valuable for metabolic diseases for which no other curative therapeutic options exist. Recently, we started a project to develop the first *in vivo* genetic repair of the brain, focusing on patients with *POLG*-related disease (**chapter 11**). By primarily focusing on the most common *POLG* variant, we hope to develop a safe and effective curative strategy to eventually treat patients before the onset of symptoms. With this project, we hope to tackle the challenges that await us, paving the way to treat patients with *POLG*-related diseases and other genes that cause genetic neurological diseases in the future.

Concluding remarks and final thoughts

These are exciting times for the field of metabolic diseases. We live in an era characterized by limitlessness. We have access to the complete human genome, unlimited computational power, artificial intelligence that can process incredible amounts of data to learn recognize patterns. New, efficient, and seemingly safe gene editing techniques are readily available. New omics techniques are rapidly being developed and help understand cellular mechanisms to depths that we never did before.

12

When I started my university studies, it was hard to imagine that twelve years later, it would be possible to edit any location of DNA precisely and efficiently. Even when I started my PhD research five years ago, various of the techniques I ended up using had not yet been developed. I can only imagine what the combination of computational power, artificial intelligence, new omics, even further improved gene editing techniques, and techniques we can't yet imagine will bring us in the next years.

I am happy to have worked on improving the molecular understanding of ARS deficiencies and developing a treatment for these severely affected patients. While further research is needed to fully understand the variations between the diseases, with new treatments available, we may perhaps soon include ARS deficiencies into a genetic newborn screening to start treatment as soon as possible to prevent further deterioration. In fact, I believe that in the future many more treatable metabolic diseases may be included in genetic newborn screening programs. Depending on the diagnosis, a personalized *in vivo* genetic editing strategy could be developed. Rapid, personalized treatment would minimize the disease's impact on the newborn and potentially permanently cure the disease. Such treatments will be developed routinely and continuously, and I wish they will become available at an affordable price. As germline editing will likely remain controversial and thus prohibited, and since to prevent is better than to cure, decent education of future parents (e.g., grown-up *in vivo* genetically corrected children) and pre-conception and pre-natal screening will be increasingly important.

New diseases that affect all organ systems will continue to be discovered, as will new variants in new genes with unknown functions. The conventional approach for understanding individual disease mechanisms and developing tailored therapies remains important and cannot be completely replaced by genetic correction. Yet, by directly modifying the underlying genetic cause of the disease, *in vivo* genetic correction has the potential to provide a more permanent and potentially more effective solution than other existing therapies.

With my research targeting various aspects of finding treatments for metabolic diseases that affect various organs, I believe to have contributed to the development of a general therapeutic strategy that may affect the future of patients with metabolic diseases.

References

1. Stevelink R & Kok G. Young scientists aim to prioritize patients. *Nature*. 2018; 558: 519.

2. Loftfield RB & Vanderjagt D. The frequency of errors in protein biosynthesis. *Biochem J*. 1972; 128: 1353–1356.

3. Young R & Bremer H. Polypeptide-chain-elongation rate in Escherichia coli B/r as a function of growth rate. *Biochem J*. 1976; 160: 185–194.

4. Simms CL, Yan LL, Qiu JK, et al. Ribosome Collisions Result in +1 Frameshifting in the Absence of No-Go Decay. *Cell Rep*. 2019; 28: 1679-1689.e4.

5. Wu CC-C, Peterson A, Zinshteyn B, et al. Ribosome Collisions Trigger General Stress Responses to Regulate Cell Fate. *Cell*. 2020; 182: 404-416.e14.

6. Lin JP, Aker M, Sitney KC, et al. First position wobble in codon-anticodon pairing: amber suppression by a yeast glutamine tRNA. *Gene*. 1986; 49: 383–388.

7. Netzer N, Goodenbour JM, David A, et al. Innate immune and chemically triggered oxidative stress modifies translational fidelity. *Nature*. 2009; 462: 522–526.

8. Ribas de Pouplana L, Santos MAS, Zhu J-H, et al. Protein mistranslation: friend or foe? *Trends Biochem Sci*. 2014; 39: 355–362.

9. Pan T. Adaptive Translation as a Mechanism of Stress Response and Adaptation. *Annu Rev Genet*. 2013; 47: 121–137.

10. Schmidt E & Schimmel P. Mutational Isolation of a Sieve for Editing in a Transfer RNA Synthetase. *Science*. 1994; 264: 265–267.

11. Zivkovic I, Ivkovic K, Cvetesic N, et al. Negative catalysis by the editing domain of class I aminoacyl-tRNA synthetases. *Nucleic Acids Res*. 2022; 50: 4029–4041.

12. Pataskar A, Champagne J, Nagel R, et al. Tryptophan depletion results in tryptophan-to-phe-nylalanine substitutants. *Nature*. 2022; 603: 721–727.

13. Rubio Gomez MA & Ibba M. Aminoacyl-tRNA synthetases. *RNA*. 2020; 26: 910–936.

14. Pataskar A, Champagne J, Nagel R, et al. Author Correction: Tryptophan depletion results in tryptophan-to-phenylalanine substitutants. *Nature*. 2022; 608: E20–E20.

15. Baranov PV & Atkins JF. Immune cells alter genetic decoding in cancer. *Nature*. 2022; 603: 582–583.

16. Behrens A, Rodschinka G & Nedialkova DD. High-resolution quantitative profiling of tRNA abundance and modification status in eukaryotes by mim-tRNAseq. *Mol Cell*. 2021; 81: 1802-1815.e7.

17. Evans ME, Clark WC, Zheng G, et al. Determination of tRNA aminoacylation levels by high-throughput sequencing. *Nucleic Acids Res*. 2017; 45: e133–e133.

18. Ingolia NT. Ribosome profiling: new views of translation, from single codons to genome scale. *Nat Rev Genet*. 2014; 15: 205–213.

19. Mendonsa S, von Kuegelgen N, Bujanic L, et al. Charcot–Marie–Tooth mutation in glycyl-tRNA synthetase stalls ribosomes in a pre-accommodation state and activates integrated stress response. *Nucleic Acids Res*. 2021; 49: 10007–10017.

20. Wu CC-C, Zinshteyn B, Wehner KA, et al. High-Resolution Ribosome Profiling Defines Discrete Ribosome Elongation States and Translational Regulation during Cellular Stress. *Mol Cell*. 2019; 73: 959-970.e5.

21. VanInsberghe M, van den Berg J, Andersson-Rolf A, et al. Single-cell Ribo-seq reveals cell cycle-dependent translational pausing. *Nature*. 2021; 597: 561–565.

12

22. Ribas de Pouplana L & Kaguni LS. The Enzymes. 1st ed. 48. Academic Press: New York; 2020.

23. Guo M, Schimmel P & Yang X-L. Functional expansion of human tRNA synthetases achieved by structural inventions. *FEBS Letters*. 2010; 584: 434–442.

24. Haijes HA, Jaeken J & Hasselt PM. Hypothesis: determining phenotypic specificity facilitates understanding of pathophysiology in rare genetic disorders. *J Inh Metab Dis*. 2020; 43: 701–711.

25. Fuchs SA, Schene IF, Kok G, et al. Aminoacyl-tRNA synthetase deficiencies in search of common themes. *Genet Med*. 2019; 21: 319–330.

26. Kok G, Tseng L, Schene IF, et al. Treatment of ARS deficiencies with specific amino acids. *Genet Med*. 2021; 23: 2202–2207.

27. Sissler M, González-Serrano LE & Westhof E. Recent Advances in Mitochondrial Aminoacyl-tRNA Synthetases and Disease. *Trends Mol Med*. 2017; 23: 693–708.

28. Del Greco C & Antonellis A. The Role of Nuclear-Encoded Mitochondrial tRNA Charging Enzymes in Human Inherited Disease. *Genes*. 2022; 13: 2319.

29. Guda P, Guda C & Subramaniam S. Reconstruction of Pathways Associated with Amino Acid Metabolism in Human Mitochondria. *Genom Proteom Bioinf*. 2007; 5: 166–176.

30. Antonellis A & Green ED. The Role of Aminoacyl-tRNA Synthetases in Genetic Diseases. *Annu Rev Genom Hum Genet*. 2008; 9: 87–107.

31. Rubio MAT, Rinehart JJ, Krett B, et al. Mammalian mitochondria have the innate ability to import tRNAs by a mechanism distinct from protein import. *Proc Natl Acad Sci USA*. 2008; 105: 9186–9191.

32. Sancho-Bru P, Najimi M, Caruso M, et al. Stem and progenitor cells for liver repopulation: can we standardise the process from bench to bedside? *Gut*. 2009; 58: 594–603.

33. Huch M, Gehart H, van Boxtel R, et al. Long-Term Culture of Genome-Stable Bipotent Stem Cells from Adult Human Liver. *Cell*. 2015; 160: 299–312.

34. Ardisasmita AI, Schene IF, Joore IP, et al. A comprehensive transcriptomic comparison of hepatocyte model systems improves selection of models for experimental use. *Commun Biol*. 2022; 5: 1094.

35. Marsee A, Roos FJM, Verstegen MMA, et al. Building consensus on definition and nomenclature of hepatic, pancreatic, and biliary organoids. *Cell Stem Cell*. 2021; 28: 816–832.

36. Squires JE, Soltys KA, McKiernan P, et al. Clinical Hepatocyte Transplantation: What Is Next? *Curr Transpl Rep*. 2017; 4: 280–289.

37. Kruitwagen HS, Oosterhoff LA, van Wolferen ME, et al. Long-Term Survival of Transplanted Autologous Canine Liver Organoids in a COMMD1-Deficient Dog Model of Metabolic Liver Disease. *Cells*. 2020; 9: 410.

38. Kok G, Verstegen MM, Houwen RH, et al. Assessment of HLA matching algorithm PIRCHE-II on liver transplantation outcomes. *Liver Transpl*. 2022; 28; 1356-1366.

39. Neumann UP, Guckelberger O, Langrehr JM, et al. Impact of human leukocyte antigen matching in liver transplantation. *Transplantation*. 2003; 75: 132–137.

40. Barrangou R. The roles of CRISPR–Cas systems in adaptive immunity and beyond. *Curr Opin Immunol*. 2015; 32: 36–41.

41. Ishino Y, Shinagawa H, Makino K, et al. Nucleotide sequence of the iap gene, responsible for alkaline phosphatase isozyme conversion in Escherichia coli, and identification of the gene product. *J Bacteriol*. 1987; 169: 5429–5433

42. Lander ES. The Heroes of CRISPR. *Cell*. 2016; 164: 18–28.

43. Gasiunas G, Barrangou R, Horvath P, et al. Cas9–crRNA ribonucleoprotein complex mediates specific DNA cleavage for adaptive immuni-

ty in bacteria. *Proc Natl Acad Sci USA*. 2012; 109: E2579-E2586.

44. Anzalone AV, Randolph PB, Davis JR, et al. Search-and-replace genome editing without double-strand breaks or donor DNA. *Nature*. 2019; 576: 149–157.

45. Schene IF, Joore IP, Oka R, et al. Prime editing for functional repair in patient-derived disease models. *Nat Commun*. 2020; 11: 5352.

46. Schene IF, Joore IP, Baijens JHL, et al. Mutation-specific reporter for optimization and enrich-

ment of prime editing. *Nat Commun*. 2022; 13: 1028.

47. Raguram A, Banskota S, Liu DR. Therapeutic in vivo delivery of gene editing agents. *Cell*. 2022; 185: 2806–2827.

48. Committee on Human Gene Editing: Scientific, Medical, and Ethical Considerations, National Academy of Sciences, National Academy of Medicine. Human Genome Editing: Science, Ethics, and Governance. National Academies Press: Washington, DC; 2017.

12

APPENDIX

....

ABSTRACT

NEDERLANDSE SAMENVATTING
(SUMMARY IN DUTCH)

LIST OF PUBLICATIONS

CURRICULUM VITAE

DANKWOORD
(ACKNOWLEDGEMENTS)

Ap

Abstract

Inborn errors of metabolism, also known as metabolic diseases, are caused by mono-genetic variants and often follow autosomal recessive inheritance. These variants cause a change in enzyme function, including a partial or total loss of function or gained abnormal function, leading to changes in cellular metabolism, e.g., synthesis, breakdown or change of cellular metabolites. Thousands of enzymes, thus thousands of metabolic diseases exist. There is an urgent need for (curative) treatment options that are applicable to multiple diseases or that can be rapidly adapted for use in different diseases. In this thesis, three levels of possible therapeutic interventions are discussed, developed for patients from our own hospital. First, using the conventional approach for IARS1 deficiency, we utilize characterization of the disease and evaluation of the molecular mechanism to develop and test a substrate therapy. This approach is specific to a single disease. We continue to test similar treatments for patients with other ARS1 deficiencies, and further explore its use in patients with various ARS2 deficiencies. Second, we target the liver, as it has a central role in metabolism. Many metabolic diseases can be treated or cured by liver transplantation, but long-term survival of transplantation recipients has remained suboptimal. With the emergence of alternatives such as bankable liver stem cells, allogenous matched or autologous ex vivo genetically corrected stem cells could be transplanted. Improved donor-recipient compatibility could help improve outcomes. We therefore investigate the effect of HLA matching on liver transplantation outcomes. Third, we explore the use of in vivo genetic correction using prime editing, a precise search-and-replace genetic editing technique, which has the potential to cure almost any metabolic disease by directly targeting the underlying genetic defect. We pave the way towards the first in vivo genetic correction therapy of the brain and liver of patients with *POLG*-related disease.

Nederlandse samenvatting

H et DNA bevat duizenden genen: locaties waarin de code voor eiwitten ligt opgeslagen. Overerfbare eigenschappen van mensen komen voort uit kleine verschillen in deze genen. Op enkele uitzonderingen na, erven de meeste van deze monogenetische eigenschappen autosomaal dominant of autosomaal recessief over. Bij autosomaal dominante overerving is het voldoende dat één van de twee kopieën van DNA is veranderd om de eigenschap tot uiting te laten komen; bij autosomaal recessieve overerving moeten beide kopieën van het DNA zijn veranderd.

Enzymen zijn speciale eiwitten die alle noodzakelijke cellulaire functies uitvoeren, waaronder de aanmaak, afbraak en het transport van voedingsstoffen en andere moleculen. Eiwitten kunnen ook belangrijk zijn voor cellulaire structuur en stabiliteit en werken als boodschappers.

DNA en RNA bestaan uit vier nucleotiden: A, T (DNA) of U (RNA), G, en C. Drie nucleotiden samen heten codons. Codons kunnen worden vertaald naar een aminozuur, de bouwstenen van eiwitten. Er zijn twintig aminozuren, dus meerdere codons kunnen voor hetzelfde aminozuur coderen. Deze aminozuren worden naar het ribosoom gedragen door transfer RNA (tRNA) dat specifiek is voor de aminozuren. Aminozuren worden gekoppeld aan tRNA door aminocyl-tRNA syntethases (ARS1). Na translatie worden de gevormde polypeptides bewerkt tot eiwitten en naar de juiste locatie vervoerd.

Mitochondriën zijn organellen die verantwoordelijk zijn voor de energieproductie van de cel. Mitochondriën zijn evolutionair ontstaan uit bacteriën en hebben dus aparte processen voor DNA kopiëren (POLG) en vertalen (mitochondriële ARS2). Menselijke cellen en hun mitochondriën zijn sterk afhankelijk van elkaar.

Metabole ziekten ontstaan uit ziektemakende monogenetische mutaties en zijn vaak autosomaal recessief overerfbaar. Doordat enzymen voor alle cellulaire processen verantwoordelijk zijn, kunnen deze veranderingen de cellulaire stabiliteit verstoren. Er bestaan duizenden enzymen en dus ook duizenden metabole ziekten met een enorme variatie in ziektebeeld en symptomen, ernst en ziektebeloop. Enkele bekende metabole ziekten zijn opgenomen in de hielprikscreening. Snelle diagnose van deze ziekten leidt tot een sterke verbetering van levenskwaliteit en overleving. Als de ziekten niet bij geboorte worden gediagnosticeerd, worden deze vaak niet ontdekt totdat er

Ap

symptomen ontstaan. Door verbeterde genetische diagnostiek worden er meer patiënten met metabole ziekten ontdekt en verschillende genen voor het eerst met deze ziekten geassocieerd. De toegenomen herkenning leidt echter nog niet tot verbeterde zorg voor de patiënten, omdat er veelal geen behandeling voorhanden is.

Behandelingen voor metabole ziekten zijn gevarieerd. Er is een urgente noodzaak voor nieuwe behandelingen die toepasbaar zijn voor meerdere ziekten of die snel aangepast kunnen worden voor verschillende ziekten. In dit proefschrift worden drie aangrijppunten voor behandelingen besproken. Deze zijn allemaal ontwikkeld voor patiënten uit ons eigen ziekenhuis, het Wilhelmina Kinderziekenhuis, Utrecht.

In **deel 2** richten we ons op de conventionele benadering voor ARS deficiënties. Deze benadering is specifiek voor deze groep metabole ziekten.

ARS enzymen, zowel cytosolaire ARS1, mitochondriële ARS2 en gecombineerd mitochondriële glycyl- en lysyl-ARS1 (GARS1, KARS1, resp.) zijn verantwoordelijk voor het binden van aminozuren aan de bijbehorende tRNA's. Mutaties in deze genen worden in toenemende mate geassocieerd met ziekte. In **hoofdstuk 2**, **hoofdstuk 3** en het **addendum bij deel 2** verkrijgen we essentieel inzicht in ARS deficiënties. Omdat onze eerste patiënt *IARS1* mutaties had, hebben we daar een bijzondere interesse in. IARS1 kan isoleucine-tRNA laden met valine, een aminozuur dat lijkt op isoleucine, maar normaal gesproken wordt deze fout hersteld. In **hoofdstuk 4** onderzoeken we het mechanisme van IARS1 deficiëntie. Bij gebrek aan essentiële aminozuren die cellen niet zelf kunnen maken, kunnen eencellige organismen soms andere aminozuren inbouwen in eiwitten. Dit vonden wij ook in gezonde menselijke cellen. Recent werd een vergelijkbaar mechanisme gevonden in menselijke tumorcellen: tryptofanyl-ARS1 (WARS1) kan tryptofaan (W) door fenylalanine (F) vervangen. In **hoofdstuk 5** analyseren we de vrij beschikbare data opnieuw om te onderzoeken of dezelfde technieken bruikbaar zijn voor het vinden van andere aminozuur verwisselingen. In **hoofdstuk 6** en **hoofdstuk 7** ontwikkelen en testen we de eerste behandelstrategie voor ARS1 deficiënties. In **hoofdstuk 8** onderzoeken we of deze behandelstrategie ook werkt voor QARS1 deficiëntie, voor gecombineerd cytosolaire en mitochondriële KARS1 deficiëntie en mitochondriële ARS2 deficiënties.

In **deel 3** richten we ons op de lever. De lever heeft een centrale rol in het metabolisme. Veel metabole ziekten kunnen worden behandeld door een levertransplantatie. Helaas blijven langetermijnoverleving en kwaliteit van leven van patiënten na

levertransplantatie suboptimaal, voornamelijk door het gebruik van medicijnen die het immuunsysteem onderdrukken. Strategieën die de noodzaak voor immunosuppressiva verlagen kunnen de levensverwachting en -kwaliteit verbeteren. Dit zou kunnen door de donorlever en de ontvanger beter op elkaar af te stemmen. Voor levertransplantaties wordt enkel gematcht op bloedgroep en hepatitisserologie. HLA-matching heeft de uitkomsten voor de meeste orgaantransplantaties verbeterd, maar bij levertransplantaties is nog niet duidelijk of het werkt. Daarom onderzoeken we in **hoofdstuk 9** of genetische HLA-matching een positief effect heeft op de uitkomsten na levertransplantatie. HLAMatchmaker en PIRCHE zijn voorbeelden van nieuwe algoritmes om HLA-matching te verbeteren. In **hoofdstuk 10** onderzoeken we of de scores van deze algoritmes correleren met de levertransplantatie uitkomsten. Aanvullend ontwikkelen we in het **addendum bij deel 3** een online toepassing om lever cel modellen te vergelijken en het beste model te kiezen voor laboratoriumonderzoek.

In **deel 4** willen we gencorrectietechnieken gebruiken om een behandeling te ontwikkelen voor DNA polymerase gamma (POLG) gerelateerde ziekten. In genvervangingstherapie, zoals op dit moment in gebruik voor spinale spieratrofie, worden extra kopieën van een gezond gen permanent of tijdelijk in patiëntcellen ingebracht. Recente ontwikkelingen in gencorrectietechnieken, die ontstaan zijn uit de Nobelprijs winnende CRISPR/Cas9 technieken, maken het mogelijk om heel precies patiëntmutaties te repareren. Prime editing is de meest belovende techniek, waarmee het mogelijk is om heel precies en veilig nagenoeg elke mutatie te corrigeren. In het **addendum bij deel 4** ontwikkelen we een methode om de techniek efficiënter te maken.

We willen deze techniek gebruiken om de meest voorkomende ziekteverwekkende mutatie van *POLG* te corrigeren. Er zijn meer dan 200 ziekteverwekkende mutaties in *POLG* en combinaties daarvan leiden tot een veelvoud aan verschillende ziekten. De meest voorkomende mutatie is c.1399G>A p.(A467T) en kan Alpers Huttenlocher syndroom veroorzaken, een ernstige ziekte met onbehandelbare epilepsie, neurologische achteruitgang en spierzwakte waarvoor nog geen behandeling bestaat. Kinderen overlijden vaak snel na het ontstaan van symptomen. In **hoofdstuk 11** timmeren we aan de weg om de eerste behandeling met gencorrectietherapie te ontwikkelen voor de meest voorkomende *POLG* mutatie.

List of publications

In this thesis

Stevelink R & **Kok G**. Young scientists aim to prioritize patients. *Nature*. 2018; 558: 519.

Fuchs SA, Schene IF*, **Kok G***, et al. Aminoacyl-tRNA synthetase deficiencies in search of common themes. *Genet Med*. 2019; 21: 319-330.

Kok G, van Karnebeek CDM & Fuchs SA. Response to Shen and Zou. *Genet Med*. 2021; 23: 589-590.

Kok G, Tseng L, Schene IF, et al. Treatment of ARS deficiencies with specific amino acids. *Genet Med*. 2021; 23: 2202-2207.

Ravel JM, Dreumont N, Mosca P, ..., **Kok G**, et al. A bi-allelic loss-of-function SARS1 variant in children with neurodevelopmental delay, deafness, cardiomyopathy, and decompensation during fever. *Hum Mutat*. 2021; 42: 1576-1583.

Kok G, van Karnebeek CDM & Fuchs SA. Response to Shen et al. *Genet Med*. 2022; 24: 506-507.

Kok G, Verstegen MMA, Houwen RHJ, et al. Assessment of HLA matching algorithm PIRCHE-II on liver transplantation outcomes. *Liver Transplant*. 2022; 28: 1356-1366.

Schene IF*, Joore IP*, Baijens JHL, Stevelink R, **Kok G**, et al. Mutation-specific reporter for optimization and enrichment of prime editing. *Nat Commun*. 2022; 13: 1028.

Ardisasmita AI*, Schene IF*, Joore IP**, **Kok G***, et al. A comprehensive transcriptomic comparison of hepatocyte model systems improves selection of models for experimental use. *Commun Biol*. 2022; 5: 1094.

Muffels IJJ, **Kok G**, Tang Z, et al. Amino acid treatment for mitochondrial ARS2 and QARS1 deficiencies. 2022
In preparation

Kok G*, Schene IF*, Ilcken EF, et al. Isoleucine-to-valine substitutions support cellular physiology during isoleucine deprivation. 2022
Conditionally accepted at Nucleic Acids Res

Kok G*, Ilcken IF*, Houwen RHJ, et al. The Effect of Genetic HLA Matching on Liver Transplantation Outcome: A Systematic Review and Meta-Analysis. 2023
In press at Ann Surg Open

Schene IF*, **Kok G***, Nieuwenhuis EES, et al. Refined analysis of open proteomics data reveals amino acid substitutions in healthy tissue. 2022
Under review

Not in this thesis

Dijkstra S*, **Kok G***, Ledford JG, Sandalova E, Stevelink R. Possibilities and pitfalls of social media for translational medicine. *Front Med*. 2018; 5.

Kok G, van de Wall BJM, Verleisdonk EJMM. Botgroeistimulatoren bij fracturen: zinnig of onzinnig? *Ned Tijdschr Geneeskd*. 2020; 164.

Curriculum vitae

After finishing bilingual secondary education, Gautam finished his Bachelor's in Biomedical Sciences (Molecular Life Sciences) at Maastricht University in 2014. Being internationally oriented, he enrolled in an Honours program in International Health and in 2013 paid a two-month visit to India to learn about its healthcare system. In 2014 he visited China with the Netherlands-Asia Honours Summer School (NAHSS) where he, besides taking summer courses at Peking University (PKU), worked on strengthening scientific and educational ties between China and The Netherlands for the Dutch Ministry of Education, Culture and Science. With special interest in research and translational medicine, Gautam studied SUMMA (Selective Utrecht Medical Master) at Utrecht University while participating in various extracurricular activities related to translational science. He then pursued a PhD in Pediatric Metabolic Diseases in the Wilhelmina Children's Hospital, where he primarily worked on the disease mechanism and treatment of a newly discovered group of diseases. He aims to become a translational scientist and a medical doctor and has a special interest in regenerative medicine, disease mechanisms and new therapeutic approaches. In his spare time, Gautam loves traveling and exploring new cultures, cooking and dining, various sports, and to play (specifically win) board games.

Dankwoord

Dit proefschrift is tot stand gekomen door inzet, gedachtewisselingen en hard werk van veel mensen. Zonder hulp en medewerking van mijn vrienden, familie, collega's, begeleiders en de patiënten was me dit nooit gelukt. Ik ben iedereen die een bijdrage heeft geleverd, het zij direct of indirect, ontzettend dankbaar. Hoewel ik weet dat het me niet zal lukken iedereen persoonlijk te bedanken, wil ik graag een poging wagen.

Dr. Fuchs, beste **Sabine**, wat hebben we een reis gemaakt. Ik ontmoette je voor het eerst bij de summer school die we samen organiseerden in 2016, toen ik nog studeerde. Je enorme enthousiasme en je waanzinnige plannen spraken me zo ontzettend aan dat ik mijzelf hier ook aan zag werken. Ik begon toch aan een ander project dan beoogd en vervolgde m'n pad als promovendus. Vanaf het begin heb ik me ontzettend welkom gevoeld en een vertrouwen, vrijheid en ondersteuning ervaren waar veel promovendi jaloers op mogen zijn. Je gaf me zelfs je huis en je hond Sam om op te passen (en wat ben ik opgelucht dat Sam dat heeft overleefd). Ik ben blij dat ik in 2016 naar je toe ben gestapt, dankbaar voor je geloof in me en trots op wat we samen hebben bereikt. Je hebt nog steeds grootse plannen en ik weet zeker dat je die gaat waarmaken. Waar de toekomst me ook brengt, ik hoop van die plannen deel uit te mogen maken en nog lang met je samen te mogen werken.

Prof. dr. Nieuwenhuis, beste **Edward**, dank je wel voor het vertrouwen dat je me gegeven. Je hebt een ontzettend fijne, gevarieerde onderzoeksgroep opgebouwd waarbinnen samenwerken niet alleen eenvoudig, maar vanzelfsprekend is. Je hebt de natuurlijke gave om mensen snel op hun gemak te laten voelen. Ik ben je dankbaar voor de kansen die je me geboden hebt. Ik waardeer je eerlijke mening en de slechte timing van je kritische maar waardevolle blik, waardoor we regelmatig op de valreep een paper helemaal moesten omschrijven.

Beste **Imre**, een heel groot deel van wat ik in het onderzoek bereikt heb, heb ik aan jou te danken. Je was de eerste promovendus van **Sabine** en mijn stagebegeleider, later mijn zeer betrokken collega. We hebben samen een groot deel van onze tijd op het lab doorgebracht. Jij leerde me vooruit te denken, tegenvallende resultaten te zien als uitdaging en dat projecten best lang mogen duren. Bovenal leerde je me dat alles in het lab gedeeld is. Je analytische blik, je enorme inzet, aandacht voor mensen, de rust die je uitstraalt als alles tegen lijkt te zitten, maar bovenal je oprechtheid en je

aandacht voor anderen, zelfs op momenten die persoonlijk zwaar voor je waren, zullen me bijblijven. Je bent een voorbeeld voor anderen, in ieder geval voor mij. Ik weet zeker dat onze paden in de toekomst zullen kruisen en ik kijk er nu al naar uit.

Natuurlijk was het onderzoek onmogelijk geweest zonder alle collega's van onze grote onderzoeksgroep. **Dr. Mokry**, dear **Michal**, your insights were useful and you taught me that it is possible to be incompatible with laboratory rules. **Dr. Lindemans**, beste **Caroline**, dank je wel voor het meedenken en richting geven van de HLA onderdelen van mijn proefschrift. **Dr. Van Hasselt**, beste **Peter**, je was altijd beschikbaar om even te sparren over een project, al kwam ik meestal met meer vragen terug. **Prof. dr. Houwen**, beste **Roderick**, ontzettend bedankt voor het meedenken en je snelle reactie op mijn manuscripten. **Dr. Kuijk**, beste **Ewart**, je kwam er pas aan het einde bij, maar was al snel onderdeel van mijn onderzoek. Dank je wel voor het meedenken en helpen na mijn vertrek. **Imre**, **Suze**, **Maaike**, **Indi**, **Ibrahim**, **Marit**, **Vivian**, **Zahra**, **Remi**, **Ema**, **Sawsan**, **Marliek**, **Matthijs**, **Martijn**, **Jorik**, **Claartje**, and all the other people and students that have been involved with our lab, I really enjoyed working on the various projects with all of you. With some of you I share projects and papers, with all of you I shared ideas, frustrations, and successes (and sometimes without asking, your laboratory materials :-) **Eveline** and **Jose**, as the newest members of our group, I am sure you will have lots of fun.

Dr. Vos, beste **Harmjan**, het was me een genoegen met je samen te mogen werken. Appen of mailen ligt je niet, dus op de meest willekeurige momenten kon ik een telefoontje verwachten. Je hebt een heerlijk ongenuanceerde blik op de wetenschap. Ik waardeer je oneindige geduld terwijl we een mass spec experiment voor de zoveelste keer moesten herhalen, en kon meegenieten in je enthousiasme toen het geduld uiteindelijk werd beloond. **Prof. dr. Prakken**, beste **Berent**, het is dankzij jou dat ik **Sabine** heb leren kennen en dit onderzoek in ben gerold. Je motiveerde mij om me samen met medestudenten in te zetten voor Apollo. Je hebt vele deuren voor me geopend, waarvoor ik je erg dankbaar ben. **Dr. Loayza-Puch**, dear **Fabricio**, and **dr. Stepanova**, dear **Ekaterina**, thank you for early scientific discussions and the various attempts at ribosome profiling. **Tim**, ook jij bedankt voor het meedenken met onze vroegste experimenten. **Prof. dr. Van Karnebeek**, beste **Clara**, na jaren met je gewerkt te hebben tijdens en na covid was het leuk je voor het eerst in persoon te ontmoeten in Freiburg. Ik wil je bedanken voor je inzet voor de ARS patiënten en ben blij dat we samen tot een behandeling hebben kunnen komen. **Dr. Spierings**, beste **Eric**, dank je wel voor het meedenken en de aanvullingen op de levetransplantatie stukken. **Prof. dr. Van der**

Laan, beste **Luc** en **dr. Verstegen**, beste **Monique**, zonder jullie waren de levertransplantatie projecten nooit van de grond gekomen. Veel dank voor het verlenen van toegang tot de dossiers, het meedenken en meelezen. **Prof. dr. Braun**, beste **Kees**, en **dr. Koeleman**, beste **Bobby**, ik ben jullie dankbaar voor jullie hulp en vertrouwen bij het opzetten van ons laatste onderzoeksidee en dat ik **Remi** een tijd heb mogen lenen.

Ik heb het genoegen gehad samen te werken met meerdere studenten. **Indi** en **Eveline**, jullie hebben je in zeer korte tijd weten te ontwikkelen tot echte onderzoekers en hebben resultaten neergezet die zo gebruikt konden worden (en werden) voor publicaties. **Indi**, overloper, ik ben blij dat je je draai snel vond bij **Imre**. **Eveline**, je toonde enorme flexibiliteit toen we door covid dicht moesten en je stage ineens stil kwam te liggen. Ik ben er stiekem best een beetje trots op dat jullie allebei aangenomen zijn en ik jullie ook als collega heb mee mogen maken. **Eline**, wat een aanstekelijke bom aan energie en enthousiasme draag jij met je mee. Je sleepte iedereen mee: borrels, uitjes, lasagne-wedstrijden, niets was je te gek (en zoals beloofd: je lasagne was lekker_der). Je hebt in korte tijd de basis weten te leggen voor een groot vervolgproject en daar heb ik veel respect voor. **Maaike**, jij hebt de uitdaging dit project naar een nog hoger niveau te tillen. Je werkt al zo snel zelfstandig en vertelt mij wat de volgende stappen zijn, dat ik er volledig van overtuigd ben dat dit geen enkel probleem voor je zal zijn. Ik hoop dat we samen kunnen blijven werken.

Allerleukste borrel club, **Suze**, **Maaike**, **Irena** en **Marliek**, ik heb genoten van onze ongedwongen samenkomsten. Door jullie was ik continue op de hoogte van de laatste en belangrijkste roddels over collega's, studenten en begeleiders. Natuurlijk was het ook heel fijn om met jullie samen te werken en ideeën uit te wisselen over de jaren. **Irena**, ik waardeer in jou een hardwerkende collega die altijd met volle moed en energie een project instapt. Je bent niet bang mij nu en dan terecht te wijzen. Ook bewonder ik je bereidheid om spontaan een biertje te drinken. Wat was het genieten om door weer en wind, covid-lockdowns en avondklokken de week te breken aan de singel.

Arrien, **Derek**, **Casper**, wat prijs ik me gelukkig dat ik jullie al sinds het begin van de middelbare school tot mijn beste vrienden mag rekenen. Wat hebben we samen veel meegemaakt. Hoewel we over de jaren heen allemaal heel andere richtingen op zijn gegroeid en heel andere levens hebben, voel ik me ontzettend vertrouwd bij jullie en weet ik dat jullie me door dik en dun steunen. Ik kijk steeds weer uit naar een stedentrips met jullie, een avondje borrelen, de eindeloze klaagzangen om alles en om niets op Whatsapp. **Arrien**, met jou proefde ik op mijn 18e tijdens onze roadtrip de

smaak van vrijheid. We waren jong en onbezonnen, maar hadden de tijd van ons leven. Ook de vele avonden in Nijmegen met je studievrienden waren heerlijke afleiding van de dagelijkse drukte. **Derek**, goed om te zien dat na de nodige jaren studeren, het werkende leven je beter af gaat. Het is telkens weer genieten je op willekeurige doordeweekse avonden over de vloer te hebben. En wat ontzettend bijzonder dat jij en **Marcella** ons dit jaar hebben verrast met **Nore**. Ik kijk er nu al naar uit haar over een aantal jaar in geuren en kleuren over onze avonturen te vertellen. **Casper**, ik heb in jou een vriend die wat serieuzer in het leven staat. Je staat altijd open voor een goed gesprek en geeft gevraagd of ongevraagd je eerlijke mening. Na mijn verdediging proost ik met jullie, op dat we vrienden blijven, voor altijd.

Lieve SUMMA vrienden, **Elise**, **Floortje**, **Siri**, **Dorine**, **Timon**, **Remi** en lieve **Simone**. Ik weet nog dat ik jullie de eerste keer uitnodigde voor mijn inmiddels fameuze Chinese aubergine. Wie had gedacht dat dat aanleiding zou zijn tot vele diners, SinterKerstEnNieuw's, tripjes naar Zwitserland, Oxford en zelfs de Waddeneilanden. Dank voor jullie vriendschap. **Jean-Luc**, dank je voor je oneindige gastvrijheid, de heerlijke wijn en de potjes squash.

Remi, wat is het leven een feest met jou als goede vriend en paranimf. Je bent niet alleen een van de slimste, maar ook een van de meest nuchtere mensen die ik ken (thans, soms). Onze wens tijdens de opleiding ooit nog samen onderzoek te doen lijkt zowaar uit kunnen laten komen. Ik heb van je geleerd dat je zo veel als haalbaar op reis moet, de rest is bijzaak. En wat hebben we een ongelofelijke dingen meegemaakt op Kalimantan, in Kirgizië, en Georgië. Via jou mag ik je lieve vriendin **Juliëtte** en vele anderen nu als vrienden beschouwen. **Jordi**, toen ik een aantal jaar geleden voor het eerst nieuwjaar bij je kwam vieren had ik nooit gedacht dat dit een traditie zou worden waar ik het hele jaar naar zou uitkijken. Ik wil jou en **Bente** bedanken voor jullie gastvrijheid, pizza's, tuica en de vele herinneringen. **Ran**, **Lennart**, **Bob** en alle andere reismaatjes, wat een gave tochten hebben we gemaakt. Ik heb hoge verwachtingen van de volgende tochten.

Dear **Shalin**, thank you for showing me there's life besides studying and research. I really enjoy our random, way over the top, extravagant city trips - although I'm not sure the amounts of wine have been very helpful in finishing my PhD. Dear **Rajumama**, I wish to thank you to for believing in me and hosting my many visits to India. Dear **Nani**, I believe that the brains in our family have come from you. Although I have always lived at a long distance from you, I have felt your support, interest and love.

———

Likewise, I am blessed to have such a large Indian family and would like to thank the many **uncles**, **aunts** and **cousins** for their hospitality. **Herco** en **Monica**, **Tim** en **Jasper**, jullie wil ik graag bedanken voor het warme welkom in jullie familie, ongevraagd advies en de heerlijke reizen naar onder meer het Kuchenbuffet.

Seema, lieve **mama**, dit proefschrift vertegenwoordigt alle waarden en normen waarmee je me hebt grootgebracht. Leren doe je voor jezelf, zei je altijd. Je hebt het positieve in me belicht en me geleerd kansen te herkennen en te grijpen, om nieuwsgierig te zijn en nooit genoegen te nemen met half werk. Dank je wel voor je begrip en geduld en onvoorwaardelijke steun. Ten slotte was het heerlijk om je steeds te horen zeggen dat ik wat rustiger aan moest doen. Dat gaf me steeds weer de kans niet naar je te luisteren en me zo weer even kind te voelen.

Lieve **Tulsi**, wat ben ik blij met jou als **zusje**. Samen konden we altijd de hele wereld aan en dat zal nooit veranderen. Ik geniet intens van onze weekendjes weg, etentjes, uitjes en alle momenten samen.

Simone, lieve **Moon**, wat gaat de tijd toch snel. Sinds onze ontmoeting in China wil je samen met mij het avontuur van het leven aangaan. Onze eerste reis naar Maleisië en de vele avontuurlijke reizen naar Kirgizië, Georgië, Roemenië, Ethiopië, India, Chili en nog veel meer, samen wielrennen, mountainbiken, weekendjes weg, een eerste huis kopen en helemaal opknappen, je deinst van weinig terug. Ik hou van je en kijk uit naar wat de toekomst voor ons in petto heeft.

Notes